Author:
De Carvalho Ferreira, Maria Luiza

Title:
Deep-sea coral records of the intermediate Atlantic Ocean during the last glacial cycle

Deep-sea coral records of the intermediate Atlantic Ocean during the last glacial cycle

Maria Luiza de Carvalho Ferreira

A dissertation submitted to the University of Bristol in accordance with the requirements for award of the degree of Doctor of Philosophy in the Faculty of Science

School of Earth Sciences

November 2022

Word Count:

37,091

Abstract

Cold-water corals are found extensively throughout the world's oceans and thus represent a valuable paleoceanographic archive – particularly at the intermediate depths (<2000 m). These corals can be radiometrically dated and therefore provide insight into millennial-centennial scale oceanic perturbations on precise age scales. In this thesis, I have paired measurements of radiocarbon (^{14}C) and Li/Mg along with U-series dating of corals to reconstruct ocean circulation and seawater temperature in the Atlantic Ocean over the last glacial interval. In addition, I have compiled a large dataset of coral occurrences (new and published coral ages) to reveal links between the distribution of corals and environmental conditions.

In Chapter 2 I investigate the temporal and spatial distribution of cold-water corals in the Northeast Atlantic over the past 150 thousand years (kyr). These data revealed that corals were thriving at low and mid-latitudes during the last glacial and deglacial intervals, but their presence at higher latitudes occurred only during warmer climates. Food supply and dissolved oxygen associated with oceanic dynamics (e.g., currents, fronts, upwelling) changed with similar timing to coral occurrence patterns suggesting a strong causal link with climate. In Chapters 3 and 4 I reconstructed seawater ^{14}C and temperature of intermediate depths in the Northeast and Southwest Atlantic. During the Last Glacial Maximum, the intermediate waters at both sites were colder than present, and the similar ^{14}C signature suggests an extension of southern-sourced waters into the Northeast Atlantic. During the early deglaciation, a pronounced warming and an increase in ^{14}C at both locations were interpreted as a result of weakened Atlantic Meridional Oceanic Circulation (AMOC) and heat export from the Southern Ocean and downwelling diffusion. Together the precisely dated coral data revealed that changes at intermediate depths are linked to perturbations in AMOC and global climate shifts.

Acknowledgements

The development of this work would not be possible without the great support of my colleagues, family and friends. I am grateful for all opportunities, friendship, kindness and also critiques that were all valuable to make me get to where I stand now – writing the final words of my PhD thesis. I strongly believe that my achievements are the result of the support, inspiration and opportunities which were offered to me by many people throughout my life. I am immensely grateful for each and every one of them.

First of all, I am very thankful to Laura Robinson. She is an excellent supervisor, very supportive and always available. She has been very supportive and patient. I am very grateful to her for having facilitated my travels to Brazil, where I had the chance to collect samples and network with researchers from my home country. Also for supporting and financing my participation in a scientific cruise to the South Sandwich Islands, several conferences and future participation in a cruise to Galapagos Islands. Equally important she had also taught me about how to create a supportive working environment, where teamwork is a key component. I feel greatly thankful for having worked with Laura.

I am also very grateful to Joseph Stewart, who supervised me through my PhD. I am thankful for providing me with training in the clean lab, ICP-MS and for discussing science and ideas. Joe is a great person, always cheerful and his excitement about science is truly inspiring. Joe is also very dedicated to maintaining the working environment as a respectful, safe and friendly place. Having worked with Joe was a great pleasure and he had contributed a great part in this project.

A big part of PhD life is work, and I had the big fortune to share this part of my life with many amazing people from the BOPP group. I am grateful for the time spent together in the labs and for all other social events. A special thanks to the coral team: Laura, Joe, Carolyn, Qian, Lorena, James, Yingchu, Maoyu, and former coral-BOPPers Tao, Ana, Ivo, Sean, and Laifeng. Without the support of each of them this work would have been a much harder task. Special thanks to Carolyn for providing lab training, maintenance of the lab and for the good chats. Joe, Tao, Ana, Qian and James also provided training on sample preparation and lab techniques, which I am very grateful for. I am also tankful to Joe, Qian, James, Lorena, Yingchu and Maoyu who had helped me with several measurements included in this thesis. Most of all, I would like to thank them all for their friendship and cooperation during my PhD.

A big thanks also goes to all members of the BIG group as well. For the discussions during the lab meetings and for the darts competitions after work. I am especially thankful to Chris, for all his help and patience during the measurements using the ICPs, as well as for all his time spent teaching me about the machines, for the maintenance of the lab and for his friendship. I am also grateful for Jamie who helped me in the lab many times.

I am grateful to Marcelo Kitahara who hosted me in CEBIMar/USP in 2018 and provided in-person training in coral identification in his lab. Also, Marcelo facilitated and accompanied me on the visit to the National Historical Museum (Rio de Janeiro, Brazil) in 2019 for the collection of the coral samples used in Chapter 4. I am also grateful to Katia Kapel who helped with the coral sampling, and to Débora Pires who was the curator of the scleractinian collection of the museum. I am also grateful to Marcelo, Laura and Michele Taylor who help me to get the CITES permission to ship the coral samples

from Brazil to the UK. I would also like to thank Christian Millo who provided additional coral samples from Tropic Seamount (included in Chapter 3) and Rio Grande Rise (included in Chapter 4). I am also grateful to Andrea Burke, Tianyu Chen and Tao Li for providing unpublished data included in Chapter 2 (and published in Deep Sea Research Part I).

I am grateful to Kate Hendry and Paul Valdes who were my APM examiners and had contributed with ideas and discussions during my PhD. I would also like to express my gratitude to Augusto Mangini and Adina Paytan, who were two important people I met who inspired me through my carrier.

I would like to thank my family for always believing in me and providing emotional and financial support throughout my life, from childhood up to now. Especially my mom, Guta, who had always supported my decisions and provided the best advice. She is my dearest friend and inspiration. I am also very grateful to my grandma (Teresa) who is an equally inspiring woman. Big thanks to my dad (Hélio) for all his support, love and kind words. My siblings Camille, Pablo e Sofia, my sister-in-law Priscila and my dear nieces Isis and Vicky, you all make my life more colourful and happier. I am exceptionally grateful to Eric, who has always supported me. He is a wonderful person and I am truly thankful that our paths crossed. I am grateful for his patience, companionship and for his scientific feedbacks too.

A big thanks to all my friends I made in Bristol. Special thanks to my housemates Chrys, Anne and Hannah, with whom I had a great time sharing chats, trips, food, and advice. You are very good friends and I am very grateful for all your support during these years. I met some great people during this period which had supported me. Especial thanks goes to Felipe, Fred, Anderson, Luana, Dave, Izzy and all the members of Bristol Wutan kung fu especially Sarer Scotthorne.

Finally, I am grateful to Schlumberger Foundation for funding my PhD through the “Faculty for the Future” fellowship. Everyone from the Schlumberger Foundation had provided excellent and committed work, and communication was always easy. Extra funding for conferences and travels was provided by the University of Bristol and NERC/FAPESP (Laura Robison and Marcelo Kitahara).

Author’s declaration

I declare that the work in this dissertation was carried out in accordance with the requirements of the University's Regulations and Code of Practice for Research Degree Programmes and that it has not been submitted for any other academic award. Except where indicated by specific reference in the text, the work is the candidate's own work. Work done in collaboration with, or with the assistance of, others, is indicated as such. Any views expressed in the dissertation are those of the author.

Maria Luiza de Carvalho Ferreira

10 November 2022

Contents

List of Figures

APPENDIX I

APPENDIX II

APPENDIX III

List of tables

Chapter 1: INTRODUCTION

1.1 MOTIVATION

Understanding the ocean's role in past and future climate change is of key scientific and societal importance. The ocean is a critical component of the climate system – acting as a conduit for the redistribution of heat, gases, and nutrients between the atmosphere, lithosphere and cryosphere. Previous studies have linked changes in atmospheric temperature and CO_2 to changes in oceanic circulation at millennial timescales (e.g., Broecker, 2018; Marcott et al., 2014; Sigman et al., 2010). For example, during the last deglaciation (18 ka to 11 ka), intervals of abrupt climate change were accompanied by changes in the ocean chemistry and dynamics (Curry and Oppo, 2005; Marchitto and Broecker, 2006; Keigwin and Boyle, 2008; Barker et al., 2009; Oppo et al., 2018; Rae et al., 2018).

To better understand past changes in our oceans, well-dated and high-resolution paleoceanographic records are needed. High quality paleoceanographic proxy data can be interpreted on its own, or used to better constrain climate models outputs which improve our the spatial/temporal resolution of reconstructions and predictions of future change. Cold-water corals represent an attractive archive for this purpose containing a host of geochemical proxy information and they can be precisely and accurately radiometrically dated (Burke and Robinson, 2012; Chen et al., 2015; Hines et al., 2015; Rae et al., 2018; Robinson et al., 2005). For instance, corals can provide high-resolution records and be used to reconstruct annual to decadal variability of local oceanographic conditions (e.g., bamboo corals; Liu et al., in review; Sherwood et al., 2009). In this thesis, however, I focused on the oceanic variability on centennial to millennial scale. For this purpose, several individuals of cold-water corals from each site were used to reconstruct a high-precision record from the last glacial and deglacial interval.

In this thesis, I have analysed and interpreted data from cold-water corals taken from strategic locations in the North and South Atlantic to reconstruct the structure and composition of the intermediate ocean (~700 m to 2000 m) during the last glacial and deglacial intervals. These data are compared with available oceanic and atmospheric records to explore the role of the ocean in dictating

climate change. The study of the intermediate ocean has climatic, oceanographic, and biological implications. For instance, intermediate waters are responsible for part of the ventilation of the ocean interior which is an important mechanism of gases (e.g., CO_2, dissolved oxygen) and nutrients (e.g., phosphate, nitrate) input to the ocean interior. Furthermore, the formation and export of intermediate waters (e.g., Antarctic Intermediate Water, AAIW) play an active role in maintaining oceanic circulation cells, such as the Atlantic Meridional Overturning Circulation (AMOC; Came et al., 2008; Talley et al. 2011a). Thus, understanding the characteristics (e.g., temperature and carbon content) and extension of intermediate waters during climatic intervals can provide a clearer picture of the climatic system.

In addition to this climatic relevance, the composition (e.g., dissolved oxygen, nutrients, temperature) and dynamics (e.g., current strength) of the intermediate waters influence directly several organisms which inhabit the continental shelves and open-seas (e.g., seamounts, ridges) including, for example, cold-water corals, sponges, crinoids (Friewald, 2002; Ramiro-Sánchez et al., 2019). The increasing number of studies of these ecosystems has highlighted their ecological relevance (e.g., acting as refugia and nurseries for several species) for the maintenance of biodiversity including vulnerable species (Sumida et al., 2021). Therefore, the temporal reconstruction of cold-water coral occurrences can help on linking environmental parameters/conditions to marine ecology dynamics and perhaps point to potential stressors and future threats (e.g., Henry et al., 2014; Wienberg et al., 2020).

1.2 OCEAN AND CLIMATE

The importance of the ocean to the climate is mainly attributed to its capacity to transport, store and release heat, gases, and nutrients. For instance, heat transported from low to high latitudes in the North Atlantic by the Gulf Stream – a warm northward flowing current from the west north Atlantic basin to the Nordic Seas – is largely responsible for the milder winters in north-western Europe, compared with more continental regions. In addition, the large capacity of the oceans to store CO_2 is important in regulating the global carbon cycle, with different parts of the ocean acting as sources or sinks of CO_2 to the atmosphere. Thus, changes in the properties of the ocean and/or its circulation can have large impacts on climate. In this regard, much research effort has been focused on reconstructing

ocean-climate coupling. At present, instrumental data can constrain models, but proxy data are need when working with geological periods.

1.2.1 Ocean circulation

While surface ocean circulation is predominantly driven by winds, the intermediate and deep circulation is mainly driven by differential buoyancy (density) related to changes in temperature and salinity (i.e. thermohaline circulation; Talley, 2013; Weaver et al., 1999). The movement of surface, intermediate, and deep waters in the Atlantic, Indian and Pacific describes the Global Overturning Circulation (Figure 1; Rahmstorf, 2002; Talley, 2013). An important piece of this global circulation is the AMOC (Figure 1), which is characterized by warm surface water transport from low to high latitudes, where they lose their heat, increase their density, sink to depth, and flow back towards the lower latitudes. In the North Atlantic, the most intense heat loss of the surface waters to the atmosphere takes place in the Nordic and Labrador seas, where deep waters are formed by deep winter convection (Dickson and Brown, 1994). This water mass, North Atlantic Deep Water (NADW), is identified by its cold and highly saline character (Broecker and Takahashi, 1980). Compared to other deep-water masses, these waters were recently in contact with the atmosphere, therefore they are oxygen- and ^{14}C-rich. NADW also receives a contribution from the Mediterranean Overflow Water in the Northeast Atlantic before continuing to flow southward, eventually being upwelled in the Southern Ocean (de Carvalho Ferreira and Kerr, 2017). Here, three water masses are formed: Antarctic Intermediate Water , Circumpolar Deep Water (CDW) and Antarctic Bottom Water (AABW). All of these southern-sourced waters are characterized by their colder temperatures, lower salinity, and higher nutrients in comparison with NADW (Talley, 2013). Additionally, these waters contain upwelled water from depths (from the North Atlantic, Pacific and Indian oceans) giving them a ^{14}C-depleted signature, especially compared with NADW. There is mounting evidence however that the structure and strength of this AMOC were different in the past and will likely change again in the future (McManus et al., 2004; Lynch-Stieglitz et al., 2007; Ferrari, 2014; Böhm et al., 2015; Rahmstorf et al., 2015; Lippold et al., 2016). Below, we explore the major changes to this system that occurred during the last glacial and deglacial interval.

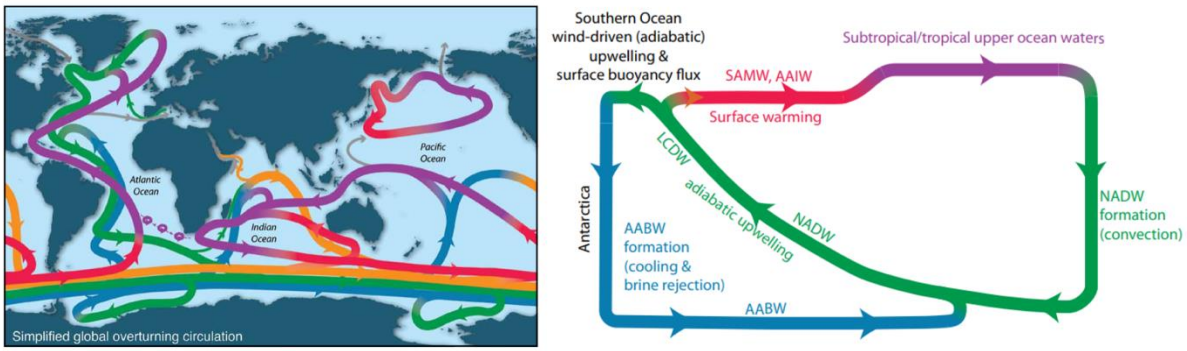

Figure 1: from Talley et al. (2013). Schematic of the global oceanic circulation (left) and simplified AMOC representation (right) highlighted the main water masses paths and formation processes. SAMW: Subantarctic Mode Water; AAIW: Antarctic Intermediate Water; NADW: North Atlantic Deep Water; LCDW: lower Circumpolar Deep Water; AABW: Antarctic Bottom Water.

1.2.2 AMOC perturbations and climate variability of the last 25,000 years

Some of the most compelling evidence implicating the ocean in global climate shifts from the last glacial to interglacial interval (last ~50 thousand years) comes from polar ice cores. Their high resolution and well-constrained chronology reveal synchronous changes in atmospheric CO_2 and Antarctica temperatures (Parrenin et al., 2013). On this timescale, the fact that the ocean can store large amounts of CO_2 (~50 times more than the atmosphere) leads to the idea of the ocean controlling the balance of the Earth's CO_2 concentrations. Furthermore, Greenland and Antarctic ice core records have revealed millennial-scale anti-phased temperature oscillations between the poles, the bipolar seesaw effect during the last deglaciation (Figure 2; Barker et al., 2009; Blunier and Brook, 2001; Marcott et al., 2014). This also points to an oceanic mechanism transporting heat between the hemispheres.

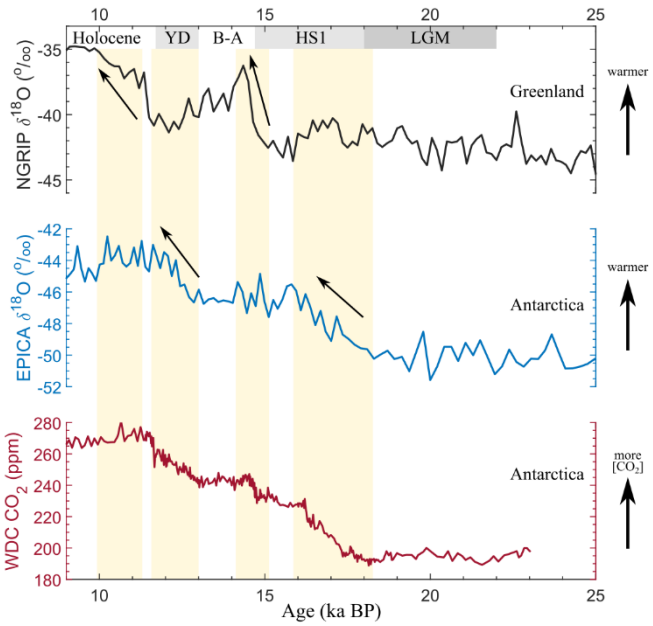

Figure 2: Atmospheric parameters from 25 ka to 9 ka. Atmospheric $\delta^{18}O$ represents temperatures of the atmosphere (higher values to the top of the figure) reconstructed from ice-cores from Greenland (black line; North Greenland Ice Core Project members, 2004) and Antarctica (blue line; Bazin et al., 2013). Atmospheric CO_2 reconstructed from West Antarctic Ice Sheet Divide ice core (WDC, red line; Marcott et al., 2014). Yellow shadings indicate intervals of atmospheric warming in Northern or Southern Hemisphere highlighting the seesaw pattern.

During the Last Glacial Maximum (LGM, 22 ka to 18 ka), atmospheric CO_2 was ~90 ppm lower and the $\Delta^{14}C$ ~400‰ higher than pre-industrial levels (Monnin et al., 2001; Reimer et al., 2020). In the ocean, several studies have suggested a more stratified Atlantic Ocean than modern (Curry and Oppo, 2005; Lynch-Stieglitz et al., 2007; Rafter et al., 2022). In agreement, it has been shown that the deep waters (>3000 m) were depleted in ^{14}C suggesting isolation of these layers from the atmosphere (Figure 3 in Skinner et al., 2017). An interesting finding was a mid-depth (~3700 m) bulge of ^{14}C observed during the LGM, which evoked a more stratified and shallower boundary between the deep and abyssal layers (Ferrari et al., 2014; Burke et al., 2015). At the same time, the intermediate layers (<1500 m) have also shown to have been more depleted in ^{14}C than the present (Adkins et al., 1998; Burke and Robinson, 2012; Chen et al., 2015; Hines et al., 2015, 2019; Robinson et al., 2005). However, the ^{14}C difference between the LGM and present of this layer is much smaller than those deeper records (Skinner and Bard, 2022). A mode of ocean circulation is suggested during the LGM through the reconstruction of seawater salinity and temperature, whereby the stratification of the ocean interior was

driven by changes in salinity rather than temperature in contrast to the thermally-driven modern circulation (Adkins et al., 2002b; Roberts et al., 2016).

The early deglaciation was marked by a gradual increase in atmospheric CO_2 parallel to warming on Antarctica (Parrenin et al., 2013). During this interval known as Heinrich Stadial 1 (HS1, 18 ka to 14.7 ka), large ice sheets that had formed in North Hemisphere during the LGM started to melt, thus decreasing high latitude surface salinity, and the formation of the NADW (Broecker et al., 1992). This process is believed to have decreased the AMOC strength (McManus et al., 2004) and its transport of heat to the Northern Hemisphere thus explaining the muted temperature change on Greenland during this interval (Barbante et al., 2006; Kindler et al., 2014). This hypothesis is supported by model results which show an intense heat accumulation in the subsurface and intermediate depths in the ocean, especially at tropical latitudes (Galbraith et al., 2016). This interval is marked by a layer of ice-rafted debris (Heinrich layers) in the North Atlantic basin due to a massive iceberg discharge (Hemming, 2004).

The subsequent deglaciation was marked by intervals of gradual increased atmospheric CO_2 in parallel with warming Antarctica temperatures that were punctuated by abrupt centennial CO_2 increases coeval with Greenland temperature shifts (Figure 2; Marcott et al., 2014). During these events, compelling evidence has supported a rapid resumption of the AMOC, and an erosion of the ^{14}C gradient between deep and intermediate layers (towards homogenized well-ventilated layers), and the outgassing of CO_2 from the deep ocean to the atmosphere (Burke and Robinson, 2012; Chen et al., 2015; Liu et al., 2009; Rae et al., 2018; Robinson et al., 2005). These findings highlight the importance of ocean circulation in driving climate change, but the processes which triggered the glacial-interglacial cycles are yet to be fully understood.

1.3 COLD-WATER CORALS

1.3.1 Characteristics and distribution

Corals are defined as "*Animals in the cnidarian classes Anthozoa and Hydrozoa that produce either calcium carbonate (aragonitic or calcitic) secretions resulting in a continuous skeleton or as numerous, usually microscopic, individual sclerites, or that have a black, horn-like, proteinaceous*

axis." (Cairns, 2007). The term cold-water corals, or deep-sea corals, used in this study refer to corals living below the photic zone, which are grouped in the azooxanthellate group because of their lack of photosymbionts. A combination of their non-dependence on light and heterotrophic feeding mechanism enables cold-water corals to live in all oceanic basins from shallow to deep depths mostly occurring from 200 m to 2000 m (e.g., Cairns, 1982; Försterra et al., 2016; Freiwald, 2002; Kitahara et al., 2010; Wienberg and Titschack, 2015). Cold-water corals are slow-growing organisms (growth rates range from 0.1 mm/yr to 3.1 mm/yr for solitary corals, and 5 to 7 mm/yr for colonial corals living below the thermocline, but higher growth rates (up to 34 mm/yr) have been reported for shallower colonial corals ; Cheng et al., 2000; Roberts et al., 2009) and can be solitary or colonial. They are found on seamounts, ridges, coral mounds, and on continental shelves and slopes (De Mol et al., 2002; Thiagarajan et al., 2013; Wienberg and Titschack, 2015; Orejas et al., 2021).

Some colonial corals are frame-building constructors and are of great importance to the maintenance of local/regional biodiversity – acting as habitats, nurseries and refugia for a large number of species (Mortensen et al., 2001; Roberts et al., 2009). Compelling studies have demonstrated that cold-water corals are threatened by traditional fishing techniques, deep sea mining, and future climate change highlighting the need for more studies exploring their life-cycle (e.g., Hebbeln et al., 2019; Kitahara, 2009; Mortensen et al., 2001; Roberts and Hirshfield, 2004). Using scleractinian solitary and colonial cold-water corals, this thesis contributes to this understanding through two approaches: (i) reconstructing the temporal and spatial coral distribution at Northeast (Chapter 2) and Southwest Atlantic (Chapter 4) and (ii) applying geochemical proxies to investigate past changes in seawater properties and their links to climate change (Chapters 3 and 4).

1.3.2 Cold-water coral geochemistry

Cold-water corals precipitate their $CaCO_3$ skeleton from an extracellular (or extracytoplasmic) calcifying fluid (ECF), which is isolated by a semi-permeable membrane. The ECF originates from seawater, but becomes enriched in Ca^{2+} through the active "pump" of a membrane-bound enzyme (CaATPase). To compensate for the input of the Ca^{2+} cations, the enzyme expels H^+, which increases the pH. This process converts HCO_3^- to CO_3^{2-}, increasing the aragonite saturation state of this

microenvironment. Furthermore, this process creates a decrease in pCO_2 and stimulates the diffusion of CO_2 into the calcifying fluid. Therefore, the high aragonite saturation state, abundant Ca^{2+} and CO_3^{2-} promote conditions for skeletal $CaCO_3$ precipitation (Cohen and McConnaughey, 2003 and references therein).

Similar to other calcifying organisms, the chemical variability of coral calcium carbonate skeletons is controlled by environmental and biological factors, the so-called "vital effects". For instance, some geochemical tracers traditionally used in foraminifera (e.g., $\delta^{13}C$ and $\delta^{18}O$) have been shown to have strong vital effects in corals indicating that internal processes rather than external (seawater) processes drive these isotopic values (Adkins et al., 2003). Additionally, intra-skeletal heterogeneity, such as the centre of calcification, exhibit different elemental/isotopic composition, for example, low $\delta^{13}C$, $\delta^{18}O$, U/Ca and high Li/Ca, Mg/Ca (Adkins et al., 2003; Robinson et al., 2006, 2014a; Case et al., 2010a). Nonetheless, some proxies have demonstrated low vital effects and good agreement with seawater measurements, such as $^{14}C/^{12}C$ ratios, uranium isotopes, Li/Mg, and neodymium isotopes (e.g., Case et al., 2010; Chen et al., 2016; Mangini et al., 1998; Robinson et al., 2004; van de Flierdt et al., 2010). The application of geochemical proxies to cold-water corals has shown a great potential to understand changes in their habitat as well as large-scale oceanic processes from centennial to glacial to deglacial time scales, which are explored in the section below.

1.3.3 Cold-water coral paleoceanography

Cold-water corals contribute to paleoceanographic reconstructions because they are distributed throughout the global ocean (Section 1.3.1). Another advantage is their applicability to accurate and precise radiometric dating methods (U-series, ^{14}C, ^{210}Pb; Robinson et al., 2014) to determine their ages and/or growth band counting. Additionally, most coral species have a lifespan of ~100 yr to 200 yr (or even a few thousand; Robinson et al., 2014), and, after they die, their skeletons can be preserved on the seafloor for hundreds of thousands of years. In some cases, one specimen can be used to reconstruct a high-resolution record, for instance analysing the growth bands of Bamboo corals (Farmer et al., 2015; Liu et al., in review.; Sherwood et al., 2009); and other paleoceanographic records can be produced using multiple individuals (Mangini et al., 1998; Schröder-Ritzrau et al., 2003; Frank et al., 2004;

Robinson, 2005; Hines et al., 2019). In this thesis, I use the latter approach, in which multiple radiometrically dated individuals collected from the same location are used to reconstruct a time series spanning the last glacial interval to the present (~50 ka). I utilize the U-series dating method to calculate the coral ages and then paired these ages with (i) ^{14}C analysis to trace potential variations in the ocean circulation and the carbon cycle and (ii) skeletal Li/Mg ratios to reconstruct the seawater temperature of the intermediate depths in the North and South Atlantic. In the sections below, a short background to these methods is provided.

1.3.4 U-series dating of cold-water corals

The high concentration of uranium in aragonitic corals (2 to 5.5 ppm) make them suitable candidates for dating using the U-series decay series (Mangini et al., 1998; Cheng et al., 2000; Edwards et al., 2003; Schröder-Ritzrau et al., 2003; Frank et al., 2004; Scholz et al., 2004; Robinson, 2005; Wefing et al., 2017; Wienberg et al., 2018a; Pratt et al., 2019). The U-series dating method is based on the disequilibrium of the decay chain of ^{238}U, where the relationship between the isotopes ^{238}U-^{234}U-^{230}Th are used. The fact that U is much more soluble than Th in seawater, provides a fractionation between these elements (Edwards et al., 2003). When corals incorporate U from seawater, their age can be calculated using the ingrowth of the ^{230}Th from the decay of ^{234}U as the system moves back to equilibrium. Modern analytical precision can resolve differences between parent to daughter ratio to ~6 half-lives, so, as the ^{230}Th has a half-life of 75,584±110 yr (Cheng et al., 2013), samples within the past ~500 ka can be measured (Cheng et al., 2000; Edwards et al., 2003).

There are two main considerations when applying the U-series dating to cold-water corals. First is consideration of initial ^{230}Th incorporated into the coral skeleton during its formation that is not from the decay of the incorporated U. Second is to assess whether the sample has been diagenetically altered after formation – i.e. has it behaved as a geochemically closed-system (no loss or gain of U or ^{230}Th post-formation). The fact that seawater [^{230}Th] increases with depth means that corals living in deeper waters will incorporate an amount of ^{230}Th that is significant, therefore the correction for initial ^{230}Th is important for cold-water corals. If this correction is not made, then the U-series measurements would result in overestimation of the age of the cold-water coral samples (Cheng et al., 2000). Unfortunately,

determining the initial ^{230}Th of the coral is not trivial. The initial [^{230}Th] of modern corals has been previously determined graphically (e.g., isochron, development diagram) by using sub-samples of a modern coral with a known age (e.g., Cheng et al., 2000; Schröder-Ritzrau et al., 2005). This method assumes that each sub-sample has same initial daughter isotopic composition (^{230}Th), similar age, and different parent-daughter ratios (^{238}U, ^{230}Th). Although it is a good and reliable approach, it also has its limitations. For instance, each sub-sample corresponds to a growth interval rather than the same age, meaning that radiogenic ^{230}Th (although small) will contribute to the total ^{230}Th of the sub-samples closer to the initiation of coral growth (Cheng et al., 2000). Additionally, the possible intraskeletal heterogeneity of ^{232}Th (used to normalize the measured ^{238}U and ^{230}Th) can also bias the values determined for the initial ^{230}Th. In this thesis, the coral age is corrected for initial [^{230}Th] using the combination of the ^{232}Th/^{238}U ratio measured in the coral together with an assumption of the seawater ^{230}Th/^{232}Th ratio. In this assumption seawater ^{230}Th/^{232}Th has activity ratio of 14.8±7.4 (the uncertainty is assumed as 50% which comprises the range of ^{230}Th/^{232}Th from intermediate open ocean waters; Robinson et al., 2004a) based on previous coral and seawater measurements (also reported as atomic ratio ^{232}Th/^{230}Th of 12500; Chen et al., 2015; Cheng et al., 2000; Robinson, 2005). This correction corresponds to the second term on the left-hand side of the equation age:

$$\left(\frac{^{230}\mathrm{Th}}{^{238}\mathrm{U}}\right)-\left(\frac{^{232}\mathrm{Th}}{^{238}\mathrm{U}}\right)\left(\frac{^{230}\mathrm{Th}}{^{232}\mathrm{Th}}\right)_{\mathrm{i}}\left(\mathrm{e}^{-\lambda_{230}\mathrm{t}}\right)=1-\mathrm{e}^{-\lambda_{230}\mathrm{t}}+\left(\frac{\delta^{234}\mathrm{U_m}}{1000}\right)\left(\frac{\lambda_{230}}{\lambda_{230}-\lambda_{234}}\right)\left(1-\mathrm{e}^{(\lambda_{234}-\lambda_{230})\mathrm{t}}\right)$$

where parenthesis refers to ratio activities, the subscripts “i” and “m” to initial and measured values, respectively, λ the decay constant of the indicated nuclide, $\delta^{234}U_m$ is the present deviation of the (^{234}U/^{238}U) ratio from secular equilibrium ($\delta^{234}U = (([^{234}U/^{238}U) - 1) \times 1000$) and “t” the age.

In this thesis, I used two methods to measure the isotopic ratios of U and Th. The first is laser ablation dating which follows the rationale and protocols of Spooner et al. (2016). The age is calculated based on the measured ^{238}U/^{230}Th ratio and the assumed value of δ^{234}U (similar to the seawater, 146±5). Additionally, no correction is made to initial ^{230}Th. This method is a valid approach as a rapid-screening dating method which requires little sample preparation, therefore it is the preferred approach when dating the samples for the first time (Spooner et al., 2016). The second method is the isotope dilution,

in which the pieces of coral skeleton pass through a rigorous (and more time-consuming) physical and chemical cleaning, and chemical separation of the U and Th fractions (e.g., column chemistry; Edwards et al., 1987; Robinson et al., 2004a; Chen et al., 2015). This method was applied to selected samples based on their U-series laser ablation ages and the time interval of interest (e.g., last glacial and deglacial interval). In both methods, the age term ("t") appears two or more times in the age equation (see equation above), therefore it needs to be calculated graphically or by iteration (Edwards et al., 2003). In this thesis, I use the Newton-Raphson iteration technique, which consists of solving the age equation starting with an initial estimate of age (e.g., 1000 yr) to produce a better "age estimate". This next estimate (t_{next}) is given by the initial estimate (t_0) minus the quotient of the age function (f(a)) and its derivative (f '(a), see formulas below). This process is repeated until the "age estimates" are invariable, so this will be defined as the coral age.

$$t_{next} = t_0 - \frac{f(a)}{f'(a)}$$

$$f(a) = 1 - e^{-\lambda_{230}t} + \left(\frac{\delta^{234}U_m}{1000}\right)\left(\frac{\lambda_{230}}{\lambda_{230} - \lambda_{234}}\right)\left(1 - e^{(\lambda_{234}-\lambda_{230})t}\right) - \left(\frac{^{230}Th}{^{238}U}\right) + \left(\frac{^{232}Th}{^{238}U}\right)\left(\frac{^{230}Th}{^{232}Th}\right)_i \left(e^{-\lambda_{230}t}\right)$$

$$f'(a) = (\lambda_{230} \cdot e^{-\lambda_{230}t}) + \left(\frac{\delta^{234}U_m}{1000}\right)\left(\frac{\lambda_{230}}{\lambda_{230} - \lambda_{234}}\right)\left((\lambda_{230} - \lambda_{234}) \cdot e^{(\lambda_{234}-\lambda_{230})t}\right) - \left(\frac{^{232}Th}{^{238}U}\right)\left(\frac{^{230}Th}{^{232}Th}\right)_i \left((\lambda_{230} \cdot e^{-\lambda_{230}t}\right)$$

To check if the coral skeleton is a closed system, the initial $\delta^{234}U_i$ (= $\delta^{234}U_m \times e^{(\lambda_{234}\, t)}$) was used. In a closed system, coral should record the $\delta^{234}U$ value of modern seawater (146.8±0.2‰; Andersen et al., 2010; Kipp et al., 2022), which has been shown not to vary more than 15‰ over the past 360 kyr (Henderson, 2002; Edwards et al., 2003). In this thesis, I used this approach as a screening criterion for diagenesis in corals. However, when a systematic change of $\delta^{234}U_i$ was observed, for instance lower $\delta^{234}U_i$ during the last glaciation, the samples were not necessarily interpreted as altered. In agreement with this latter approach, smaller magnitude changes in seawater $\delta^{234}U$ (e.g., ~7‰) have been proposed during glacial to interglacial time scales in response of changes in continental weathering (Robinson et al., 2004b; Esat and Yokoyama, 2006; Chen et al., 2016; Chutcharavan et al., 2018). The results of these studies indicate lower $\delta^{234}U_i$ (by ~7‰ to 4‰ from the modern seawater) during the last glaciation and an increase towards modern-like values during the last deglaciation. The evoked mechanisms are related

with increased ^{234}U input to the sea. The deglacial increase in continental weathering, rainfall, sea level and ice-sheet melting likely played a role in changing the seawater $\delta^{234}U$ by adding ^{234}U-enriched waters into the sea (Robinson et al., 2004b; Esat and Yokoyama, 2006; Chen et al., 2016; Chutcharavan et al., 2018).

U-series dating in cold-water corals has been widely used as it offers a precise and accurate method to calculate ages. Several studies have used the coral ages to investigate the temporal distribution of coral populations, as well as to calculate coral mounds aggradation rates (e.g., Frank et al., 2011; McCulloch et al., 2010; Raddatz et al., 2020; Schröder-Ritzrau et al., 2005; Wienberg et al., 2020, 2018). These studies have contributed to the understanding of environmental and climatic conditions associated with the success and demise of corals. It is noteworthy that some studies have used ^{14}C dating with similar aims, which also produced important insights for similar questions (e.g., Burke et al., 2010; Margolin et al., 2014; Thiagarajan et al., 2013; Titschack et al., 2015). In Chapter 2, I used the U-ages of a suite of fossil corals from the Northeast Atlantic to investigate the temporal distribution of corals and the associated environmental impacts over the past 150 ka. It was observed a northwards shift in coral occurrence in response to the change from glacial to interglacial conditions. The changing spatial pattern is linked with food supply and dissolved oxygen controlled by oceanic dynamics (e.g., currents, fronts, upwelling).

1.3.5 ^{14}C of cold-water corals as a proxy for ocean circulation

Radiocarbon (^{14}C) is formed in the atmosphere as the result of the interaction between neutrons and nitrogen atoms (^{14}N) induced by cosmic rays. The "bombarded" ^{14}N atoms capture a neutron and expel a proton forming the ^{14}C atom, which combines with oxygen to form $^{14}CO_2$ and enters the surface ocean through sea-air mixing (Broecker, 2014; Skinner and Bard, 2022). Once surface waters sink to the ocean interior, inorganic ^{14}C is transported to deeper layers mainly through water masses mixing. There, the ^{14}C will decay to ^{14}N according to its half-life of 5730±40 yr (Godwin, 1962). in this way, the ^{14}C signature of a water mass will depend on the time elapsed from its last contact with the atmosphere, and on the mixing with adjacent waters (which may have different ^{14}C signatures). Thus, ^{14}C provides a way to trace oceanic circulation and/or mixing changes (see review by Skinner and Bard,

2022). The modern distribution of ^{14}C in the ocean illustrates the applicability of ^{14}C to trace ocean circulation (Figure 3). For instance, in the North Atlantic, deep waters are directly formed from the sinking of surface waters and, thus, are ^{14}C-rich (Figure 3). On the other hand, deep waters formed in the Southern Ocean have large contributions of "old" waters (e.g., from the Pacific Ocean) and are thus ^{14}C-depleted (Figure 3).

Cold-water corals have been shown to record seawater ^{14}C signatures and have been used in several studies to reconstruct seawater ^{14}C variability and circulation through time (Mangini et al., 1998; Schröder-Ritzrau et al., 2003; Frank et al., 2004; Robinson, 2005; Eltgroth et al., 2006; Li et al., 2020). By convention, the ^{14}C of the sample is reported as a fraction of the modern (Fm) defined by the ratio between the $\delta^{13}C$-normalized ($\delta^{13}C = -25‰$) ^{14}C of the sample relative to the $\delta^{13}C$-normalized ($\delta^{13}C = -19‰$) ^{14}C of an oxalic standard. Here, the "modern" means the year of 1950 (or year "0 BP" (Stuiver and Polach, 1977; Adkins et al., 2002a). The ^{14}C age is then calculated by applying the Libby mean life (8033, half-life of 5568 yr) to this "fraction modern" following the equation:

$$^{14}C\ age = -8033 \times \ln(Fm)$$

The modern and paleo cold-water coral ^{14}C data are presented in delta notation which represents the age-corrected ^{14}C ($\Delta^{14}C$; Adkins and Boyle, 1997; Chen et al., 2015). This correction is necessary to account for the radioactive decay of ^{14}C between the measurement date (^{14}C age) and the time the sample formed (in this study the coral's U-series age). So, the seawater $\Delta^{14}C$ can be reconstructed using the following the equation:

$$\Delta^{14}C = \left(\frac{e^{-\,^{14}C\ age/8033}}{e^{-\,Useries\ age/8267}} - 1 \right) \times 1000$$

Even though the $\Delta^{14}C$ is a useful parameter to compare coral data with the atmosphere, it is affected by changes in the atmospheric ^{14}C decay inventory (Reimer et al., 2020). To account for this varying atmospheric radiocarbon inventory, we use the B-atmosphere term (B-atm), which is the difference between the ^{14}C age of the ocean (R_{coral}) and the contemporary ^{14}C age of the atmosphere (R_{atm}):

$$B\text{-}atm = R_{coral} - R_{atm}$$

This parameter is an effective way to investigate changes related to oceanic processes because it represents the direct age offset between seawater and the contemporaneous atmosphere. Great effort has gone into reconstructing the atmospheric radiocarbon composition by compiling data from tree rings, plant macrofossils, speleothems, surface corals and foraminifera (Reimer et al., 2020, 2013 and studies therein). This calibration serves as a basis for several studies focusing on the carbon cycle using ^{14}C as a tracer of CO_2 from different reservoirs. Amongst them, speleothem-based ^{14}C has revealed intervals of highly elevated $\Delta^{14}C$ correlated with weakening of Earth's magnetic field, and suggestions of oceanic-driven variations during the last deglaciation (e.g., Beck et al., 2001; Cheng et al., 2018; Southon et al., 2012). In the ocean, ^{14}C has shown a tight correlation with atmospheric CO_2, revealing intervals of carbon storage in the deep ocean (Adkins and Boyle, 1997; Barker et al., 2010; Skinner et al., 2010, 2017), and short-lived events of CO_2 rise and ^{14}C decrease indicating pulses of intense oceanic mixing (Burke and Robinson, 2012; Chen et al., 2015; Freeman et al., 2015; Hines et al., 2015; Thiagarajan et al., 2014). In Chapters 3 and 4, I use the $\Delta^{14}C$ of corals and compare these data with the contemporary atmosphere.

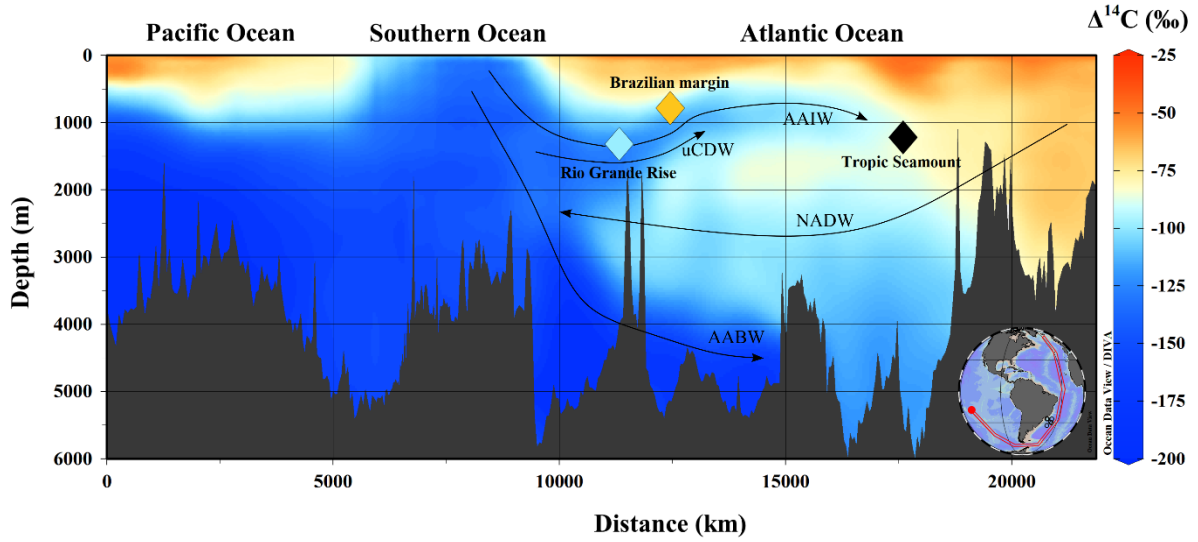

Figure 3: Modern bomb-corrected $\Delta^{14}C$ distribution in the Pacific (left), Southern (middle) and Atlantic (right) oceans. Dark blue indicates ^{14}C-depleted waters (e.g., deep Pacific, Southern Ocean and deep Atlantic) and red indicates ^{14}C-rich waters (surface and thermocline waters, and North Atlantic). Diamonds indicate the locations of the cold-water corals presented in this thesis: Tropic Seamount, Chapters 2 and 3), Brazilian margin and Rio Grande Rise (Chapter 4).

1.3.6 Seawater temperatures reconstruction using Li/Mg ratios of cold-water corals

Trace elements Li and Mg are incorporated into a coral's ECF from seawater and precipitated by substitution into the aragonite lattice (Sinclair and Risk, 2006; Case et al., 2010). Similarly low partition coefficients mean that Li and Mg are similarly discriminated against during the precipitation of aragonite and therefore have similar responses to growth induced effects such as Rayleigh fractionation, kinetic effects, and growth entrapment (Case et al., 2010). However, the incorporation of these elements into biogenic carbonates have opposing dependencies with temperature (Mg increases while Li decreases), thus ratioing Li/Mg produces a highly sensitive temperature proxy where growth induced effects have been largely cancelled (Montagna et al., 2014). Case et al. (2010) were the first to show strong correlation between the Li/Mg of cold-water corals and temperature, that was independent of salinity and carbonate ion concentration, supporting the robustness of Li/Mg as a temperature proxy. Subsequent studies on corals and aragonitic foraminifera also support a strong correlation between the Li/Mg and seawater temperature (Bryan and Marchitto, 2008; Case et al., 2010; Hathorne et al., 2013; Raddatz et al., 2013; Marchitto et al., 2018; Cuny-Guirriec et al., 2019; Stewart et al., 2020). The most recent study by Stewart et al. (2020) incorporated more data from cold-water corals including corals of the family Stylasteridae, and proposed a universal calibration for all aragonitic organisms (Figure 4) following the equation:

$$Li/Mg = 5.42\ e^{-(0.05\times T)}$$

where Li/Mg corresponds to the ratio measured in the aragonitic organism and T to the seawater temperature (°C). The strong correlation between the Li/Mg ratios and seawater temperature and the limited impact of growth induced "vital effects" point to the great potential of the Li/Mg paleothermometer in biogenic carbonates. For example, this proxy was applied to aragonitic benthic foraminifera from the Florida Straits revealing cold intermediate waters during the LGM and large variability during the last deglaciation in association with AMOC strength (Valley et al., 2019). In this thesis, the Li/Mg of cold-water corals are used to reconstruct the temperature of intermediate waters in the Northeast Atlantic (Chapter 3) and Southwest Atlantic (chapter 4) over the past 50 ka. Together

with ^{14}C data measured in the same corals, the responses of oceanic circulation during climatic perturbations are explored.

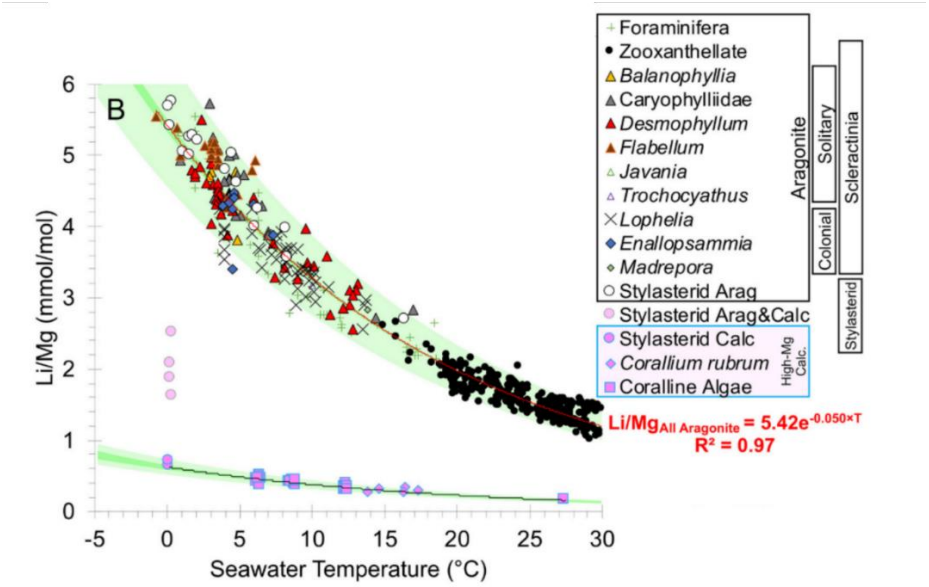

Figure 4: from Stewart et al. (2020). Calibration curve of Li/Mg and temperature from a compilation of aragonitic organisms (cold-water corals, surface corals and foraminifera).

1.4 OBJECTIVES

The overall aim of this thesis is to investigate the link between the ocean and the climate. As stated in the sections above, the intermediate ocean is an important piece of the climatic system, connecting the atmosphere with the ocean interior (and vice versa), and impacting the oceanic circulation. Additionally, climate-driven perturbations in the ocean can impact a large number of organisms inhabiting the intermediate depths. Therefore, the specific objectives of this thesis were:

- investigate the impact of the climate variability of the past 150 kyr on the spatial distribution of cold-water corals in the Northeast Atlantic focusing on coral populations from open-ocean sites, and including colonial and solitary species;
- reconstruct the ^{14}C and temperature of seawater during the past 35 kyr on the Tropic Seamount (Northeast Atlantic) to investigate the impacts of AMOC perturbations in the regional intermediate waters;
- reconstruct the temperature record in the intermediate South Atlantic and explore possible mechanisms for its variability during the last glacial to interglacial interval.

1.5 THESIS STRUCTURE

In this thesis, I generate new cold-water coral ages of the Northeast and South Atlantic. The coral ages are combined with published data to investigate the temporal distribution of coral from both the North and South Atlantic. I use paired U-series ages and ^{14}C data to investigate oceanographic changes of Atlantic intermediate waters during the last glacial, deglacial and interglacial intervals. I reconstruct past seawater temperature using the Li/Mg proxy to investigate the thermal response of the ocean during intervals of oceanic circulation change. This thesis is divided into four subsequent chapters.

Chapter 2 contains the temporal distribution of cold-water corals in the Northeast Atlantic over the past 150 ka. I add ~600 new U-series ages of cold-water corals to a compilation of ~700 previously published coral ages. The study highlights a striking similarity between the temporal distribution of the coral population from the open-ocean and continental margin sites, and both solitary and colonial corals, showing that that broad environmental parameters controlled by climate impact the coral distribution in the Northeast Atlantic. This chapter was recently published in "Deep-sea Research Part I".

Chapter 3 presents seawater ^{14}C and temperature from the past 35 ka at Tropic Seamount (Northeast Atlantic). The results suggest that both parameters respond to periods of AMOC perturbation. The comparison between the temperatures of intermediate waters at Tropic Seamount and deep North and South Atlantic during the LGM support a glacial ocean stratification not controlled by temperature. Furthermore, the ^{14}C data during the LGM and HS1 indicate large contributions of AAIW in the Northeast Atlantic, which likely played a role in the deglacial warming observed during the HS1.

In Chapter 4, I present U-series dated corals from two sites in the Southwest Atlantic: Rio Grande Rise and Brazilian margin. These data are used to explore the distribution of cold-water corals in the Southwest Atlantic over the past 270 ka. Additionally, the first reconstruction of seawater ^{14}C and temperature of an open-ocean site in the Southwest Atlantic across the last glacial to interglacial interval are presented. We compared these with new and published data from the continental margin and the Southern Ocean, which suggested a persistent connection with the atmosphere, and rapid transport of climate anomalies to our site.

Chapter 5 summarizes the main findings discussed in this thesis and elaborates on future perspectives.

Chapter 2: SPATIAL AND TEMPORAL DISTRIBUTION OF COLD-WATER CORALS IN THE NORTHEAST ATLANTIC OCEAN OVER THE LAST 150 THOUSAND YEARS

Abstract

Scleractinian cold-water corals are found across the Northeast Atlantic, providing structure for important habitats that support high biodiversity. Climate-driven perturbations on parameters such as carbonate chemistry, oxygen, bottom currents, productivity and temperature have the potential to impact the abundance and diversity of these cold-water coral communities. One way to explore the linkage between corals and climate is to examine historic coral distributions during times of past climate change. Previous coral dating efforts in the Northeast Atlantic (n ~ 700) have focused on reef-forming colonial coral communities from shelf and slope areas. However, there are far fewer data from open-ocean settings or from solitary coral species, thus precluding assessment of basin-wide controls on coral occurrence. Here, we contribute >600 new U-series ages for both solitary and colonial coral species from open-ocean sites including the Reykjanes Ridge and seamounts in the mid and low latitudes to map the changing distribution of Northeast Atlantic cold-water corals over the last 150,000 years. The temporal occurrences of solitary and colonial corals from our offshore sites are broadly similar to the distributions along the nearer-shore sites at the same latitudes. In the cold-temperate and high-latitude Northeast Atlantic, corals are most abundant during warm climate intervals, with the Reykjanes Ridge (60°N) representing the northernmost limit of corals in the Northeast Atlantic during Marine Isotope Stage (MIS) 5, MIS 3 and Bølling-Allerød. This biogeographical distribution expanded northwards to the Norwegian margin at the onset of the Holocene when the ice sheets retreated and modern-like oceanographic conditions were established. We interpret the abundance of corals at these northerly sites to be linked with increased food supply and favourable hydrological conditions. By contrast, coral sites south of 45°N are characterised by glacial and deglacial occurrences, with a marked decline during the Holocene. This distribution is also linked to food supply, potentially driven by shifts in dust fertilization and upwelling, in addition to changes in dissolved oxygen concentration and temperature. Together, these findings emphasize the links between climate, oceanic processes, and cold-water coral distribution, pointing to low food supply and low oxygen concentration as limiting factors for cold-water coral populations. Both parameters are changing in the modern ocean, with implications for future coral communities.

Contributions

This chapter was published in Deep-Sea Research Part I in October 2022 (https://doi.org/10.1016/j.dsr.2022.103892). Co-authors on the paper were Prof Laura F. Robinson (University of Bristol), Dr Joseph A. Stewart (University of Bristol), Dr Tao Li (Nanjing University), Dr Tianyu Chen (Nanjing University), Dr Andrea Burke (University of St Andrews), Dr Marcelo Kitahara (University of Sao Paulo, Brazil), Prof Nicholas J. White (University of Cambridge). In this paper we presented the discussion of ~690 new cold-water coral U-series ages from Equatorial Atlantic, Reykjanes Ridge (off Iceland) and Tropic Seamount (Northeast Atlantic). I dated the samples from the Tropic Seamount (~60 ages) with the help of Tao Li and Joseph Stewart. The age calculation were done by me using a Matlab script written by Tianyu Chen (Nanjing University, former post-doc researcher in the University of Bristol). Tao Li and Tianyu Chen dated the samples from the Equatorial Atlantic (~450 ages), and Andrea Burke dated the samples from Reykjanes Ridge (~180 ages). In addition, I compiled ~700 published cold-water coral ages. I interpreted the data and wrote the manuscript with comments from the co-authors. During the peer-review process, Dr Sophia Hines and two anonymous reviewers provided constructive comments which were incorporated into the final version of the paper. The table of the new coral ages are in the Appendix I, as well as published in the Pangaea database (https://doi.pangaea.de/10.1594/PANGAEA.945280). The coral age compilation is in the Pangaea database only. Supplementary figures S1 to S6 are in the Appendix I.

2.1 INTRODUCTION

Ecosystem interactions with the climate system are a complex topic of much interest in the scientific literature (Blois et al., 2013; Canadell et al., 2021). Marine life is influenced by climate change, for example by habitat gain or loss (Henry et al., 2014), but marine species can also contribute to the modulation of climate via their role in carbon cycling (e.g., Sigman and Hain, 2012). With rising atmospheric CO_2 the ocean is warming, whilst seawater pH and saturation state are reducing (Canadell et al., 2021), triggering changes to the food web, for instance decreasing primary production in the North Atlantic (Capuzzo et al., 2018). These changes have stimulated research into the effects of rapid climate change on marine fauna (e.g., Miller et al., 2011). One way to investigate the interactions between ecosystems and the marine environment is to look back in the past (Hebbeln et al., 2019), comparing well-dated coral samples with paleoclimate records from intervals of climate change (Thiagarajan et al., 2013; Stewart et al., 2021).

Cold-water corals are keystone taxa that can form structural habitats for diverse and abundant marine fauna (Roberts et al., 2006). In addition, their carbonate skeletons can be dated using radiometric techniques, and the ages can then be used to reconstruct the timing of coral mound formation and changing coral population distributions over tens of thousands of years (Eisele et al., 2008; Mienis et al., 2009; Wienberg et al., 2009; Douarin et al., 2013; Thiagarajan et al., 2013; Margolin et al., 2014; Titschack et al., 2015; Victorero et al., 2016). There are about 700 published ages for corals from the Northeast Atlantic, primarily from colonial species sampled on continental shelves and slopes (Table 1). These data have shown that the spatial and temporal distribution of cold-water coral communities changed with timings aligned with major global climate change events (Frank et al., 2011; Schröder-Ritzrau et al., 2005). For example, during glacial and deglacial intervals corals thrived in tropical and warm-temperate latitudes of the Northeast Atlantic (Schröder-Ritzrau et al., 2005; Eisele et al., 2011; Frank et al., 2011; Wienberg et al., 2018), but these communities decreased in abundance at the onset of the Holocene. By contrast, the opposite behaviour has been detected in northerly regions (>45°N) such as the colder and more productive Celtic and Nordics Seas where prolific cold-water coral reefs were established or re-colonised at the onset of the Holocene (Dorschel et al., 2007; Eisele et al., 2008;

Frank et al., 2009, 2011; Van der Land et al., 2010; Wienberg et al., 2020; Bonneau et al., 2018; De Mol et al., 2011; Dorschel et al., 2005; Douarin et al., 2013; López Correa et al., 2012; Mienis et al., 2009; Raddatz et al., 2016; Victorero et al., 2016). With growing evidence for climate-induced latitudinal displacement of cold-water coral populations in the Northeast Atlantic over the last 150,000 years (Schröder-Ritzrau et al., 2005; Frank et al., 2009; Wienberg et al., 2010; Frank et al., 2011) it is important to consider the impact of ongoing changing environmental conditions on coral and coral associated communities.

Scleractinian cold-water corals are suspension-feeders that rely on food supply from particulate organic matter either falling from surface water primary production or brought in by the hydrodynamic action of bottom currents (Roberts et al., 2006; Davies and Guinotte, 2011; Mohn et al., 2014; Morato et al., 2020). As a result, modern framework-forming cold-water coral distributions occur preferentially within high productivity and high energy areas (Freiwald, 2002; Mohn et al., 2014). Other factors important to coral health may include dissolved oxygen concentration (Dodds et al., 2007; Thiagarajan et al., 2013; Stewart et al., 2021), carbonate saturation state (Guinotte et al., 2006; Thiagarajan et al., 2013), and seawater density gradients (associated with temperature and salinity characteristics of water masses; De Mol et al., 2011; Dullo et al., 2008; Flögel et al., 2014). Bottom currents can also play a role in the dispersal of coral larvae (Henry et al., 2014). Complicating the picture, recent findings raise questions about the limiting environmental conditions that cold-water corals can withstand. Unexpectedly, thriving cold-water reefs have been found under hypoxic and warm conditions off the Angola margin (Southeast Atlantic; Hanz et al., 2019; Hebbeln et al., 2020; Orejas et al., 2021). There, coral success has been linked to the high abundance and quality of organic matter as a food source (Hanz et al., 2019).

A combination of factors is needed to explain coral population distributions – both today and in the past. For example, the success of coral communities in the southern Gulf of Cádiz is thought to be related to productivity, which in turn is driven by a combination of enhanced dust input and frontal upwelling (Foubert et al., 2008; Wienberg et al., 2009, 2010). In the Holocene a frontal zone shift and an increase in seawater temperature have been linked to the subsequent demise of the coral population (Wienberg et al., 2010). The development of coral mounds along the Mauritanian margin during the

last glacial and deglacial has also been linked to increased surface ocean productivity (Eisele et al., 2011). However, dissolved oxygen and temperature may also have been important factors. For instance modern corals are only found inhabiting canyons off Mauritania, where cascading events are thought to episodically deliver food and well-oxygenated waters from the surface to the deep (Wienberg et al., 2018).

Thus far, most data from the Northeast Atlantic come from reef-forming cold-water corals along the continental margin. The few ages from seamounts in the open-ocean and/or from solitary corals are generally in line with the timing of observations from shelf areas, suggesting that there could be a common controlling mechanism across the basin (Schröder-Ritzrau et al., 2003, 2005; Wienberg et al., 2009, 2010; Frank et al., 2011). However, the limited data from these open-ocean sites or from solitary species prevent us from determining whether nearshore mound forming communities are being controlled by local (e.g., coastal upwelling and local productivity change) or basin-wide processes that would dictate scleractinian cold-water coral occurrence regardless of species or habitat type.

Here we present 616 new ages obtained from solitary and colonial scleractinian cold-water corals from open-ocean habitats including volcanic ridges and seamounts in the Northeast Atlantic. These sites provide a direct contrast to the majority of existing data from the region. Our new coral ages, combined with ~700 existing published data from the Norway shelf to the Mauritanian margin, represent the most up to date temporal distribution of cold-water corals from the Northeast Atlantic. We use this combined dataset to test whether productivity (food supply) is the major control on cold-water corals, including an assessment of basin-wide patterns and potential differences between the continental margin and open ocean settings, and solitary and reef forming species over the last 150 thousand years.

Table 1: List of references used for the cold-water coral compilation from Northeast Atlantic Ocean coral sites. Reference numbers correspond to locations in Figure 1.

Regions	Latitude range (°N)	Ref. number	References	Location
Norwegian shelf	70°49`N to 59°N	1	Raddatz et al. (2016)	Lopphavet, Oslofjord and Sula Reef
		2	López Correa et al. (2012)	Trænadjupet and Stjernsund
		3	Schröder-Ritzrau et al. (2005)	Kosterfjord and Sula Reef
		20	Frank et al. (2011)	Trænadjupet
		24	Titschack et al. (2015)	Stjernsund, Træna and Røst Reef

		30	Lindberg & Mienert (2006)	Fugløy Reef
Northern Northeast Atlantic	62°56'N to 42°47'N	4	Douarin et al. (2013)	Scottish margin
		5	Frank et al. (2004)	Rockall Trough
		6	Frank et al. (2009)	Porcupine Seabight
		20	Frank et al. (2011)	Porcupine Seabight
		7	Dorschel et al. (2007)	Porcupine Seabight
		8	de Mol et al. (2011)	Bay of Biscay
		9	Schröder-Ritzrau et al. (2003)	Rockall Trough
		3	Schröder-Ritzrau et al. (2005)	Bay of Biscay Faroe Island Porcupine Seabight
		22	van der Land et al. (2010)	Rockall Trough
		23	van der Land et al. (2014)	Porcupine Seabight
		25	Bonneau et al. (2018)	Rockall Trough
		26	Victorero et al. (2016)	Rockall Trough
		27	Wienberg et al. (2020)	Porcupine Seabight
		28	Eisele et al. (2008)	Porcupine Seabight
		29	Mienis et al. (2009)	Rockall Trough
mid-North Atlantic	42°N to 33°12'N	10	Adkins et al. (1998)	mid-North Atlantic
		11	Eltgroth et al. (2006)	mid-North Atlantic
		9	Schröder-Ritzrau et al. (2003)	Azores
Gulf of Cádiz	36°11'N to 35°N	12	Wienberg et al. (2009)	Gulf of Cádiz
		13	Wienberg et al. (2010)	Gulf of Cádiz
		9	Schröder-Ritzrau et al. (2003)	Gulf of Cádiz
		3	Schröder-Ritzrau et al. (2005)	Gulf of Cádiz
		20	Frank et al. (2011)	Gulf of Cádiz
		21	Dubois-Dauphin et al. (2016)	Gulf of Cádiz
Temperate seamounts	36°58'N to 29°49'N	9	Schröder-Ritzrau et al. (2003)	Lars Seamount Conception Seamount
		3	Schröder-Ritzrau et al. (2005)	Galicia Bank Conception Seamount Lars Seamount Ampère Seamount Last Minute Seamount Josephine Seamount Lion Seamount Annika Seamount Unicorn Seamount Filho do Funchal
Mauritania margin	20°15'N to 17°29'N	14	Wienberg et al. (2018)	off Mauritania
		15	Eisele et al. (2011)	off Mauritania
Northeast Equatorial Atlantic	9°13'N to 2°19'N	16	Mangini et al. (1998)	Equatorial Atlantic
		17	Chen et al. (2015)	Equatorial Atlantic
		18	Chen et al. (2016)	Equatorial Atlantic
		19	Chen et al. (2020)	Equatorial Atlantic

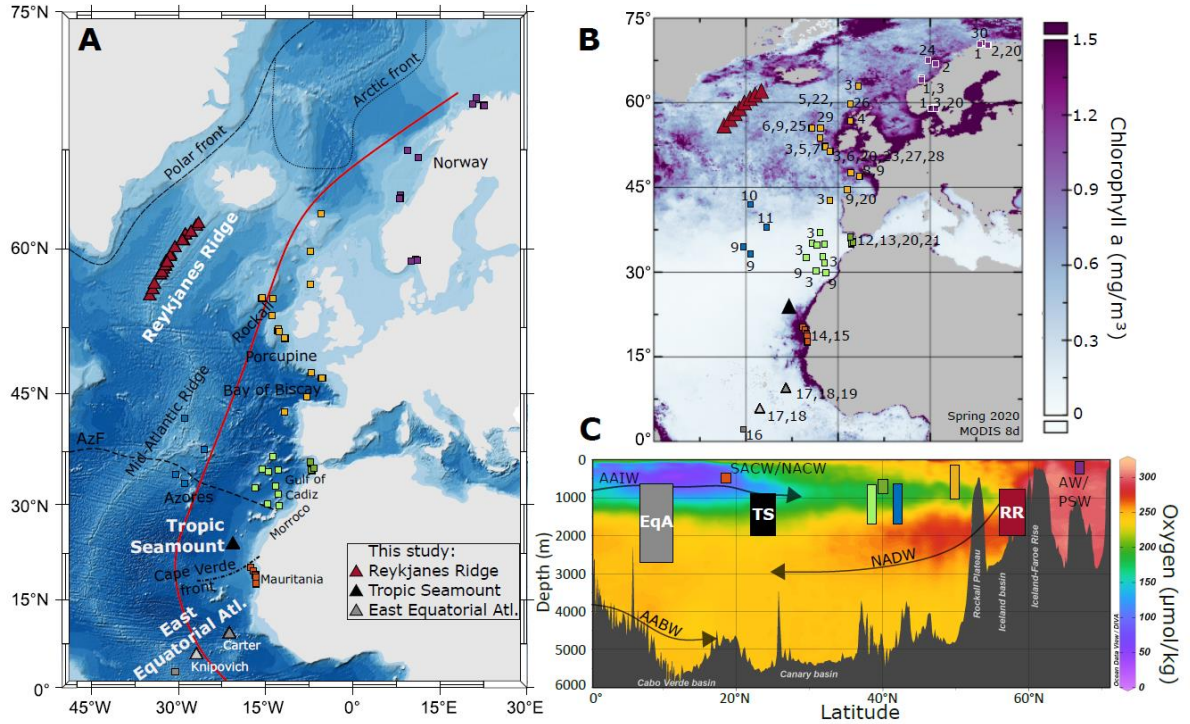

Figure 1: Locations of available cold-water corals discussed in the text, and oceanic parameters. (A) Cold-water coral records presented in main discussion. Published (squares) and new records (triangles) from Tropic Seamount (black), East Equatorial Atlantic (grey) and Reykjanes Ridge (red). Regions are grouped by colour (purple to Norwegian shelf, yellow to northern Northeast Atlantic, blue for mid-North Atlantic, dark green for Gulf of Cádiz, light green for temperate seamounts, and orange for Mauritania margin, see Table 1 for details). Dashed lines indicate modern position of Polar and Arctic fronts (Eynaud et al., 2009). Red line indicates profile section illustrated in Panel C. (B) Chlorophyll-a concentration map (from MODIS Aqua 8-daily resolution, period of March to June 2020 at https://giovanni.gsfc.nasa.gov; Panoply). Numbers correlate to the references used for cold-water coral compilation listed in Table 1. (C) Dissolved oxygen profile (Olsen et al., 2020; GLODAP) depth distribution of corals from each region (indicated by same colour as map) and position of main water masses. AAIW, Antarctic Intermediate Water; AABW, Antarctic Bottom Water; SACW/NACW, South and North Central Water; NADW, North Atlantic Deep Water; AW, Atlantic Water; PSW, Polar Surface Water.

2.2 SITE DESCRIPTIONS

The new U-series ages obtained from scleractinian cold-water corals come from three locations: the Reykjanes Ridge (57°N to 61°N, 28°W to 33°W); the Tropic Seamount (23°55'N, 20°45'W); and the East Equatorial Atlantic from Carter (9°N, 21°W) and Knipovich seamounts (5°N, 27°W; Figure 1, Table 2). Fossil and living corals from Reykjanes Ridge were collected from 35 dredge sites along the axis and western flank of this part of the Mid-Atlantic Ridge. The presence of modern cold-water corals at Reykjanes Ridge has been previously documented, with high species richness but smaller colonies compared to higher latitude shelf areas (Mortensen et al., 2008). Corals from Tropic Seamount

(extending from 4100 m to its summit around 1000 m) were collected by ROV *Isis* from the seamount top and the upper part of the flanks (down to 1800 m; Murton, 2016). The known modern coral population consists of solitary corals (e.g., *Javania cailleti* presented in this study) and small colonies of *Solenosmilia variabilis,* which have a patchy distribution along ledges. Rich coral gardens mostly consisting of octocorals are found at the eastern and western sites of the seamount (Murton, 2016; Ramiro-Sánchez et al., 2019). The corals from the Equatorial Atlantic seamounts were also collected by ROV *Isis* (Robinson, 2014; Chen et al., 2015, 2016, 2020) during 16 dives at five sites, however only data from seamounts in the Northeast Atlantic are presented in this study (Carter and Knipovich; some authors refer to Carter Seamount as Annan Seamount (e.g., Victorero et al., 2018)). On these seamounts, the modern occurrences of scleractinian corals are patchy, with dense octocoral gardens and *Enallopsammia* sp. observed, particularly on the southern edge of Carter Seamount (Victorero et al., 2018).

Table 2: Site, sampling, and taxa information of cold-water coral sites presented in this study. Depth of Reykjanes Ridge samples corresponds to the mean depth of dredge on and off bottom. Taxa corresponds to all identified species. *One sample collected at 265 m.**One sample collected at 2814 m.

Location	**Lat. (°N)**	**Lon. (°W)**	**Depth (m)**	**Cruise**	**Year**	**Sampling method**	**Taxa**
Reykjanes Ridge (125 ages)	57 to 61	28 to 33	768 to 2022	CE08-06	2008	dredge	*Madrepora* sp. *Desmophyllum pertusum* *Solenosmilia* sp. *Desmophyllum dianthus* *Caryophyllia* sp. *Flabellum* sp.
Tropic Seamount (36 ages)	23°55’	20°45’	970 to 1797	JC142	2016	ROV	*Desmophyllum dianthus* *Solenosmilia variabilis* *Caryophyllia* sp. *Javania caelleti* *Madrepora oculata*
Carter Seamount - East Equatorial Atlantic (308 ages)	9	21	639* to 2160	JC094	2013	ROV	*Caryophyllia* sp. *Desmophyllum dianthus* *Enallopsammia* sp. *Javania* sp. *Madrepora* sp. *Polymyces* sp. *Dasmosmillia* sp.
Knipovich Seamount - East Equatorial Atlantic (132 ages)	5	26	749 to 2599**	JC094	2013	ROV	*Caryophyllia* sp. *Desmophyllum dianthus* *Enallopsammia* sp. *Javania* sp.

2.2.1 Oceanographic settings

2.2.1.1 Reykjanes Ridge

The bathymetry of the Reykjanes Ridge controls the modern position of the Sub-Arctic Front, corresponding to the maximum extent of winter drift sea-ice (Moros et al., 2012). This front marks the interaction between the warm, saline waters of the poleward flowing North Atlantic Current (NAC), and the cold and relatively fresh polar waters flowing southward along the Greenland margin. The intermediate waters mostly consist of Labrador Sea Water (Rhein et al., 2002), and a smaller contribution of Subpolar Mode Water that includes recirculated central waters transported by the NAC and modified by sea-ice interaction to a cold, fresh and nutrient-rich water (García-Ibáñez et al., 2015). The deeper layers include denser, oxygen-rich overflow waters from the Nordic Seas (Iceland-Scotland Overflow Water and Denmark Strait Overflow Water; de Carvalho Ferreira and Kerr, 2017). The corals in this study are from the intermediate and deep layers within the influence of these northern-sourced water masses (Figure 1).

2.2.1.2 Tropic Seamount and East Equatorial Atlantic Sites

Tropic Seamount is situated in the southern Canary Island Seamount Province around 500 km from the Northwest African coast which is a highly-productive upwelling region (Romero et al., 2008). The eutrophic upwelled waters are exported offshore as upwelling filaments and eddies as far as Tropic Seamount (Hernández-Guerra et al., 2005; Figure 1). Additionally, subsurface particle-rich layers (enriched in organic matter) extend as far as 600 km offshore from the African shelf between 400 m and 800 m depth (Karakaş et al., 2006), potentially acting as a food source for corals.

The sites within the east Equatorial Atlantic are within the zonal Equatorial Current system, the modern position of the Intertropical Convergence Zone and the African dust plume (Figure S1). Dust and nutrient-rich upwelling waters fertilize the surface ocean, stimulating primary productivity (Zarriess and Mackensen, 2010). Dust dispersion is controlled by the trade winds and continental aridity, on seasonal as well as millennial-scales.

The upper water column of these low latitude sites comprises warm surface (0 to 50 m) and thermocline (<700 m) waters, which include North Atlantic Central Water and South Atlantic Central

Water (Pastor et al., 2015). The modern oxygen minimum zone lies between 600 m and 1000 m within the boundary between the thermocline waters and Antarctic Intermediate Water (AAIW). AAIW is recognized by its low salinity and high dissolved silicate sourced from the Southern Ocean (Pastor et al., 2015; de Carvalho Ferreira and Kerr, 2017). Deeper layers (>1500 m) predominantly consist of North Atlantic Deep Water (NADW). In the context of the modern hydrography, the cold-water corals from both sites are within AAIW (approx. 600 m to 1500 m) and NADW.

2.3 DATING METHODS

Two U-series methods were applied to date the new samples. U-series laser ablation dating was used to provide a rapid determination of coral age (Spooner et al., 2016). Other samples were dated by more accurate and precise U-series isotope-dilution (per-mil versus per-cent level for the laser ablation dating; Cheng et al., 2000; Spooner et al., 2016).

The samples dated by U-series laser ablation were cut and polished before ablation using a Photon Machines Analyte G2 193 nm laser. The ^{230}Th and ^{238}U isotopes were measured simultaneously using a Neptune Multi-Collector Inductivity Coupled Plasma Mass Spectrometer (MC-ICP-MS) on a central ion counter and a Faraday cup respectively (Spooner et al., 2016). Final ages were calculated using the measured ^{230}Th/^{238}U ratios, and the assumption that there has been no open-system behaviour and that its initial ^{230}Th is negligible (Spooner et al., 2016). The age was calculated by the Newton-Raphson iteration method, using the (^{230}Th/^{238}U) of the sample corrected for background (laser cell gas blank) and scaled to an in-house inorganic aragonite standard (Table S1; Spooner et al., 2016), and the approximate δ^{234}U of the seawater value (as 146‰ added to 5‰ multiplicated by random numbers 100,000 times (Monte Carlo technique) to simulate uncertainty in the values of δ^{234}U).

For U-series isotope-dilution dating, approximately 0.15 g of sample was physically cleaned and then oxidatively and reductively cleaned following established chemical protocols (Cheng et al., 2000). Once clean, the samples were dissolved in HNO_3 (7.5 M) and gravimetrically-spiked with a ^{236}U-^{229}Th mixed spike calibrated to uncertainty of 4.1‰ (2s; Burke and Robinson, 2012). U and Th in samples were co-precipitated with Fe-hydroxide, then separated and purified by anion-exchange columns (Chen et al., 2015c). The U and Th were measured separately by bracketing standard methods (international

U standard U112a and in-house Th standard SGS) on a Neptune MC-ICP-MS. Repeat analysis of the Harwell uraninite standard HU1 (uranium) and ThB (in-house thorium solution of ^{229}Th, ^{230}Th, ^{232}Th; Auro et al., 2012) standards gave an accuracy of 1‰ (1*s*) and long-term reproducibility of 1.3‰ (1*s*) for both ^{238}U/^{234}U and ^{230}Th/^{229}Th. Additionally, a pure ^{236}U spike was added to the Th fraction to allow measurement of ^{230}Th and ^{229}Th by ^{236}U normalization (Chen et al., 2015). It is worth noting that the ^{236}U spike was used in a previous study to show the low percentage of U (0.9%) into the Th fraction during column chemistry (Robinson et al., 2004a). Furthermore, contributions of ^{230}Th in the ^{236}U spike is believed not to be significant. Uncertainties related to machine and procedural blank were first propagated for each measured isotopic ratios, including uncertainties associated with the spike (estimated to 0.7‰ for ^{236}U and 2‰ for ^{229}Th per gram of spike, and 0.00004 g on the weight of spike). Then, the final uncertainties included the application of random numbers to the error of each variable (isotope ratios, ^{232}Th/^{230Th} uncertainty set as 50%, and decay constants) prior to solving the age equation. The final ages were calculated iteratively, solved 100,000 times by Monte Carlo simulation and corrected for initial ^{230}Th using the (^{232}Th/^{230}Th) atomic ratio of 12,500 based on modern seawater ratios (Cheng et al., 2000; Robinson et al., 2005). All dates are given as years before present (BP), where the present is the calendar year 1950 (Table S2).

Previously published U-Th ages (n=580) were included following the original publication. We did not apply the quality controls that we applied to our samples (e.g., initial δ^{234}U, [^{238}U] and [^{232}Th], see Section 2.4.1) to these compiled coral data, since similar issues were addressed in the relevant publications. Within the compilation there are a few datapoints (n=20) which fall outside our 15‰ initial δ^{234}U tolerance (see Section 2.4.1), however inclusion or exclusion of these data does not change our overall findings. Radiocarbon ages (n=85; Douarin et al., 2013; Frank et al., 2004; Titschack et al., 2015; Victorero et al., 2016; Wienberg et al., 2020, 2009) were re-calibrated using the Calib8.1 software and the new Marine20 calibration curve (Heaton et al., 2020a). To account for the offset between deep water and surface water radiocarbon in the past we apply an offset from the contemporaneous Marine20 value (Table S3; details in supplementary material). When the original, non-calibrated ^{14}C ages were not reported in the original publication (n=12; Frank et al., 2011, 2009), we used the reported calibrated ages.

2.4 RESULTS

2.4.1 Dating results and data quality

2.4.1.1 U-series laser ablation ages

A total of 140 samples from Reykjanes Ridge and 434 samples from the east Equatorial Atlantic were dated by U-series laser ablation and yielded ages from 150 kyr BP to 0.3 kyr BP (Table S1). Spooner et al. (2016) reported expected uncertainties based on coral isotopic heterogeneity and counting statistics to be approximately ±0.8 kyr, ±1.5 kyr and ±15 kyr at 10 kyr BP, 20 kyr BP and 125 kyr BP, respectively (Figure S2). We use these assumptions as a basis for the acceptable upper age limit for our samples, with ages with uncertainties above this level being rejected. Samples younger than 1 kyr BP were included in the compilation only when the absolute error was lower than the calculated age. In total, 44 sample ages were rejected (n=31 Reykjanes Ridge and n=13 east Equatorial Atlantic) resulting in 530 U-series laser ablation ages (n=109 Reykjanes Ridge and n=421 east Equatorial Atlantic; Table S1) included to the final database. Even if these ages had been included, there would be no change to the overall interpretation.

2.4.1.2 U-series isotope dilution ages

U-series isotope-dilution ages (n=118, including duplicates) ranged from 148 kyr BP to 0.1 kyr BP (Table S2). The [^{232}Th] from Tropic Seamount samples averaged 2.9 ppb (maximum 16.8 ppb), from Reykjanes Ridge averaged 0.9 ppb (max 3.9 ppb) and from east Equatorial Atlantic averaged 4.2 ppb (max 18.1 ppb). We applied three quality control measures: concentration of ^{232}Th; concentration of ^{238}U; and the initial δ^{234}U ($\delta^{234}U_i = \delta^{234}U \times e^{(\lambda_{234}\, t)}$). The 86 U-series isotope dilution ages (n=36 Tropic Seamount, n=32 Reykjanes Ridge, n=18 east Equatorial Atlantic) which pass these quality measures were included in the final database. Where replicate measurements are available, the highest quality sub-sample for each coral was selected based on quality control parameters described below (Table S2).

Samples with [^{232}Th] >6 ppb were not included in the compilation because of the large associated age uncertainty (Table S2), though inclusion of these data would not change the main findings. Four samples from Tropic Seamount showed anomalously low ^{238}U concentrations (< 1.6 ppm) and were

also not included in the compilation (Table S2). We inferred from trace metal analysis that two of these samples included high magnesium calcite, perhaps from encrusting organisms such as bryozoans.

The $\delta^{234}U_i$ screening criterion was used to assess open-system behaviour resulting from diagenetic alteration (Cheng et al., 2000; Robinson et al., 2006). The $\delta^{234}U_i$ results (Figure S3, Table S2) for the majority of our samples are within 10‰ of modern seawater values (146.8 ±0.1‰; Andersen et al., 2010), within the expected variability range for the seawater over the past 360 kyr (~15‰; Chen et al., 2015; Henderson, 2002). Three samples (two from Tropic Seamount and one from Reykjanes Ridge; Table S2) were thought to be affected by diagenetic alteration because they fall outside the expected variation range of seawater (±15‰ from modern seawater; Henderson, 2002) thus they were excluded from the compilation.

2.4.2 Temporal distribution of corals at new sites

2.4.2.1 Reykjanes Ridge

Coral samples from Reykjanes Ridge (n=141) ranged in age from 110 kyr BP to recent. Colonial corals were found only after 13.9 kyr BP, while solitary corals clustered in four time intervals within MIS 5, 3 and 1 (Figure 2). Three samples dated within the interval of 110 to 95 kyr BP, and eight samples between 80 and 70 kyr BP. In the following age cluster, the corals fall within 55 to 35 kyr BP (Figure 3). There are no corals from 35 to 15 kyr BP. The youngest age cluster extends from the onset of the Bølling-Allerød (B-A, 14.7 to 13 kyr BP; Figure 3) to recent, when corals show distinct peak for both solitary and colonial forms during the last 2 kyr BP (Figure 2).

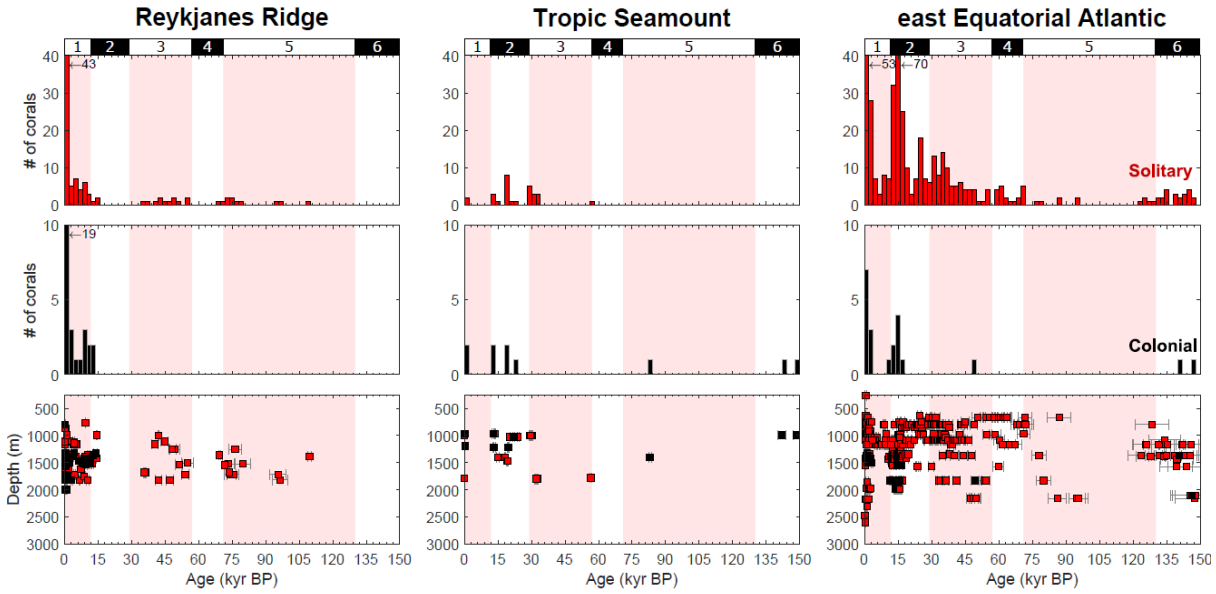

Figure 2: Age distribution of new U-series dated cold-water corals from Reykjanes Ridge (n=141), Tropic Seamount (n=36) and east Equatorial Atlantic (n=439). Solitary corals are shown in red and colonial corals are shown in black. Histograms show 2000-year bins. Error bars (2*s*) are shown in bottom panels. Top labels indicate MIS periods (1 to 6) and red shading marks MIS 5, 3 and 1.

2.4.2.2 Tropic Seamount

Tropic Seamount cold-water corals dated from 148 to 0.1 kyr BP (n=36), with two live-collected samples (Figure 2). Solitary corals were found at (i) 56 kyr BP, (ii) 34 to 12 kyr BP, and (iii) recent. Colonial corals comprise four age ranges: (i) 150 to 140 kyr BP, (ii) around 82 kyr BP, (iii) 32 to 12 kyr BP, and (iv) recent. The two oldest corals at Tropic Seamount (142 and 148 kyr BP) are from MIS 6 (Figure 2). Over the subsequent ~100 kyr, cold-water corals remained sparse with only two coral samples dated at 82 kyr BP (colonial) and 56 kyr BP (solitary). A significant increase in coral abundance began at the end of MIS 3 (~32 kyr BP) and extended to the beginning of the Younger Dryas (YD; 13 to 11.7 kyr BP), with a transient peak (n=11) during the Last Glacial Maximum (LGM, 22 to 18 kyr BP; Figure 3). However, there are no corals recorded from 29 to 24.5 kyr BP (coincident with Heinrich Stadial 2, HS2) nor from 18 to 15.5 kyr BP (coincident with Heinrich Stadial 1 (18 to 14.7 kyr BP, HS1); Figure 3). Next, there is a gap of ~12.5 kyr throughout the mid-YD and Holocene, including the last African Humid Period (8.2 to 5.5 kyr BP; Adkins et al., 2006), followed by the occurrence of four recent samples younger than 0.2 kyr BP (Figure 3).

2.4.2.3 East Equatorial Atlantic Sites

In addition to the corals dated in this study (n=439), 92 previously published ages from the east Equatorial Atlantic are included in this discussion (Mangini et al., 1998; Chen et al., 2015, 2016, 2020). Considered together, the full dataset includes ages that range from 147 kyr BP to present (Figure 2), and most of the corals are solitary (n=503, with 28 colonial specimens). Solitary corals are found in this region throughout the last 147 kyr, except for the interval 120 to 95 kyr BP, while there are only three instances of colonial corals dated older than 17 kyr BP: at 146 kyr BP, 140 kyr BP, and 49 kyr BP (Figure 2 and Figure S4).

The occurrence of solitary corals in the Equatorial Atlantic is semi-continuous from 95 kyr BP, with increasing abundance from 50 kyr BP and a distinct peak between 16 to 14 kyr BP (HS1 and B-A). The latter peak is also observed for colonial corals. Subsequently, both solitary and colonial coral populations show a decrease from 12 to 4 kyr BP, and a recovery after 4 kyr BP (Figure 2). The east Equatorial Atlantic dataset is distributed across three locations (Figure 1): Carter Seamount (total n=363 ages; 307 new ages and 56 published); Knipovich Seamount (total n=167 ages; 132 new ages and 35 published); and the mid-Atlantic ridge at 2300 m depth aged 14.1 kyr BP (total n=1; 1 age published; Mangini et al., 1998). Corals from both Carter and Knipovich seamounts show peak abundance during the HS1 and the B-A transition, and after 4 kyr BP (Figure 2 and Figure S4). A notable observation is that there are very few corals reported between 8.5 kyr BP and 4 kyr BP during the last African Humid Period (Figure 3).

Another feature observed in the east Equatorial Atlantic is an apparent deeper coral occurrence (below ~1600 m) during warm climatic phases (MIS 5, 3 and 1) as well as during mid-MIS 6 and the last deglaciation, contrasting with shallower occurrences during glacial intervals (MIS 6, 4 and 2, Figure 3). Intriguingly, the “deepening” in coral occurrence down to ~2000 m during the last deglaciation occurs at the same time as an increase in depth range (1800 m to 2600 m) of coral populations at seamounts in the Northwest Atlantic (Thiagarajan et al., 2013). However, given few sites with sampling across a wide depth range we do not make any further interpretations on depth distribution in this study.

2.5 DISCUSSION

2.5.1 North to South differences in coral occurrence across the Northeast Atlantic

A key observation from previous publications in the Northeast Atlantic is the latitudinal difference in coral occurrences over time (Frank et al., 2011). Corals from low and mid latitudes flourished during glacial and deglacial periods, whereas corals from higher latitudes were abundant during warm climate intervals – expanding their northernmost extent to the Norwegian margin after the Younger Dryas (López Correa et al., 2012). Our new dataset allows us to explore whether this feature is also apparent across the wider basin, and for solitary coral species which are underrepresented in the fossil record of the Northeast continental margin. Our data show that open-ocean habitats also exhibit distinct differences between high (Reykjanes Ridge) and low latitudes (east Equatorial Atlantic and Tropic Seamount), with the same warm/cold periods seesaw pattern observed in shelf settings (Frank et al., 2011).

Open-ocean corals from the Reykjanes Ridge are typically found during warm climate intervals at MIS 5, 3 and 1. During MIS 5, these ages are similar to those from coral mounds from the Porcupine Seabight and Rockall Trough (Dorschel et al., 2007; Frank et al., 2009, 2011; van der Land et al., 2010, 2014; Wienberg et al., 2020). During MIS 3, however, solitary corals are present at Reykjanes Ridge (n=13 from 55 to 35 kyr BP), while they are largely absent on the continental margin north of 45°N (Figure 4) with the exception of one coral age at Porcupine Seabight (53 ka; Dorschel et al., 2007). After a gap of 20,000 years, coinciding with the LGM and early deglaciation, solitary and colonial corals re-occur at Reykjanes Ridge during the B-A and show an increasing abundance through the Holocene (Figure 4). Thus, the data suggest that during warm climatic phases prior to the Holocene (MIS 5, MIS 3 and B-A) the Reykjanes Ridge (~60°N) represented the northernmost limit of corals in the Northeast Atlantic (Figure 4, Figure 5). During the Holocene corals re-occur at Porcupine Seabight and Rockall Trough, and as far north as the Norwegian margin (Figure S5; Frank et al., 2011; Lindberg and Mienert, 2006; López Correa et al., 2012; Raddatz et al., 2016; Schröder-Ritzrau et al., 2005; Titschack et al., 2015; Wienberg et al., 2020) and at the Faroe Islands (Schröder-Ritzrau et al., 2005) pointing to a more northerly distribution.

Further south, corals from Tropic and east Equatorial Atlantic seamounts are more abundant during glacials (MIS 3 to 2; Figure 2 and Figure 4), similar to the Gulf of Cádiz (Wienberg et al., 2009, 2010), temperate latitude seamounts (Schröder-Ritzrau et al., 2003, 2005), and off Mauritania (Figure 4; Eisele et al., 2011; Wienberg et al., 2018). All of these sites also share the following similarities: sparse or no coral occurrence during MIS 6 and 5, a reduction at the onset of the Holocene and a re-appearance in the last thousand years (Figure 4). Of course, the sparse occurrence of corals during MIS 6 and 5 might be related to sampling limitations, for instance the use of short sediment cores on coral mounds.

Together, these observations from the combined coral dataset highlight basin-scale controls on both solitary and colonial corals from the continental shelf and slope as well as open-ocean habitats (e.g., seamounts and mid-ocean ridges). In the next sections we explore the controls in more detail.

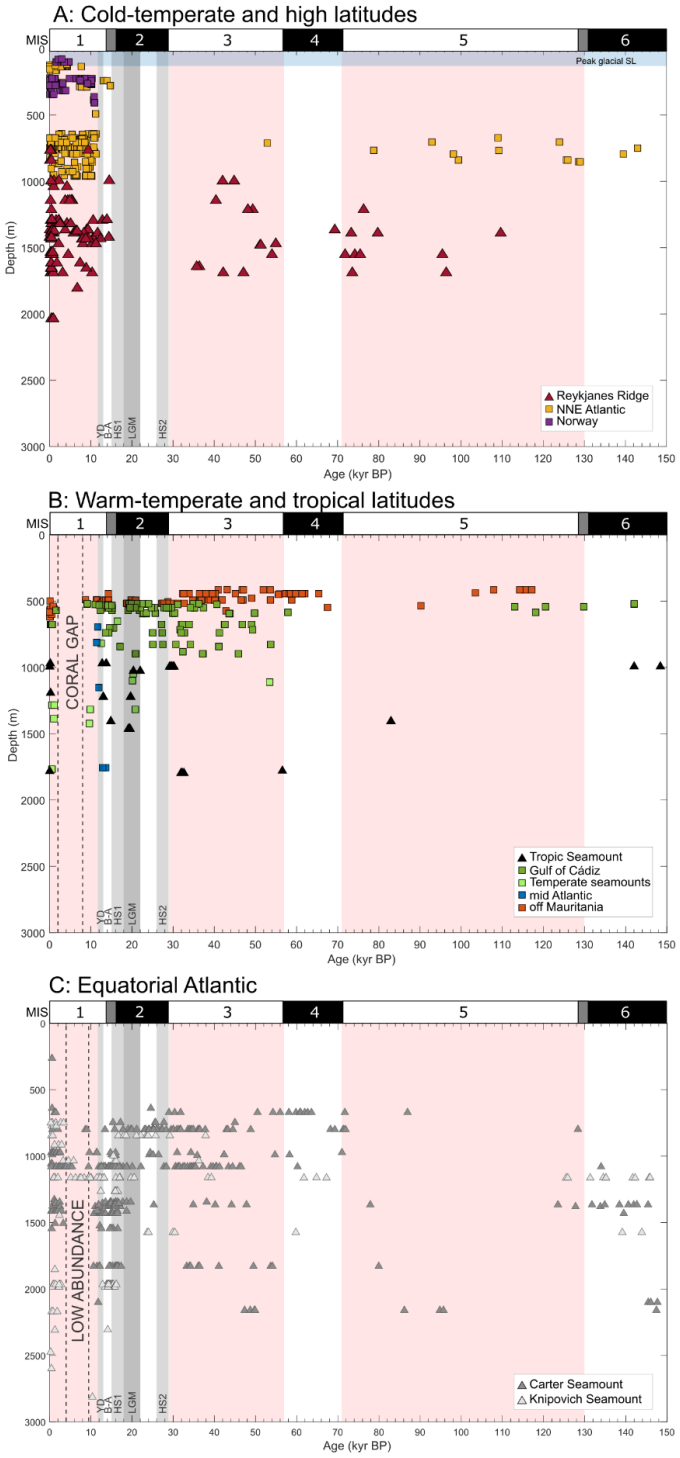

Figure 3: Temporal depth distribution of cold-water corals from the Northeast Atlantic divided by region: (**A**) cold-temperate and high latitudes coral sites (note that Reykjanes Ridge samples are plotted as mean depths from maximum and minimum depths of dredges when on the seafloor); (**B**) tropical and warm-temperate coral sites; (**C**) east Equatorial Atlantic coral sites (see Table 1 and Figure 1 for references). Square symbols represent previously published data and triangles represent coral sites from this study. Red shading indicates MIS 5, 3 and 1, and blue shading on panel A indicates the lowest glacial sea level (~130 m). Top labels indicate MIS periods (1 to 6), and glacial terminations 2 (130 kyr BP) and 1 (14 kyr BP) are indicated by dark grey bars. Shaded gray bars indicate climatic periods as follow: HS2 (Heinrich stadial 2, 28 to 24 kyr BP); LGM (Last Glacial Maximum, 22 to 18 kyr BP); HS1 (Heinrich stadial 1, 18 to 14.7 kyr BP); B-A (Bølling-Allerød, 14.7 to 13 kyr BP); YD (Younger Dryas, 13 to 11.7 kyr BP).

2.5.2 Environmental drivers of coral distribution in the cold-temperate and high latitudes

The occurrence of coral mounds in cold, temperate latitudes has previously been linked to enhanced bottom water hydrodynamics as a main control of food and sediment fluxes (Frank et al., 2009, 2011; Wienberg et al., 2020). Additionally, corals from these locations and high latitudes were found to be situated within a narrow band of water density constraining the importance of oceanic circulation (Dullo et al., 2008; De Mol et al., 2011; Flögel et al., 2014). In this section, we first discuss the mechanisms associated with the higher (lower) coral abundance at these locations during warm (cold) climate intervals. Then, we compare the timing of coral occurrence at these sites and discuss the associated mechanisms during the last 15 kyr.

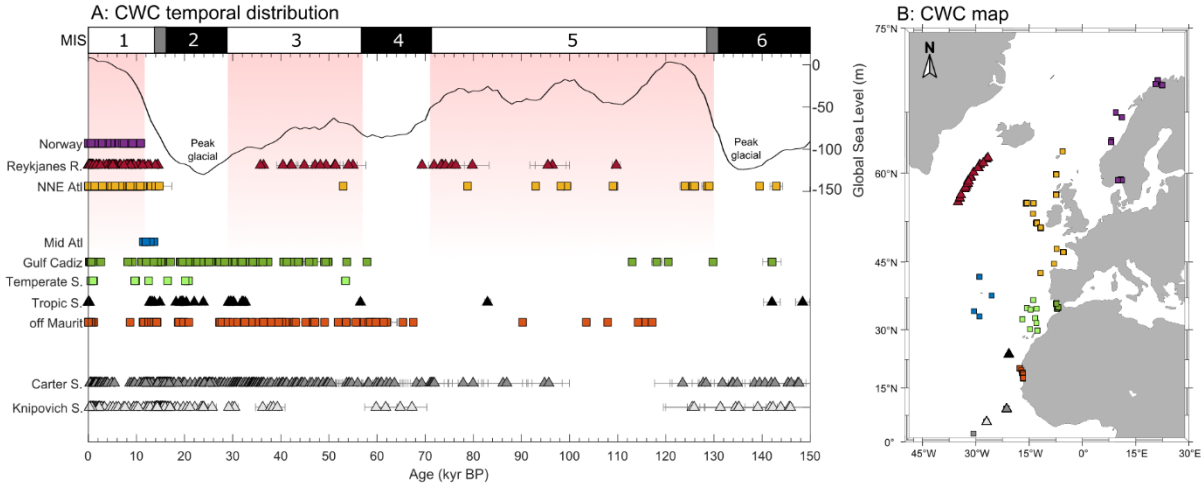

Figure 4: (A) Compiled age distributions of cold-water corals from the Northeast Atlantic (see Table 1 and Figure 1 for references) and global sea level reconstruction (Spratt and Lisiecki, 2016). Red shading indicates MIS 5, 3 and 1, coincident with intervals of abundant high latitude corals. Top labels indicate MIS periods (1 to 6), and glacial terminations 2 (130 kyr BP) and 1 (14 kyr BP) are indicated by dark grey bars. (B) Map of cold-water corals shown and colour matched with panel A. Square symbols represent previously published data and triangles represent coral sites from this study (Reykjanes Ridge, Tropic Seamount, Carter Seamount and Knipovich Seamount).

2.5.2.1 Comparison of warm and cold climatic intervals

During warm intervals, warm waters transported by the NAC reached the Nordic Seas and recirculated within the seas south of Iceland, and the Polar Front is thought to have shifted northward compared to colder intervals (Figure 5; de Vernal et al., 2005; Pflaumann et al., 2003; Toucanne et al., 2021). This displacement would have diminished regional sea-ice formation, stimulating primary

productivity and increasing food availability for benthic communities (Matul et al., 2018). Analogous to the modern day, the waters transported by the NAC would also have acted as an additional source of biomass through advection of phytoplankton towards the Nordic Seas and Arctic Ocean (Vernet et al., 2019). Therefore, we argue that these changes in oceanic circulation together with the associated increase in temperature and food availability would have affected coral communities, driving high coral abundances in the northern Northeast Atlantic during MIS 5 and 1 (Figure 4; for discussion of MIS 1 see Section 2.5.2.2). During the MIS 3, a similar mechanism is expected to be associated with the occurrence of corals at Reykjanes Ridges. This is supported by evidence of a decrease in polar waters and an increase of temperate waters occurring south of Iceland during early and mid-MIS 3 (Bashirova et al., 2014). However, the contrasting low occurrence or absence of corals at Porcupine Seabight and the Rockall Trough point towards additional forcing, for instance hydrodynamic processes controlling food and sediment flux (Wienberg et al., 2020).

The opposite mechanism likely explains the sparseness of corals in cold-temperate and high latitude locations during glacial intervals (e.g. MIS 4 and 2, Figure 4). During these cold periods, primary productivity was likely limited by enhanced sea-ice cover following a southward shift in the Polar Front (Figure 5; Löfverström et al., 2014). This shift would have been particularly important at latitudes north of 45°N when the NAC is thought to have shifted towards to a nearly zonal position around 40°N - 50°N (Figure 5; Eynaud et al., 2009). Supporting this frontal shift, reconstructions of sea surface temperature and salinity south of Iceland suggest a large winter sea-ice expansion during the LGM (Thornalley et al., 2011a), paired with the absence of corals at Reykjanes Ridge (Figure 5). In summary, coral occurrences from cold-temperate and high latitudes have been responding to intervals of increased food availability paced by warm climate intervals.

2.5.2.2 The last 15 kyr

During the last 15 kyr corals re-occur at Reykjanes Ridge during the interstadial B-A, followed by a re-aggradation of coral mounds at Porcupine Seabight and Rockall Trough, and a northward migration of corals up to the Norwegian shelf (Schröder-Ritzrau et al., 2003; Frank et al., 2004; Schröder-Ritzrau et al., 2005; Dorschel et al., 2007; Eisele et al., 2008; Frank et al., 2009; Mienis et al., 2009; van der

Land et al., 2010; Frank et al., 2011; Douarin et al., 2013; van der Land et al., 2014; Victorero et al., 2016; Bonneau et al., 2018; Wienberg et al., 2020).

The re-occurrence of cold-water corals (both solitary and colonial) at Reykjanes Ridge during the B-A (Figure 4 and Figure S5) parallels a regional increase of organic matter (high abundance of benthic foraminifera *Cassidulina teretis*; Matul et al., 2018) and an increase in the export of dense, oxygen-rich overflow waters from the Nordic Seas (1179 m; Ezat et al., 2017). These findings suggest that the coral community at Reykjanes Ridge benefited from the enhanced food supply and likely enhanced oxygenation of subsurface waters promoted by the increased flow of the deep waters.

The timing of the coral re-occurrence at Reykjanes Ridge around 14.5 kyr BP aligns with an increase in abundance of corals in the Bay of Biscay (Figure 5; note there are only 12 ages available from the Bay of Biscay; De Mol et al., 2011; Schröder-Ritzrau et al., 2003), however, coral mound formation at Porcupine Seabight and Rockall Trough remained inactive until 11.3 kyr BP (Dorschel et al., 2007; Frank et al., 2009, 2011; van der Land et al., 2010, 2014; Wienberg et al., 2020). One potential reason put forth for this inactivity is related to sluggish bottom currents (Wienberg et al., 2020). Later on, during the onset of the Holocene, it has been suggested that the location of the coral mounds within a highly dynamic transition zone may have promoted hydrodynamic conditions favourable to coral growth, such as enhanced food and sediment supply (Figure 5; Wienberg et al., 2020). This could have been a result of the invigoration of the MOW, and the establishment of its modern depth and intensity flow pattern (Rogerson et al., 2005; Wienberg et al., 2020).

Further north, the onset of coral growth at the Norwegian shelf occurred at 10.9 kyr BP, around 400 yr after re-growth at coral mounds in the Porcupine Seabight and Rockall Trough suggesting a rapid climate driven coral migration (Frank et al., 2011; López Correa et al., 2012). The start of the Norwegian coral ecosystems is contemporaneous with the establishment of modern-like warm climatic conditions and oceanographic patterns (López Correa et al., 2012). Additionally, evidence based on genetic traits of modern coral communities has been used to suggest that coral larvae were coming from the Mediterranean Sea and out into the British Isles and Norwegian shelf at the onset of the Holocene (Henry et al., 2014). This evidence has been supported by Boavida et al. (2019) who demonstrated a northward expansion of cold-water corals after the end of the last glacial from the Mediterranean Sea

to the North Atlantic, with a nearly homogenised genetic signature of *Desmophyllum pertusum* (*Lophelia pertusa*) from the Bay of Biscay to the Iceland margin. Overall, the overflow waters from the Mediterranean Sea may play an important role in the Northeast Atlantic coral community by influencing regional hydrodynamics, food supply and larvae dispersion.

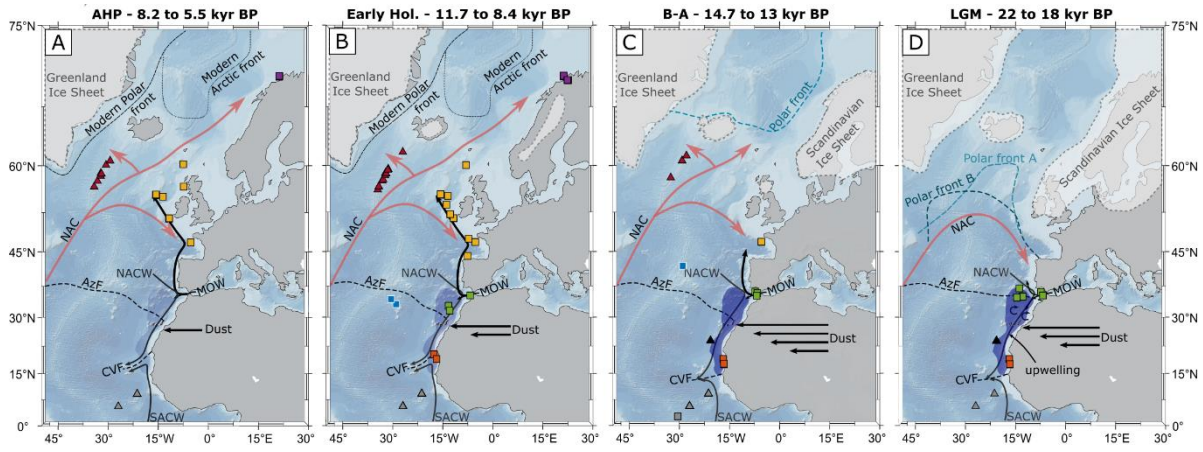

Figure 5: Schematic representation of main mechanisms associated with cold-water coral distribution in the Northeast Atlantic Ocean at four time slices: (A) African Humid Period (AHP, 8.2 to 5.5 kyr BP), (B) early Holocene (11.7 to 8.4 kyr BP), (C) Bølling-Allerød (B-A, 14.7 to 13 kyr BP), and (D) Last Glacial Maximum (LGM, 22 to 18 kyr BP). Polar Front A and B (panel D) corresponds to reconstructions by Pflaumann et al., (2003) and de Vernal et al., (2005) respectively; and Polar Front (panel C) follows Xiao et al. (2017). Approximate position of ice sheets and Polar and Arctic Fronts (panels B and A) after (Pflaumann et al., 2003; De Vernal et al., 2005; Hughes et al., 2016). Schematic dust fluxes are according to (McGee et al., 2013). Coastal and frontal upwelling at the Northwest African margin are shown with the shaded blue area (Romero et al., 2008; Zarriess and Mackensen, 2010; Bradtmiller et al., 2016). Main pathway of Mediterranean Overflow Water (MOW) is indicated by black arrows exiting the Strait of Gibraltar (Rogerson et al., 2005). The North Atlantic Current (NAC) is indicated by red arrows (Matul et al., 2018; Thornalley et al., 2011). Inferred positions of North Atlantic Central Water (NACW) and South Atlantic Central Water (SACW) are indicated by dark gray arrows (Wienberg et al., 2018). Cape Verde (CVF) and Azores (AzF) frontal positions are after (Romero et al., 2008; Wienberg et al., 2010, 2018).

2.5.3 Environmental drivers of coral distribution in the low and mid-latitudes

The temporal distribution of corals from low and mid-latitudes in the Northeast Atlantic contrasts with the distribution of corals further north by having the most prolific growth during the last glacial interval, and a strong decrease in abundance at the onset of the Holocene. Previous studies attributed this pattern to productivity, shifts in oceanographic fronts, and hydrological conditions such as temperature and dissolved oxygen (Eisele et al., 2011; Frank et al., 2011; Wienberg et al., 2018, 2010, 2009). The similar occurrence pattern observed for corals from the east Equatorial Atlantic and Tropic Seamount point towards basin-scale mechanisms paced by climatic shifts. In this section we present a

discussion of the mechanisms associated with this coral pattern during four time intervals: the last glaciation, HS1, early-Holocene, and African Humid Period and present.

2.5.3.1 Last glacial interval and LGM

During the onset of the MIS 4, an increase in coral population in the east Equatorial Atlantic (Figure 2 and Figure S4) is associated with higher total organic carbon (TOC) and biogenic opal compared to interglacials (Wagner, 2000). At the same time, coral mounds off Mauritania re-initiated as a response to an increased in food supply (Eisele et al., 2011; Wienberg et al., 2018; Portilho-Ramos et al., 2022). In addition to productivity, Wienberg et al. (2018) suggests that a southward displacement of Cape Verde Frontal Zone would have placed these coral mounds within the oxygen-rich North Atlantic Central Water, promoting favourable conditions for coral growth.

During the LGM and deglaciation, high coral abundances at Gulf of Cádiz, temperate latitude seamounts, Tropic Seamount and Mauritania margin occur at the same time as aeolian fluxes were up to two times higher than the present (Figure 6; McGee et al., 2013; Middleton et al., 2018; Rowland et al., 2021). The high aeolian fluxes and the increase in coastal and frontal upwelling (Adkins et al., 2006; Romero et al., 2008) resulted in high productivity off Northwest Africa (Bradtmiller et al., 2016) and in the Gulf of Cádiz (Wienberg et al., 2010) providing additional food resources to corals. The contemporaneous high coral abundance at Tropic Seamount suggests that these organic-rich waters reached the offshore location of the seamount, increasing food supply and sustaining favourable conditions for corals (Figure 5). Contrasting to this prolific coral growth, corals from the east Equatorial Atlantic show a reduced occurrence. In fact, there was a reduction of the organic matter export to the sea floor (e.g., low TOC) in the Equatorial Atlantic during the LGM (Zarriess and Mackensen, 2010), further demonstrating the strong link between productivity and east Equatorial Atlantic corals.

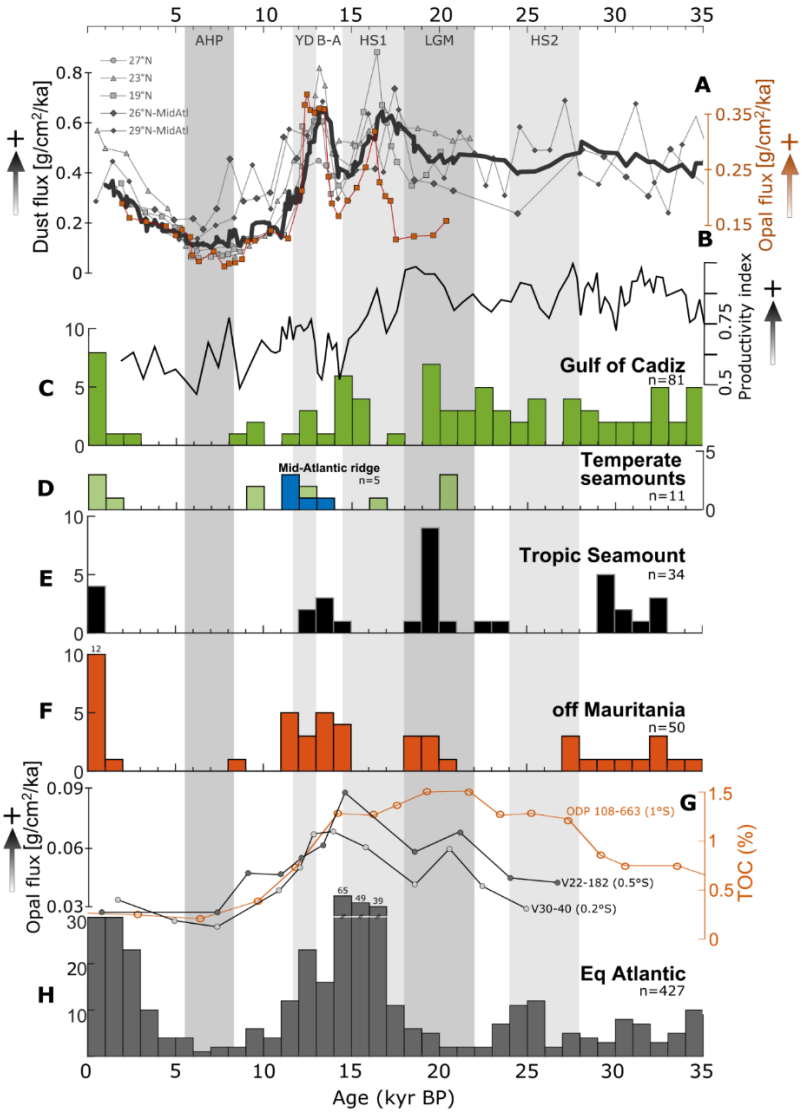

Figure 6: Age distribution of cold-water corals from the tropical and central Northeast Atlantic and environmental proxies from the past 35 kyr BP. (A) Compilation of dust fluxes from Northwest Africa from cores OC437-7 GC68 (19°N, scaled down 6 times), GC49 (23°N), GC37 (27°N) (McGee et al., 2013), KN207-2 GGC3 (26°N), GGC6 (29°N) (Middleton et al., 2018), black line corresponds to the 6-point moving average . Opal flux from the Mauritanian margin (orange symbols, same core as dust record at 19°N; Bradtmiller et al., 2016). (B) Productivity index at Gulf of Cádiz based on planktonic foraminiferal assemblages from core GeoB9064 (Wienberg et al., 2010). (C) Histogram of cold-water corals of Gulf of Cádiz (green; Dubois-Dauphin et al., 2016; Frank et al., 2011; Schröder-Ritzrau et al., 2005, 2003; Wienberg et al., 2010, 2009). (D) Histogram of cold-water corals from seamounts at temperate latitudes (light green; Schröder-Ritzrau et al., 2005, 2003) and mid-Atlantic (blue; Adkins et al., 1998; Eltgroth et al., 2006; Schröder-Ritzrau et al., 2005, 2003). (E) Histogram of cold-water corals from Tropic Seamount (this study). (F) Histogram of cold-water corals from the Mauritanian margin (Eisele et al., 2011; Wienberg et al., 2018). (G) Opal fluxes from Equatorial Atlantic from cores V22-182 and V30-40 (Bradtmiller et al., 2007) and total organic carbon (TOC) from core ODP 108-663 (Wagner, 2000). (H) Histogram of cold-water corals from east Equatorial Atlantic (this study; Chen et al., 2020, 2016, 2015; Mangini et al., 1998). Histograms show number of corals dated and total number of samples (n). Shaded bars indicate climatic periods as follow: LGM (Last Glacial Maximum, 22 to 18 kyr BP); HS1 (Heinrich stadial 1, 18 to 14.7 kyr BP); B-A (Bølling-Allerød, 14.7 to 13 kyr BP); YD (Younger Dryas, 13 to 11.7 kyr BP); AHP (African Humid Period, 8.2 to 5.5 kyr BP). For site location references see Figure S1.

2.5.3.2 Heinrich Stadial 1

While productivity seems to be the dominant driver of coral abundance (Section 2.5.3.1), a different mechanism may have dominated during Heinrich Stadial 1. At this time, reconstructions of productivity from the Equatorial Atlantic and NW African margin show a pronounced increase (Romero et al., 2008; Zarriess and Mackensen, 2010; McKay et al., 2014; Bradtmiller et al., 2016), which occurred during the most pronounced coral abundance peak in the east Equatorial Atlantic (Figure 6). By contrast, corals were absent at the Mauritanian margin and Tropic Seamount (Figure 6 and Figure S5).

During HS1, the presence of the oxygen-poor South Atlantic Central Water on the Mauritanian continental shelf and slope may have reduced coral mound growth (Wienberg et al., 2018). A similar pattern of coral growth observed at our new Tropic Seamount site suggests that deoxygenation of the water column at this time may also have occurred further offshore and at deeper depths (between 1000 m and 1500 m in contrast with corals off Mauritania at ~500 m). It is unlikely that the same mechanism (e.g., coral site location within the central waters) would explain this lowering in seawater oxygen content at Tropic Seamount. Instead, we argue that the high input of organic matter onto the sea floor may have promoted low benthic oxygen conditions. In agreement with this idea, an increase in abundance of local benthic foraminifera tolerant to low oxygen is described at the continental slope (~2500 m) off Mauritania during the HS1 (McKay et al., 2014).

2.5.3.3 Early-Holocene

During the early-Holocene, a pronounced decrease in coral population is observed in the east Equatorial Atlantic, Tropic Seamount, Gulf of Cádiz, temperate latitude seamounts and Mauritania margin (Figure 6). In fact, the abundance pattern of corals in the east Equatorial Atlantic mimics the pattern of dust fluxes and productivity, with a coral gap of more than 12 thousand years at Tropic Seamount coeval with low values for these two parameters (Figure 6). The reduced dust fluxes during the early Holocene (e.g., McGee et al., 2013; Middleton et al., 2018; Rowland et al., 2021) could have directly impacted primary productivity decreasing “iron fertilization” of surface ocean (Mark Moore et al., 2009; Wienberg et al., 2010). Furthermore, the associated weakened trade winds are thought to have

reduced coastal upwelling intensity as suggested by low opal flux and organic carbon observed at the entire Northwest African margin between 19°N and 27°N (Bradtmiller et al., 2016). In addition, diatom assemblages from the continental slope off Mauritania also indicate low productivity during the Holocene in agreement with a reduced coastal upwelling (McKay et al., 2014). Recently, Portilho-Ramos et al. (2022) demonstrated that coral occurrences on the Mauritania margin and Gulf of Cádiz are strongly associated with food supply. They attributed the lack of coral occurrence during the onset of the Holocene to a decrease in organic matter flux and weakened bottom currents (Portilho-Ramos et al., 2022).

In addition to coastal upwelling, the absence of corals on the upper slope off Mauritania in the Holocene has been attributed to the presence of the oxygen-poor South Atlantic Central Water due to the northward shift of the Cape Verde Frontal Zone (Figure 5). At the same time, the southward position of the Azores Front (~30°N; Figure 5) displaced the higher productivity area away from the Gulf of Cádiz, thus decreasing food supply (Wienberg et al., 2010). In addition to these oceanographic and hydrological changes, warmer seawater temperatures after the Younger Dryas was thought to be a potential extra stressor for the local coral community (Wienberg et al., 2010, 2018). However, the recent Mauritania margin and Gulf of Cádiz study suggests that temperature played little role in coral demise during the Holocene (Portilho-Ramos et al., 2022).

2.5.3.4 African Humid Period and present

In the east Equatorial Atlantic, the coral population sharply decreases from the onset of the Holocene until it reaches the lowest coral abundance during the last African Humid Period (Figure 6). During this interval, African vegetation and precipitation combined with weaker trade winds led to low dust flux and a pronounced decrease in coastal upwelling (Figure 5; Adkins et al., 2006; Bradtmiller et al., 2016). Similarly, corals are absent on the Mauritania margin, Tropic Seamount, Gulf of Cádiz and temperate seamounts throughout the last African Humid Period (Figure 5). Our data indicate that the influence of these changes in productivity extended across the basin, and that this interval, together with the shifts on oceanographic fronts and hydrological conditions (Section 2.5.3.3), represents the most unfavourable conditions for coral growth at mid to low latitudes within the Holocene.

The modern coral communities at all mid to low latitude sites are characterized by a patchy occurrence and low numbers which seems to be controlled by specific and local conditions (e.g., enhanced hydrodynamics supplying food and oxygen), differing considerably from the thriving glacial/deglacial reefs. For instance, modern corals at Tropic Seamount are mostly observed on the eastern and western flanks, where higher current and energy may increase food supply. And at the Mauritanian margin, late-Holocene corals are observed exclusively within canyons, where episodic events can deliver food and well-oxygenated surface waters into the deep (Wienberg et al., 2018). In summary, productivity seems to be the main driver of coral abundance across the region. Other parameters as oxygen concentration and temperature however may still act as stressors controlling coral growth, with local factors also influencing coral distributions.

2.6 CONCLUSIONS

We have combined >600 new U-series dates of fossil scleractinian cold-water corals from the tropical and high latitude Northeast Atlantic Ocean with previous published data to yield a database of over 1300 coral dates. Systematic analysis of the temporal distribution of the coral population shows that the corals are affected by basin wide climate-driven oceanographic and hydrologic change. We demonstrate that the timing of colonial and solitary cold-water coral occurrence is similar, suggesting similar survival needs. Furthermore, we reveal an analogous temporal distribution between coral population from continental shelf, slope and open-sea regime. This extensive database includes equatorial regions, where corals show contrasting distribution patterns compared to the high latitude Northeast Atlantic.

Sites in the cold-temperate and high latitude Northeast Atlantic reveal peak coral occurrences during warm climate intervals over the past 150 kyr BP, and the Reykjanes Ridge (~60°N) represents the known biogeographical limit of cold-water corals during MIS 5 and 3. Regionally, cold-water coral success is thought to be controlled by oceanic dynamics, especially the inflow of warm Atlantic waters by NAC, the Polar Front position, and the influence of MOW at coral mounds on continental margins, all mechanisms associated with food and sediment supply. During the early Holocene, the biogeographical limit of cold-water corals expands from Reykjanes Ridge (~60°N) to the Norwegian

shelf (~70°N), a time when full interglacial conditions and modern-like circulation patterns were established.

A contrasting pattern is observed in the low and mid latitude Northeast Atlantic, where corals show prolific growth during the last glacial and deglacial intervals, and a pronounced decline during the early and mid-Holocene. This finding had been based mainly on observations of corals mounds on the continental slope off Northwest Africa (Wienberg et al., 2010, 2018; Eisele et al., 2011; Frank et al., 2011). Our new and extensive record of Equatorial Atlantic corals however confirms the broad scale of this pattern. We find the glacial / deglacial large scale coral occurrence is linked to surface water productivity driven by enhanced dust fertilization and stronger upwelling systems. Additionally, water column oxygenation is shown as an important factor to coral growth mainly driven by frontal zone positions or organic matter remineralization. The collapse of central and equatorial Northeast Atlantic coral populations during the Holocene occurs with a drastic decrease in wind strength and aridity in Africa. Moreover, lower concentrations of dissolved oxygen and higher temperatures, may have acted as additional stressors to corals inhabiting the continental slope.

Past climate-driven shifts in cold-water corals towards higher latitudes during warm intervals mean that future warming and associated sea ice reduction, if moderate and gradual, may open new niches for corals. However, the fast rates of warming have already impacted key regions of the ocean declining primary productivity (Capuzzo et al., 2018) and oxygen concentration (Santos et al., 2016). These factors combined with ocean acidification/aragonite saturation horizon shoaling (Guinotte et al., 2006; Carvalho-Borges et al., 2018) will doubtless present challenges to calcifying organisms with unknown consequences for the future of cold-water corals and the important habitats that they engineer.

2.7 ACKNOWLEDGEMENTS

We acknowledge the crew and researchers on board the research cruises JC142 (Tropic Seamount in 2016; project ‘MarineE-tech’; grants NE/M011186/1, awarded to B. Murton and NE/M011151/1, awarded to P. Lusty), JC094 (Equatorial Atlantic in 2013) and CE08-06 (Reykjanes Ridge in 2008) who obtained the samples for this study. We thank Christopher Coath, Carolyn Taylor and Yun-Ju Sun for their help with laboratory work. We thank the editors, Sophia Hines, and two other reviewers for

their comments which considerably improved this manuscript. Funding was provided by NERC grants awarded to L.F.R. (NE/S001743/1 and NE/R005117/1) and by Schlumberger Foundation who provided the PhD scholarship “Faculty for the Future Fellowship”. M.V.K. acknowledges the support from the São Paulo Research Foundation (FAPESP #2017/50229-5) and from the National Council for Scientific and Technological Development (CNPq #301436/2018-5). The new data and compilation reported in this paper are archived in Pangaea (https://doi.pangaea.de/10.1594/PANGAEA.945280).

Chapter 3: MULTI-PROXY COLD-WATER CORAL RECORDS FROM TROPIC SEAMOUNT DURING THE PAST 35 THOUSAND YEARS

Abstract

The ocean is an important part of the Earth's climate system responsible for transporting heat across the Northern and Southern Hemispheres and for exchanging CO_2 with the atmosphere. During the last ice age and deglaciation, the climate changed from a cold and CO_2 depleted atmosphere to the present interglacial conditions – warmer temperatures and higher CO_2. It is thought that perturbations of the oceanic circulation had a crucial role in these changes, however the mechanisms are yet to be fully understand. In this context, data from the intermediate depths of the ocean (600 m to 2000 m) have are not consistent, with some data suggesting a reservoir of old-carbon, but some data suggesting a well-ventilated signature. In this study, we used U-series dated deep-sea corals collected from the Tropic Seamount in the tropical Northeast Atlantic to investigate the composition of the intermediate waters from the past 35 thousand years. The U-ages were paired with ^{14}C data, and the temperatures were reconstructed from Li/Mg ratios. The results suggest that the intermediate waters at Tropic Seamount remained more well ventilated than deep layers of the ocean during the Last Glacial Maximum (LGM) and early deglaciation. During the LGM, the waters at Tropic Seamount show a rapid ^{14}C excursion towards signatures of the Antarctic Intermediate Water (AAIW), in agreement with data from equatorial Atlantic and Southern Ocean. The transition between the LGM and early deglaciation was marked by a large increase in both temperature and ^{14}C content. This warming parallels other records from South, equatorial and North Atlantic which demonstrate a large scale thermal response of the intermediate ocean to an interval of weakened AMOC. Furthermore, the ^{14}C-signature of AAIW shown by the corals at Tropic Seamount may suggest a South-to-North heat export during the early deglaciation.

Contributions

The coral samples from this chapter are from the collections of Prof Laura F. Robinson (University of Bristol) and Prof Christian Millo (USP, University of Sao Paulo, Brazil). The sample preparation and U-series dating were done by myself. The age calculation were done by me using a Matlab script written by Dr Tianyu Chen (Nanjing University, former post-doc researcher in the University of Bristol). The samples' cleaning for the trace elements analysis was done by myself, James Kershaw (University of Bristol) and Yun-Ju Sun (University of Bristol). The majority of the trace elements analysis was done by James Kershaw, Dr Joseph A. Stewart (University of Bristol) and myself, and a few samples were measured by Yun-Ju Sun and Maoyu Wang (University of Bristol). I prepared and cleaned the radiocarbon samples with the graphitization being carried out by Paul Monaghan (University of Bristol) and the radiocarbon analysis and data processing by Dr Timothy Knowles (University of Bristol). This chapter was written by me. This chapter was written as paper format because we intend to submit it to Paleoceanography and Paleoclimatology journal.

3.1 INTRODUCTION

During the last glaciation, the ocean is thought to have undergone significant changes in response to a colder and more CO_2-depleted atmosphere (Monnin et al., 2001; Schneider von Deimling et al., 2006; Marcott et al., 2014). Reconstructions of nutrients and stable isotopes from the Atlantic Ocean during the LGM (22 ka to 18 ka), suggest a shallowing of deep waters and more voluminous southern-sourced waters at abyssal depths (Curry and Oppo, 2005; Gebbie, 2014). The large ice sheets in the North Atlantic as well as extended sea ice in both high latitude regions are linked with the development of this different oceanic configuration. It has been suggested that the Atlantic Ocean may have consisted of two overturning circulation cells (upper and lower) with reduced mixing between them, and that these cells were salinity controlled (Adkins et al., 2002b; Marchitto and Broecker, 2006; Ferrari et al., 2014; Roberts et al., 2016). The majority of previous observations have been carried out at surface and deep depths of the Atlantic Ocean, for instance using planktic and benthic foraminifera from sediment cores.

Several studies have observed ^{14}C-depleted deep and abyssal waters in the Atlantic Ocean during the last glaciation, especially during the LGM (Barker et al., 2010; Skinner et al., 2010; Freeman et al., 2016). They interpreted this signal as a deep ocean more isolated from the atmosphere compared with the modern, which also also corroborated by $\delta^{13}C$ data that indicates different oceanic configuration during this period (Lynch-Stieglitz et al., 2007). Additionally, it was postulated that the lower CO_2 concentration observed in the atmosphere was the result of CO_2 accumulation in these deep layers of the ocean (Keigwin, 2004; Skinner et al., 2010). Recently, compiled evidence of the intermediate depths (~1000 m to 2000 m) of the Atlantic Ocean show that the waters have remained ^{14}C-enriched during the LGM, indicating the close relationship between the intermediate waters and the atmosphere (De Pol-Holz et al., 2010; Freeman et al., 2016; Chen et al., 2020). However, the ventilation of intermediate layers is still debated due to other records showing glacial ^{14}C depleted signatures, for example in the east Pacific Ocean, North Atlantic and Southern Ocean (Robinson et al., 2005; Stott et al., 2009; Thornalley et al., 2011b; Burke and Robinson, 2012). This discrepancy demonstrates the need for

studying the dynamic intermediate layer, which might provide insights on regional and larger scale oceanic processes.

As the climate changed to deglacial conditions, the atmospheric CO_2 content increased in parallel with an increase in the ^{14}C content of the deep and intermediate waters, indicating a ventilation of these layers (Skinner and Shackleton, 2004; Skinner et al., 2010; Burke and Robinson, 2012; Chen et al., 2015). Several studies suggest a crucial role of the Southern Ocean in the atmospheric CO_2 rise, for instance the increase of upwelling of deep CO_2-enriched and consequent degassing of CO_2 (Burke and Robinson, 2012; Rae et al., 2018; Li et al., 2020; Stewart et al., 2021). Moreover, intermediate waters have shown a dynamic behaviour during the past abrupt atmospheric variability at the last deglaciation further pointing out the quick response of the waters at these depths to climatic variability (Chen et al., 2015, 2020).

Another key climatic component is temperature, a critical driver of the global oceanic overturning circulation which transports warm waters from low to high latitudes, where surface waters lose buoyancy due to sea-air heat loss and sink to the ocean interior (Talley, 2013). During the last deglaciation, high-resolution reconstructions of the atmosphere show two intervals of a gradual increase in atmospheric CO_2 coincident with Southern Hemisphere warming and a cold Northern Hemisphere (see Figure 2 in Chapter 1). These intervals saw reduced strength of AMOC, leading to the hypothesis that heat was accumulated in the Southern Hemisphere due to the decreased of northward transport of heat (seesaw pattern; Barker et al., 2009; Shakun et al., 2012; Marcott et al., 2014). In contrast, events of rapid reassumption of AMOC are thought to have driven episodes of deglacial CO_2 peaks synchronous with warming in the Northern Hemisphere (Marcott et al., 2014). In the equatorial Atlantic and Southern Ocean, coral data showed an erosion of ^{14}C gradient at intermediate depths demonstrated a link with AMOC overshoot and atmospheric CO_2 peak during the last deglaciation (Burke and Robinson, 2012; Chen et al., 2015).

There is evidence that intermediate waters may have played a crucial role in connecting high and low latitudes, transferring climatic signal (e.g., heat, nutrients), and thus modulating the Earth's climate (Pena et al., 2013; Romahn et al., 2014). However, during events of oceanic reorganization, the limited and contradictory data from intermediate depths provide equivocal evidence about intermediate waters

(e.g., Antarctic Intermediate Water, AAIW) on oceanic circulation. For instance, during Heinrich Stadial 1 (HS1, 18 ka to 14.7 ka) and the Younger Dryas (YD, 13 ka to 14.7 ka) some studies suggest a larger entrainment of southern-sourced waters at intermediate depths (Pahnke et al., 2008), while others argued for minor changes (Huang et al., 2014; Howe et al., 2016), or even a decrease in southern-sourced waters (Xie et al., 2012). Available proxy and model data demonstrate contemporaneous warming of the intermediate tropical ocean in response to a weakened AMOC during YD and HS1 (Came et al., 2007; Weldeab et al., 2016; Poggemann et al., 2018; Umling et al., 2019; Valley et al., 2019). However, the explanation for this warming is also divergent, where some studies attribute it to surface and/or subsurface changes in the Northern latitudes (Came et al., 2007; Weldeab et al., 2016; Valley et al., 2019) while others to the Southern latitudes (Poggemann et al., 2018), or both (Umling et al., 2019). Therefore, the use of accurately dated archives and paired information about the circulation and heat content may promote invaluable information to better constrain the timing and magnitude of such events, and to shed light on the possible associated mechanisms.

Here, we investigate the oceanic circulation and temperature evolution of the intermediate depths of the tropical Northeast Atlantic using deep-sea corals. We used paired U-Th and ^{14}C data as a proxy for oceanic ventilation, and Li/Mg ratios to reconstruct the temperature. These data were compared with previous published data to provide new insights into the role of the intermediate ocean during global climate reorganisations.

3.2 METHODOLOGY

3.2.1 Samples and oceanographic settings

Deep-sea coral samples (Plate 1, Appendix II) for this study were collected by the ROV *Isis* during cruise JC142 on the RSS *James Cook* from Tropic Seamount (23°55'N, 20°45'W) in 2016 (Figure 1). The scleractinian corals (n=38) analysed consist of four species, three solitary: *Desmophyllum dianthus* (n=25), *Caryophyllia sp.* (n=4), *Javania cailleti* (n=2), and one colonial: *Solenosmilia variabilis* (n=7). The fossil and live collected corals are from depths ranging between 970 m and 1952 m. This depth range today is bathed by Antarctic Intermediate Water (AAIW) and North Atlantic Deep Water (NADW) (Bashmachnikov et al., 2015; Pastor et al., 2015). AAIW is identify by a low-salinity and

nutrient-rich core centred at 900 m, while NADW is found below approximately 1500 m (Figure 1). The coral samples were dated by U-series isotopic dilution method at the facilities of the Bristol Isotope Group (University of Bristol) following established protocol (Cheng et al., 2000; Burke and Robinson, 2012; Chen et al., 2015). The details of the dating results are found at Chapter 2 which consist of a paper recently published in Deep Sea Research Part I (de Carvalho Ferreira et al., 2022). All data from the U-series dating and photos of each species (Plate 1) are in the Appendix II.

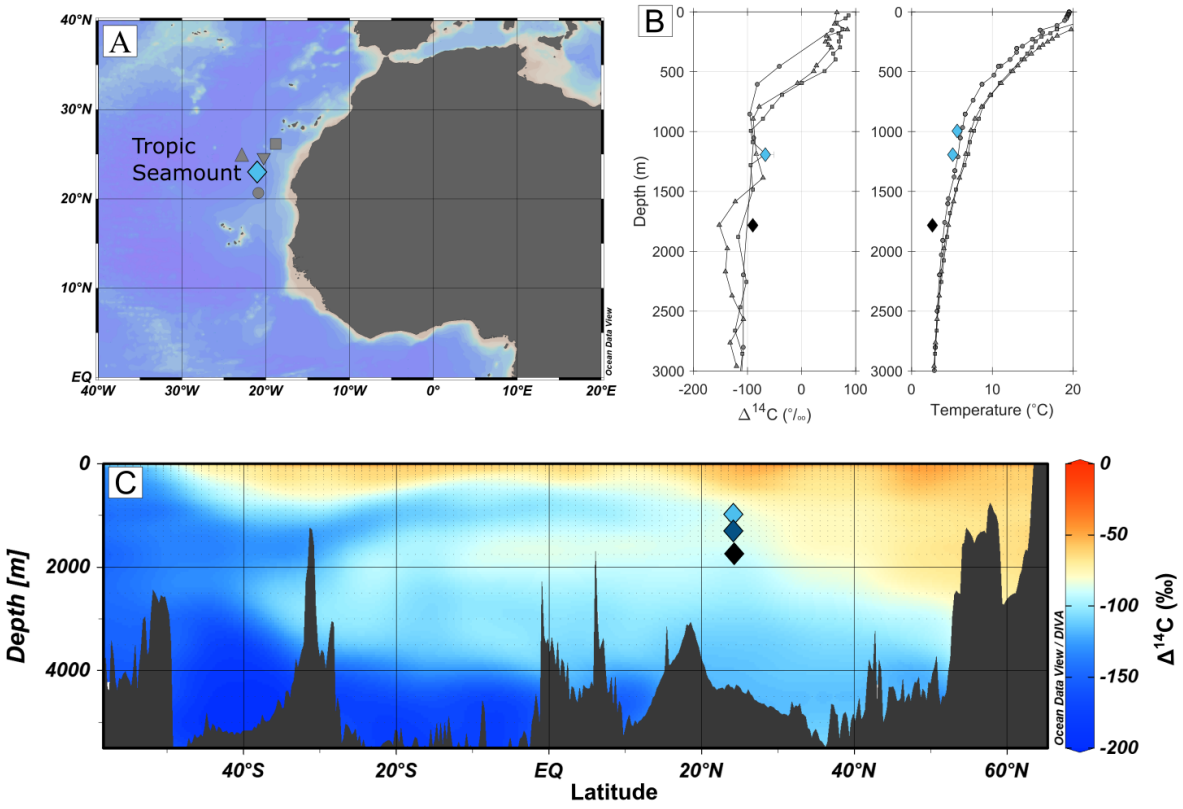

Figure 1: Tropic Seamount location and seawater properties. (A) Map of coral location (Tropic Seamount) and seawater stations used in the profiles. (B) Seawater profiles of $\Delta^{14}C$ and temperature diamonds indicate values measured/reconstructed using modern corals from Tropic Seamount. (C) Seawater $\Delta^{14}C$ bomb-corrected section at Atlantic Ocean (data from GLODAP v2.2020; Olsen et al., 2020), diamonds indicate the location and depth of Tropic Seamount corals.

3.2.2 Radiocarbon analysis

3.2.2.1 Sample preparation

Coral pieces for the radiocarbon analysis were cut and physically cleaned using a drilling tool. Next, approximately 0.03 g of sample were separated from same material used for U-Th isotope dilution

dating after being rigorously oxidative cleaned. Subsequently, the corals were leached in hydrochloric acid (HCl) to remove any potentially adsorbed CO_2. In this process approximately 35% to 50% of total mass of the coral was removed, and the residual sample (~12 mg) were sent for ^{14}C analysis.

3.2.2.2 Analytical techniques and ^{14}C ages

Radiocarbon analyses were performed using a MICADAS accelerator mass spectrometer at University of Bristol (Bristol Accelerator Mass Spectrometer facility, BRAMS). The samples were converted to CO_2 by hydrolyses using phosphoric acid (H_3PO_4), then the CO_2 was converted to graphite by adding H_2 into reaction tubes containing a conditioned iron catalyst (Adkins et al., 2002a; Knowles et al., 2019). Finally, the $^{14}C/^{12}C$ of the graphite was analysed at BRAMS.

Three deep-sea corals were used as matrix-matched standard and blank, which were size matched with the samples and run in the same magazine. The coral standards were U-dated to ~10 ka giving a reproducibility of 1.8‰ (2 s; n=7). Prior to calculating the radiocarbon age of the corals, the fraction modern (Fm) of the coral blank (Fm = 0.002±0.00023 (2 standard deviation, n=7), corresponding to an age of 50.5 ka) was used to correct the Fm of the samples. In addition, oxalic acids standards were run on every batch of samples, which were used to normalize the radiocarbon ages (Knowles et al., 2019). The radiocarbon age (^{14}C age) was calculated using the blank corrected Fm and the Libby mean life (8033, half-life of 5568 yr):

$$^{14}C \text{ age} = -8033 \times \ln(Fm)$$

Analytical uncertainties were processed using the software "BATS" for data reduction (Wacker et al., 2010; Knowles et al., 2019).

3.2.2.3 Calculations of $\Delta^{14}C$ and B-atmosphere

The modern and paleo deep-sea coral radiocarbon data are presented in delta notation which is the age-corrected $\Delta^{14}C$ (Adkins and Boyle, 1997; Chen et al., 2015). This notation accounts for the difference between the conventional ^{14}C age and the calendar age of the sample. The former is calculated using the Libby half-life (see Section 3.2.2.2), while the calendar age is divided by the "real" mean life of ^{14}C (8267, half-life of 5730 yr; Godwin, 1962). The seawater $\Delta^{14}C$ can be reconstructed by

using the U-series age ("Useries age", in years before 1950) and the radiocarbon age ("^{14}C age") of the coral:

$$\Delta^{14}C = \left(\frac{e^{-\,{}^{14}\text{C age}/8033}}{e^{-\,\text{Useries age}/8267}} - 1 \right) \times 1000$$

However, Δ^{14}C is affected by changes in the atmospheric ^{14}C decay inventory. To account for this varying atmospheric radiocarbon inventory, we use the B-atmosphere (B-atm), which is the difference between the radiocarbon age of the coral (^{14}C age) and the contemporary radiocarbon age of the atmosphere ($^{14}Cage_{atm}$):

$$\text{B-atm} = {}^{14}\text{Cage} - {}^{14}\text{Cage}_{atm}$$

This parameter is an effective way to investigate changes related with oceanic processes (e.g., oceanic ventilation, water masses mixing; Chen et al., 2015; Li et al., 2020). In this study, we use the Δ^{14}C of corals to compare with the atmosphere; and the B-atm is preferred to compare the oceanic radiocarbon variability through time. Both atmospheric values are extracted from the calibration curve Intcal20 (Reimer et al., 2020). The data of the radiocarbon parameters is in the Appendix II.

3.2.3 Trace metal analysis

3.2.3.1 Sample preparation

Coral pieces for trace metals analysis were cut and physically cleaned using a drilling tool. Pieces of septa and attached theca were preferred for the solitary cup corals (*Desmophyllum*, *Caryophyllia*, *Javania*), while only the calyxes-theca of colonial corals (*Solenosmilia*) were used, in order to reduce microstructural biases as far as possible (Stewart 2020). Briefly, 10 mg to 20 mg of each sample was crushed using a pestle and mortar. Then, approximately 5 mg of homogeneous powder was oxidative cleaned in warm 1% H_2O_2 (80°C; buffered in NH_4OH), followed by a weak acid polish (0.0005 M HNO_3), followed by dissolution in distilled 0.5 M HNO_3 (Boyle 1981; Rae 2011; Stewart 2020). All samples were replicated to check possible coral skeletal heterogeneity and consequent impact on proxies.

3.2.3.2 Analytical techniques

Trace metal analysis were performed at University of Bristol using a Thermo Element2 ICP-MS. Prior the analysis, the calcium concentration of each sample was measured and then diluted to match 4 mM [Ca] matrix. Aliquots of coral samples were dissolved in 0.5 M HNO_3 and analysed together with matrix-matched, synthetic solutions standards (Stewart et al., 2020) using bracketing standards. All samples were acid-blank corrected, and reference materials (NIST RM 8301c, NIST RM 8301f and JCp-1) were measured at the start and end of the run to check for instrumental drift. The long-term reference materials (n=29) yielded analytical precision of <±1.7% (1 standard deviation) for Li/Ca, Mg/Ca and Sr/Ca. The trace element data are shown in Appendix II.

3.2.3.3 Estimating seawater temperatures

The Li/Mg ratio of the skeleton of aragonitic organisms, including cold-water corals, show a strong correlation with seawater temperature (Case et al., 2010; Montagna et al., 2014; Marchitto et al., 2018). The use of the ratio between Li/Ca and Mg/Ca considerably minimizes the biological vital effects observed in other trace metal and isotope ratios measured in corals (e.g., $\delta^{18}O$, Mg/Ca), making Li/Mg the most suitable proxy for paleo-reconstruction. Here, we use the most recently published curve calibration (Figure 2, uncertainty (2s) of ±3.4°C on 95% prediction interval; Stewart et al., 2020), which demonstrates an exponential relation between seawater temperature (°C) and Li/Mg (mmol/mol) considering a wide range of aragonitic organisms from different locations, and a temperature range of ~30°C to ~0°C.

$$Li/Mg_{coral} = 5.42 \times e^{-0.05 \times T}$$

3.2.4 Compiled data

The ^{14}C data from the atmospheric curve IntCal20 (data available at http://intcal.org/; Reimer et al., 2020) were used to calculate the B-atm of the corals from Tropic Seamount (Section 3.2.2.3). In addition, the three main datasets (atmospheric, marine and speleothem) which comprises the IntCal20 were plotted separately to compare the raw data distribution with the coral data from the interval 33 ka

to 29 ka (Section 3.4.1). The B-atm reconstructions for all data discussed in this chapter were recalibrated to IntCal20 to permit a direct comparison with the new deep-sea coral data from Tropic Seamount.

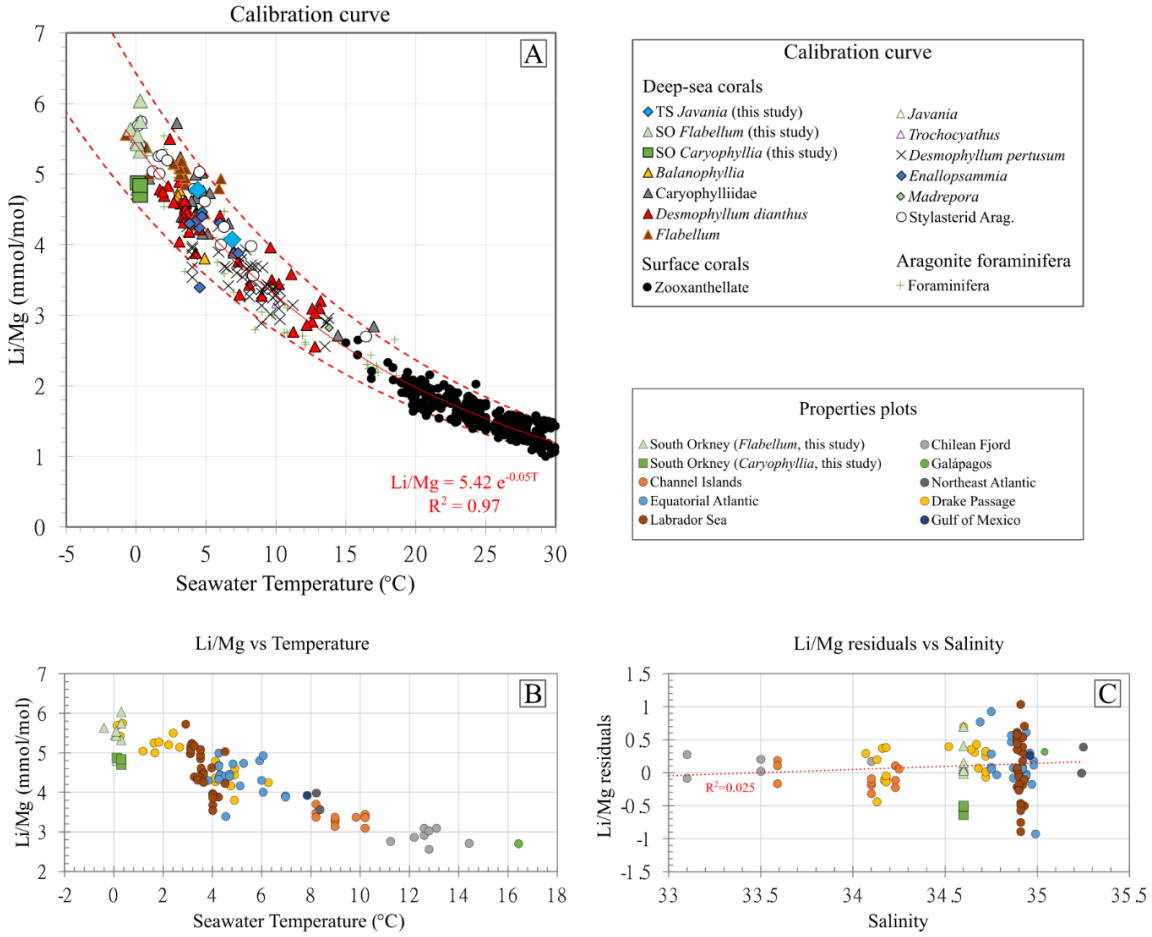

Figure 2: (A) Calibration curve of Li/Mg to seawater temperature for all aragonitic organism (Stewart et al. 2020) including new deep-sea corals from Tropic Seamount: "TS *Javania*" (*Javania caelleti*, light blue diamonds), South Orkney Island: "SO *Flabellum*" (*Flabellum* sp., green triangles) and "SO *Caryophyllia*" (*Caryophyllia* sp., green squares). Dashed lines indicate prediction intervals. (B) Li/Mg ratios of deep-sea corals plotted against temperature coloured by location, data from Stewart et al. (2020). (C) Li/Mg residuals (using the calibration equation from panel A) plotted against salinity. Scatter distribution and no linear correlation (R^2=0.025) reinforces previous findings of low or any impact of salinity on the incorporation of Li/Mg in deep-sea coral skeleton (Case et al., 2010).

3.3 RESULTS

3.3.1 $\Delta^{14}C$ and B-atmosphere

The ^{14}C coral results are presented below using the latest version of the atmospheric calibration curve IntCal20 to derive $\Delta^{14}C$ and B-atm (Reimer et al., 2020). The seawater $\Delta^{14}C$ reconstructed using corals from Tropic Seamount extends from 32.6 ka to 12.8 ka, and two modern samples, a total of 35 corals (Figure 3 and Appendix II). The geochemical analysis of two samples at 1800 m depth suggests they might be altered. The first is a coral dated at 32.62 ka, which has high Mn/Ca and Al/Ca ratios (Figure 4); the other coral dated at 32.22 ka, has $\delta^{234}Ui$ outside the expected values of seawater (Figure 4). $\delta^{234}Ui$ is used as an indicator of closed-system behaviour of the U isotopic system when coral values are within ~7‰ to 10‰ from the seawater values (146.8±0.1‰; Andersen et al., 2010), otherwise it can be an indicative of diagenetic alteration (Cheng et al., 2000; Henderson, 2002; Edwards, 2003; Robinson et al., 2004b). These samples show $\Delta^{14}C$ ~150‰ depletion and similar to the atmosphere, respectively. The other two coral samples from the same depth (~1800 m) aged 32 ka and 31.9 ka show $\Delta^{14}C$ between 200‰ and 300‰ above the atmospheric curve, however there are no geochemical evidence of alteration. The nine shallower-depth (995 m) corals aged between 31.9 ka and 29.1 ka plotted near the atmospheric curve (Figure 3). From 30 ka to 29 ka, the corals show a decrease of $\Delta^{14}C$ similar to the trend in the atmosphere and coinciding with the end of Heinrich Stadial 3 (HS3, 31.5 ka to 29.5 ka).

From 24 ka to the mid-LGM, the $\Delta^{14}C$ values remain near the 100‰ depletion line in comparison with the atmosphere (Figure 3). At 19.5 ka, intermediate-depth corals (1450 m) register a rapid $\Delta^{14}C$ decrease of 107‰ occurring in ~500 yr, therefore shifting from 100‰ to 200‰ depletion compared to the atmosphere (Figure 3). This negative excursion corresponds to a B-atm increase of 520 yr, meaning that the relative age of the local waters shifted from 680 yr at 20 ka to 1200 yr at the mid/end of the LGM in comparison with the contemporaneous atmosphere (Figure 3).

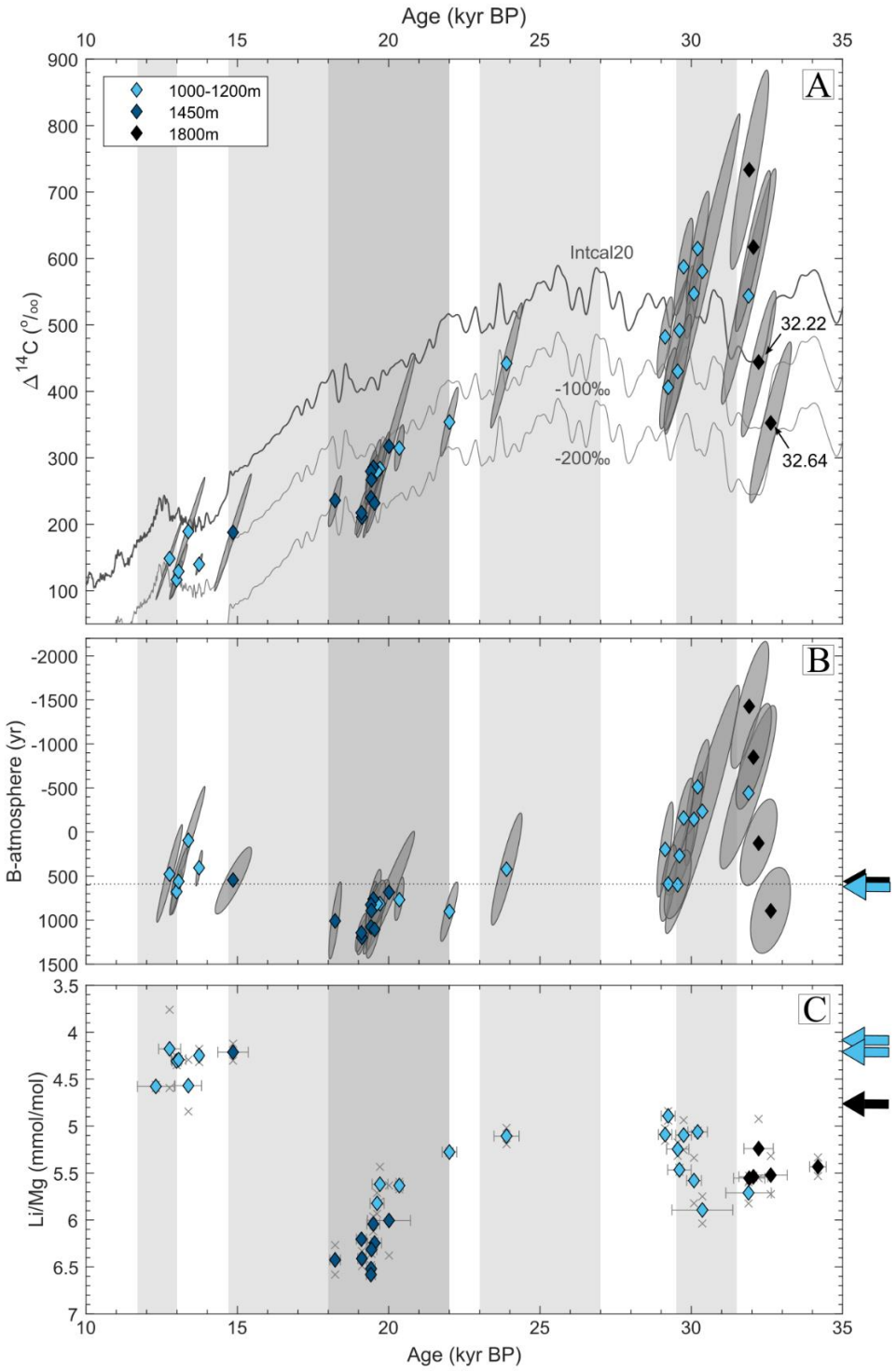

Figure 3: (A) $\Delta^{14}C$, (B) B-atmosphere and (C) Li/Mg ratios of deep-sea corals from Tropic Seamount. (A) The two samples likely altered (indicated by high $\delta^{234}Ui$, and Al/Ca and Mn/Ca, see text) are indicated on the top panel by an arrow and their ages (32.62 ka and 32.22 ka). Grey line indicates IntCal20 (Reimer et al., 2020), and light grey lines show 100‰ and 200‰ depletion in comparison with IntCal20. (B) Arrows on the right-hand side of the B-atmosphere panel indicate values of modern corals, and the colour represents the depth. Errors (2s) are plotted as ellipses, and the colours of the diamonds represent coral depths (see legend). (C) Error bars indicate U-series age errors (2s), "x" symbols indicate replicates, and diamond symbols are the average of the replicates. Arrows on the right-hand side of the panels indicate values of modern corals, the colour represents the depth. Grey shadings indicate climatic intervals: Heinrich Stadial 3 (HS3), Heinrich Stadial 2 (HS2), Last Glacial Maximum (LGM), Heinrich Stadial 1 (HS1), and Younger Dryas (YD).

The $\Delta^{14}C$ shift from 200‰ depletion during the LGM to ~100‰ depletion at the end of HS1, corresponding to B-atm change from 1010 yr to 545 yr, respectively (Figure 3). During the mid Bølling-Allerød (B-A, 14.7 ka to 13 ka), one coral at 13.7±0.09 ka shows a slightly less ^{14}C depleted signature compared to with other deglacial and modern data, equivalent to B-atm value of 406 yr (Figure 3). At 13.4±0.4 ka, another coral shows a low B-atm (94 yr), however this sample exhibits a larger uncertainty and its $\delta^{234}Ui$ value plotted near the accepted variance (~7‰) from the modern seawater value which could indicate some level of diagenetic alteration.

At the start of the YD, the corals from 1223 m and 970 m depth record modern-like ^{14}C values and mean B-atm is 577±200 yr (Figure 3). Two modern samples (*Solenosmilia variabilis* and *Javania caelleti*) from 1193 m and 1783 m depths show B-atm of 615 yr and 559 yr, respectively. These values correspond to a $\Delta^{14}C$ depletion of 67‰ and 90‰, in agreement with modern seawater values (Figure 1B). Therefore, we observed that the Tropic Seamount corals show similar B-atm values to those of modern seawater from the end of HS1 (18.2 ka) and throughout the deglacial interval (15 ka to 12 ka).

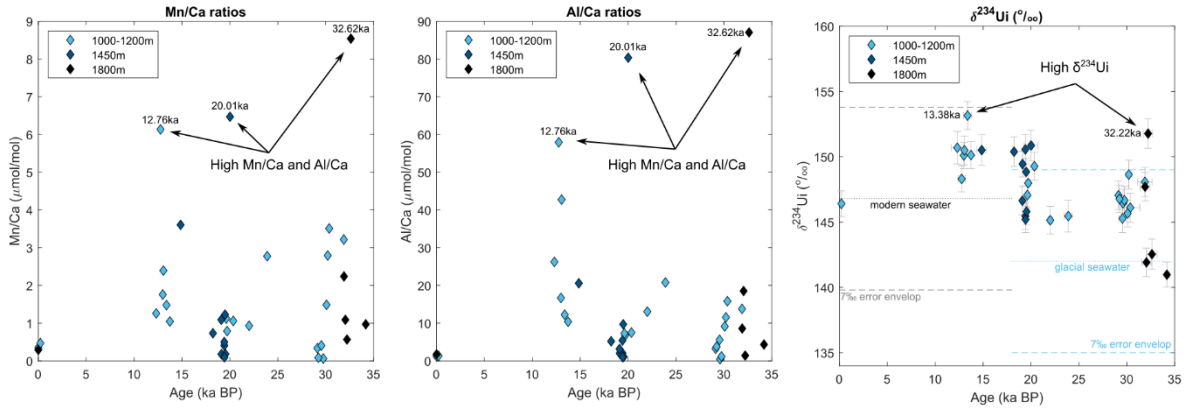

Figure 4: Geochemical parameters indicative of alteration or contamination. Mn/Ca (left), Al/Ca (middle) and $\delta^{234}Ui$ plotted against U-series ages (corrected) of deep-sea corals from Tropic Seamount.

3.3.2 Li/Mg ratios

A total of 38 coral samples were analysed, and the element/Ca ratios reported here (Appendix II) are the average of the replicates. Li/Mg ratios of deep-water coral samples ranged from 4.1 mmol/mol to 6.6 mmol/mol (Figure 3). The difference between the Li/Mg ratios measured in each replicate had a median value of 0.1 mmol/mol, ranging from 0.004 mmol/mol to 0.8 mmol/mol. These ratios

correspond to reconstructed temperatures of 0.4°C (median), 0.01°C and 4°C, respectively. The largest variability within the replicates was found for a sample aged ~12.76 ka suggesting skeletal heterogeneity (Figure 3, Appendix II), one of the replicates show higher Mn/Ca, Al/Ca and Li/Ca (and only slightly higher Mg/Ca) resulting in a reconstructed temperature of 3.3°C (while the other replicate show reconstructed temperature of 7.3°C; Appendix II). Apart from this sample, all the temperature values are within the uncertainties predicted for the calibration curve (±3.4°C, 2*s*) and demonstrate that our samples show minor intra-skeletal variability. Several samples from the LGM show Li/Mg ratios ranging from 6 mmol/mol to 6.6 mmol/mol, which correspond to temperatures of −2°C to −3.9°C (Figure 5) when using the calibration curve equation (Section 3.2.3.3; Stewart et al., 2020). Because the seawater freezing point (for a salinity of ~35) is around −2 °C, temperatures lower than this reconstructed temperature value is unlikely to be correct. In the section below (Section 3.3.3), this extreme low temperature during the LGM is addressed, including the Li/Mg ratio results of 12 new modern deep-sea coral samples from low temperature waters.

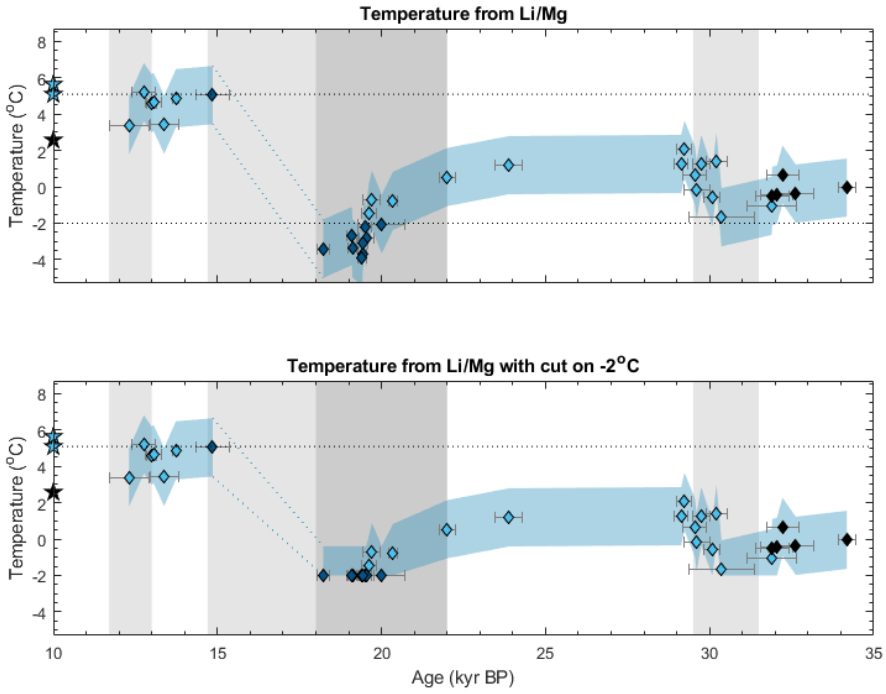

Figure 5: Seawater temperature reconstructed from Li/Mg ratios from deep-sea corals. Top panel show temperatures using Li/Mg calibration equation (Section 2.3.3; Stewart et al., 2020), while lower panel includes a cut-off value of −2°C (see Section 3.3 for details). Dotted lines at 5°C indicate modern seawater temperature at depth of 1000 m for reference, and dotted line at −2°C indicates the seawater freezing temperature used as cut-off value (Section 3.3). Stars in the left y axis of the panels indicate values of modern corals, the colour represents the depth.

3.3.3 Investigating low temperatures derived from the Li/Mg proxy

During the LGM, direct use of the existing calibration causes the Li/Mg ratios to convert to apparent temperatures as cold as −3.9°C (Section 3.3.2; Figure 5). This temperate is below the freezing point of seawater, so cannot be real. Here, three ideas were explored to investigate possible explanations for this apparently low temperature: (i) increased salinity of LGM seawater and corresponding lowering in seawater's freezing point; (ii) salinity effects on the Li/Mg ratios; and (iii) testing the calibration at low temperatures by the measurement of 12 live-collected corals from cold (~0°C) seawater from the South Orkney Islands (60°S, 45°W).

During the LGM, the ocean was approximately 3‰ saltier than modern (Adkins et al., 2002b). To test if this change in salinity could account for the change on the seawater freezing point from −2°C to −3.9°C, the following equation (Fofonoff and Millard Jr, 1983) can be applied to calculate the freezing point of seawater (T in °C), which is a function of salinity (S) and pressure (p in dbar):

$$T_f(S,p)=\left(-0.0575 + 1.7105\ 10^{-3}\ \sqrt{S}\ - 2.1545\ 10^{-4}\ S\right) S\ - 7.53\ 10^{-3}\ p$$

The calculated freezing temperature of the seawater at the sea surface (p = 0) for a salinity of 35 (global modern average) is −1.922°C. For a hypothetical 3‰ saltier LGM seawater (salinity of 38) the freezing point would drop to −2.095°C, a difference of only 0.17°C. The salinity required to reproduce temperatures of −3.9°C occurring at the sea surface without freezing would be ~68, which is unrealistic. Therefore, we rule out the possibility that seawater temperatures would have reached −3.9°C during the LGM.

To investigate the possible effect of the salinity on coral Li/Mg ratios, we calculated the residuals of the Li/Mg from the temperature calibration, using the dataset of Stewart et. al (2020) and the new Li/Mg ratios of the corals from South Orkney (see also below). The residuals were then cross plotted against seawater salinity data, which show no correlation (Figure 2C). In agreement, the effect of salinity into the incorporation of Li and Mg on deep-sea corals has been previously investigated by Case et al. (2010). They showed an insignificant correlation between Li/Mg and salinity for a salinity range of 34 to 36.5 (Case et al., 2010). Together these evidence suggest little influence of salinity on the incorporation of Li and Mg.

The low number of samples at temperatures around or below 0°C of the calibration curve (Stewart et al., 2020), motivated the new measurements presented here of 12 live-collected scleractinian corals (*Flabellum* sp. and *Caryophyllia* sp.) from waters of temperatures ranging from −0.4°C to 0.3°C from the South Orkney Islands. The Li/Mg ratios ranged from 4.6 mmol/mol to 6.3 mmol/mol (Figure 2A), which corresponds to a temperature range of 3°C, thus within the predicted uncertainty of the existing curve (±3.4°C, 2s; Stewart et al., 2020). The new samples plotted near the calibration curve, and there is no significant change between the updated calibration equation and the one from Stewart et al. (2020). This finding supports the applicability of the calibration curve for aragonitic organisms from 25°C to −0.4°C.

Despite our findings above, it is of course possible that the future development of local-specific and/or species-specific calibrations may improve the Li/Mg conversion to temperature. Thus, further measurements of Li/Mg ratios from modern aragonitic organisms living in other regions of extremely cold waters would be valuable improve our understanding on the biomineralization mechanisms and its temperature relation. As well as the assessment of the diagenetic alterations of fossil corals into their Li/Mg ratios. Given that we know that the freezing point of seawater is around −1.9°C, then , we apply a minimum of −2°C as a cutoff value for samples of high Li/Mg (Figure 5).

3.3.4 Seawater temperature from Li/Mg ratios

During the last glacial interval (34 ka to 18 ka), the reconstructed seawater temperatures of Tropic Seamount show values lower than modern seawater, consistently lower than 2°C (Figure 5). From 30.4 ka to 29.1 ka, a warming of ~3.5°C is observed coinciding with the end of HS3 (Figure 5). Then, a gradual cooling is observed from 23.9 ka until the mid-LGM, when the waters at 1450 m reach temperatures of −2°C (Figure 5). Finally, temperatures increased towards modern-like values around 5°C during at 15 ka (Figure 5). Two slightly colder temperatures (~3.4°C) are observed at 13.4 ka and 12.3 ka, coincident with the B-A and YD (Figure 5). However, this variation is within the uncertainties of the modern-like temperate. In comparison, reconstructed temperatures of three modern corals were 5.6°C (*Javania caelleti*), 5.1°C (*Solenosmilia variabilis*) and 2.6°C (*Javania caelleti*), for depths of 995

m, 1220 m, and 1780 m. These values are in good agreement with modern seawater temperature (Figure 1B).

3.4 DISCUSSION

3.4.1 High ^{14}C values between 33 ka to 29 ka?

Our radiocarbon data from the interval between 33 ka and 29 ka suggests enrichment in ^{14}C of intermediate waters (Figure 6; 1000 m to 1800 m). In some cases, the $\Delta^{14}C$ even plots above the atmospheric curve. These elevated and highly variable $\Delta^{14}C$ values of the corals from this interval are an intriguing feature. In this section, a brief discussion is presented considering the possible reasons for the ^{14}C signature of these corals, including coral diagenesis, uncertainties of the atmospheric calibration curve, and the large variability of $\Delta^{14}C$ from previously published data from this interval.

Previous studies had investigated the potential sources of CO_2 contamination in deep-sea corals (Adkins et al., 2002a). They demonstrate that the cleaning of the samples is crucial for an accurate determination of the seawater $\Delta^{14}C$. The first is the removal of the Fe-Mn crusts that often covers fossil corals and which may contain organic carbon from secondary precipitation (Adkins et al., 2002a). The removal of this crust is effectively made on the first physical cleaning of the sample, additionally all radiocarbon samples pass through a rigorous oxidative cleaning (Section 3.2.2.1). Another factor for concern is absorption of modern CO_2 into the coral skeleton. To account for this potential source of contamination, all coral samples are leached in weak HCl immediately prior to the CO_2 graphitization procedure, this leaching removed ~35% of the sample mass. This is a well-established procedure, and it is shown to successfully remove modern CO_2 in coral samples with at least 5% of its mass leached (Adkins et al., 2002a).

The observation that the $\Delta^{14}C$ of the intermediate depths of the ocean (Tropic Seamount) are higher than the contemporaneous atmosphere is clearly in odds with the fact that the atmosphere is the source of radiocarbon to the oceans. An alternative explanation for this "elevated" $\Delta^{14}C$ registered by the deep-sea corals at Tropic Seamount could be related to the uncertainties on both the ^{14}C of the corals and the atmospheric ^{14}C record. The IntCal20 at this time interval is reconstructed using ^{14}C data of plant macrofossil (Lake Suigetsu varved sediment macrofossil data), speleothem (Hulu cave), tree-ring (New

Zealand kauri) and foraminifera (Reimer et al., 2020 and references herein). One complicating factor is the age model of each of these data sets, but sophisticated statistical approaches are applied to the IntCal20 to account for such uncertainties on calendar ages (Heaton et al., 2020b). However, the authors point out that it is specifically challenging when comparing, for instance, Hulu cave and Lake Suigetsu. Even though the same features are observed in both data sets, the timescales are slightly offset. If the datasets are not precisely aligned, then merging them together could result on either an overly smooth or the complete loss of some features (Heaton et al., 2020b).

Nonetheless, here we do not intend to discuss the assumptions and corrections that are applied to each of these records but to point out the wide scatter on the dataset which comprises the IntCal20 around these ages. When we plot our deep-sea coral-based $\Delta^{14}C$ together with data from IntCal20, we observe that they fall within the variability of this overall dataset, even though they are higher than the average curve (Figure 6). Similar observations are made when comparing our ^{14}C data, IntCal20 and previous published surface corals and deep-sea corals (Figure 6). For instance, in the South Atlantic (Brazilian margin; Mangini et al., 2010), Southern Ocean (off Tasmania; Hines et al., 2015), and Northwest Atlantic (Robinson et al., 2005) deep-sea coral based $\Delta^{14}C$ also show atmospheric-like (or above) values from similar time interval (Figure 6). Similar high ^{14}C was also recorded by benthic foraminifera at Baja California (Cariaco Basin, south Caribbean Sea) around 36 to 33 ka (Marchitto et al., 2007). Furthermore, radiocarbon values higher than the average IntCal20 curve are also observed for surface corals at tropical Atlantic and Pacific oceans, especially around 30 ka and older than 35 ka (Figure 6; Fairbanks et al., 2005; Durand et al., 2013). Together this evidence suggest that the radiocarbon values of the atmosphere could be higher than shown by the average IntCal20 curve, or that some features could be underrepresented.

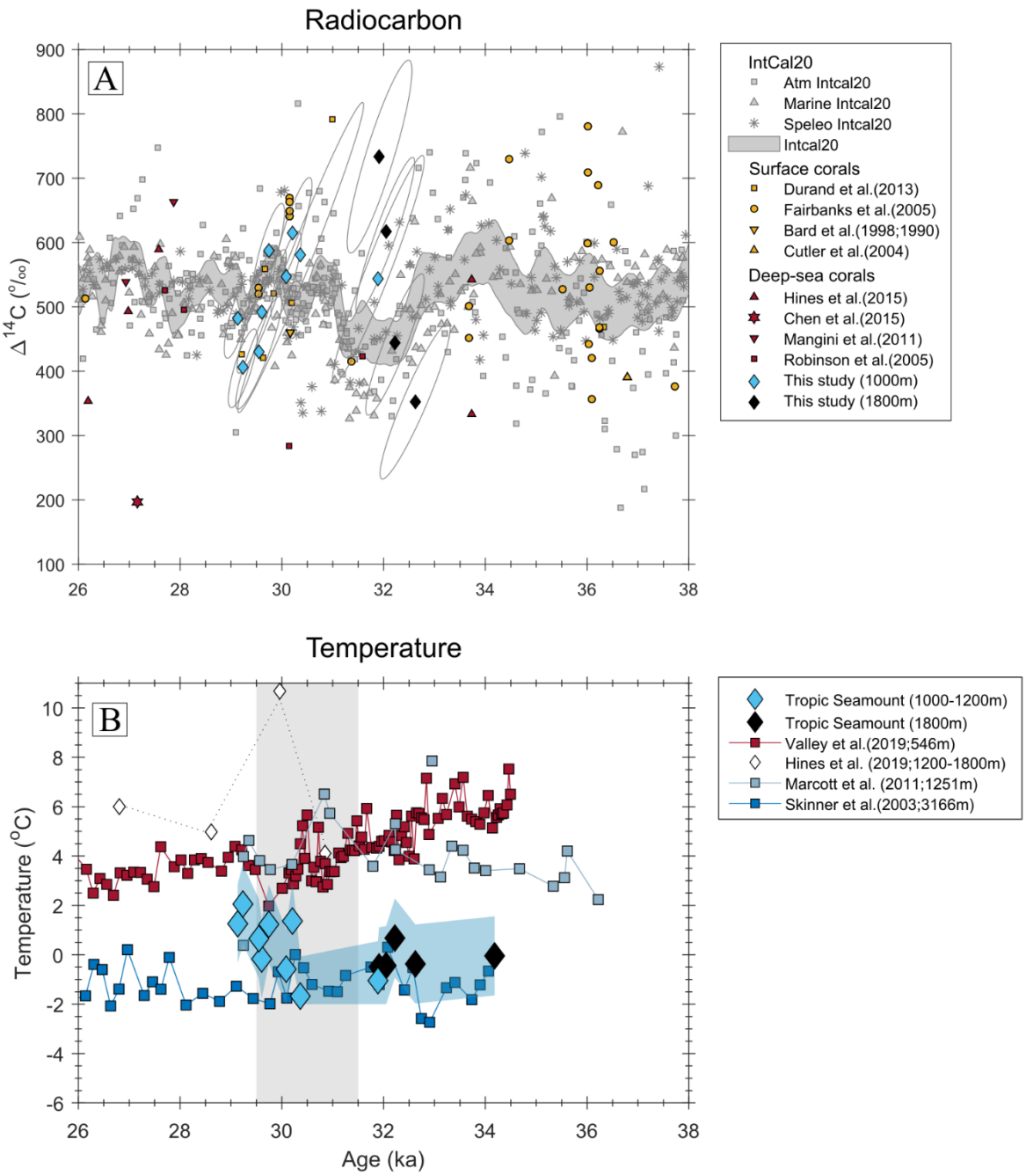

Figure 6: Radiocarbon and temperature from Tropic Seamount corals compared to published data from the interval of 26 ka to 38 ka. (A) $\Delta^{14}C$ of Tropic Seamount (blue and black diamonds) compared with reconstructions of IntCal20 (grey symbols representing atmospheric, marine and speleothem), surface corals (yellow symbols) and previous published deep-sea corals (red symbols). Large scatter is observed on all records for this time interval. (B) Temperature of Tropic Seamount (blue and black diamonds) compared with reconstructions of intermediate Northwest Atlantic (Marcott et al., 2011; Valley et al., 2019; Hines et al., 2019) and deep Northeast Atlantic (Skinner et al., 2003).

3.4.2 HS3: a well-ventilated intermediate ocean?

Taking into account the considerations from section 3.4.1, observations of the ^{14}C and temperature changes during 33 ka to 29 ka are discussed below. Overall, the radiocarbon data from this interval suggest that the intermediate waters were more elevated in ^{14}C, and the temperatures colder than modern seawater at Tropic Seamount (Figure 6). The cooler oceanic temperatures are expected because this interval is within the last glaciation, although it precedes the LGM. At the mid- to end of HS3 (30 ka to 29 ka), the corals at Tropic Seamount registered a warming of ~3.5°C (Figure 6) simultaneous with a drop in $\Delta^{14}C$ towards the depletion line of -100‰ which agrees with modern-like values (Figure 6). The contemporaneous decrease in $\Delta^{14}C$ at Tropic Seamount and in the atmosphere (Reimer et al., 2020) suggests that the intermediate waters (995 m depth) at Tropic Seamount maintained a close link with the atmosphere.

During Heinrich Stadials, models suggest that a decrease in AMOC strength, and corresponding decrease in cold deep-water convection, would promote a warming of subsurface and intermediate depth waters (Galbraith et al., 2016; Umling et al., 2019). Previous reconstructions of temperature in the North Atlantic support this hypothesis showing a warming of intermediate depth waters (1250 m) started pre-HS3 and peaking at the mid-HS3, and no changes in deeper depths (3100 m; Figure 6; Skinner et al., 2010; Marcott et al., 2011). In contrast, temperature reconstruction from the tropical Northwest Atlantic show a cooling trend punctuated by a rapid warming at mid- and late-HS3 (Figure 6; Valley et al., 2019). The temperature reconstruction from Tropic Seamount show a warming from mid- to late-HS3 (~29.5 ka) which resembles the late warming observed in the tropical Northwest Atlantic (Figure 6). Coral data from ~1650 m in the Northwest Atlantic also suggests a warming during the mid-HS3, however the low resolution hinder further interpretation (Figure 6; Hines et al., 2019). Curiously, a low magnitude temperature increase is observed in Antarctic and Greenland ice cores at a similar time (Bazin et al., 2013; Kindler et al., 2014). In the intermediate South Atlantic, temperatures show a warming at depths of the modern NADW (1300 m and 1900 m) but not at shallower depths (~1100 m; Umling et al., 2019). Together this evidence likely suggests that the warming during the end of HS3 observed in the tropical North Atlantic, and perhaps the deeper (>1300 m) site at South Atlantic,

was not advected from the Southern Hemisphere, but possibly from the North Atlantic, and/or heat gain via downward diffusion.

3.4.3 LGM: northward AAIW extension

During the LGM, the intermediate waters at Tropic Seamount show larger ^{14}C age offsets from the contemporary atmosphere (B-atm around 750 to 1200 yr-^{14}C) compared with deglacial and modern values (B-atm ~600 yr-^{14}C; Figure 7). Overall, this result is in agreement with observations of deep and intermediate waters in the wider North Atlantic (Freeman et al., 2016; Ezat et al., 2017; Skinner et al., 2017), South Atlantic (Barker et al., 2010) and Southern Ocean (Hines et al., 2015; Li et al., 2020), all suggesting more depleted ^{14}C waters than modern during the LGM. Despite this overall similarity, a radiocarbon gradient is observed between the intermediate and deep waters. The ^{14}C values of the intermediate depths at the Tropic Seamount agrees with other intermediate water sites (Cléroux et al., 2011; Sortor and Lund, 2011; Chen et al., 2015; Lund et al., 2015; Freeman et al., 2016; Skinner et al., 2017), which remain about 500 to 1000 ^{14}C-yr less depleted than the deep waters at North and South Atlantic (Barker et al., 2010; Freeman et al., 2016; Skinner et al., 2017; Ausín et al., 2021). Curiously, our glacial temperatures are in agreement with temperature reconstructions of both deep North Atlantic and intermediate high-latitude South Atlantic, all showing values close to freezing point of seawater (Figure 8; Adkins et al., 2002b; Skinner et al., 2003; Roberts et al., 2016). The occurrence of similar cold temperatures at intermediate depths at Tropic Seamount, high latitude South Atlantic and deep North Atlantic, but significantly different ^{14}C values between the intermediate and deep Atlantic, favour the hypothesis of a glacial ocean stratification not controlled by temperature, but other properties, perhaps salinity as previous proposed (Adkins et al., 2002b; Roberts et al., 2016).

Two main mechanisms have been discussed to explain the depletion of ^{14}C observed in the glacial ocean: a less efficient sea-air ^{14}C exchange due to lower atmospheric CO_2 partial pressure and oceanic surface conditions (e.g., extended sea-ice); and changes in the global overturning circulation (Rahmstorf, 2002; Ferrari et al., 2014; Galbraith et al., 2015). The lower atmospheric CO_2 partial pressure during the LGM was estimated to account for approximately 250 ^{14}C-yr depletion in comparison with the modern surface water age (Galbraith et al., 2015). During the early-LGM, our

deep-water coral-based B-atm show a difference of ~180 ^{14}C-yr compared to the modern B-atm values, which could be explained solely by the low-CO_2 partial pressure effect. However, at 19.5 ka, this B-atm difference at Tropic Seamount rapidly increases to ~500 yr-^{14}C while no change is observed at the atmospheric CO_2 concentration, nor at the atmospheric $\Delta^{14}C$ of Northern Hemisphere (Marcott et al., 2014; Reimer et al., 2020), pointing towards an oceanic mechanism to explain this variation.

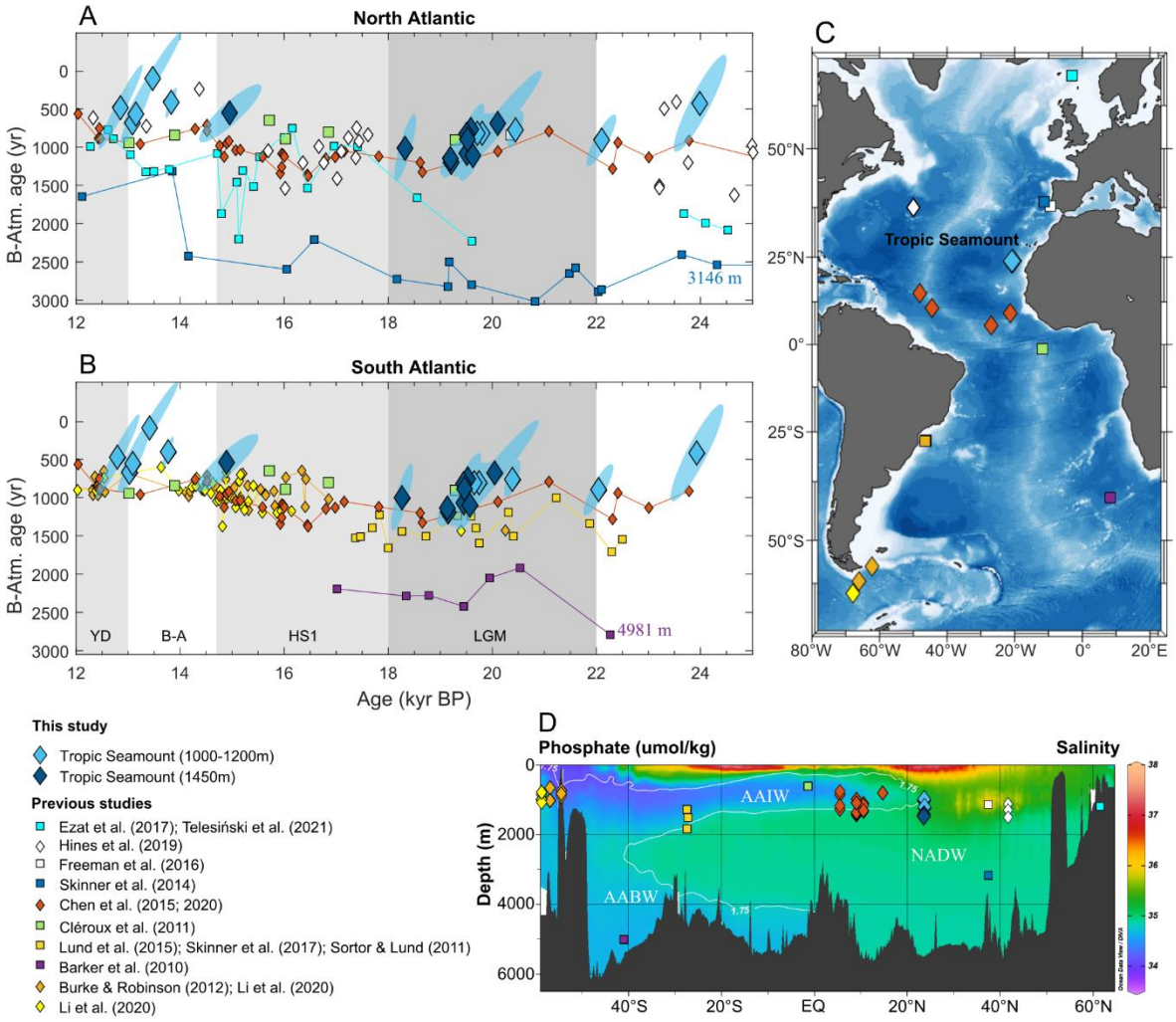

Figure 7: B-atmosphere compilation from sites at Atlantic Ocean and new coral data at Tropic Seamount from 12 ka to 25 ka. B-atm values of deep-sea corals (diamonds) and benthic foraminifera (squares) from (A) North and (B) South Atlantic. B-atm errors (2s) of corals from Tropic Seamount are plotted as ellipses, compiled data are shown without errors. (C) Map of Atlantic Ocean indicating the sites location shown at A and B. (D) South-North Atlantic Ocean section indicating the depth distribution of the sites shown at A and B, colours represent seawater salinity, and white line indicate phosphate concentration of 1.75 µmol/kg. The intermediate depth tongue indicated by phosphate concentrations >1.75 µmol/kg and lower salinities (~34.5, blue colour) represents Antarctic Intermediate Water (AAIW) extension; the North Atlantic Deep Water (NADW) is recognized by higher salinities (~35, green colour), and the Antarctic Bottom Water (AABW) are the waters near the sea floor at Southern latitudes (hydrological data from GLODAP v2.2020; Olsen et al., 2020).

The B-atm excursion at 19.5 ka observed at Tropic Seamount shifted from 680 yr-^{14}C to 1200 yr-^{14}C in approximately 500 yr. ^{14}C reconstructions from other locations of the Atlantic and Southern oceans do not show similar rapid changes (Sortor and Lund, 2011; Chen et al., 2015, 2020; Lund et al., 2015; Skinner et al., 2017), so we speculate that this signal must be related to increased mixing with ^{14}C-depleted water rather than changes in the ^{14}C signature of the water masses. However, it is worth mentioning that the lack on observed ^{14}C excursion in other locations could be an artefact of a lower resolution of these records compared with our reconstruction which has a large abundance of corals during this short time interval. This high abundance also strengthens our confidence on this trend being a real feature.

Studies focusing on reconstructing the AMOC strength have suggested a decrease starting prior HS1 (McManus et al., 2004; Meckler et al., 2013; Ng et al., 2018). Several studies have linked this AMOC perturbation to changes in seawater properties and ocean configuration. For instance, a weakened AMOC is associated with a warming of intermediate waters at North Atlantic, due to less formation of NADW (Marcott et al., 2011); an expansion of AAIW to equatorial Atlantic (Pahnke et al., 2008; Poggemann et al., 2017); and a deepening and thickening of AAIW at Atlantic Ocean (Gu et al., 2017). In the modern water column configuration, the depth where the ^{14}C excursion occurred (1450 m) is the transition zone between AAIW and NADW (Figure 7). This makes our site suitable for tracing the contribution of each of these water masses during AMOC perturbations. We found that the glacial B-atm values of deep and intermediate-North Atlantic (2500 ^{14}C-yr and 2000 ^{14}C-yr; Skinner et al., 2010; Ezat et al., 2017; Telesiński et al., 2021) are larger than the B-atm of waters at modern depths of AAIW (and upper Circumpolar Deep Water, uCDW) at the Drake Passage (1430 ^{14}C-yr; Figure 7; Li et al., 2020). The latter are within error of the B-atm observed at the intermediate waters of Tropic Seamount (1200 ^{14}C-yr), thus suggesting larger contribution of AAIW during the mid to late-LGM at this location.

An alternative mechanism to explain the mid LGM radiocarbon decrease would be a shoaling of NADW as suggested by a number of biochemical proxies at the LGM (Curry and Oppo, 2005; Yu et al., 2008; Gebbie, 2014). However, the B-atm values at Tropic Seamount (1200 ^{14}C-yr) are still significantly more ^{14}C enriched than records of NADW, which shows values around 2000 ^{14}C-yr

(Skinner et al., 2003; Ezat et al., 2017; Telesiński et al., 2021). This observation again supports the larger contribution of AAIW, and not NADW, to the Tropic Seamount during the LGM.

3.4.4 Deglaciation: transition to modern-like seawater configuration

The most pronounced changes in temperature and radiocarbon in our new record occur during the last deglaciation, when the intermediate waters at Tropic Seamount shift to modern-like seawater values (~500 ^{14}C-yr; Figure 8). From the LGM to the end of HS1, the corals from Tropic Seamount register a warming of approx. 7°C and a decrease of 460 ^{14}C-yr in B-atm. During this time, a gradual increase of Antarctic δ^{18}O is interpreted as a Southern Hemisphere atmospheric warming of ~6°C (Figure 8; Parrenin et al., 2013). In contrast, the δ^{18}O of Northern Greenland (NGRIP) indicates a cold period followed up by an abrupt warming at the transition of HS1 and B-A suggesting a later warming of the Northern Hemisphere atmosphere (Figure 8; Kindler et al., 2014). The assessment of the timing of the start of temperature and radiocarbon change at Tropic Seamount is impeded by a temporal gap in coral occurrence during HS1 (de Carvalho Ferreira et al., 2022). Furthermore, the age uncertainty (±506 yr, 2s) of the coral sample at late-HS1 makes it difficult to correlate with Southern or Northern atmospheric warming events. Therefore, we compare our data to previous published studies from different sites at the Atlantic Ocean to investigate the mechanisms and sources of this switch to modern-like conditions.

During HS1, several proxies indicate a weakening of the AMOC (McManus et al., 2004; Böhm et al., 2015; Ng et al., 2018). Paleoceanographic and modelling results suggest that during a weak AMOC the subsurface and intermediate waters would warm as a response to lesser formation and export of the cold NADW; and/or a build-up of heat at lower latitudes and a downward diffusion of heat to the ocean interior (Rühlemann et al., 2004; Marcott et al., 2011; He et al., 2020). Indeed, several studies show a warmer tropical and equatorial Atlantic during the HS1, what seems to validate this hypothesis (Marcott et al., 2011; Thiagarajan et al., 2014; Weldeab et al., 2016; Poggemann et al., 2018; Max et al., 2022).

Recently, temperature reconstructions from the intermediate depth of the South Atlantic suggest a correlation between HS1 warming and weaker AMOC (Umling et al., 2019). The authors further show that a warming at 1000 m and 2000 m depths is likely a result of the transport of warmer southern and northern sourced waters, respectively. In agreement, a warming is also reported in the North Atlantic

during the HS1 (Poggemann et al., 2018; Hines et al., 2019; Valley et al., 2019). But in this case, the interpretations diverge from southern-source warming (Poggemann et al., 2018), northern source warming (Valley et al., 2019), and downward heat diffusion (Weldeab et al., 2016; Hines et al., 2019). Independently of the heat source, all studies demonstrate that the intermediate Atlantic Ocean thermally responds to perturbations of AMOC. Our temperature reconstruction at Tropic Seamount corroborates with this observation of a generalized warmer intermediate waters at Atlantic Ocean during a weakened AMOC. To investigate the source of the intermediate waters at Tropic Seamount, the ^{14}C signature of seawater at different sites is compiled and compared with our data.

During early-HS1 (~18 ka to 16 ka), the intermediate waters in the Drake Passage, equatorial Atlantic, tropical Atlantic and North Atlantic all show a similar ^{14}C signature suggesting that these waters had remained well-ventilated (Figure 8; Burke and Robinson, 2012; Chen et al., 2015, 2020; Ezat et al., 2017; Hines et al., 2019; Li et al., 2020). During the late-HS1, the waters from the Faroe-Shetland Channel show a B-atm increase of 1200 ^{14}C-yr (Figure 8), indicating either a reduction of the formation of this water mass or an increased contribution of a ^{14}C-depleted waters (Ezat et al., 2017; Telesiński et al., 2021). Independently of the mechanism, this signal is not shown to be transported to the equatorial Atlantic (Figure 8; Chen et al., 2015, 2020). Instead, the intermediate depth equatorial Atlantic remains well-ventilated in close agreement with the ^{14}C signature of the waters from the Drake Passage (Figure 8; Burke and Robinson, 2012; Li et al., 2020). This evidence points to a lesser contribution of waters from the Faroe-Shetland Channel (NADW) to equatorial and tropic North Atlantic during the late-HS1.

It is worth noting that a study using benthic foraminifera from south of Iceland (1237 to 2303 m) suggested "extremely" ^{14}C-depleted waters during deglacial cold intervals (e.g., HS1 and YD; Thornalley et al., 2011b). Similarly, deep-sea coral data off the Brazilian margin (621 m and 781 m) also show a trend towards ^{14}C-depleted water, although of a smaller magnitude during HS1 and YD (Mangini et al., 2010). Both studies evoke the presence of ^{14}C-depleted AAIW. The former study has been suggested to be biased by the use of some species of benthic foraminifera which poses challenges in the interpretations (Ezat et al., 2017). The latter study reconstruct the ^{14}C using deep-sea corals from a sediment core in pockmark fields, although the authors had ruled out the influence of methane due to

the low correlation and no significant change of $\delta^{13}C$ (Mangini et al., 2010). However, the "extremely" depleted ^{14}C signatures observed during the YD and early-Holocene (B-atm up to 3300 ^{14}C yrs) in comparison with records from the South and North Atlantic (850 to 500 ^{14}C yrs) suggest an alternative source of C to this corals. A possible process would be the influence of ^{14}C-dead CO_2 and carbon-rich fluids on the coral skeleton after they were buried. This process was suggested to account for several ^{14}C depletions on records in the Pacific Ocean (Stott et al., 2019). However the implications of this process for the carbon cycle remain puzzling (Skinner and Bard, 2022).

Based on our ^{14}C and temperature compilation, we suggest that the waters at Tropic Seamount during the early glaciation was mainly composed of southern-sourced waters (AAIW/uCDW). An increase of AAIW contributions to tropical Atlantic Ocean is further supported by increased Cd_w (Figure 8), lower $\delta^{18}O$ and $\delta^{13}C$ data (Poggemann et al., 2017; Valley et al., 2017). During its northward transport, AAIW likely incorporated warmth through downward diffusion in the South Atlantic, equatorial and tropical North Atlantic reaching the Tropic Seamount as a ^{14}C-enriched and warm water. During the YD, the ^{14}C signature of both Northern and Southern waters agrees with the values at equatorial and tropical Atlantic (Figure 8), likely indicating the influence of both water masses to the intermediate waters. This scenario is in line with the modern circulation and composition of intermediate waters at tropical Atlantic, where AAIW is mixed and incorporated into other water masses (Talley et al., 2011a).

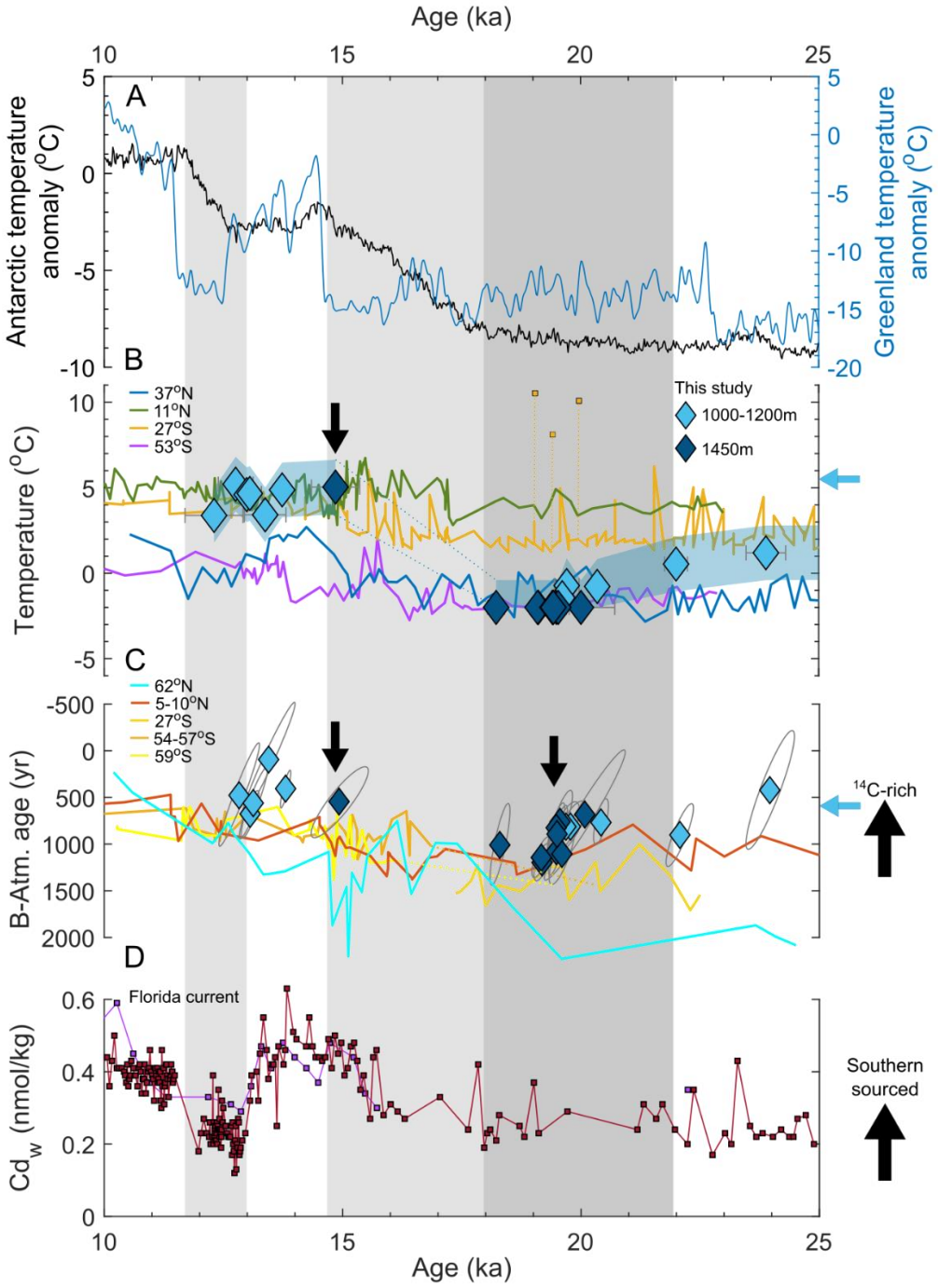

Figure 8: Compiled climatic records from 25 ka to 10 ka. (A) Antarctic (back line) and Greenland (blue line) temperatures anomalies in relation to Holocene temperatures (Parrenin et al., 2013; Kindler et al., 2014). (B) Seawater temperature reconstructions at Atlantic Ocean sites: Tropic Seamount (23°N, blue diamonds, this study), Iberian margin (37°N, 3146 m, dark blue line, Skinner et al., 2003), tropical NW Atlantic (11°N, 852 m, green line, Poggemann et al., 2018), Brazilian margin (27°S, 1100 m, yellow line, Umling et al., 2019), Drake Passage (53°S, 598 m, purple line, Roberts et al., 2016). Blue shading indicates 1s (±1.6°C), blue arrow at left y axis indicates modern temperature at Tropic Seamount. (C) B-atm reconstructions at Atlantic Ocean sites: Tropic Seamount (23°N, blue diamonds, this study), Faroe-Shetland Channel (62°N, 1179 m, Ezat et al., 2017), equatorial North Atlantic (5°N to 10°N, 749 m to 1431 m, Chen et al., 2015, 2020), Brazilian margin (27°S, 1268 m to 1820 m, Lund et al., 2015; Skinner et al., 2017; Sortor & Lund, 2011), Drake Passage "AAIW" (54°S to 57°S, 648 m to 1012 m, (Burke and Robinson, 2012; Li et al., 2020), Drake Passage "uCDW" (59°S, 776 m to 1064 m, Li et al., 2020). Error ellipses indicates 2s, blue arrow at left y axis indicates modern B-atm at Tropic Seamount. (D) Cd_w reconstruction at Florida strait (Valley et al., 2019) and Florida current (Came et al., 2008).

3.5 CONCLUSIONS

The new results of radiocarbon combined with temperature at the intermediate waters support a tight link between South Atlantic and Tropic Seamount, and points to a thermal response of intermediate ocean to AMOC perturbations. Elevated ^{14}C during the interval between 33 ka and 29 ka suggests a well-ventilated intermediate ocean. We demonstrated that there is a wide scatter in the available data during this interval, including the data set of the Northern Hemisphere Atmospheric curve (IntCal20), which agrees with our deep-sea coral data. During the LGM, a rapid depletion in ^{14}C gives the intermediate waters at Tropic Seamount a characteristic AAIW (and uCDW) ^{14}C-signature in similarity with values measured in the equatorial Atlantic, South Atlantic and Drake Passage. These findings support a similar water mass extending from South to tropical North Atlantic maintaining a well-ventilated intermediate-depth Atlantic Ocean.

During HS1 the intermediate waters at Tropic Seamount warmed and increased its ^{14}C content reaching modern-like conditions. This warming agrees with a general warmer subsurface and intermediate Atlantic Ocean likely associated with a weakened AMOC. Based on an Atlantic Ocean ^{14}C compilation, we argue that, during the early deglaciation, the intermediate waters at Tropic Seamount are mainly composed of AAIW, which incorporates heat during its transport northwards through downward diffusion in South Atlantic, equatorial and tropical North Atlantic. Finally, we addressed the extremally low temperatures resulted from high Li/Mg ratios during the LGM. We found that the hypothesized saltier glacial ocean could not account for such low temperatures, and that Li/Mg ratios in modern corals show no correlation with salinity. The measurement of additional 12 live collected coral samples from low temperature seawater demonstrate the reliability of the Li/Mg calibration curve, but point out the need to apply a cut off limit of −2°C to high Li/Mg.

Chapter 4: LINKING OCEANIC CIRCULATION AND TEMPERATURE VARIABILITY IN THE SOUTHWEST ATLANTIC SINCE 50 KA USING ^{14}C AND LI/MG IN DEEP-SEA CORALS

Abstract

The ocean is a key player in regulating the climate. During the last glacial to deglacial interval perturbations in the Atlantic Meridional Overturning Circulation (AMOC) have been linked with atmospheric CO_2 and temperature changes. Perturbations of the AMOC have also been hypothesized to have caused oceanic temperature variations. To test this hypothesis, we reconstructed the temperature of the intermediate Southwest Atlantic using Li/Mg ratios of deep-sea corals over the past 50 ka. During the last glaciation, the temperature remained colder than the modern seawater. Pronounced warming of ~4.5°C was observed during the last deglaciation, reaching modern-like temperatures at the onset of the Holocene. During this interval, new paired measurements of ^{14}C and U-series coral ages indicate signatures of southern-sourced waters. Additionally, the timing of the temperature changes in the Southwest Atlantic closely resembles the temperature pattern of waters from the Drake Passage. A final observation was a cooling that occurred during the mid- to late-Holocene at depths ~2000 m, which was also registered in the intermediate depths of the Drake Passage, the surface Southern Ocean and recorded by ice-cores in Antarctica. This study demonstrates a close link between the intermediate waters in the Southwest Atlantic, AMOC perturbations and seawater properties changes in the Southern Ocean during millennial and centennial scale events.

Contributions

The coral samples from this chapter are from the collections of the National Historical Museum (MNRJ, Museu Nacional do Rio de Janeiro, Brazil) and Prof Christian Millo (USP, University of Sao Paulo, Brazil). The corals were sampled in the MNRJ by me, Dr Marcelo V. Kitahara (USP, Brazil) and Dr Katia C. C. Capel (USP, Brazil). I am grateful to Prof Débora Pires who was the curator of scleractinian corals at MNRJ, and to Prof Christian Millo for the donation of his samples. The permits for shipping the samples were done by myself, Dr Marcelo Kitahara, Dr Michelle Taylor (University of Essex, UK) and Prof Laura F. Robinson (University of Bristol). The sample preparation and U-series dating were done by myself. The age calculation were done by me using a Matlab script written by Dr Tianyu Chen (Nanjing University, former post-doc researcher in the University of Bristol). The samples' cleaning for the trace elements analysis was done by myself, and the analysis by Dr Joseph A. Stewart (University of Bristol) and myself. I prepared and cleaned the radiocarbon samples with the graphitization being carried out by Paul Monaghan (University of Bristol) and the radiocarbon analysis and data processing by Dr Timothy Knowles (University of Bristol). This chapter was written by me. This chapter was written as paper format because we intend to submit it for publication.

4.1 INTRODUCTION

Ocean circulation plays an important role in the climatic system. It is responsible for transporting heat from low to high latitudes sustaining atmospheric conditions and impacting biogeochemical cycles in the ocean, such as promoting suitable conditions for primary productivity and sea-air exchange of CO_2. The impacts of the ocean on the carbon cycle have been demonstrated to be of central importance on glacial to deglacial timescales, by acting as a source or sink during periods of different ocean circulation, in particular associated with changes in the Atlantic Meridional Oceanic Circulation (AMOC; Marcott et al., 2014; Rae et al., 2018; Skinner et al., 2010; Yu et al., 2022). In a similar manner, AMOC perturbations have been suggested to drive changes in heat storage and release in the ocean, impacting climatic components, and promoting ice shelf melting at high latitudes (Marcott et al., 2011). Despite the progressive increase in our understanding of the systematics of ocean-climate dynamics, most studies have taken place at deep depths in the North Atlantic Ocean and, to a lesser extent, in the Southern Ocean. Thus, records focussing on the South Atlantic and at intermediate depths of the ocean (800 m to 2000 m) remain sparse, thus clouding our understanding of oceanic linkages across the Atlantic basin.

An effective approach to trace water column modifications and oceanic circulation is the use of radiocarbon (^{14}C). Radiocarbon is formed in the atmosphere and enters the surface ocean through sea-air mixing. Once the surface waters sink to the ocean interior, their ^{14}C content decreases due to the decay of the ^{14}C with a half-life of 5,730 years (Libby et al., 1949; Godwin, 1962; Skinner and Bard, 2022). Therefore, the ^{14}C of a water parcel is a function of the time elapsed since was last in contact with the atmosphere (Adkins et al., 2002; Mangini et al., 1998). In addition to this process, the ^{14}C content of a water parcel is also dependent on the mixing proportions with adjacent waters during its flow to and within the ocean interior (Burke et al., 2015; Skinner and Bahr, 2022).

Amongst marine ^{14}C archives, deep-sea corals have the advantage that they can be dated by an independent method (U-series dating). Previous studies using deep-sea corals had demonstrated long-term (glacial/deglacial) and rapid (centennial-scale) ^{14}C changes associated with largescale AMOC perturbations (Hines et al., 2015; Robinson et al., 2005; Thiagarajan et al., 2014). For instance, through

the analysis of ^{14}C in deep-sea corals, a sudden AMOC resumption (and overshoot) was observed contemporaneously in the Equatorial Atlantic and Drake Passage regions which corresponded to the onset of the Bølling-Allerød interval (B-A, 14.7 ka to 13 ka; Burke and Robinson, 2012; Chen et al., 2015). Furthermore, studies of the intermediate depths of the ocean have revealed the dynamic and well-ventilated properties of these waters, suggesting a continuous link between the intermediate waters and the atmosphere (De Pol-Holz et al., 2010; Hines et al., 2019; Chen et al., 2020).

During the last deglaciation, atmospheric temperatures in the high-latitude Northern and Southern Hemisphere warmed in a "seesaw" pattern (Barker et al., 2009; Shakun et al., 2012; Marcott et al., 2014). For instance, during Heinrich stadial 1 (HS1, 18 ka to 15 ka) at the beginning of the last deglaciation Greenland saw relatively cold temperatures while Antarctica gradually warmed. This was followed by a pronounced temperature peak in the Northern Hemisphere accompanied by cooling of the Southern Hemisphere during the B-A. Both of these events were characterized by AMOC perturbations, thought to be a key driver of this global temperature variability (Clark et al., 2002; Shakun et al., 2012). Intermediate depths of the ocean may have stored large amounts of heat during the HS1 and released it to high latitudes of the North Atlantic during the reinvigoration of a strong state of AMOC (Marcott et al., 2011; Thiagarajan et al., 2014; Valley et al., 2019). In agreement with this theory, recent studies from the Brazilian margin have shown an AMOC response to heat storage and transport at upper and intermediate depths of the water column (Umling et al., 2019; Meier et al., 2021; Santos et al., 2022). However, the impact of AMOC in the intermediate waters in the Brazilian margin remain puzzling. For instance, Mangini et al. (2010) documented waters extremely depleted in ^{14}C during HS2, HS1 and YD, which were interpreted as less presence of the ^{14}C-enriched NADW or larger contributions of ^{14}C-depleted waters from the Pacific Ocean.

The extensive presence of deep-sea corals in the Brazilian continental margin and offshore islands (Sumida et al., 2004; Kitahara, 2007; Pires, 2007; Cordeiro et al., 2014) highlight the potential of this location to reveal the connection of ocean circulation and climate on glacial to deglacial scales (Sumida et al., 2004; Kitahara, 2007; Pires, 2007; Cordeiro et al., 2014; Henry et al., 2014; Raddatz et al., 2020; Sumida et al., 2021; Trevizani et al., 2022). To this end, we present coupled U-ages and radiocarbon analysis of deep-sea corals from the Brazilian margin and the Rio Grande Rise (open-ocean site) for the

last 22 kyr. In addition, we reconstruct the temperature of intermediate waters at these locations by using Li/Mg measurements in the same coral samples enabling us to track temperature variability through the past glacial, deglacial and interglacial intervals (50 ka to present). Lastly, we combine our new coral ages with previously published coral ages from the Brazilian margin to discuss the temporal distribution of U-dated deep-sea corals over the past 270 kyr.

4.2 SAMPLES AND OCEANOGRAPHIC SETTINGS

The deep-sea corals used in this study (Plate 2, Appendix III) were collected from the Rio Grande Rise (34°S to 24°S, 36°W to 30°W) and the Brazilian continental margin (28°S to 21°S, 46°W to 39°W; Figure 1). The majority coral samples were collected using trawling or dredges by research vessels (e.g., Marion Dufresne, Prof. W. Bernard, RRS Discovery) or fishing vessels (e.g., Mar Salada, Toisa Canqueror). All samples were provided by the National Historical Museum, Brazil (MNRJ, from Portuguese: Museu Nacional do Rio de Janeiro) and by Prof Christian Millo (USP, from Portuguese: Universidade de São Paulo). The scleractinian solitary corals analysed in this study are of the taxa: *Caryophyllia berteriana, Caryophyllia* sp., *Desmophyllum dianthus, Trochocyathus rawsonii*, *Crispatotrochus squiresi*, *Paracyathus* sp. (Marcelo Kitahara, personal communication). The colonial identified species were: *Enallopsammia rostrata, Solenosmilia variabilis*, *Madrepora oculata* and *Bathelia candida* (Marcelo Kitahara, personal communication). The corals are distributed across a depth range of 600 m to 2600 m, which correspond to modern-day Antarctic Intermediate Water (AAIW), upper Circumpolar Deep Water (uCDW) and upper North Atlantic Deep Water (uNADW; Figure 2).

The water column of the study location is composed of Tropical Water above ~100 m, underlain by Subtropical Mode Waters (precursor of South Atlantic Central Water). The latter consists of surface waters subducted northwards to depths between 100 m and 600 m to form the permanent thermocline (Souza et al., 2018). Most of the corals are found at depths bathed today by AAIW, characterized by a low-salinity and high-nutrient core between 600 m and 1900 m at the South Atlantic Subtropical Gyre (Figure 1; Santos et al., 2016; Talley et al., 2011). The AAIW is composed of a mixture of the Subantarctic Mode Water, formed in the Pacific Ocean, with adjacent water at the Drake Passage.

During its transit, AAIW becomes colder and denser, and it is transported northward to the South Atlantic Ocean.

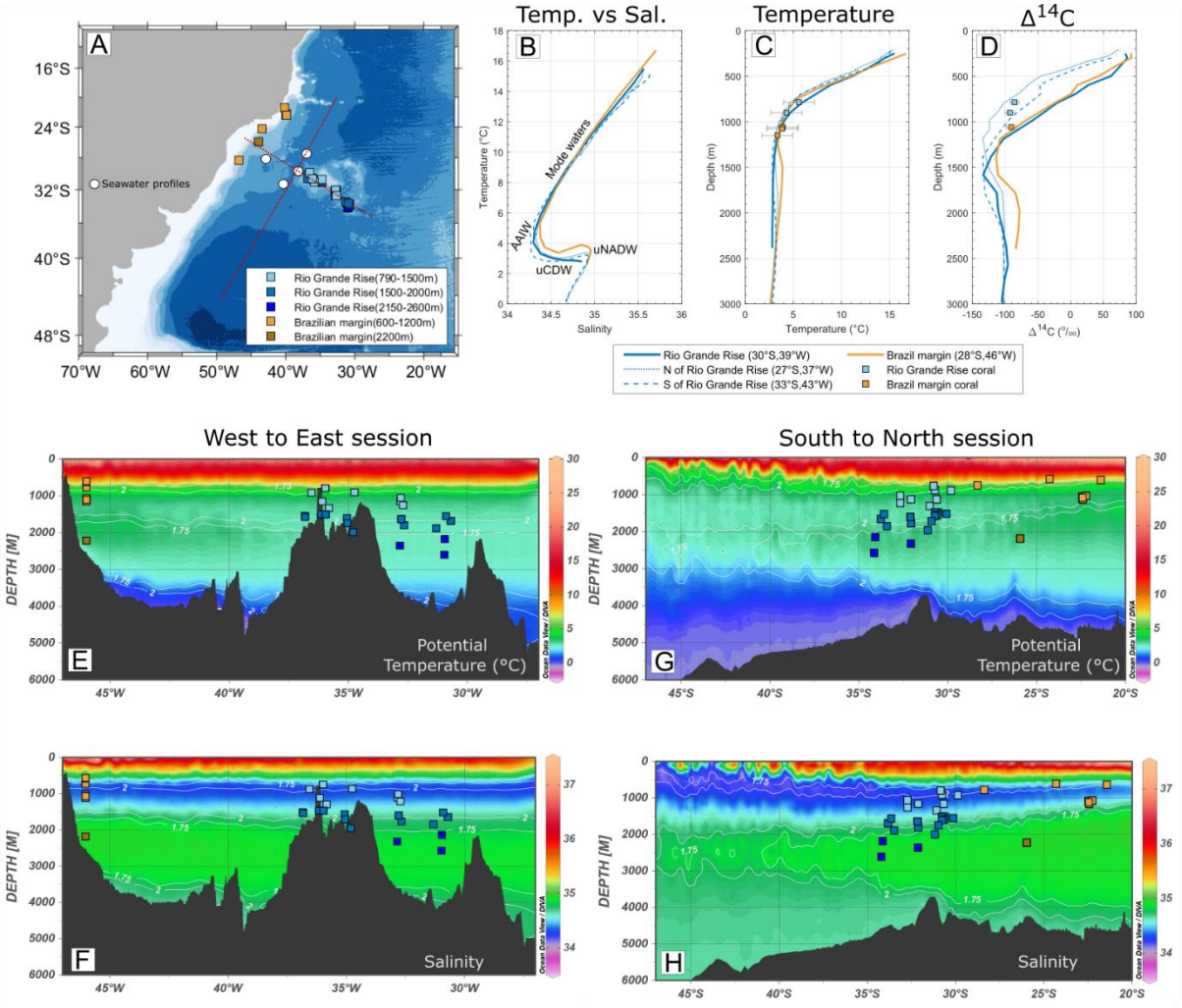

Figure 1: (A) Map of deep-sea coral studied sites in the Southwest Atlantic Ocean, Rio Grande Rise (blue squares) and Brazilian margin (yellow squares). The locations of the seawater profiles are shown by blue and yellow dots on the map. Red dotted lines indicate sections of panels E to H. Seawater modern profiles of (A) salinity versus temperature, (B) temperature versus depth, and (C) $\Delta^{14}C$ versus depth. (E) West to east section of potential temperature with coral locations. (E) West to east section of salinity with coral locations. (G) North to south section of potential temperature with coral locations. (E) North to south section of salinity with coral locations. Modern seawater parameters extracted from GLODAP database (Olsen et al., 2020).

The uCDW is found just below the AAIW, characterized by a constant temperature of ~3°C (see Figure 1B) and is coincident with an oxygen minimum layer (Maamaatuaiahutapu et al., 1992; Talley et al., 2011b). The uCDW is partially formed by deep waters from the Pacific, North Atlantic and the Indian Ocean that enter and mix within the Antarctic Circumpolar Current (Talley, 2013). Then, the uCDW upwells at ACC and mixes with less-dense shelf waters from the Antarctic Shelf, before being exported northwards to the South Atlantic. NADW is found in South Atlantic at depths between 2000

m and 4000 m (de Carvalho Ferreira and Kerr, 2017), and it is characterized by a deep-salinity maximum and low-nutrient concentrations (Figure 1). The upper part of NADW is mainly composed of waters from the Labrador Sea (de Carvalho Ferreira and Kerr, 2017), where dense waters are formed by deep convection of surface waters during the winter (Talley et al., 2011a).

The formation and composition of each water mass will aid in our understanding of the distribution of modern temperature and $\Delta^{14}C$. The Mode waters and AAIW show higher $\Delta^{14}C$ than uCDW, which is characterized by the lowest $\Delta^{14}C$ at intermediate depths (Figure 1). The uNADW shows a bulge of higher $\Delta^{14}C$, decreasing at abyssal depths due to the entrainment of Antarctic Bottom Waters (Figure 1).

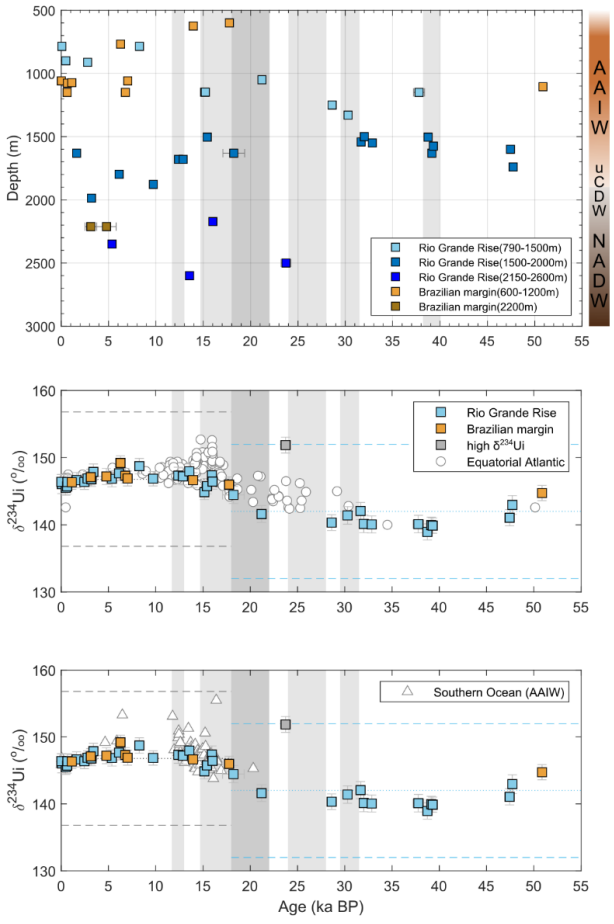

Figure 2: Depth versus age and $\delta^{234}U_i$ from deep-sea corals from the Rio Grande Rise (blue squares, this study), Brazilian margin (yellow squares, this study), Equatorial Atlantic (white dots; Chen et al., 2015, 2020), and South Atlantic at depths corresponding to AAIW (white triangles; Li et al., 2020). The grey square shows the coral sample with high $\delta^{234}U_i$ which potentially shows open-system behaviour. Error bars (2s) of the new coral data are indicated, and in some cases they are smaller than the symbols. Compiled data are plotted without uncertainties. Grey shadings indicate climatic intervals from right to left: Heinrich Stadial 3 (31.5 ka to 29.5 ka), Heinrich Stadial 2 (28 ka to 24 ka), Last Glacial Maximum (22 ka to 18 ka), Heinrich Stadial 1 (18 ka to 14.7 ka), and Younger Dryas (13 ka to 11.7 ka).

4.3 METHODOLOGY

4.3.1 U-series dating

Two methods of U-series dating were applied to the deep-sea coral samples of this study at the University of Bristol detailed below: (i) rapid laser ablation "reconnaissance" dating and (ii) high accuracy isotope dilution dating.

First, the age of 77 samples was screened by laser ablation dating using a previously established protocol (Spooner et al., 2016). This method is the first dating approach to new and unknown-age coral samples because it requires low sample preparation time and provides age uncertainties at the percent level (Spooner et al., 2016). For this, samples were cut into small pieces (~0.5 cm long) and polished before laser ablation using the Photon Machines Analyte G2 193 nm laser coupled to a Neptune Multi-Collector Inductivity Coupled Plasma Mass Spectrometer (MC-ICP-MS). The low abundance ^{230}Th isotope was measured simultaneously with ^{238}U on a central ion counter and a Faraday cup respectively Table 1; Spooner et al., 2016). Samples were analysed using a bracketing standard procedure where an in-house standard (inorganic aragonite vein) and background blank (laser cell gas blank) were measured every three samples. Then, the ^{230}Th/^{238}U ratio of each sample was corrected for background, and the ages were calculated by Newton-Raphson iteration. Here, it is assumed that there has been no open-system behaviour and that the initial ^{230}Th is negligible (Spooner et al., 2016). Therefore, the approximate δ^{234}U of the seawater value (as 146‰ added to 5‰ multiplicated by random numbers 100,000 times (Monte Carlo technique) to simulate uncertainty in the values of δ^{234}U) is used in the age calculation (Chapter 1).

Table 1: Cup configuration of U-series laser ablation (laser) and isotope-dilution (ID uranium and ID thorium) dating methods. H1 to H4 are Faraday cups, and IC1 is the central ion counter. Note that the cup positions are the same in both thorium configurations.

	IC1	H1	H2	H3	H4
Laser	^{230}Th				^{238}U
ID uranium	^{234}U	^{235}U	^{236}U	^{238}U	
ID thorium	^{230}Th	^{232}Th		^{236}U	^{238}U
	^{229}Th		^{232}Th		^{236}U

After acquiring the LA U-Th ages, 37 corals younger than 50 ka were selected for the more precise U-series isotope-dilution dating to better characterise the last deglaciation (per mil accuracy versus

percent level for the laser ablation dating; Cheng et al., 2000; Spooner et al., 2016). Prior to the analysis, 0.15 g of sample was physically cleaned and then oxidatively and reductively cleaned following established chemical protocols (Shen and Boyle, 1988; Cheng et al., 2000). Subsequently, samples were weighed, dissolved in HNO_3 (7.5 M) and gravimetrically-spiked with a ^{236}U-^{229}Th mixed spike calibrated to an uncertainty of 4.1‰ (2s; Burke and Robinson, 2012). U and Th were separated from the coral matrix by co-precipitation with Fe-hydroxide, then separated and purified by anion-exchange chromatography (Edwards et al., 1987; Chen et al., 2015).

The purified aliquots of U and Th were measured in separate runs both by bracketing standard methods (international U standard U112a and in-house Th standard SGS) on the same MC-ICP-MS used for laser dating. The standards Harwell uraninite standard (HU1) and ThB (in-house thorium solution of ^{229}Th, ^{230}Th, ^{232}Th; Auro et al., 2012) were measured every four samples and gave accuracy of 0.07‰ for $^{238}U/^{234}U$ and 1.6‰ for $^{230}Th/^{229}Th$. In the Th measurement, ^{229}Th and ^{230}Th were measured on a secondary electron multiplier by peak jumping. A pure-^{236}U spike was added to the Th fraction which is used to correct for signal instability during peak jumping by normalizing ^{230}Th and ^{229}Th to ^{236}U (Chen et al., 2015). The final ages were calculated iteratively and solved 100,000 times by Monte Carlo simulation. Differently from the laser ablation method, the ages were corrected for initial ^{230}Th using the $^{232}Th/^{230}Th$ activity ratio of 14.8±7.4 (the uncertainty is assumed as 50% which comprises the range of $^{230}Th/^{232}Th$ from intermediate open ocean waters; Robinson et al., 2004a) based on modern seawater ratios (Cheng et al., 2000; Robinson et al., 2005). Uncertainties related to machine and procedural blank were first propagated for each measured isotopic ratios, including uncertainties associated with the spike (estimated to 0.7‰ for ^{236}U and 2‰ for ^{229}Th per gram of spike, and 0.00004 g on the weight of spike). Then, the final uncertainties included the application of random numbers to the error of each variable (isotope ratios, $^{232}Th/^{230}Th$ uncertainty set as 50%, and decay constants) prior to solving the age equation.All dates are given as years before present (BP), where the present is the calendar year 1950. All data from the U-series dating is in the Appendix III.

4.3.2 Radiocarbon

Approximately 0.02 g of 18 samples from the same material used for the U-series dilution were separated for radiocarbon (^{14}C) analysis after a thorough oxidative cleaning procedure. Prior to graphitization, the samples were leached in weak hydrochloric acid (~0.1% HCl) to remove ~35% of its mass to account for any potentially adsorbed CO_2. The remaining sample (~13 mg) is dissolved in phosphoric acid (H_3PO_4) and evolved CO_2 is converted to graphite. The samples were pressed into aluminium targets and measured at the Bristol Accelerator Mass Spectrometer (BRAMS) facility using standard hydrolysis, together with oxalic acid standards, along with two coral samples which have been repeatedly measured as an internal standard and a blank, with U-series ages of 10.5 and 300 ka, respectively. The full dating procedure is described by Adkins et al. (2002). Briefly, the $^{14}C/^{12}C$ of the sample is measured and normalized to a $\delta^{13}C$ value of −25‰. The radiocarbon activities are reported as fraction modern (Fm) relative to the activity of the oxalic acid standard in the year of 1950 (normalized to $\delta^{13}C$=−19‰; Adkins et al., 2002 and references therein). Before converting the Fm to ^{14}C age (= −8033×ln(Fm)), the Fm of each sample is corrected using the Fm of the "coral blank" (Fm=0.0023±0.00007). Analytical uncertainties were processed using BATS data reduction software (Knowles et al., 2019).

The seawater $\Delta^{14}C$ (‰) was reconstructed using the ^{14}C age (^{14}C age) and the U-series (isotope dilution method) ages (Useries age) according to the expression:

$$\Delta^{14}C = \left(\frac{e^{-\,^{14}C\ age/8033}}{e^{-\ Useries\ age/8267}} - 1 \right) \times 1000$$

where the Libby mean life is 8033 and the "real" mean life of ^{14}C is 8267. The notation $\Delta^{14}C$ represent the relative difference between the ^{14}C in the international standard in 1950 and the ^{14}C in the sample corrected for age. When comparing these $\Delta^{14}C$ with the contemporaneous atmosphere, it is preferable to use the B-atmosphere (B-atm) nomenclature which is the direct difference between the ^{14}C age of the sample with the ^{14}C of the contemporary atmosphere (B-atm = $^{14}C age_{coral} - {}^{14}C age_{atm}$; atmospheric data extracted from IntCal20; Reimer et al., 2020). This offset, in years, accounts for changes in the radiocarbon inventory and is an effective way to compare with other oceanic records. All data from the radiocarbon analysis is in the Appendix III.

4.3.3 Trace elements analysis

The samples for trace elements were cut and physically cleaned using the same approach as for U-series dating. All samples were replicated to check coral skeletal heterogeneity (see brief discussion in Section 4.3.4). Approximately 10 mg to 15 mg of each sample was crushed, and 5 mg of this powder was oxidatively cleaned in warm 1% H_2O_2 (80°C; buffered in NH_4OH), followed by a weak acid polish (0.0005 M HNO_3), and dissolved in distilled 0.5 M HNO_3 (Boyle, 1981; Rae et al., 2011; Stewart et al., 2020). The solutions were then analysed using a Thermo Element2 ICP-MS. The calcium concentration of all samples was measured using a diluted 20 µl sample aliquot before the samples were again diluted to a matched 4 mM [Ca] matrix. Subsequently, the samples were measured by bracketing standard method using matrix-matched synthetic gravimetric standards (Stewart et al., 2020). All samples were corrected to measured acid-blanks, and reference materials (NIST RM 8301 (Coral), NIST RM 8301 (Foraminifera) and JCp-1) were measured at the start and end of the run to check assess accuracy and precision. This yielded a long-term analytical precision of <±1.7% (1 standard deviation; n=29) for Li/Ca, Mg/Ca and Sr/Ca for the reference materials yielded analytical precision of for Li/Ca, Mg/Ca and Sr/Ca. The seawater temperature was reconstructed using the exponential calibration curve for aragonitic organisms published by Stewart et al. (2020), the following equation:

$$Li/Mg_{coral} = 5.42 \times e^{(-0.05 \times T)}$$

where Li/Mg_{coral} is the ratio measured and T is the seawater temperature. All data from the trace elements analysis is in the Appendix III.

4.3.4 Quality control

The first parameter we use for checking diagenetic alteration is the initial $\delta^{234}U$ ($\delta^{234}U_i = \delta^{234}U \times e^{(\lambda_{234}\, t)}$). The $\delta^{234}U_i$ of deep-sea corals has been traditionally used as an indicator of a closed-system for U, because modern and fossil corals $\delta^{234}U_i$ agree with seawater values (Cheng et al., 2000; Robinson et al., 2006; Kipp et al., 2022). The expected variability range for the $\delta^{234}U_i$ of seawater over the past 360 kyr is ~15‰ (Chen et al., 2015; Henderson, 2002). Recently, studies have shown that $\delta^{234}U_i$ of seawater may have been lower than modern during glacial intervals (Chen et al., 2016; Chutcharavan et al., 2018). Nonetheless, this variability does not exceed a range of ±7‰ the value of modern seawater

(146.8 ±0.1‰; Andersen et al., 2010; Henderson, 2002; Robinson et al., 2004). All samples are within the expected seawater variability, except one sample aged 23.74 ka showing high $\delta^{234}U_i$ (Figure 2), so is not be included in the discussion. Additionally, two samples aged 1.7 ka and 18.3 ka show anomalous [^{238}U] of 9.3 ppm and 1.2 ppm, these samples are shown in the figures, but will not be included in the discussion.

The other parameter investigated is the Li/Mg reproducibility between the replicated coral samples (Figure 3). For instance, the centre of calcification of corals has been discussed to show different trace elements composition as higher Li/Ca, and Mg/Ca (Robinson et al., 2014; Stewart et al., 2020). For each coral sample, two individual pieces are cut, cleaned, and analysed to scan for intra-skeleton heterogeneity (Figure 3; Stewart et al., 2020). One modern *Solenosmilia variabilis* aged 0.65 ka on the Brazil margin shows a large difference between the two samples, one sample has a Li/Mg ratio of 4.5 mmol/mol and the other 5.6 mmol/mol, which corresponds to 3.8°C and −0.6°C, respectively. This difference likely indicates an intra-skeleton heterogeneity or contamination. A closer look into these poorly replicated samples shows that one of them has the highest Al/Ca ratio (148 μmol/mol) compared with all other samples. Additionally, this sample also shows high Mn/Ca and Fe/Ca, which could be an indicator of oxide or silicate contamination. Therefore, we rejected this replicate and kept only the measurement with low Al/Ca, Mn/Ca and Fe/Ca. The reconstructed temperature of this replicate (3.8°C) is in good agreement with the next coral chronologically aged 0.63 ka (3.3°C) on the Brazilian margin. The Li/Mg ratio difference between all the other replicates averaged 0.15 mmol/mol and a maximum of 0.57 mmol/mol corresponding to 0.6°C and 2.2°C respectively (Figure 3).

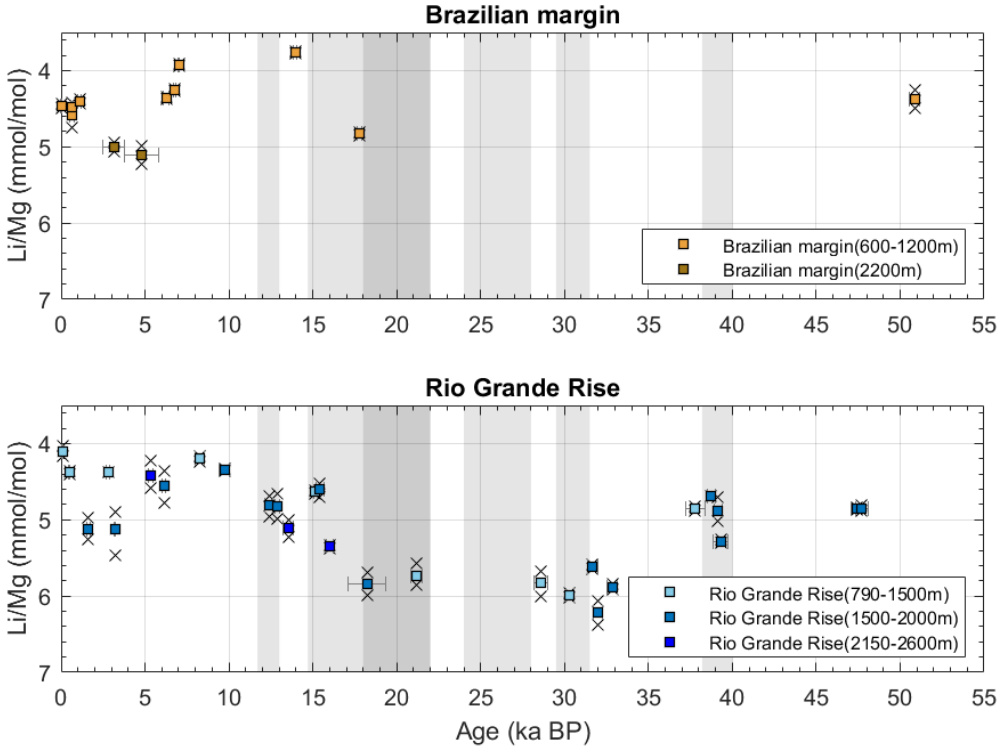

Figure 3: Li/Mg ratios of deep-sea corals from the Rio Grande Rise and Brazilian margin. Replicates are indicated by "x" symbols, and squares indicate the mean value of the replicates. Error bars (2s) of U-series ages are indicated, and in some cases they are smaller than the symbols. Grey shadings indicate climatic intervals from right to left: Heinrich Stadial 4 (40 ka to 38.2 ka), Heinrich Stadial 3 (31.5 ka to 29.5 ka), Heinrich Stadial 2 (28 ka to 24 ka), Last Glacial Maximum (22 ka to 18 ka), Heinrich Stadial 1 (18 ka to 14.7 ka), and Younger Dryas (13 ka to 11.7 ka).

4.4 RESULTS

4.4.1 U-age distribution

A total of 78 deep-sea corals were dated using the U-series laser ablation method, from which 54 samples were from Rio Grande Rise and 24 samples were from the Brazilian continental margin. The age uncertainties of the laser ablation dated corals are ±1 ka, ±2 ka and <±40 ka at 30 ka, 50 ka and 270 ka. These uncertainties are better than the expected uncertainties based on coral isotopic heterogeneity and counting statistics (Spooner et al., 2016). From this laser ablation dataset, 26 samples from Rio Grande Rise and 11 samples from the Brazilian margin were selected and dated by U-series isotope dilution method, improving the precision and accuracy of these ages. Additionally, 5 samples from Rio Grande Rise were solely dated by isotope dilution methods. The uncertainties of the U-series isotope dilution ages correlate with [^{232}Th] which demonstrates that the main source of the uncertainty results

from the initial ^{230}Th correction. The correction of initial ^{230}Th for deep-sea corals is necessary because the seawater [^{230}Th] increases with depth, and the corals incorporate a significant amount of Th during their growth (Cheng et al., 2000; Edwards, 2005). Therefore, the ^{232}Th/^{238}U ratio measured at the coral and the seawater ^{230}Th/^{232}Th is used to estimate the initial ^{230}Th in the coral. The [^{232}Th] of ~70% of the samples were below 4.2 ppt, corresponding to age uncertainties better than ±0.4 ka. Three samples show higher [^{232}Th] of 5.7 ppt, 6.7 ppt, and 9.6 ppt, which corresponds to uncertainties of ±0.6 ka, ±0.6 ka and ±1 ka.

Fifty-eight corals on the Rio Grande Rise were dated and show an age range from 247 ±4 ka to 1.6 ±1 ka (Figure 4). The majority of the corals are solitary (71%) and are distributed at a depth range from 780 m to 2600 m. The larger abundance of the solitary corals occurs within the last glacial and interglacial interval spanning the last 40 kyr to the present (Figure 4). Only three colonial corals on the Rio Grande Rise show ages older than 10 ka, including the oldest coral aged 263±37 ka. The colonial corals are distributed in a narrower depth range from 780 m to 1150 m, except for one coral aged 95±4 ka at 2500 m, and two corals ~5 ka at 1500 m (Figure 4). On the Brazilian continental margin, 25 corals were dated, the majority were colonial corals (87%), contrasting with only three solitary corals (Figure 4). The oldest colonial coral on the Brazilian margin was dated 51 ±0.3 ka, and the others clustered at ages younger than 20 ka. Their depth range is from 600 m to 1150 m, similar to the colonial corals on Rio Grande Rise (Figure 4). The three solitary corals show ages of 6.3 ±0.2 ka (at 768 m depth), 4.8 ±1 ka and 3.1 ±0.6 ka (both at depths of 2200 m).

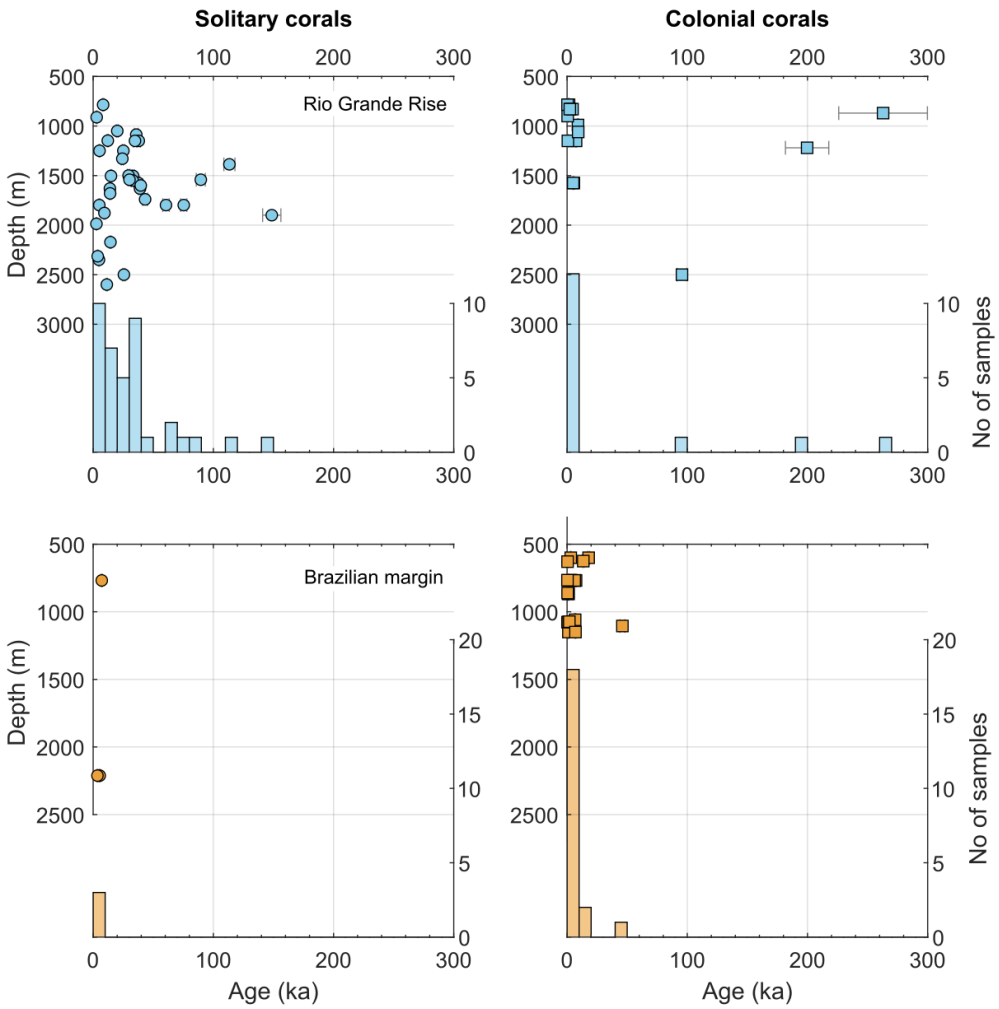

Figure 4: Temporal distribution of deep-sea coral from the Rio Grande Rise (blue symbols) and the Brazilian margin (yellow symbols). Left panels show solitary deep-sea corals and right panels show colonial deep-sea corals. Error bars (2s) of U-series ages are indicated, and in some cases they are smaller than the symbols. Histograms show 10,000-year bins.

4.4.2 Initial $\delta^{234}U_i$ values

The use of $\delta^{234}U_i$ as a diagenetic indicator was discussed in section 4.3.4, which demonstrates that in general, the corals on Rio Grande Rise and the Brazilian margin have behaved as a closed-system. The seawater $\delta^{234}U_i$ ratio has also been previously discussed to have been lower during the last glaciation and increased to modern seawater values during the early deglaciation (Chen et al., 2016; Chutcharavan et al., 2018). The $\delta^{234}U_i$ of the corals from this study agree with this finding showing an average of 141±1.5‰ (1s) during the last glacial interval (50 ka to 20 ka; Figure 2). During the early-deglaciation, the $\delta^{234}U_i$ increases to 146‰ between 18.2 ka and 17.8 ka coinciding with the onset of

HS1 (Figure 2). After 16.1 ka, the $\delta^{234}U_i$ of the corals show an average of 146.9 ±0.9‰ (1*s*) in agreement with modern values of seawater (146.8 ±0.1; Andersen et al., 2010).

4.4.3 Seawater temperature reconstruction from Li/Mg ratios

The reconstructed temperature range using the Li/Mg ratios on Rio Grande Rise is 7.3°C and −2.7°C (Figure 5). Only one sample aged 32 ka on Rio Grande Rise showed a temperature that was unfeasibly below the seawater freezing point (approx. −2°C). Following the same approach discussed in Chapter 2 (section 3.3) the temperature of this sample was approximated to be −2°C. The temperatures of corals younger than 0.6 ka on Rio Grande Rise (one *Enallopsammia rostrata* and one *Madrepora oculata*) and Brazilian margin (three specimens of *Solenosmilia variabilis*) closely agree with nearby modern seawater measurements (Figure 1) demonstrating that Li/Mg in the coral skeleton is a reliable tool for reconstructing water column temperature.

The overall temperature pattern on Rio Grande Rise is a decreasing trend from 50 ka to 34 ka, near freezing temperatures between 34 ka and 18 ka coinciding with the Last Glacial Maximum (LGM, 22 ka to 18 ka; Figure 5). During the deglaciation, the corals at the three depth ranges show a temperature increase of ~6°C until the onset of the Holocene (Figure 5). At the mid to late-Holocene, one coral at 2000 m depth show a cooling of 2.3°C while the temperatures recorded by the corals between 800 m and 900 m remain relatively stable (note that the youngest coral is from a slightly shallower depth that could account for the apparent warmer temperatures). When looking in more detail, we observed three features: (i) warming of ~2.4°C around 39 ka coinciding with the HS4; (ii) warming of ~4.5°C of magnitude during the HS1; and (iii) a second warming of ~ 2°C between the YD and the onset of the Holocene (Figure 5).

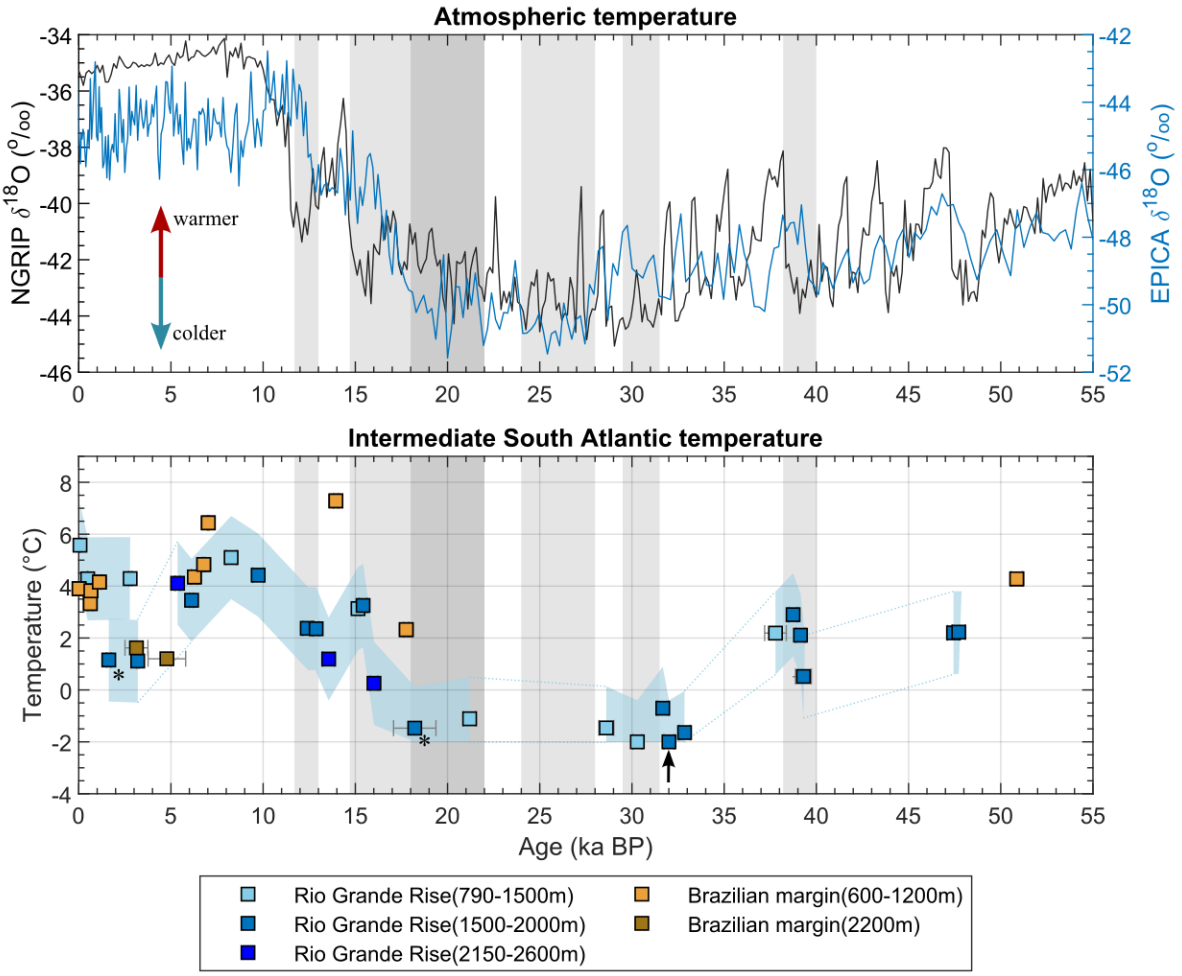

Figure 5: Temperature reconstruction from deep-sea corals from the Rio Grande Rise and Brazilian margin. Top panel show $\delta^{18}O$ of Greenland ice-core (NGRIP, black line; North Greenland Ice Core Project members, 2004) and $\delta^{18}O$ of Antarctic ice-core (EPICA, blue line; Bazin et al., 2013). Red and blue arrows indicate higher and lower atmospheric temperatures. Blue shading indicates prediction interval uncertainty from the calibration curve (1s=1.6°C; Stewart et al., 2020). Black arrow indicates the sample of temperature approximated to −2°C. Asterisk symbols indicate samples with high and low ^{238}U. Grey shadings indicate climatic intervals from right to left: Heinrich Stadial 4 (40 ka to 38.2 ka), Heinrich Stadial 3 (31.5 ka to 29.5 ka), Heinrich Stadial 2 (28 ka to 24 ka), Last Glacial Maximum (22 ka to 18 ka), Heinrich Stadial 1 (18 ka to 14.7 ka), and Younger Dryas (13 ka to 11.7 ka).

The reconstructed temperatures on the Brazilian margin show a similar pattern to the Rio Grande Rise. During the deglaciation, corals at ~600 m depth show warming of a similar magnitude (~4.9°C) to the deglacial corals on Rio Grande Rise (Figure 5). During the mid and late-Holocene, temperatures were relatively stable (between 4.8°C and 3.3°C) at depths between 750 m and 1200 m, except for one higher temperature (6.4°C) observed at 7 ka. In the mid-Holocene, two corals at 2200 m depth aged 4.8 ka and 3.1 ka show lower temperatures (~1.4°C) than modern seawater (3.3°C), similar to the contemporaneous corals at deeper depths on Rio Grande Rise.

4.4.4 Radiocarbon parameters

The $\Delta^{14}C$ of deep-sea corals from Rio Grande Rise and Brazilian margin <22 ka ranged from −106‰ to 320‰, corresponding to B-atm values of 205 ^{14}C yrs and 909 ^{14}C yrs. On the Brazilian margin, a specimen of *Solenosmilia variabilis* aged 0.02 ±0.02 ka shows $\Delta^{14}C$ of −90±7‰ in good agreement of nearby seawater measurements (-111‰; Figure 1; Olsen et al., 2020). At Rio Grande Rise, two corals (*Enallopsammia rostrata* and *Madrepora oculata*) younger than 0.5 ka show $\Delta^{14}C$ of −85±6‰ and −92±7‰. These values are within the $\Delta^{14}C$ range observed nearby modern seawater (Figure 1; Olsen et al., 2020).

During the LGM and HS1, the corals on Rio Grande Rise and the Brazilian margin show $\Delta^{14}C$ below the 100‰ depletion line with the atmosphere, corresponding to a mean B-atm of 840±51 ^{14}C yrs (n=2; Figure 6). This B-atm value corresponds to 130 ^{14}C yr and 400 ^{14}C yr depletion with modern seawater values on Rio Grande Rise and the Brazilian margin respectively. During the deglaciation, the corals show an increase in the seawater ^{14}C. During the B-A, one coral at ~600 m depth on the Brazilian margin show B-atm of 463±239 ^{14}C yr, which is in agreement with modern seawater measurements (~488 ^{14}C yr; Figure 6; Olsen et al., 2020). During the YD, two corals from ~1700 m on the Rio Grande Rise aged 12.9 ka and 12.4 ka show B-atm ages of 205±172 ^{14}C yr and 282±245 ^{14}C yr, which is ~550 ^{14}C yr more enriched than the modern seawater (Figure 6).

During the Holocene, four corals between 780 m and 920 m on Rio Grande Rise show a gradual depletion in ^{14}C towards modern-like conditions, they show B-atm of 250±420 ^{14}C yr, 405±126 ^{14}C yr and 721±80 ^{14}C yr at 8.2 ka, 2.8 ka and 0.07 ka (Figure 6). At similar times, the corals at 700 m and 1200 m on the Brazilian Margin remain with B-atm (mean value of 850±96 ^{14}C yr, n=5) similar to modern seawater (~750 ^{14}C yr). Only one coral (*Stephanocyathus diadema*) at 2200 m on the Brazilian margin was analysed for its ^{14}C content. It was dated 3±0.6 ka and has a B-atm age of 539±616 ^{14}C yr (Figure 6). This value is in agreement with modern seawater B-atm of ~630 ^{14}C yr, and with a ^{14}C enriched bulge centred at ~2000 m observed within the modern seawater profile (Figure 1). However, its uncertainty is too large to draw any conclusion, therefore no further interpretations will be made using this sample.

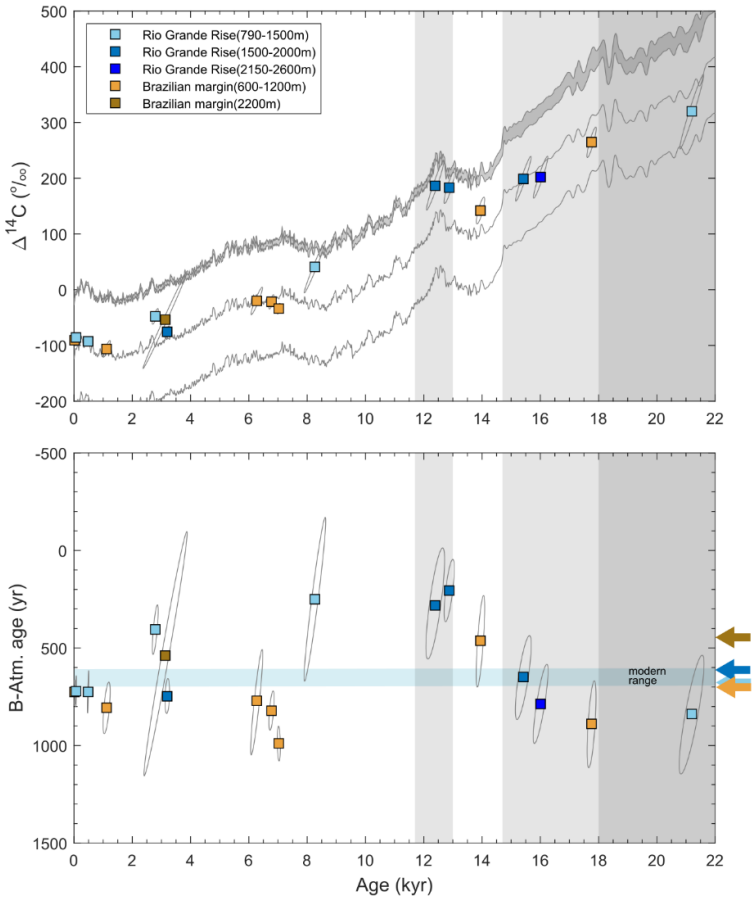

Figure 6: Radiocarbon parameters $\Delta^{14}C$ and B-atmosphere (B-atm) of deep-sea corals from the Rio Grande Rise and the Brazilian margin from 22 ka to present. Thick grey line in the top panel indicates the reconstructed $\Delta^{14}C$ atmospheric curve (IntCal20; Reimer et al., 2020), thin grey lines indicate 100‰ and 200‰ depletion to the atmosphere. Errors (2s) are plotted as ellipses. Coloured arrows indicate modern seawater B-atm values. Grey shadings indicate climatic intervals from right to left: Last Glacial Maximum (22 ka to 18 ka), Heinrich Stadial 1 (18 ka to 14.7 ka), and Younger Dryas (13 ka to 11.7 ka).

4.5 DISCUSSION

4.5.1 Deep-sea coral distribution in South Atlantic

Modern occurrences of deep-sea corals in the Southwest Atlantic are reported extending from the Argentinean continental margin to the equatorial Brazilian margin (Kitahara et al., 2010; Carranza et al., 2012; Schejter et al., 2016; Cordeiro et al., 2020; Sumida et al., 2020). Recent studies have suggested that the aggradation of coral mounds on the Brazilian margin may occur in short pulses of ~4 ka in contrast with longer occurrences (covering glacial or deglacial intervals) observed at the Northeast Atlantic (Wienberg and Titschack, 2015; Raddatz et al., 2020; de Carvalho Ferreira et al., 2022). Here, we compare our results of U-series dated corals on the Rio Grande Rise and the Brazilian margin with three previously published U-ages of deep-sea corals from the Brazilian margin (Henry et al., 2014;

Mangini et al., 2010; Raddatz et al., 2020). Note that the sampling of the corals in this study did not follow systematic planning, therefore any interpretation of their distribution (e.g., depth, age, location, coral type) will be subject to some sampling bias. Nevertheless, the description of their temporal distribution contributes to the current understudied fossil deep-sea coral occurrence in the South Atlantic.

The first observation from our coral abundance data is that the oldest occurrences of solitary (*Caryophyllia berteriana*) and colonial (*Bathelia candida*, *Solenosmilia variabilis*) on Rio Grande Rise are the oldest coral occurrences in the Southwest Atlantic reported so far (Figure 7). The comparison between the corals from the Rio Grande Rise with the Brazilian margin show two main features. First is the greater abundance of corals between 40 ka and 30 ka on the Rio Grande Rise, contrasting with one single occurrence (and with low aggradation rate) of *Solenosmilia variabilis* on the Brazilian margin (Raddatz et al., 2020). Second is the colonial coral occurrence which cluster during the Holocene on Rio Grande Rise, while on the Brazilian margin the corals show larger abundance between 20 ka and ~15 ka (Figure 7). The main difference observed between our new coral-ages and the previously published records on the Brazilian margin is the high abundance during the Holocene (Figure 7).

The relation between coral occurrence and oceanic dynamics has been investigated by the authors mentioned above. It is suggested that southern-sourced waters may have played an important role in larval transport positively impacting the local coral community (Henry et al., 2014; Raddatz et al., 2020). Additionally, a multi-proxy study related the cold-water coral growth to intervals of enhanced organic matter supply and strong bottom currents off the Brazilian margin (Bahr et al., 2020). The increased food supply and bottom currents were suggested to be caused by AMOC weakening, lower sea level, and increased precipitation and river runoff (Bahr et al., 2020). The addition of these new coral-ages to the previously published data seems to show an uninterrupted coral occurrence on the Brazilian margin extending over the last 30 kyr (Figure 7). This could potentially indicate a higher resilience of cold-water corals from this site to climate induced change, in comparison, for instance, with corals in the Northeast Atlantic (de Carvalho Ferreira et al., 2022). Interestingly, a recent study on shallow water corals suggests a less susceptibility to coral bleaching of coral in the South Atlantic due to specific features (e.g., high tolerance to seawater turbidity and nutrification; Mies et al., 2020).

However, as stated above, we cannot rule out the possibility of sampling bias on the cold-water coral distribution presented in this study, therefore we opt not to further interpret this coral distribution pattern until further observations are obtained.

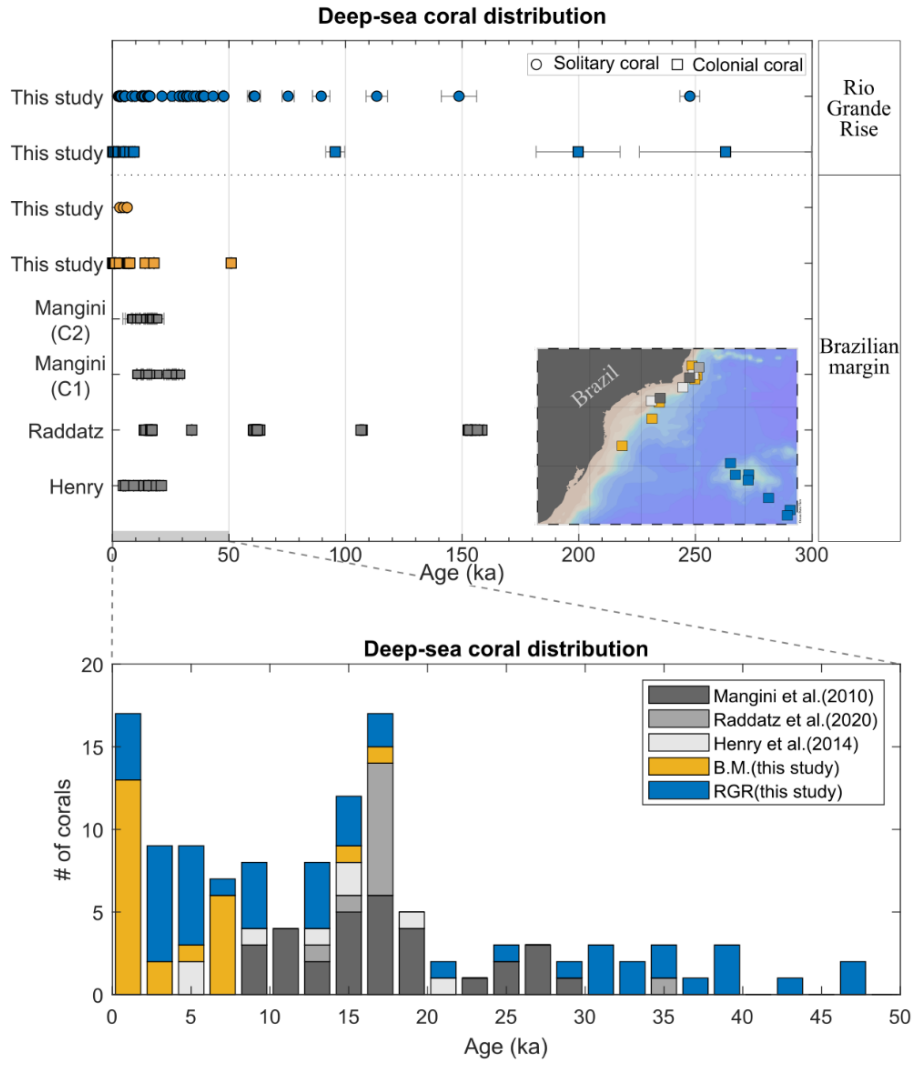

Figure 7: Deep-sea coral distribution from the Southwest Atlantic Ocean. Dot symbols represent solitary deep-sea corals and square symbols colonial deep-sea corals. Rio Grande Rise (blue symbols, RGR, this study), Brazilian margin (yellow symbols, B. M., this study), previous studies from the Brazilian margin (grey symbols, Henry et al., 2014; Mangini et al., 2010; Raddatz et al., 2020). Inset map show site locations (colour code follows histogram graph). Histograms show number of corals dated, in bins of 2,000 years.

4.5.2 Increasing $\delta^{234}U_i$ during the HS1 as a weathering tracer

The $\delta^{234}U_i$ ratio has been suggested as a potential proxy for past continental weathering flux (Chen et al., 2016; Chutcharavan et al., 2018). In modern seawater the $^{234}U/^{238}U$ ratio is in disequilibrium (~15‰ above secular equilibrium) due to the more mobile nature of ^{234}U compared with ^{238}U. During

the decay of ^{238}U to ^{234}U within mineral grains, the mineral lattice is believed to be damaged, such that ^{234}U is preferentially mobilized during weathering (Edwards, 2003; Robinson et al., 2004b). An interesting observation from our deep-sea corals in the Southwest Atlantic is that the glacial-deglacial $\delta^{234}U_i$ pattern parallels observations at low-latitude Atlantic (Figure 2; Chen et al., 2016; Chutcharavan et al., 2018). Overall, $\delta^{234}U_i$ was lower during the last glaciation and increased to modern-like values during HS1 (Figure 2). This increase was likely a result of input of ^{234}U-enriched waters from melting of basal icesheets at high latitudes during the last deglaciation (Chen et al., 2016; Chutcharavan et al., 2018). Our results support this interpretation and demonstrate that the increase in the seawater $\delta^{234}U_i$ show similar timing at both locations contemporaneous with the onset of the last glaciation (LGM to HS1 transition; Figure 2).

However, during the mid-HS1, the $\delta^{234}U_i$ peak observed at the low-latitude Atlantic contrasts with a more muted signal observed in our new data from the Southwest Atlantic (Figure 2). Coral data from the Southern Ocean - coinciding with the modern depth range of the AAIW and the depth range of the majority of our corals - also do not show such a pronounced peak of $\delta^{234}U_i$ during this time interval (Figure 2; Li et al., 2020). We speculate that the rapid increased in $\delta^{234}U_i$ observed at the low-latitude Atlantic sites may have been a feature particular to the North Atlantic basin, perhaps because of the proximity to the large icesheets expended during the last glacial interval. Additionally, increased overturning circulation of the Atlantic occurred at the transition between HS1 and B-A that may have more effectively mixed this signal (Burke and Robinson, 2012; Chen et al., 2015).

4.5.3 Warming and ventilation of the intermediate waters at HS1

Our most pronounced feature is the increase in temperature and radiocarbon at intermediate depths in the Southwest Atlantic during the early deglaciation (Figure 8). Towards the end of HS1, it is thought that the lower limb of the AMOC experienced an increase in strength based on Pa/Th (McManus et al., 2004; Böhm et al., 2015; Ng et al., 2020). At the same time, a switch for more radiogenic Nd signature in several records across the Atlantic indicated a larger contribution of northern-sourced waters (Lippold et al., 2016). In agreement, radiocarbon data from the intermediate depths from the Equatorial Atlantic and Southern Ocean suggest an erosion of the glacial stratification of the ocean interior

culminating in an AMOC "overshot" around 15 ka (Burke and Robinson, 2012; Chen et al., 2015). This event occurred during an atmospheric CO_2 increase which led to the hypothesis that degassing of old-carbon from the deep Southern Ocean to the atmosphere occurred due to increased upwelling (Burke and Robinson, 2012; Marcott et al., 2014; Rae et al., 2018). The intense mixing of the sea surface with the atmosphere could promote a "younging" of the waters which are then advected to intermediate depths along the Rio Grande Rise and the Brazilian margin supporting the observed decreasing trend of B-atm in our data. Another pronounced feature of our data during this interval is the intense warming of ~4.5°C observed at both sites, Rio Grande Rise and Brazilian margin, suggesting a link between ocean circulation and temperature of the ocean interior (Figure 9).

HS1 is known as a cold stadial event in the Northern Hemisphere, contrasting with a warming of the Southern Hemisphere (bipolar seesaw; Barker et al., 2009). This was a result of a sluggish ocean circulation where less cold water from the North Atlantic would be transported to the deeper limb of AMOC, and heat would be less effectively transported from south to north in the upper limb of AMOC. Thus, with less efficient AMOC mixing during the early deglaciation, a warming of the upper layer <2000 m has been proposed as indicated by model results and proxy data (Marcott et al., 2011; Galbraith et al., 2016; Umling et al., 2019). A recent reconstruction of temperature at Southern Ocean at depths corresponding to AAIW and uCDW shows a similar warming pattern and magnitude to our temperatures on Rio Grande Rise (Figure 8; Stewart et al., in review). The authors argue that this warming was caused by contemporaneous warming of the atmosphere. Our temperature data suggest that this warmer AAIW was advected to the Southwest Atlantic exporting heat to the ocean interior. In support of this finding is the similar ^{14}C-signature of these waters and the ^{14}C content of our corals. It is noteworthy that the warming observed during the HS4 (~39 ka) parallel with increased temperatures in Antarctica (synchronous with a cooling in Greenland) could also be caused by similar mechanism.

On the Brazilian margin, the temperature reconstructed from our corals at 600 m depth shows a similar magnitude of warming, but absolute values are higher than on the Rio Grande Rise (~1500 m; Figure 8). This temperature difference can be explained by the difference in the depth of the corals, as the same temperature difference (~4°C) is observed for these depths at the modern seawater temperature profile. When compared with the modern seawater profile, it is noted that the temperature after this

deglacial warming at both sites approaches modern-like conditions (Figure 9). Similar warming was previously described for the sea surface based on Mg/Ca and at intermediate depths (1100 m to 1900 m) based on Li/Mg both on foraminifera from the Brazilian margin (Santos et al., 2017, 2022; Umling et al., 2019). Our results contribute to the observations of deglacial warming of the sea surface, base of the thermocline, and intermediate depths down to 2700 m depth in the Southwest Atlantic.

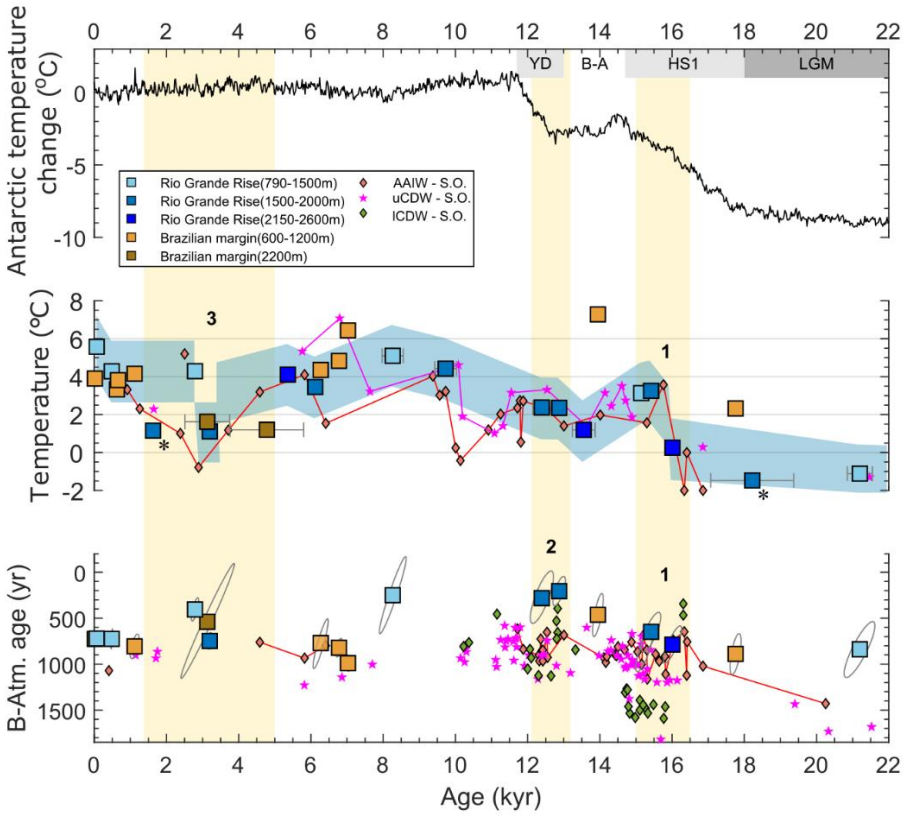

Figure 8: Radiocarbon and temperature from new coral data from the Rio Grande Rise (blue squares) and Brazilian margin (yellow squares). Published records from the Drake Passage are divided by modern depths of the water masses: Antarctic Intermediate Water (AAIW, orange diamonds), upper Circumpolar Deep Water (uCDW, pink stars), and lower Circumpolar Deep Water (lCDW, green diamonds) (Burke and Robinson, 2012; Li et al., 2020; Stewart et al., in review). Yellow shading marks the main discussion topics: (1) parallel increase of radiocarbon and temperature at Heinrich Stadial 1 (HS1), (2) ^{14}C-enrichent of intermediate waters at Younger Drays (YD) on Rio Grande Rise in agreement with data from lCDW, (3) cooling of waters >1600 m during the mid to late-Holocene. Asterisk symbols indicate samples with high and low ^{238}U. Acronyms on the top of the figure indicate climatic intervals: Last Glacial Maximum (LGM, 22 ka to 18 ka), HS1 (18 ka to 14.7 ka), Bølling Allerød (B-A, 14.7 ka to 13 ka), and Younger Dryas (13 ka to 11.7 ka).

4.5.4 ^{14}C-enriched waters during the Younger-Dryas

An intriguing feature during the Younger-Dryas (YD), is the large ^{14}C enrichment of the waters at 1700 m on Rio Grande Rise (Figure 8), when the B-atm show values around 200 and 280 ^{14}C yrs that are better ventilated than modern waters (modern waters at similar depth B-atm ~ 830 ^{14}C yrs). This ^{14}C

enrichment marked by the corals in the Rio Grande Rise is consistent with a steep increase in the atmospheric $\Delta^{14}C$ suggesting a connection between these ^{14}C inventories (Figure 6). In the modern water column configuration, these depths are in the transition zone between uCDW and AAIW, while NADW is found deeper at depths below ~2000 m. Pa/Th data of several deep-sea sites in the Atlantic Ocean indicates a weaker AMOC than modern during the YD, which could result in less formation of NADW (Lippold et al., 2016; Ng et al., 2018). In agreement, a coral-based ^{14}C reconstruction in the North Atlantic (~1700 m) show a sharp shift to a ^{14}C-depleted waters at the onset of YD indicative of less proportion of NADW (Eltgroth et al., 2006). Together, these observations indicate that the ^{14}C enrichment observed on Rio Grande Rise during the YD may not be associated with ventilation of northern-sourced waters, but instead with processes influencing southern-sourced waters (e.g., AAIW, CDW). Indeed, radiocarbon data from deep-sea corals in the Southern Ocean show a pronounced short-lived positive excursion of ^{14}C at the depths of modern lCDW (Figure 8; Li et al., 2020). The authors attribute this rapid event to a deepening of the mixed layer to open-ocean deep convection. Therefore, we propose that the ^{14}C-enriched waters of the Southern Ocean were rapidly advected to the Rio Grande Rise, prompting this well-ventilated signature.

4.5.5 Cool intermediate waters during the mid to late-Holocene

During the Holocene, a cooling of ~3°C is observed at depths greater than 1600 m on Rio Grande Rise reconstructed using specimens of the genus *Caryophyllia* (*C. berteriana* and *C. scobinosa*). Three corals aged 9.7±0.3, ka 6.1±0.1ka, and 5.4±0.1 ka show an average temperature of 4.4°C, and one coral aged 3.2±0.6 ka show temperature of 1.1°C (a note that another coral aged 1.6±1.1 ka at 1600 m also record temperature of 1.1°C, but this sample showed high ^{238}U concentrations). Furthermore, two corals (*Stephanocyathus diadema*) aged 4.8±1 ka and 3.1±0.6 ka at 2200 m depth on the Brazilian margin also show cold temperatures of 1.4°C. Together, these data suggest that this cooling of ~3°C (Figure 9) likely occurred around 5 ka and 4 ka (Figure 8).

Temperature reconstructions using deep-sea corals in the Southern Ocean, suggest a contemporaneous and gradual decrease of ~4°C at depths corresponding to modern AAIW, which is in agreement to the cooling we observed in our data (Figure 8; Stewart et al., in review). Reconstructions

of mean global atmospheric temperatures during the Holocene, suggest a warmer period until the mid-Holocene (~6 ka) followed by a gradual cooling (Marcott et al., 2013). This global temperature however is dominated by records from the Northern Hemisphere, and a stacked temperature for latitudes >30°S suggest an earlier cooling started around 10 ka (Marcott et al., 2013). While this temperature reconstruction can be biased by the spatial cover of proxies, ice-cores from Greenland and Antarctica both record similar warmer conditions in the earlier Holocene (i.e., "Holocene optimum") interrupted by shorter-scale events (Masson et al., 2000; Masson-Delmotte et al., 2005).

Studies focusing on reconstructing sea surface conditions show a cooling event started around 6 ka to 5 ka in the East Atlantic sector of the Southern Ocean in phase with a cooling trend in Antarctic temperatures (Masson et al., 2000; Hodell et al., 2001; Nielsen et al., 2004). Evidence for contemporaneous colder sea surface temperatures is also presented at the western Antarctica Peninsula (Shevenell et al., 2011). These sea surface temperature changes are interpreted as a response to a decline in summer insolation at high-latitude Southern Hemisphere amplified by regional climatic feedbacks (Hodell et al., 2001; Nielsen et al., 2004; Shevenell et al., 2011). An example of a regional feedback is the extension of sea ice during the mid-Holocene interpreted from diatom abundances at the East Atlantic Southern Ocean (Shevenell et al., 2011). This sea ice extension was related to a decrease in the strength (or change in position) of the westerlies leading to less upwelling of warmer deep waters (e.g., CDW; Shevenell et al., 2011). Regardless of the mechanism, the colder waters at depths greater than 1600 m on Rio Grande Rise and the Brazilian margin during the mid to late-Holocene parallels with regional cooling of the Antarctic atmosphere, several records of sea surface temperature, and a general cooling of AAIW in the Southern Ocean. Therefore, we argue that the interaction of seawater with lower atmospheric temperatures and the incorporation of colder sea surface waters, would both impact the temperature of AAIW exported to our sites.

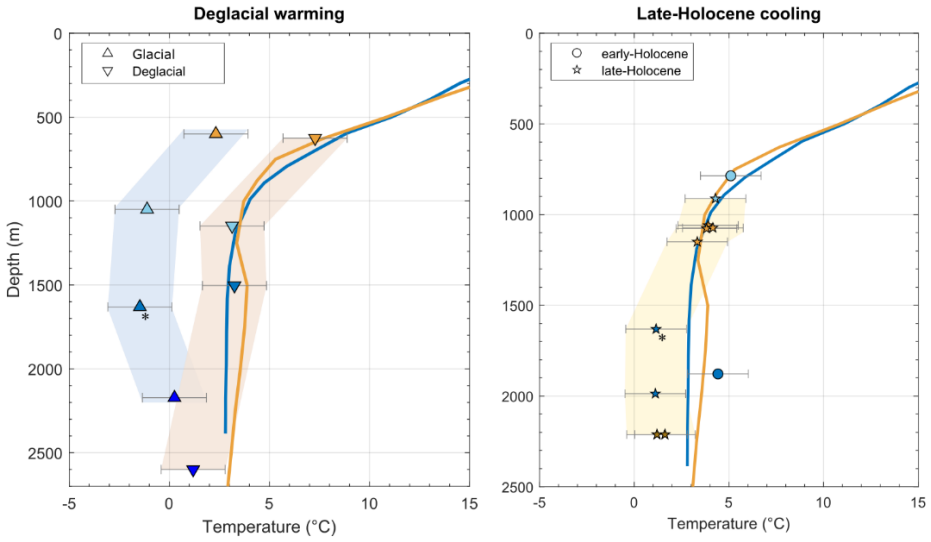

Figure 9: Coral-based reconstructed temperatures profile from the early-deglaciation (left) and late-Holocene (right). Modern seawater profiles are shown by the coloured lines. Blue symbols and line are temperatures from the Rio Grande Rise, and yellow symbols and line are temperatures from the Brazilian margin. Glacial coral ages ranged from 21.2 ka to 16 ka, deglacial coral ages ranged from 15.4 ka to 13.5 ka. Early-Holocene corals aged 9.7 ka and 8.3 ka, late-Holocene corals have ages <4.8 ka. Asterisk symbols indicate samples with high and low ^{238}U.

4.6 CONCLUSIONS

In this study we used deep-sea corals from the Rio Grande Rise and the Brazilian margin to investigate the response of intermediate waters to climatic changes since the last glaciation. The U-series ages of 58 deep-sea corals from Rio Grande Rise and 25 from the Brazilian margin were compiled with previous published coral ages providing a nearly continuous colonial coral occurrence record on the Brazilian margin. Moreover, we find the oldest reported coral occurrence in the Southwest Atlantic. They consist of two colonial coral specimens (*Solenosmilia variabilis* and *Bathelia candida*) aged 263 ka and 199 ka and one solitary coral (*Caryophyllia berteriana*) aged 247 ka on the Rio Grande Rise.

Through the analysis of ^{14}C and Li/Mg temperature reconstructions at our study sites, we observed a pronounced ^{14}C-enrichment and warming of the intermediate waters towards modern-like conditions, during HS1. We attributed this shift to changes in the properties of the southern sourced waters advected to our studied site, in agreement with coral-based reconstructions in the Atlantic sector of the Southern Ocean. Furthermore, the strong perturbations of AMOC during the early deglaciation may have been the main force driving warming of the Southern Hemisphere, and the intermediate waters in the

Southwest Atlantic likely maintained connection with the atmosphere. During the YD, two corals at 1700 m depth on the Rio Grande Rise showed considerably more ^{14}C-enriched waters compared with modern conditions. The evidence of a weaker AMOC and similar ^{14}C positive excursion observed at the intermediate depths in the Southern Ocean led to the conclusion that well ventilated waters of the Southern Ocean were rapidly transported to our sites.

Finally, a cooling of ~3°C at water depths greater than 1600 m on Rio Grande Rise and the Brazilian margin during the mid-Holocene parallel with colder temperatures on Antarctica and surface waters of the Southern Ocean. The mechanisms associated with this might be related to a decrease in the duration of summer insolation and regional feedbacks. The results presented in this study demonstrate the highly dynamic behaviour of intermediate waters and the response of climate. Intermediate waters in the Southwest Atlantic respond to AMOC perturbations while atmospheric temperature variability and sea-air exchanges occurred in the Southern Ocean during millennial and centennial scale events.

Chapter 5: CONCLUSION AND PERSPECTIVES

In this thesis, cold-water corals were used to investigate the temporal distribution of corals and to reconstruct the ^{14}C and temperature of the intermediate waters in the Atlantic Ocean over the last glacial, deglacial and interglacial intervals. The intermediate ocean plays a key role in maintaining AMOC, and it is a valuable conduit linking the atmosphere and the ocean interior, such as transporting heat, gases and nutrients. Additionally, the so-called "deep-sea" ecosystems (e.g., cold-water corals reefs, gardens, sponges) are found in these intermediate depths, which are increasingly being recognized by their ability to main the regional (perhaps even global) biodiversity.

Here, I used two U-series dating methods: rapid laser ablation "reconnaissance" dating and high accuracy isotope dilution solution analysis. The reconnaissance method was performed to obtain ages for the larger coral dataset. Selected samples from the last glacial to interglacial interval were then more precise and accurately dated by isotope dilution methods. Radiocarbon and Li/Mg ratios measured in corals from the Northeast and Southwest Atlantic were used as proxies of ocean circulation and seawater temperature. These proxy records provided insights into the role of the intermediate depth waters in driving millennial and centennial scale climate change.

5.1 COLD-WATER CORAL TEMPORAL DISTRIBUTION

This study was motivated by previously observed latitudinal shifts in Northeast Atlantic coral occurrence that are potentially paced by past warm and cold climates (Frank et al., 2011). This hypothesis was based mainly on colonial corals inhabiting continental shelves (Frank et al., 2011). Therefore, in this thesis, corals from open-ocean sites and a large number of solitary corals were dated and incorporated to the dataset. Approximately 600 new corals from Reykjanes Ridge, Tropic Seamount, and seamounts in the equatorial Atlantic were dated by U-series laser ablation and isotope dilution methods. These samples were collected in previous research cruises and are part of the large cold-water coral collection of Prof Laura F. Robinson (University of Bristol). The new ages were

combined with ~700 previous published coral ages to explore the temporal distribution of corals over the last 150,000 years.

In chapter 2, the temporal coral occurrence amongst the new open-ocean sites and the previous published continental shelf was strikingly similar suggesting that these latitudinal shifts were driven by a common basin-wide climate forcing. The solitary coral ages from the Northeast Atlantic also showed similar distribution patterns to colonial corals, wherever data of both coral types were available. In each region the presences of corals was linked to times when sediment based proxies indicated increased food availability, while events of corals demise or gaps in the records were potentially associated with less food and/or lower dissolved oxygen in seawater.

A second coral distribution analysis was also performed for the Southwest Atlantic (Chapter 4) using samples from the National Historical Museum (MNRJ, Museu Nacional do Rio de Janeiro, Brazil) and the collection of Prof Christian Millo (USP, University of Sao Paulo, Brazil). Here, new U-series coral ages from Rio Grande Rise and the Brazilian margin showed a temporal distribution spanning the last 260 kyr. A high abundance of corals was observed on the Brazilian margin during the Holocene, differing from the previous published coral ages clustering during the last glacial and deglacial interval. When combining these two coral datasets from the Brazilian margin, corals showed a virtually continuous occurrence from ~30 ka to present, or from ~40 ka including the coral distribution from the Rio Grande Rise. This occurrence may indicate a high resilience of cold-water corals from these sites to climate induced change, perhaps reassembling their shallower waters equivalents, which have been suggested to be less susceptible to coral bleaching due to specific features (e.g., high tolerance to seawater turbidity and nutrification; Mies et al., 2020). However, further study is needed to identify the relation between environmental drivers (e.g. food supply, temperature, pH, circulation) and the cold-water coral distribution in the Southwest Atlantic.

5.2 INTERMEDIATE WATER ^{14}C AND TEMPERATURE IN THE ATLANTIC OCEAN OVER THE LAST 30 KYR

5.2.1 North Atlantic

This study was motivated by the current debate on the role of intermediate waters in oceanic circulation during the last glacial and deglacial interval. While some studies point to a northward expansion of AAIW during a weakened AMOC (e.g., HS1 and YD) at low-mid North Atlantic, others argue for the presence of NADW (Pahnke et al., 2008; Xie et al., 2012). Furthermore, although there is a broad consensus of a warming of the ocean interior in response to a weakened AMOC during the last deglaciation, the mechanisms remain unclear (e.g., advection vs downward mixing of heat, freshening of North Atlantic; Poggemann et al., 2018; Came et al., 2007).

The radiocarbon and temperature results from the Tropic Seamount in the Northeast Atlantic (Chapter 3) showed a close connection with other intermediate waters from the South Atlantic (Cléroux et al., 2011; Sortor and Lund, 2011; Lund et al., 2015; Skinner et al., 2017; Umling et al., 2019). During Heinrich Stadial 3 (HS3) the ^{14}C values suggest well-ventilated waters and a ^{14}C drop parallel with atmospheric ^{14}C. Some datapoints plotted at or above the atmospheric curve, however, this may relate to uncertainty in the average atmospheric curve itself. Additionally, our new data are within the scatter of published archives (Fairbanks et al., 2005; Robinson et al., 2005; Hoffmann et al., 2010; Hines et al., 2015).

During the last glaciation, the Mg/Li based temperature records from intermediate waters from the Tropic Seamount showed near freezing temperatures. Similar temperatures have been observed at intermediate depth South Atlantic and deep North Atlantic sites (Skinner et al., 2003; Roberts et al., 2016). The ^{14}C values are also similar to the general pattern of a glacial ocean that was more depleted in ^{14}C relative to the present. Despite this general agreement, intermediate waters in the Tropic Seamount remained better ventilated than the deep layers (>3000 m; Barker et al., 2010; Skinner et al., 2014).

During the LGM, a rapid negative ^{14}C excursion of 107‰ at Tropic Seamount reached values similar to those recorded in Antarctic Intermediate Water (AAIW) and upper Circumpolar Water (uCDW), suggesting a major contribution of these southern-sourced waters to the study site (Sortor and

Lund, 2011; Lund et al., 2015; Skinner et al., 2017; Li et al., 2020). In the late-HS1, the intermediate waters at the Tropic Seamount showed an increase in ^{14}C values, with this increase aligned with changes in southern-sourced water values. During this time, my new data showed a warming of ~7°C in the intermediate waters at the Tropic Seamount which occurred alongside a weakened lower limb of Atlantic Meridional Oceanic Circulation (AMOC; McManus et al., 2004; Böhm et al., 2015; Ng et al., 2018). This warming was attributed to an increase in temperatures of southern-sourced waters and downward accumulation of heat from the surface during the northward transport of these waters.

5.2.2 South Atlantic

The scarcity of studies in the South Atlantic (especially compared with North Atlantic) motivated the development of Chapter 4. Studies using cold-water corals as paleo-proxies in the Southern Ocean, low latitude Atlantic and North Atlantic suggest that the intermediate ocean had remained more well-ventilated than the deeper layer and that it responds quickly to oceanic perturbations (e.g., AMOC "overshoot" during B-A; Burke and Robinson 2012; Chen et al., 2016; Robinson et al., 2005). More recently, the thermal response of the ocean interior to such ocean perturbations had received much attention (Marcott et al., 2011; Valley et al. 2019; Stewart et al., in review). In Chapter 4, I reconstructed the temporal variability of seawater ^{14}C and temperature (Li/Mg ratios) from the South Atlantic and compared it with other locations in the Atlantic Ocean.

The ^{14}C and temperature results reconstructed from corals from the Rio Grande Rise and the Brazilian margin (Chapter 4) support a close link between atmospheric variability, perturbations in AMOC and the intermediate water dynamics. During HS1, the intermediate waters at both study sites shifted from lower ^{14}C and colder temperatures towards modern-like conditions. At the same time, coral-based reconstructions of temperature and ^{14}C from the Drake Passage (Southern Ocean) showed similar changes, which lead to the interpretation that the waters obtained their ^{14}C and temperature signature in the Drake Passage and were exported to our study sites (Stewart et al., in review).

Another indicator of water mass connectivity between Rio Grande Rise and the Drake Passage is the peak in ^{14}C observed at both locations during the Younger Dryas and the overall pattern of initial $\delta^{234}U$. In the mid-Holocene, waters deeper than 1600 m at Rio Grande Rise and the Brazilian margin

showed colder temperatures than modern at a time of cooling of AAIW in the Drake Passage. Furthermore, similar cooling was documented in atmospheric records in the Antarctica and in the surface Southern Ocean.

5.2.3 Low temperatures from the Li/Mg proxy

During the LGM, the temperatures calculated using the Li/Mg ratio measured in the corals from the Tropic Seamount resulted in values down to −3.9°C using the calibration of Stewart et al. (2020). The data fall within error of the freezing point of water (−2°C), when the full uncertainty (2*s* = 3.4°C) on the calibration is taken into account. However, temperatures below the seawater freezing point are unfeasible. This motivated a discussion on a few ideas that could be driving this low temperatures in Chapter 3. I addressed the effect of a saltier glacial ocean during the LGM, the effect of the salinity into the Li/Mg ratios, and including new Li/Mg measurements of corals from cold-waters. I demonstrated that the suggested 3‰ increase in salinity during the LGM (Adkins et al., 2002b) would account for an insignificant change in the freezing point of seawater (a difference of <0.2°C). I analysed the residuals of the Li/Mg plotted against the salinity which also do not show any significative relationship. Then, I analysed 12 new live-collected corals from waters ~0°C from the South Orkney Island. These new samples fell within error of the existing calibration curve (Stewart et al., 2020) supporting its applicability for a large range of temperature, including samples at ~0°C. Although the reason for these low temperatures (high Li/Mg) were not uncovered, I suggested and used the approach of approximating the temperatures less than or equal to −2°C.

5.3 SUMMARY AND OUTLOOK

In this thesis, I carried out extensive studies of cold-water corals in relation to past distributions and to climate change. Their temporal and spatial distribution can be associated with changes in environmental parameters which in turn are dictated by climate shifts. Other proxies, such as ^{14}C and Li/Mg, can provide direct ways to reconstruct seawater parameters. Furthermore, the advantage of dating scleractinian coral using U-series methods provide precise and accurate ages. An overall

observation from my work is that coral-based oceanic reconstructions are emphasising the dynamic behaviour of the intermediate waters and their role in responding and influencing the climate system.

A continuation of this study would be a focus on coral sampling efforts in specific areas (either in situ or from collections) to fill the spatial gaps on the current coral database (Figure 1). An immediate target could be the South Atlantic, specifically open-ocean sites and the Southeast Basin. For instance, this basin is where the waters from the Indian Ocean enters into the Atlantic contributing to the upper limb of AMOC, and where a branch of the Deep Western Boundary Current flows eastwards contributing to the export of NADW to the Indian Ocean (Bower et al., 2019). In this sense, a recent study linked the AMOC strength variability with changes in water export from the Indian Ocean to the Atlantic Ocean and the monsoons (Cheng et al., 2021). They used a suite of centennial-scale resolution speleothems in the Southern Hemisphere to demonstrate that a larger input of the Agulhas leakage to the Atlantic may had enhanced AMOC strength and led to the termination of the Heinrich Event 4 (40 ka to 38 ka; Cheng et al., 2021). The processes evoked were the southward positioning of the Southern Westerly winds and Subtropical Front, and a lesser fresh water input from the Amazon river. A missing piece of this puzzle is an oceanic record, in which corals could considerably contribute. For instance, (i) the temporal distribution of coral population can indicate changes in oceanographic fronts (Margolin et al., 2014; Wienberg et al., 2018; Stewart et al., 2021), (ii) geochemical proxies applied to corals (e.g., Li/Mg, ^{14}C, $\delta^{11}B$, Ba/Ca, clumped isotopes; Hines et al., 2019; Montagna et al., 2014; Spooner et al., 2018; Stewart et al., 2020) can directly reflect seawater parameters, and (iii) there are records of corals off the coast of South Africa, on the Walvis Ridge (submarine ridge at Southeast Atlantic ~20°S to 25°S) and a few seamounts between Africa and Antarctica (Figure 1). Therefore, efforts on sampling and measuring corals from the Southeast Atlantic basin could be valuable to understanding the connections between the Atlantic and Indian oceans and the implications for AMOC during the past glacial intervals.

Finally, coral collections should be combined with seawater measurements (e.g., salinity, temperature, dissolved oxygen, carbon system parameters (pH, alkalinity), nutrients, and trace elements concentration (e.g., Ba)). This would allow to better constrain geochemical proxies application in corals. Additionally, the retrieve of sediment cores nearby the coral collection could provide a suite of other

environmental proxies (e.g., sortable silt (for bottom current speed), particulate and dissolved carbon (for food supply), foraminifera assemblages (for surface and/or bottom water conditions)). Of course that this would depend on local conditions (e.g., sedimentation rate), but, for instance, studies of coral-bearing sediment cores have shown a good application of combining these archives on glacial scales (Wienberg et al., 2010; Bahr et al., 2020). Perhaps this could be an interesting approach to study places of coral occurrences coinciding with high sedimentation rates such as off the delta of the Amazon river (Cordeiro et al., 2015).

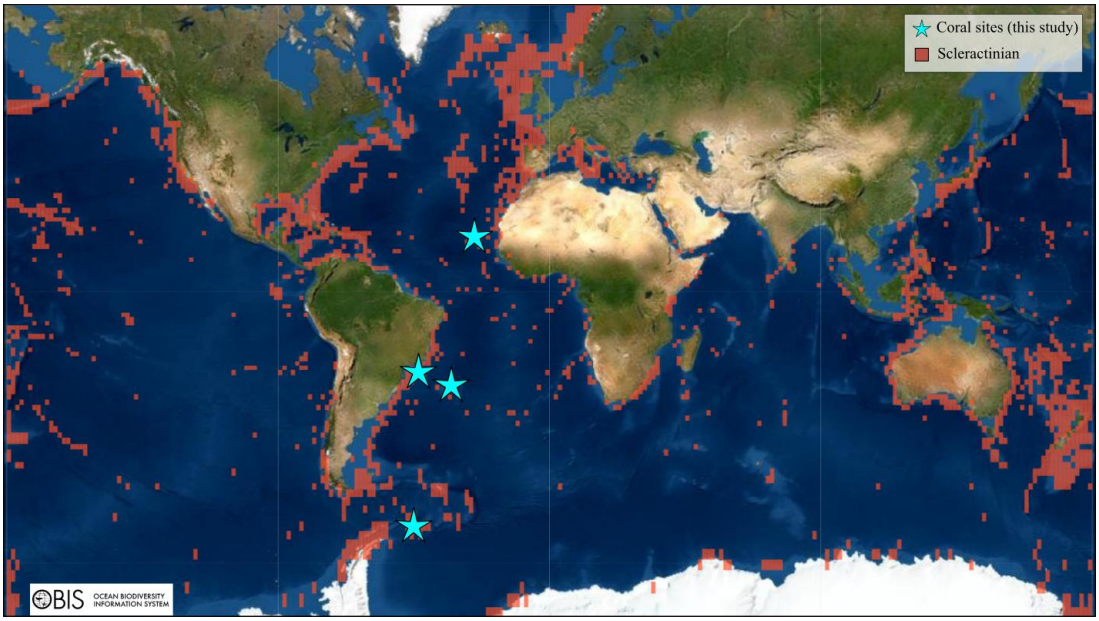

Figure 1: Global occurrence of scleractinian corals deeper than 150 m. Blue stars indicate the coral sites analysed in this thesis. Map and data extracted from OBIS database (https://obis.org/ accessed on the 02 November 2022).

PUBLISHED AND SUBMITTED PUBLICATIONS OF THE AUTHOR

de Carvalho Ferreira, M. L., Robinson, L. F., Stewart, J. A., Li, T., Chen, T., Burke, A., Kitahara, M. V., White, N. J., 2022. Spatial and temporal distribution of cold-water corals in the Northeast Atlantic Ocean over the last 150 thousand years. Deep Sea Research Part I: Oceanographic Research Papers, 190, https://doi.org/10.1016/j.dsr.2022.103892

de Carvalho Ferreira, Maria Luiza; Robinson, Laura F; Stewart, Joseph A; Li, Tao; Chen, Tianyu; Burke, Andrea; Kitahara, Marcelo V; White, Nicholas J (2022): U-Th and 14C ages of cold-water corals at Northeast Atlantic from the past 150 thousand years. PANGAEA, https://doi.org/10.1594/PANGAEA.945280

Kershaw, J., Stewart, J. A., Strawson, I., **de Carvalho Ferreira, M. L.**, Robinson, L. F., Hendry, K. R., Samperiz, A., Burke, A., Rae, J. W. B., Day, R. D., Etnoyer, P. J., Williams, B., Häussermann, V. Ba/Ca of stylasterid coral skeletons records dissolved seawater barium concentrations. In review at Chemical Geology.

Stewart, J. A., Robinson, L. F., Rae, J. W. B., Burke, A., Chen, T., Li, T., **de Carvalho Ferreira, M. L.**, Fornari, D. Deep-sea corals reveal Antarctic climate pacing of low latitude deglacial warming. In review at Science Advances.

REFERENCES

Adkins, J., P. deMenocal, and G. Eshel. 2006. The “African humid period” and the record of marine upwelling from excess 230Th in Ocean Drilling Program Hole 658C. Paleoceanography, 21(4):1–14, https://doi.org/10.1029/2005PA001200.

Adkins, J. F., E. A. Boyle, W. B. Curry, and A. Lutringer. 2003. Stable isotopes in deep-sea corals and a new mechanism for “vital effects.” Geochimica et Cosmochimica Acta, 67(6):1129–1143, https://doi.org/10.1016/S0016-7037(02)01203-6.

Adkins, J. F., S. Griffin, M. Kashgarian, H. Cheng, E. R. M. Druffel, E. A. Boyle, R. Lawrence Edwards, and C.-C. Shen. 2002a. Radiocarbon Dating of Deep-Sea Corals. Radiocarbon, 44(2):567–580, https://doi.org/10.1017/S0033822200031921.

Adkins, J. F., K. McIntyre, and D. P. Schrag. 2002b. The Salinity, Temperature, and δ 18 O of the Glacial Deep Ocean. Science, 298(5599):1769–1773, https://doi.org/10.1126/science.1076252.

Adkins, J. F., H. Cheng, E. A. Boyle, E. R. M. Druffel, and R. L. Edwards. 1998. Deep-Sea Coral Evidence for Rapid Change in Ventilation of the Deep North Atlantic 15,400 Years Ago. Science, 280(5364):725–728, https://doi.org/10.1126/science.280.5364.725.

Adkins, J. F., and E. A. Boyle. 1997. Changing atmospheric Δ 14 C and the record of deep water paleoventilation ages. Paleoceanography, 12(3):337–344, https://doi.org/10.1029/97PA00379.

Andersen, M. B., C. H. Stirling, B. Zimmermann, and A. N. Halliday. 2010. Precise determination of the open ocean 234U/238U composition. Geochemistry, Geophysics, Geosystems, 11(12) https://doi.org/10.1029/2010GC003318.

Auro, M. E., L. F. Robinson, A. Burke, L. I. Bradtmiller, M. Q. Fleisher, and R. F. Anderson. 2012. Improvements to 232-thorium, 230-thorium, and 231-protactinium analysis in seawater arising from GEOTRACES intercalibration. Limnology and Oceanography: Methods, 10(JULY):464–474, https://doi.org/10.4319/lom.2012.10.464.

Ausín, B., M. Sarnthein, and N. Haghipour. 2021. Glacial-to-deglacial reservoir and ventilation ages on the southwest Iberian continental margin. Quaternary Science Reviews, 255:106818, https://doi.org/10.1016/j.quascirev.2021.106818.

Bahr, A., M. Doubrawa, J. Titschack, G. Austermann, A. Koutsodendris, D. Nürnberg, A. L. Albuquerque, O. Friedrich, and J. Raddatz. 2020. Monsoonal forcing of cold-water coral growth off southeastern Brazil during the past 160 kyr. Biogeosciences, 17(23):5883–5908, https://doi.org/10.5194/bg-17-5883-2020.

Barbante, C., J. M. Barnola, S. Becagli, J. Beer, M. Bigler, C. Boutron, T. Blunier, E. Castellano, O. Cattani, J. Chappellaz, D. Dahl-Jensen, M. Debret, B. Delmonte, D. Dick, S. Falourd, S. Faria, U. Federer, H. Fischer, J. Freitag, A. Frenzel, D. Fritzsche, F. Fundel, P. Gabrielli, V. Gaspari, R. Gersonde, W. Graf, D. Grigoriev, I. Hamann, M. Hansson, G. Hoffmann, M. A. Hutterli, P. Huybrechts, E. Isaksson, S. Johnsen, J. Jouzel, M. Kaczmarska, T. Karlin, P. Kaufmann, S. Kipfstuhl, M. Kohno, F. Lambert, A. Lambrecht, A. Lambrecht, A. Landais, G. Lawer, M. Leuenberger, G. Littot, L. Loulergue, D. Lüthi, V. Maggi, F. Marino, V. Masson-Delmotte, H. Meyer, H. Miller, R. Mulvaney, B. Narcisi, J. Oerlemans, H. Oerter, F. Parrenin, J. R. Petit, G. Raisbeck, D. Raynaud, R. Röthlisberger, U. Ruth, O. Rybak, M. Severi, J. Schmitt, J. Schwander,

U. Siegenthaler, M. L. Siggaard-Andersen, R. Spahni, J. P. Steffensen, B. Stenni, T. F. Stocker, J. L. Tison, R. Traversi, R. Udisti, F. Valero-Delgado, M. R. Van Den Broeke, R. S. W. Van De Wal, D. Wagenbach, A. Wegner, K. Weiler, F. Wilhelms, J. G. Winther, and E. Wolff. 2006. One-to-one coupling of glacial climate variability in Greenland and Antarctica. Nature, 444(7116):195–198, https://doi.org/10.1038/nature05301.

Barker, S., G. Knorr, M. J. Vautravers, P. Diz, and L. C. Skinner. 2010. Extreme deepening of the Atlantic overturning circulation during deglaciation. Nature Geoscience, 3(8):567–571, https://doi.org/10.1038/ngeo921.

Barker, S., P. Diz, M. J. Vautravers, J. Pike, G. Knorr, I. R. Hall, and W. S. Broecker. 2009. Interhemispheric Atlantic seesaw response during the last deglaciation. Nature, 457(7233):1097–1102, https://doi.org/10.1038/nature07770.

Bashirova, L. D., E. S. Kandiano, V. V. Sivkov, and H. A. Bauch. 2014. Migrations of the North Atlantic Polar front during the last 300 ka: Evidence from planktic foraminiferal data. Oceanology, 54(6):798–807, https://doi.org/10.1134/S0001437014060010.

Bashmachnikov, I., Â. Nascimento, F. Neves, and T. Menezes. 2015. Distribution of intermediate water masses in the subtropical northeast Atlantic. Ocean Science Discussions, 12(3):769–822, https://doi.org/10.5194/osd-12-769-2015.

Bazin, L., A. Landais, B. Lemieux-Dudon, H. Toyé Mahamadou Kele, D. Veres, F. Parrenin, P. Martinerie, C. Ritz, E. Capron, V. Y. Lipenkov, M.-F. Loutre, D. Raynaud, B. M. Vinther, A. M. Svensson, S. O. Rasmussen, M. Severi, T. Blunier, M. C. Leuenberger, H. Fischer, V. Masson-Delmotte, J. A. Chappellaz, and E. Wolff. 2013. Delta18O measured on ice core EDML on AICC2012 chronology https://doi.org/https://doi.org/10.1594/PANGAEA.824888.

Beck, J. W., D. A. Richards, R. L. Edwards, B. W. Silverman, P. L. Smart, D. J. Donahue, S. Hererra-Osterheld, G. S. Burr, L. Calsoyas, A. J. T. Jull, and D. Biddulph. 2001. Extremely large variations of atmospheric 14C concentration during the last glacial period. Science, 292(5526):2453–2458, https://doi.org/10.1126/science.1056649.

Blois, J. L., P. L. Zarnetske, M. C. Fitzpatrick, and S. Finnegan. 2013. Climate Change and the Past, Present, and Future of Biotic Interactions. Science, 341(6145):499–504, https://doi.org/10.1126/science.1237184.

Blunier, T., and E. J. Brook. 2001. Timing of Millennial-Scale Climate Change in Antarctica and Greenland During the Last Glacial Period. Science, 291(5501):109–112, https://doi.org/10.1126/science.291.5501.109.

Boavida, J., R. Becheler, M. Choquet, N. Frank, M. Taviani, J. Bourillet, A. Meistertzheim, A. Grehan, A. Savini, and S. Arnaud-Haond. 2019. Out of the Mediterranean? Post-glacial colonization pathways varied among cold-water coral species. Journal of Biogeography, 46(5):915–931, https://doi.org/10.1111/jbi.13570.

Böhm, E., J. Lippold, M. Gutjahr, M. Frank, P. Blaser, B. Antz, J. Fohlmeister, N. Frank, M. B. Andersen, and M. Deininger. 2015. Strong and deep Atlantic meridional overturning circulation during the last glacial cycle. Nature, 517(7532):73–76, https://doi.org/10.1038/nature14059.

Bonneau, L., C. Colin, E. Pons-Branchu, F. Mienis, N. Tisnérat-Laborde, D. Blamart, M. Elliot, T. Collart, N. Frank, L. Foliot, and E. Douville. 2018. Imprint of Holocene Climate Variability on Cold-Water Coral Reef Growth at the SW Rockall Trough Margin, NE Atlantic. Geochemistry, Geophysics, Geosystems, 19(8):2437–2452, https://doi.org/10.1029/2018GC007502.

Bower, A., S. Lozier, A. Biastoch, K. Drouin, N. Foukal, H. Furey, M. Lankhorst, S. Rühs, and S. Zou. 2019. Lagrangian Views of the Pathways of the Atlantic Meridional Overturning Circulation. Journal of Geophysical Research: Oceans, 124(8):5313–5335, https://doi.org/10.1029/2019JC015014.

Boyle, E. A. 1981. Cadmium, zinc, copper, and barium in foraminifera tests. Earth and Planetary Science Letters, 53(1):11–35, https://doi.org/10.1016/0012-821X(81)90022-4.

Bradtmiller, L. I., D. McGee, M. Awalt, J. Evers, H. Yerxa, C. W. Kinsley, and P. B. DeMenocal. 2016. Changes in biological productivity along the northwest African margin over the past 20,000 years. Paleoceanography, 31(1):185–202, https://doi.org/10.1002/2015PA002862.

Bradtmiller, L. I., R. F. Anderson, M. Q. Fleisher, and L. H. Burckle. 2007. Opal burial in the equatorial Atlantic Ocean over the last 30 ka: Implications for glacial-interglacial changes in the ocean silicon cycle. Paleoceanography, 22(4):n/a-n/a, https://doi.org/10.1029/2007PA001443.

Broecker, W. 2018. CO2: Earth's Climate Driver. Geochemical Perspectives, 7(2):117–196, https://doi.org/10.7185/geochempersp.7.2.

Broecker, W. S. 2014. Radiocarbon; Pp. 257–271. In Treatise on Geochemistry. Vol. 4. Elsevier https://doi.org/10.1016/B978-0-08-095975-7.00409-5.

Broecker, W., G. Bond, M. Klas, E. Clark, and J. McManus. 1992. Origin of the northern Atlantic's Heinrich events. Climate Dynamics, 6(3–4):265–273, https://doi.org/10.1007/BF00193540.

Broecker, W. ., and T. Takahashi. 1980. Hydrography of the central Atlantic—III. The North Atlantic deep-water complex. Deep Sea Research Part A. Oceanographic Research Papers, 27(8):591–613, https://doi.org/10.1016/0198-0149(80)90076-X.

Bryan, S. P., and T. M. Marchitto. 2008. Mg/Ca-temperature proxy in benthic foraminifera: New calibrations from the Florida Straits and a hypothesis regarding Mg/Li. Paleoceanography, 23(2):1–17, https://doi.org/10.1029/2007PA001553.

Burke, A., A. L. Stewart, J. F. Adkins, R. Ferrari, M. F. Jansen, and A. F. Thompson. 2015. The glacial mid-depth radiocarbon bulge and its implications for the overturning circulation. Paleoceanography, 30(7):1021–1039, https://doi.org/10.1002/2015PA002778.

Burke, A., and L. F. Robinson. 2012. The Southern Ocean's Role in Carbon Exchange During the Last Deglaciation. Science, 335(February):557–562, https://doi.org/10.1126/science.1208163.

Burke, A., L. F. Robinson, A. P. McNichol, W. J. Jenkins, K. M. Scanlon, and D. S. Gerlach. 2010. Reconnaissance dating: A new radiocarbon method applied to assessing the temporal distribution of Southern Ocean deep-sea corals. Deep-Sea Research Part I: Oceanographic Research Papers, 57(11):1510–1520, https://doi.org/10.1016/j.dsr.2010.07.010.

Cairns, S. D. 2007. DEEP-WATER CORALS: AN OVERVIEW WITH SPECIAL REFERENCE TO DIVERSITY AND DISTRIBUTION OF DEEP-WATER SCLERACTINIAN CORALS. Bulletin of Marine Science, 81(3):311–322,.

Cairns, S. D. 1982. Antarctic and Subantarctic Scleractinia. (January 1983):1–74, https://doi.org/10.1029/AR034p0001.

Came, R. E., D. W. Oppo, W. B. Curry, and J. Lynch-Stieglitz. 2008. Deglacial variability in the surface return flow of the Atlantic meridional overturning circulation. Paleoceanography, 23(1):1–10, https://doi.org/10.1029/2007PA001450.

Came, R. E., W. B. Curry, D. W. Oppo, A. J. Broccoli, R. J. Stouffer, and J. Lynch-Stieglitz. 2007. North atlantic intermediate depth variability during the younger dryas: Evidence from benthic foraminiferal Mg/Ca and the GFDL R30 coupled climate model. Geophysical Monograph Series, 173(January):247–263, https://doi.org/10.1029/173GM16.

Canadell, J. G., P. M. S. Monteiro, M. H. Costa, L. C. da Cunha, P. M. Cox, A. V. Eliseev, S. Henson, M. Ishii, S. Jaccard, C. Koven, A. Lohila, P. K. Patra, S. Piao, J. Rogelj, S. Syampungani, S. Zaehle, and K. Zickfeld. 2021. Global Carbon and other Biogeochemical Cycles and Feedbacks; Pp. In Climate Change 2021: The Physical Science Basis. Contribution of Working Group I to the Sixth Assessment Report of the Intergovernmental Panel on Climate Change. V. Masson-Delmotte,, P. Zhai,, A. Pirani,, S. L. Connors,, C. Péan,, S. Berger,, N. Caud,, Y. Chen,, L. Goldfarb,, M. I. Gomis,, M. Huang,, K. Leitzell,, E. Lonnoy,, J.B.R.Matthews,, T. K. Maycock,, T. Waterfield,, O. Yelekçi,, R. Yu, and B. Zhou, eds, Cambridge University Press.

Capuzzo, E., C. P. Lynam, J. Barry, D. Stephens, R. M. Forster, N. Greenwood, A. McQuatters-Gollop, T. Silva, S. M. van Leeuwen, and G. H. Engelhard. 2018. A decline in primary production in the North Sea over 25 years, associated with reductions in zooplankton abundance and fish stock recruitment. Global Change Biology, 24(1):e352–e364, https://doi.org/10.1111/gcb.13916.

Carranza, A., A. M. Recio, M. Kitahara, F. Scarabino, L. Ortega, G. López, P. Franco-Fraguas, C. de Mello, J. Acosta, and A. Fontan. 2012. Deep-water coral reefs from the Uruguayan outer shelf and slope. Marine Biodiversity, 42(3):411–414, https://doi.org/10.1007/s12526-012-0115-6.

Carvalho-Borges, M. de, I. B. M. Orselli, M. L. de C. Ferreira, and R. Kerr. 2018. Seawater acidification and anthropogenic carbon distribution on the continental shelf and slope of the western South Atlantic Ocean. Journal of Marine Systems, 187(August 2017):62–81, https://doi.org/10.1016/j.jmarsys.2018.06.008.

Case, D. H., L. F. Robinson, M. E. Auro, and A. C. Gagnon. 2010. Environmental and biological controls on Mg and Li in deep-sea scleractinian corals. Earth and Planetary Science Letters, 300(3–4):215–225, https://doi.org/10.1016/j.epsl.2010.09.029.

Chen, T., L. F. Robinson, A. Burke, L. Claxton, M. P. Hain, T. Li, J. W. B. Rae, J. Stewart, T. D. J. Knowles, D. J. Fornari, and K. S. Harpp. 2020. Persistently well-ventilated intermediate-depth ocean through the last deglaciation. Nature Geoscience, 13(11):733–738, https://doi.org/10.1038/s41561-020-0638-6.

Chen, T., L. F. Robinson, M. P. Beasley, L. M. Claxton, M. B. Andersen, L. J. Gregoire, J. Wadham, D. J. Fornari, and K. S. Harpp. 2016. Ocean mixing and ice-sheet control of seawater 234 U/ 238 U during the last deglaciation. Science, 354(6312):626–629, https://doi.org/10.1126/science.aag1015.

Chen, T., L. F. Robinson, A. Burke, J. Southon, P. Spooner, P. J. Morris, and H. C. Ng. 2015. Synchronous centennial abrupt events in the ocean and atmosphere during the last deglaciation. Science, 349(6255):1537–1541, https://doi.org/10.1126/science.aac6159.

Cheng, H., Y. Xu, X. Dong, J. Zhao, H. Li, J. Baker, A. Sinha, C. Spötl, H. Zhang, W. Du, B. Zong, X. Jia, G. Kathayat, D. Liu, Y. Cai, X. Wang, N. M. Strikis, F. W. Cruz, A. S. Auler, A. K. Gupta, R. K. Singh, S. Jaglan, S. Dutt, Z. Liu, and R. L. Edwards. 2021. Onset and termination of Heinrich Stadial 4 and the underlying climate dynamics. Communications Earth and Environment, 2(1) https://doi.org/10.1038/s43247-021-00304-6.

Cheng, H., R. Lawrence Edwards, J. Southon, K. Matsumoto, J. M. Feinberg, A. Sinha, W. Zhou, H. Li, X. Li, Y. Xu, S. Chen, M. Tan, Q. Wang, Y. Wang, and Y. Ning. 2018. Atmospheric

14C/12C changes during the last glacial period from hulu cave. Science, 362(6420):1293–1297, https://doi.org/10.1126/science.aau0747.

Cheng, H., R. Lawrence Edwards, C. C. Shen, V. J. Polyak, Y. Asmerom, J. Woodhead, J. Hellstrom, Y. Wang, X. Kong, C. Spötl, X. Wang, and E. Calvin Alexander. 2013. Improvements in230Th dating,230Th and234U half-life values, and U-Th isotopic measurements by multi-collector inductively coupled plasma mass spectrometry. Earth and Planetary Science Letters, 371–372:82–91, https://doi.org/10.1016/j.epsl.2013.04.006.

Cheng, H., J. Adkins, R. L. Edwards, and E. A. Boyle. 2000. U-Th dating of deep-sea corals. Geochimica et Cosmochimica Acta, 64(14):2401–2416, https://doi.org/10.1016/S0016-7037(99)00422-6.

Chutcharavan, P. M., A. Dutton, and M. J. Ellwood. 2018. Seawater234U/238U recorded by modern and fossil corals. Geochimica et Cosmochimica Acta, 224:1–17, https://doi.org/10.1016/j.gca.2017.12.017.

Clark, P. U., N. G. Pisias, T. F. Stocker, and A. J. Weaver. 2002. The role of the thermohaline circulation in abrupt climate change. Nature, 415(6874):863–869, https://doi.org/10.1038/415863a.

Cléroux, C., P. deMenocal, and T. Guilderson. 2011. Deglacial radiocarbon history of tropical Atlantic thermocline waters: Absence of CO2 reservoir purging signal. Quaternary Science Reviews, 30(15–16):1875–1882, https://doi.org/10.1016/j.quascirev.2011.04.015.

Cohen, A. L., and T. A. McConnaughey. 2003. Geochemical Perspectives on Coral Mineralization. Reviews in Mineralogy and Geochemistry, 54(1):151–187, https://doi.org/10.2113/0540151.

Cordeiro, R. T., B. M. Neves, M. V. Kitahara, R. C. Arantes, and C. D. Perez. 2020. First assessment on Southwestern Atlantic equatorial deep-sea coral communities. Deep-Sea Research Part I: Oceanographic Research Papers, 163(June) https://doi.org/10.1016/j.dsr.2020.103344.

Cordeiro, R. T. S., B. M. Neves, J. S. Rosa-Filho, and C. D. Pérez. 2015. Mesophotic coral ecosystems occur offshore and north of the Amazon River. Bulletin of Marine Science, 91(4):491–510, https://doi.org/10.5343/bms.2015.1025.

Cordeiro, R. T. S., M. V. Kitahara, and F. D. Amaral. 2014. New records and range extensions of azooxanthellate scleractinians (Cnidaria: Anthozoa) from Brazil. ANZIAM Journal, 5(3):1–6, https://doi.org/10.1017/S175526721200019X.

Cuny-Guirriec, K., E. Douville, S. Reynaud, D. Allemand, L. Bordier, M. Canesi, C. Mazzoli, M. Taviani, S. Canese, M. McCulloch, J. Trotter, S. D. Rico-Esenaro, J. A. Sanchez-Cabeza, A. C. Ruiz-Fernández, J. P. Carricart-Ganivet, P. M. Scott, A. Sadekov, and P. Montagna. 2019. Coral Li/Mg thermometry: Caveats and constraints. Chemical Geology, 523(April):162–178, https://doi.org/10.1016/j.chemgeo.2019.03.038.

Curry, W. B., and D. W. Oppo. 2005. Glacial water mass geometry and the distribution of δ 13 C of ΣCO 2 in the western Atlantic Ocean. Paleoceanography, 20(1):n/a-n/a, https://doi.org/10.1029/2004PA001021.

Davies, A. J., and J. M. Guinotte. 2011. Global Habitat Suitability for Framework-Forming Cold-Water Corals. PLoS ONE, 6(4):e18483, https://doi.org/10.1371/journal.pone.0018483.

de Carvalho Ferreira, M. L., L. F. Robinson, J. A. Stewart, T. Li, T. Chen, A. Burke, M. Kitahara, and N. J. White. 2022. Spatial and temporal distribution of cold-water corals in the Northeast Atlantic

Ocean over the last 150 thousand years. Deep Sea Research Part I: Oceanographic Research Papers, https://doi.org/10.1016/j.dsr.2022.103892.

de Carvalho Ferreira, M. L., and R. Kerr. 2017. Source water distribution and quantification of North Atlantic Deep Water and Antarctic Bottom Water in the Atlantic Ocean. Progress in Oceanography, 153:66–83, https://doi.org/10.1016/j.pocean.2017.04.003.

De Mol, L., D. Van Rooij, H. Pirlet, J. Greinert, N. Frank, F. Quemmerais, and J.-P. Henriet. 2011. Cold-water coral habitats in the Penmarc'h and Guilvinec Canyons (Bay of Biscay): Deep-water versus shallow-water settings. Marine Geology, 282(1–2):40–52, https://doi.org/10.1016/j.margeo.2010.04.011.

De Mol, B., P. Van Rensbergen, S. Pillen, K. Van Herreweghe, D. Van Rooij, A. McDonnell, V. Huvenne, M. Ivanov, R. Swennen, and J. P. Henriet. 2002. Large deep-water coral banks in the Porcupine Basin, southwest of Ireland. Marine Geology, 188(1–2):193–231, https://doi.org/10.1016/S0025-3227(02)00281-5.

De Pol-Holz, R., L. Keigwin, J. Southon, D. Hebbeln, and M. Mohtadi. 2010. No signature of abyssal carbon in intermediate waters off Chile during deglaciation. Nature Geoscience, 3(3):192–195, https://doi.org/10.1038/ngeo745.

de Vernal, A., F. Eynaud, M. Henry, C. Hillaire-Marcel, L. Londeix, S. Mangin, J. Matthiessen, F. Marret, T. Radi, A. Rochon, S. Solignac, and J. L. Turon. 2005. Reconstruction of sea-surface conditions at middle to high latitudes of the Northern Hemisphere during the Last Glacial Maximum (LGM) based on dinoflagellate cyst assemblages. Quaternary Science Reviews, 24, 897–924, https://doi.org/10.1016/j.quascirev.2004.06.014.

Dickson, R. R., and J. Brown. 1994. The production of North Atlantic Deep Water: sources, rates, and pathways. Journal Of Geophysical Research, 99(C6):12319, https://doi.org/10.1029/94JC00530.

Dodds, L. A., J. M. Roberts, A. C. Taylor, and F. Marubini. 2007. Metabolic tolerance of the cold-water coral Lophelia pertusa (Scleractinia) to temperature and dissolved oxygen change. Journal of Experimental Marine Biology and Ecology, 349(2):205–214, https://doi.org/10.1016/j.jembe.2007.05.013.

Dorschel, B., D. Hebbeln, A. Rüggeberg, and C. Dullo. 2007. Carbonate budget of a cold-water coral carbonate mound: Propeller Mound, Porcupine Seabight. International Journal of Earth Sciences, 96(1):73–83, https://doi.org/10.1007/s00531-005-0493-0.

Dorschel, B., D. Hebbeln, A. Rüggeberg, W. C. Dullo, and A. Freiwald. 2005. Growth and erosion of a cold-water coral covered carbonate mound in the Northeast Atlantic during the Late Pleistocene and Holocene. Earth and Planetary Science Letters, 233(1–2):33–44, https://doi.org/10.1016/j.epsl.2005.01.035.

Douarin, M., M. Elliot, S. R. Noble, D. Sinclair, L.-A. Henry, D. Long, S. G. Moreton, and J. Murray Roberts. 2013. Growth of north-east Atlantic cold-water coral reefs and mounds during the Holocene: A high resolution U-series and 14C chronology. Earth and Planetary Science Letters, 375:176–187, https://doi.org/10.1016/j.epsl.2013.05.023.

Dubois-Dauphin, Q., L. Bonneau, C. Colin, J.-C. Montero-Serrano, P. Montagna, D. Blamart, D. Hebbeln, D. Van Rooij, E. Pons-Branchu, F. Hemsing, A.-M. Wefing, and N. Frank. 2016. South Atlantic intermediate water advances into the North-east Atlantic with reduced Atlantic meridional overturning circulation during the last glacial period. Geochemistry, Geophysics, Geosystems, 17(6):2336–2353, https://doi.org/10.1002/2016GC006281.

Dullo, W.-C., S. Flögel, and A. Rüggeberg. 2008. Cold-water coral growth in relation to the hydrography of the Celtic and Nordic European continental margin. Marine Ecology Progress Series, 371:165–176, https://doi.org/10.3354/meps07623.

Durand, N., P. Deschamps, E. Bard, B. Hamelin, G. Camoin, A. L. Thomas, G. M. Henderson, Y. Yokoyama, and H. Matsuzaki. 2013. Comparison of 14 C and U-Th Ages in Corals from IODP #310 Cores Offshore Tahiti. Radiocarbon, 55(4):1947–1974, https://doi.org/10.2458/azu_js_rc.v55i2.16134.

Edwards, R. L. L., C. D. D. Gallup, and H. Cheng. 2003. Uranium-series Dating of Marine and Lacustrine Carbonates; Pp. 363–405. In Reviews in Mineralogy and Geochemistry. Vol. 52. https://doi.org/10.2113/0520363.

Edwards, R. L., J. H. Chen, and G. J. Wasserburg. 1987. 238U-234U-230Th-232Th systematics and the precise measurement of time over the past 500,000 years. Earth and Planetary Science Letters, 81(2–3):175–192, https://doi.org/10.1016/0012-821X(87)90154-3.

Eisele, M., N. Frank, C. Wienberg, D. Hebbeln, M. López Correa, E. Douville, and A. Freiwald. 2011. Productivity controlled cold-water coral growth periods during the last glacial off Mauritania. Marine Geology, 280(1–4):143–149, https://doi.org/10.1016/j.margeo.2010.12.007.

Eisele, M., D. Hebbeln, and C. Wienberg. 2008. Growth history of a cold-water coral covered carbonate mound — Galway Mound, Porcupine Seabight, NE-Atlantic. Marine Geology, 253(3–4):160–169, https://doi.org/10.1016/j.margeo.2008.05.006.

Eltgroth, S. F., J. F. Adkins, L. F. Robinson, J. Southon, and M. Kashgarian. 2006. A deep-sea coral record of North Atlantic radiocarbon through the Younger Dryas: Evidence for intermediate water/deepwater reorganization. Paleoceanography, 21(4):1–12, https://doi.org/10.1029/2005PA001192.

Esat, T. M., and Y. Yokoyama. 2006. Variability in the uranium isotopic composition of the oceans over glacial-interglacial timescales. Geochimica et Cosmochimica Acta, 70(16):4140–4150, https://doi.org/10.1016/j.gca.2006.06.013.

Eynaud, F., L. De Abreu, A. Voelker, J. Schönfeld, E. Salgueiro, J. L. Turon, A. Penaud, S. Toucanne, F. Naughton, M. F. Sánchez Goñi, B. Malaizé, and I. Cacho. 2009. Position of the Polar Front along the western Iberian margin during key cold episodes of the last 45 ka. Geochemistry, Geophysics, Geosystems, 10(7) https://doi.org/10.1029/2009GC002398.

Ezat, M. M., T. L. Rasmussen, D. J. R. R. Thornalley, J. Olsen, L. C. Skinner, B. Hönisch, and J. Groeneveld. 2017. Ventilation history of Nordic Seas overflows during the last (de)glacial period revealed by species-specific benthic foraminiferal 14 C dates. Paleoceanography, 32(2):172–181, https://doi.org/10.1002/2016PA003053.

Fairbanks, R. G., R. A. Mortlock, T. C. Chiu, L. Cao, A. Kaplan, T. P. Guilderson, T. W. Fairbanks, A. L. Bloom, P. M. Grootes, and M.-J. J. Nadeau. 2005. Radiocarbon calibration curve spanning 0 to 50,000 years BP based on paired 230Th/234U/238U and 14C dates on pristine corals. Quaternary Science Reviews, 24(16–17):1781–1796, https://doi.org/10.1016/j.quascirev.2005.04.007.

Farmer, J. R., L. F. Robinson, and B. Hönisch. 2015. Growth rate determinations from radiocarbon in bamboo corals (genus Keratoisis). Deep-Sea Research Part I: Oceanographic Research Papers, 105:26–40, https://doi.org/10.1016/j.dsr.2015.08.004.

Ferrari, R., M. F. Jansen, J. F. Adkins, A. Burke, A. L. Stewart, and A. F. Thompson. 2014. Antarctic sea ice control on ocean circulation in present and glacial climates. Proceedings of the National Academy of Sciences, 111(24):8753–8758, https://doi.org/10.1073/pnas.1323922111.

Flögel, S., W.-C. Dullo, O. Pfannkuche, K. Kiriakoulakis, and A. Rüggeberg. 2014. Geochemical and physical constraints for the occurrence of living cold-water corals. Deep-Sea Research Part II, 99:19–26, https://doi.org/10.1016/j.dsr2.2013.06.006.

Fofonoff, N. P., and R. C. Millard Jr. 1983. Algorithms for the computation of fundamental properties of seawater. UNESCO Technical Papers in Marine Sciences, 53, https://doi.org/https://doi.org/10.25607/OBP-1450.

Försterra, G., V. Häussermann, and J. Laudien. 2016. Animal Forests in the Chilean Fjords: Discoveries, Perspectives and Threats in Shallow and Deep Waters; Pp. 1–35. In Marine Animal Forests. Springer International Publishing, Cham https://doi.org/10.1007/978-3-319-17001-5_3-1.

Foubert, A., D. Depreiter, T. Beck, L. Maignien, B. Pannemans, N. Frank, D. Blamart, and J. Henriet. 2008. Carbonate mounds in a mud volcano province off north-west Morocco: Key to processes and controls. Marine Geology, 248(1–2):74–96, https://doi.org/10.1016/j.margeo.2007.10.012.

Frank, N., A. Freiwald, M. L. Correa, C. Wienberg, M. Eisele, D. Hebbeln, D. Van Rooij, J.-P. Henriet, C. Colin, T. van Weering, H. de Haas, P. Buhl-Mortensen, J. M. Roberts, B. De Mol, E. Douville, D. Blamart, and C. Hatte. 2011. Northeastern Atlantic cold-water coral reefs and climate. Geology, 39(8):743–746, https://doi.org/10.1130/G31825.1.

Frank, N., E. Ricard, A. Lutringer-Paquet, C. van der Land, C. Colin, D. Blamart, A. Foubert, D. Van Rooij, J.-P. Henriet, H. de Haas, and T. van Weering. 2009. The Holocene occurrence of cold water corals in the NE Atlantic: Implications for coral carbonate mound evolution. Marine Geology, 266(1–4):129–142, https://doi.org/10.1016/j.margeo.2009.08.007.

Frank, N., M. Paterne, L. Ayliffe, T. van Weering, J.-P. Henriet, and D. Blamart. 2004. Eastern North Atlantic deep-sea corals: tracing upper intermediate water Δ14C during the Holocene. Earth and Planetary Science Letters, 219(3–4):297–309, https://doi.org/10.1016/S0012-821X(03)00721-0.

Freeman, E., L. C. Skinner, C. Waelbroeck, and D. Hodell. 2016. Radiocarbon evidence for enhanced respired carbon storage in the Atlantic at the Last Glacial Maximum. Nature Communications, 7(May):1–8, https://doi.org/10.1038/ncomms11998.

Freeman, E., L. C. Skinner, A. Tisserand, T. Dokken, A. Timmermann, L. Menviel, and T. Friedrich. 2015. An Atlantic-Pacific ventilation seesaw across the last deglaciation. Earth and Planetary Science Letters, 424:237–244, https://doi.org/10.1016/j.epsl.2015.05.032.

Freiwald, A. 2002. Reef-Forming Cold-Water Corals; Pp. 365–385. In Ocean Margin Systems. G. Wefer,, D. Billett,, D. Hebbeln,, B. Jorgensen,, M. Schluter, and T. van Weering, eds, Springer Berlin Heidelberg, Berlin, Heidelberg https://doi.org/10.1007/978-3-662-05127-6_23.

Galbraith, E. D., T. M. Merlis, and J. B. Palter. 2016. Destabilization of glacial climate by the radiative impact of Atlantic Meridional Overturning Circulation disruptions. Geophysical Research Letters, 43(15):8214–8221, https://doi.org/10.1002/2016GL069846.

Galbraith, E. D., E. Y. Kwon, D. Bianchi, M. P. Hain, and J. L. Sarmiento. 2015. The impact of atmospheric pCO2 on carbon isotope ratios of the atmosphere and ocean. Global Biogeochemical Cycles, 29(3):307–324, https://doi.org/10.1002/2014GB004929.

García-Ibáñez, M. I., P. C. Pardo, L. I. Carracedo, H. Mercier, P. Lherminier, A. F. Ríos, and F. F. Pérez. 2015. Structure, transports and transformations of the water masses in the Atlantic Subpolar Gyre. Progress in Oceanography, 135:18–36, https://doi.org/10.1016/j.pocean.2015.03.009.

Gebbie, G. 2014. How much did Glacial North Atlantic Water shoal? Paleoceanography, 29(3):190–209, https://doi.org/10.1002/2013PA002557.

Godwin, H. 1962. Half-life of Radiocarbon. Nature, 195(4845):984–984, https://doi.org/10.1038/195984a0.

Gu, S., Z. Liu, J. Zhang, J. Rempfer, F. Joos, and D. W. Oppo. 2017. Coherent Response of Antarctic Intermediate Water and Atlantic Meridional Overturning Circulation During the Last Deglaciation: Reconciling Contrasting Neodymium Isotope Reconstructions From the Tropical Atlantic. Paleoceanography, 32(10):1036–1053, https://doi.org/10.1002/2017PA003092.

Guinotte, J. M., J. Orr, S. Cairns, A. Freiwald, L. Morgan, and R. George. 2006. Will human-induced changes in seawater chemistry alter the distribution of deep-sea scleractinian corals? Frontiers in Ecology and the Environment, 4:141–146, https://doi.org/https://doi.org/10.1890/1540-9295(2006)004[0141:WHCISC]2.0.CO;2.

Hanz, U., C. Wienberg, D. Hebbeln, G. Duineveld, M. Lavaleye, K. Juva, W.-C. Dullo, A. Freiwald, L. Tamborrino, G.-J. Reichart, S. Flögel, and F. Mienis. 2019. Environmental factors influencing benthic communities in the oxygen minimum zones on the Angolan and Namibian margins. Biogeosciences, 16(22):4337–4356, https://doi.org/10.5194/bg-16-4337-2019.

Hathorne, E. C., T. Felis, A. Suzuki, H. Kawahata, and G. Cabioch. 2013. Lithium in the aragonite skeletons of massive Porites corals: A new tool to reconstruct tropical sea surface temperatures. Paleoceanography, 28(1):143–152, https://doi.org/10.1029/2012PA002311.

He, C., Z. Liu, J. Zhu, J. Zhang, S. Gu, B. L. Otto-Bliesner, E. Brady, C. Zhu, Y. Jin, and J. Sun. 2020. North Atlantic subsurface temperature response controlled by effective freshwater input in "Heinrich" events. Earth and Planetary Science Letters, 539:116247, https://doi.org/10.1016/j.epsl.2020.116247.

Heaton, T. J., P. Köhler, M. Butzin, E. Bard, R. W. Reimer, W. E. N. Austin, C. Bronk Ramsey, P. M. Grootes, K. A. Hughen, B. Kromer, P. J. Reimer, J. Adkins, A. Burke, M. S. Cook, J. Olsen, and L. C. Skinner. 2020a. Marine20 - The Marine Radiocarbon Age Calibration Curve (0-55,000 cal BP). Radiocarbon, 62(4):779–820, https://doi.org/10.1017/RDC.2020.68.

Heaton, T. J., M. Blaauw, P. G. Blackwell, C. Bronk Ramsey, P. J. Reimer, and E. M. Scott. 2020b. The IntCal20 Approach to Radiocarbon Calibration Curve Construction: A New Methodology Using Bayesian Splines and Errors-in-Variables. Radiocarbon, 62(4):821–863, https://doi.org/10.1017/RDC.2020.46.

Hebbeln, D., C. Wienberg, W.-C. Dullo, A. Freiwald, F. Mienis, C. Orejas, and J. Titschack. 2020. Cold-water coral reefs thriving under hypoxia. Coral Reefs, 39(4):853–859, https://doi.org/10.1007/s00338-020-01934-6.

Hebbeln, D., R. da C. Portilho-Ramos, C. Wienberg, and J. Titschack. 2019. The fate of cold-water corals in a changing world: A geological perspective. Frontiers in Marine Science, 6(MAR):1–8, https://doi.org/10.3389/fmars.2019.00119.

Hemming, S. R. 2004. Heinrich events: Massive late Pleistocene detritus layers of the North Atlantic and their global climate imprint. Reviews of Geophysics, 42(1) https://doi.org/10.1029/2003RG000128.

Henderson, G. M. 2002. Seawater (234 U/ 238 U) during the last 800 thousand years. Earth and Planetary Science Letters, 199(1–2):97–110, https://doi.org/10.1016/S0012-821X(02)00556-3.

Henry, L.-A., N. Frank, D. Hebbeln, C. Wienberg, L. Robinson, T. van de Flierdt, M. Dahl, M. Douarin, C. L. Morrison, M. López Correa, A. D. Rogers, M. Ruckelshausen, and J. M. Roberts. 2014. Global ocean conveyor lowers extinction risk in the deep sea. Deep Sea Research Part I: Oceanographic Research Papers, 88(1):8–16, https://doi.org/10.1016/j.dsr.2014.03.004.

Hernández-Guerra, A., E. Fraile-Nuez, F. López-Laatzen, A. Martínez, G. Parrilla, and P. Vélez-Belchí. 2005. Canary Current and North Equatorial Current from an inverse box model. Journal of Geophysical Research, 110(C12):C12019, https://doi.org/10.1029/2005JC003032.

Hines, S. K. V., J. M. Eiler, J. R. Southon, and J. F. Adkins. 2019. Dynamic Intermediate Waters Across the Late Glacial Revealed by Paired Radiocarbon and Clumped Isotope Temperature Records. Paleoceanography and Paleoclimatology, 34(7):1074–1091, https://doi.org/10.1029/2019PA003568.

Hines, S. K. V., J. R. Southon, and J. F. Adkins. 2015. A high-resolution record of Southern Ocean intermediate water radiocarbon over the past 30,000 years. Earth and Planetary Science Letters, 432:46–58, https://doi.org/10.1016/j.epsl.2015.09.038.

Hodell, D. A., S. L. Kanfoush, A. Shemesh, X. Crosta, C. D. Charles, and T. P. Guilderson. 2001. Abrupt Cooling of Antarctic Surface Waters and Sea Ice Expansion in the South Atlantic Sector of the Southern Ocean at 5000 cal yr B.P. Quaternary Research, 56(2):191–198, https://doi.org/10.1006/qres.2001.2252.

Hoffmann, D. L., J. W. Beck, D. A. Richards, P. L. Smart, J. S. Singarayer, T. Ketchmark, and C. J. Hawkesworth. 2010. Towards radiocarbon calibration beyond 28 ka using speleothems from the Bahamas. Earth and Planetary Science Letters, 289(1–2):1–10, https://doi.org/10.1016/j.epsl.2009.10.004.

Howe, J. N. W., A. M. Piotrowski, T. L. Noble, S. Mulitza, C. M. Chiessi, and G. Bayon. 2016. North Atlantic Deep Water Production during the Last Glacial Maximum. Nature Communications, 7(June):11765, https://doi.org/10.1038/ncomms11765.

Huang, K. F., D. W. Oppo, and W. B. Curry. 2014. Decreased influence of Antarctic intermediate water in the tropical Atlantic during North Atlantic cold events. Earth and Planetary Science Letters, 389:200–208, https://doi.org/10.1016/j.epsl.2013.12.037.

Hughes, A. L. C., R. Gyllencreutz, Ø. S. Lohne, J. Mangerud, and J. I. Svendsen. 2016. The last Eurasian ice sheets - a chronological database and time-slice reconstruction, DATED-1. Boreas, 45(1):1–45, https://doi.org/10.1111/bor.12142.

Karakaş, G., N. Nowald, M. Blaas, P. Marchesiello, S. Frickenhaus, and R. Schlitzer. 2006. High-resolution modeling of sediment erosion and particle transport across the northwest African shelf. Journal of Geophysical Research: Oceans, 111(6):1–13, https://doi.org/10.1029/2005JC003296.

Keigwin, L. D., and E. A. Boyle. 2008. Did North Atlantic overturning halt 17,000 years ago? Paleoceanography, 23(1):n/a-n/a, https://doi.org/10.1029/2007PA001500.

Keigwin, L. D. 2004. Radiocarbon and stable isotope constraints on Last Glacial Maximum and Younger Dryas ventilation in the western North Atlantic. Paleoceanography, 19(4):n/a-n/a, https://doi.org/10.1029/2004PA001029.

Kindler, P., M. Guillevic, M. Baumgartner, J. Schwander, A. Landais, and M. Leuenberger. 2014. Temperature reconstruction from 10 to 120 kyr b2k from the NGRIP ice core. Climate of the Past, 10(2):887–902, https://doi.org/10.5194/cp-10-887-2014.

Kipp, M. A., H. Li, M. J. Ellwood, S. G. John, R. Middag, J. F. Adkins, and F. L. H. Tissot. 2022. 238U, 235U and 234U in seawater and deep-sea corals: A high-precision reappraisal. Geochimica et Cosmochimica Acta, 336:231–248, https://doi.org/10.1016/j.gca.2022.09.018.

Kitahara, M. V., R. R. Capítoli, and N. O. Horn Filho. 2010. Distribuição das espécies de corais azooxantelados na plataforma e talude continental superior do sul do Brasil. Iheringia. Série Zoologia, 99(3):223–236, https://doi.org/10.1590/s0073-47212009000300001.

Kitahara, M. V. 2009. A pesca demersal de profundidade e os bancos de corais azooxantelados do sul do Brasil. Biota Neotrop. Biota Neotrop, 9, https://doi.org/10.1590/S1676-06032009000200003.

Kitahara, M. V. 2007. Species richness and distribution of azooxanthellate Scleractinia in Brazil. Bulletin of Marine Science, 81(2):497–518.

Knowles, T. D. J., P. S. Monaghan, and R. P. Evershed. 2019. Radiocarbon Sample Preparation Procedures and the First Status Report from the Bristol Radiocarbon AMS (BRAMS) Facility. Radiocarbon, 61(5):1541–1550, https://doi.org/10.1017/RDC.2019.28.

Li, T., L. F. Robinson, T. Chen, X. T. Wang, A. Burke, J. W. B. Rae, A. Pegrum-Haram, T. D. J. Knowles, G. Li, J. Chen, H. C. Ng, M. Prokopenko, G. H. Rowland, A. Samperiz, J. A. Stewart, J. Southon, and P. T. Spooner. 2020. Rapid shifts in circulation and biogeochemistry of the Southern Ocean during deglacial carbon cycle events. Science Advances, 6(42):eabb3807, https://doi.org/10.1126/sciadv.abb3807.

Libby, W. F., E. C. Anderson, and J. R. Arnold. 1949. Age Determination by Radiocarbon Content: World-Wide Assay of Natural Radiocarbon. Science, 109(2827):227–228, https://doi.org/10.1126/science.109.2827.227.

Lindberg, B., and J. Mienert. 2006. Sedimentological and geochemical environment of the Fugløy Reef off northern Norway. Cold-Water Corals and Ecosystems, 633–650, https://doi.org/10.1007/3-540-27673-4_31.

Lippold, J., M. Gutjahr, P. Blaser, E. Christner, M. L. de Carvalho Ferreira, S. Mulitza, M. Christl, F. Wombacher, E. Böhm, B. Antz, O. Cartapanis, H. Vogel, and S. L. Jaccard. 2016. Deep water provenience and dynamics of the (de)glacial Atlantic meridional overturning circulation. Earth and Planetary Science Letters, 445:68–78, https://doi.org/10.1016/j.epsl.2016.04.013.

Liu, Q., L. F. Robinson, E. Hendy, M. G. Prokopenko, J. A. Stewart, T. D. J. Knowles, T. Li, and A. Samperiz. In press. Reinterpreting radiocarbon records in bamboo corals – new insights from the tropical North Atlantic. In review at Geochimica et Cosmochimica Acta,.

Liu, Z., B. L. Otto-Bliesner, F. He, E. C. Brady, R. Tomas, P. U. Clark, A. E. Carlson, J. Lynch-Stieglitz, W. Curry, E. Brook, D. Erickson, R. Jacob, J. Kutzbach, and J. Cheng. 2009. Transient simulation of last deglaciation with a new mechanism for bolling-allerod warming. Science, 325(5938):310–314, https://doi.org/10.1126/science.1171041.

Löfverström, M., R. Caballero, J. Nilsson, and J. Kleman. 2014. Evolution of the large-scale atmospheric circulation in response to changing ice sheets over the last glacial cycle. Climate of the Past, 10(4):1453–1471, https://doi.org/10.5194/cp-10-1453-2014.

López Correa, M., P. Montagna, N. Joseph, A. Rüggeberg, J. Fietzke, S. Flögel, B. Dorschel, S. L. Goldstein, A. Wheeler, and A. Freiwald. 2012. Preboreal onset of cold-water coral growth

beyond the Arctic Circle revealed by coupled radiocarbon and U-series dating and neodymium isotopes. Quaternary Science Reviews, 34:24–43, https://doi.org/10.1016/j.quascirev.2011.12.005.

Lund, D. C., A. C. Tessin, J. L. Hoffman, and A. Schmittner. 2015. Southwest Atlantic water mass evolution during the last deglaciation. Paleoceanography, 30(5):477–494, https://doi.org/10.1002/2014PA002657.

Lynch-Stieglitz, J., J. F. Adkins, W. B. Curry, T. Dokken, I. R. Hall, J. C. Herguera, J. J.-M. Hirschi, E. V Ivanova, C. Kissel, O. Marchal, T. M. Marchitto, I. N. McCave, J. F. McManus, S. Mulitza, U. Ninnemann, F. Peeters, E.-F. Yu, and R. Zahn. 2007. Atlantic Meridional Overturning Circulation During the Last Glacial Maximum. Science, 316(5821):66–69, https://doi.org/10.1126/science.1137127.

Maamaatuaiahutapu, K., V. C. Garçon, C. Provost, M. Boulahdid, and A. P. Osiroff. 1992. Brazil-Malvinas Confluence: Water mass composition. Journal of Geophysical Research, 97:9493, https://doi.org/10.1029/92JC00484.

Mangini, A., J. M. Godoy, M. L. Godoy, R. Kowsmann, G. M. Santos, M. Ruckelshausen, A. Schroeder-Ritzrau, and L. Wacker. 2010. Deep sea corals off Brazil verify a poorly ventilated Southern Pacific Ocean during H2, H1 and the Younger Dryas. Earth and Planetary Science Letters, 293(3–4):269–276, https://doi.org/10.1016/j.epsl.2010.02.041.

Mangini, A., M. Lomitschka, R. Eichstädter, N. Frank, S. Vogler, G. Bonani, I. Hajdas, and J. Patzold. 1998. Coral provides way to age deep water. Nature, 392(6674):347–348, https://doi.org/10.1038/32804.

Marchitto, T. M., S. P. Bryan, W. Doss, M. T. McCulloch, and P. Montagna. 2018. A simple biomineralization model to explain Li, Mg, and Sr incorporation into aragonitic foraminifera and corals. Earth and Planetary Science Letters, 481:20–29, https://doi.org/10.1016/j.epsl.2017.10.022.

Marchitto, T. M., S. J. Lehman, J. D. Ortiz, J. Flückiger, and A. van Geen. 2007. Marine Radiocarbon Evidence for the Mechanism of Deglacial Atmospheric CO 2 Rise. Science, 316(5830):1456–1459, https://doi.org/10.1126/science.1138679.

Marchitto, T. M., and W. S. Broecker. 2006. Deep water mass geometry in the glacial Atlantic Ocean: A review of constraints from the paleonutrient proxy Cd/Ca. Geochemistry, Geophysics, Geosystems, 7(12) https://doi.org/10.1029/2006GC001323.

Marcott, S. A., T. K. Bauska, C. Buizert, E. J. Steig, J. L. Rosen, K. M. Cuffey, T. J. Fudge, J. P. Severinghaus, J. Ahn, M. L. Kalk, J. R. McConnell, T. Sowers, K. C. Taylor, J. W. C. White, and E. J. Brook. 2014. Centennial-scale changes in the global carbon cycle during the last deglaciation. Nature, 514(7524):616–619, https://doi.org/10.1038/nature13799.

Marcott, S. A., J. D. Shakun, P. U. Clark, and A. C. Mix. 2013. A Reconstruction of Regional and Global Temperature for the Past 11,300 Years. Science, 339(6124):1198–1201, https://doi.org/10.1126/science.1228026.

Marcott, S. A., P. U. Clark, L. Padman, G. P. Klinkhammer, S. R. Springer, Z. Liu, B. L. Otto-Bliesner, A. E. Carlson, A. Ungerer, J. Padman, F. He, J. Cheng, and A. Schmittner. 2011. Ice-shelf collapse from subsurface warming as a trigger for Heinrich events. Proceedings of the National Academy of Sciences of the United States of America, 108(33):13415–13419, https://doi.org/10.1073/pnas.1104772108.

Margolin, A. R., L. F. Robinson, A. Burke, R. G. Waller, K. M. Scanlon, M. L. Roberts, M. E. Auro, and T. van de Flierdt. 2014. Temporal and spatial distributions of cold-water corals in the Drake Passage: Insights from the last 35,000 years. Deep-Sea Research Part II: Topical Studies in Oceanography, 99:237–248, https://doi.org/10.1016/j.dsr2.2013.06.008.

Mark Moore, C., M. M. Mills, E. P. Achterberg, R. J. Geider, J. LaRoche, M. I. Lucas, E. L. McDonagh, X. Pan, A. J. Poulton, M. J. A. Rijkenberg, D. J. Suggett, S. J. Ussher, and E. M. S. Woodward. 2009. Large-scale distribution of Atlantic nitrogen fixation controlled by iron availability. Nature Geoscience, 2(12):867–871, https://doi.org/10.1038/ngeo667.

Masson-Delmotte, V., A. Landais, M. Stievenard, O. Cattani, S. Falourd, J. Jouzel, S. J. Johnsen, D. Dahl-Jensen, A. Sveinsbjornsdottir, J. W. C. White, T. Popp, and H. Fischer. 2005. Holocene climatic changes in Greenland: Different deuterium excess signals at Greenland Ice Core Project (GRIP) and NorthGRIP. Journal of Geophysical Research D: Atmospheres, 110(14):1–13, https://doi.org/10.1029/2004JD005575.

Masson, V., F. Vimeux, J. Jouzel, V. Morgan, M. Delmotte, P. Ciais, C. Hammer, S. Johnsen, V. Y. Lipenkov, E. Mosley-Thompson, J.-R. Petit, E. J. Steig, M. Stievenard, and R. Vaikmae. 2000. Holocene Climate Variability in Antarctica Based on 11 Ice-Core Isotopic Records. Quaternary Research, 54(3):348–358, https://doi.org/10.1006/qres.2000.2172.

Matul, A., M. S. Barash, T. A. Khusid, P. Behera, and M. Tiwari. 2018. Paleoenvironment variability during termination I at the Reykjanes Ridge, north Atlantic. Geosciences (Switzerland), 8(10):1–14, https://doi.org/10.3390/geosciences8100375.

Max, L., D. Nürnberg, C. M. Chiessi, M. M. Lenz, and S. Mulitza. 2022. Subsurface ocean warming preceded Heinrich Events. Nature Communications, 13(1):4217, https://doi.org/10.1038/s41467-022-31754-x.

McCulloch, M., M. Taviani, P. Montagna, M. López Correa, A. Remia, and G. Mortimer. 2010. Proliferation and demise of deep-sea corals in the Mediterranean during the Younger Dryas. Earth and Planetary Science Letters, 298(1–2):143–152, https://doi.org/10.1016/j.epsl.2010.07.036.

McGee, D., P. B. DeMenocal, G. Winckler, J. B. W. Stuut, and L. I. Bradtmiller. 2013. The magnitude, timing and abruptness of changes in North African dust deposition over the last 20,000yr. Earth and Planetary Science Letters, 371–372:163–176, https://doi.org/10.1016/j.epsl.2013.03.054.

McKay, C. L., H. L. Filipsson, O. E. Romero, J. B. W. Stuut, and B. Donner. 2014. Pelagic-benthic coupling within an upwelling system of the subtropical northeast Atlantic over the last 35kaBP. Quaternary Science Reviews, 106:299–315, https://doi.org/10.1016/j.quascirev.2014.04.027.

McManus, J. F., R. Francois, J.-M. Gherardi, L. D. Keigwin, and S. Brown-Leger. 2004. Collapse and rapid resumption of Atlantic meridional circulation linked to deglacial climate changes. Nature, 428(6985):834–837, https://doi.org/10.1038/nature02494.

Meckler, A. N., D. M. Sigman, K. A. Gibson, R. François, A. Martínez-García, S. L. Jaccard, U. Röhl, L. C. Peterson, R. Tiedemann, and G. H. Haug. 2013. Deglacial pulses of deep-ocean silicate into the subtropical North Atlantic Ocean. Nature, 495(7442):495–498, https://doi.org/10.1038/nature12006.

Meier, K. J. F., A. Bahr, C. M. Chiessi, A. L. Albuquerque, J. Raddatz, and O. Friedrich. 2021. Role of the Tropical Atlantic for the Interhemispheric Heat Transport During the Last Deglaciation. Paleoceanography and Paleoclimatology, 36(5) https://doi.org/10.1029/2020PA004107.

Middleton, J. L., S. Mukhopadhyay, C. H. Langmuir, J. F. McManus, and P. J. Huybers. 2018. Millennial-scale variations in dustiness recorded in Mid-Atlantic sediments from 0 to 70 ka. Earth and Planetary Science Letters, 482:12–22, https://doi.org/10.1016/j.epsl.2017.10.034.

Mienis, F., C. van der Land, H. C. de Stigter, M. van de Vorstenbosch, H. de Haas, T. Richter, and T. C. E. van Weering. 2009. Sediment accumulation on a cold-water carbonate mound at the Southwest Rockall Trough margin. Marine Geology, 265(1–2):40–50, https://doi.org/10.1016/j.margeo.2009.06.014.

Mies, M., R. B. Francini-Filho, C. Zilberberg, A. G. Garrido, G. O. Longo, E. Laurentino, A. Z. Güth, P. Y. G. Sumida, and T. N. S. Banha. 2020. South Atlantic Coral Reefs Are Major Global Warming Refugia and Less Susceptible to Bleaching. Frontiers in Marine Science, 7(June):1–13, https://doi.org/10.3389/fmars.2020.00514.

Miller, K. J., A. A. Rowden, A. Williams, and V. Häussermann. 2011. Out of their depth? Isolated deep populations of the cosmopolitan coral desmophyllum dianthus may be highly vulnerable to environmental change. PLoS ONE, 6(5) https://doi.org/10.1371/journal.pone.0019004.

Mohn, C., A. Rengstorf, M. White, G. Duineveld, F. Mienis, K. Soetaert, and A. Grehan. 2014. Linking benthic hydrodynamics and cold-water coral occurrences: A high-resolution model study at three cold-water coral provinces in the NE Atlantic. Progress in Oceanography, 122:92–104, https://doi.org/10.1016/j.pocean.2013.12.003.

Monnin, E., A. Indermühle, A. Dällenbach, J. Flückiger, B. Stauffer, T. F. Stocker, D. Raynaud, and J. M. Barnola. 2001. Atmospheric CO2 concentrations over the last glacial termination. Science, 291(5501):112–114, https://doi.org/10.1126/science.291.5501.112.

Montagna, P., M. McCulloch, E. Douville, M. López Correa, J. Trotter, R. Rodolfo-Metalpa, D. Dissard, C. Ferrier-Pagès, N. Frank, A. Freiwald, S. Goldstein, C. Mazzoli, S. Reynaud, A. Rüggeberg, S. Russo, and M. Taviani. 2014. Li/Mg systematics in scleractinian corals: Calibration of the thermometer. Geochimica et Cosmochimica Acta, 132:288–310, https://doi.org/10.1016/j.gca.2014.02.005.

Morato, T., J. González-Irusta, C. Dominguez-Carrió, C. Wei, A. Davies, A. K. Sweetman, G. H. Taranto, L. Beazley, A. García-Alegre, A. Grehan, P. Laffargue, F. J. Murillo, M. Sacau, S. Vaz, E. Kenchington, S. Arnaud-Haond, O. Callery, G. Chimienti, E. Cordes, H. Egilsdottir, A. Freiwald, R. Gasbarro, C. Gutiérrez-Zárate, M. Gianni, K. Gilkinson, V. E. Wareham Hayes, D. Hebbeln, K. Hedges, L. Henry, D. Johnson, M. Koen-Alonso, C. Lirette, F. Mastrototaro, L. Menot, T. Molodtsova, P. Durán Muñoz, C. Orejas, M. G. Pennino, P. Puerta, S. Á. Ragnarsson, B. Ramiro-Sánchez, J. Rice, J. Rivera, J. M. Roberts, S. W. Ross, J. L. Rueda, Í. Sampaio, P. Snelgrove, D. Stirling, M. A. Treble, J. Urra, J. Vad, D. Oevelen, L. Watling, W. Walkusz, C. Wienberg, M. Woillez, L. A. Levin, and M. Carreiro-Silva. 2020. Climate-induced changes in the suitable habitat of cold-water corals and commercially important deep-sea fishes in the North Atlantic. Global Change Biology, 26(4):2181–2202, https://doi.org/10.1111/gcb.14996.

Moros, M., E. Jansen, D. W. Oppo, J. Giraudeau, and A. Kuijpers. 2012. Reconstruction of the late-Holocene changes in the Sub-Arctic Front position at the Reykjanes Ridge, north Atlantic. Holocene, 22(8):877–886, https://doi.org/10.1177/0959683611434224.

Mortensen, P. B., L. Buhl-Mortensen, A. V. Gebruk, and E. M. Krylova. 2008. Occurrence of deep-water corals on the Mid-Atlantic Ridge based on MAR-ECO data. Deep-Sea Research Part II: Topical Studies in Oceanography, 55(1–2):142–152, https://doi.org/10.1016/j.dsr2.2007.09.018.

Mortensen, P. B., T. Hovland, J. H. Fosså, and D. M. Furevik. 2001. Distribution, abundance and size of Lophelia pertusa coral reefs in mid-Norway in relation to seabed characteristics. Journal of the Marine Biological Association of the United Kingdom, 81(4):581–597, https://doi.org/10.1017/S002531540100426X.

Murton, B. J. 2016. MarineE-Tech Project: To Map the Cobalt-Rich Ferromanganese Crusts of Tropic Seamount , NE Atlantic Ocean Ocean. pp.

Ng, H. C., L. F. Robinson, G. H. Rowland, S. S. Chen, and J. F. McManus. 2020. Coupled analysis of seawater and sedimentary 231Pa/230Th in the tropical Atlantic. Marine Chemistry, 227(September):103894, https://doi.org/10.1016/j.marchem.2020.103894.

Ng, H. C., L. F. Robinson, J. F. McManus, K. J. Mohamed, A. W. Jacobel, R. F. Ivanovic, L. J. Gregoire, and T. Chen. 2018. Coherent deglacial changes in western Atlantic Ocean circulation. Nature Communications, 9(1):2947, https://doi.org/10.1038/s41467-018-05312-3.

Nielsen, S. H. H., N. Koç, and X. Crosta. 2004. Holocene climate in the Atlantic sector of the Southern Ocean: Controlled by insolation or oceanic circulation? Geology, 32(4):317, https://doi.org/10.1130/G20334.1.

North Greenland Ice Core Project members. 2004. High-resolution record of Northern Hemisphere climate extending into the last interglacial period. Nature, 431(7005):147–151, https://doi.org/10.1038/nature02805.

Olsen, A., N. Lange, R. M. Key, T. Tanhua, H. C. Bittig, A. Kozyr, M. Álvarez, K. Azetsu-Scott, S. Becker, P. J. Brown, B. R. Carter, L. Cotrim Da Cunha, R. A. Feely, S. Van Heuven, M. Hoppema, M. Ishii, E. Jeansson, S. Jutterström, C. S. Landa, S. K. Lauvset, P. Michaelis, A. Murata, F. F. Pérez, B. Pfeil, C. Schirnick, R. Steinfeldt, T. Suzuki, B. Tilbrook, A. Velo, R. Wanninkhof, and R. J. Woosley. 2020. An updated version of the global interior ocean biogeochemical data product, GLODAPv2.2020. Earth System Science Data, 12(4):3653–3678, https://doi.org/10.5194/essd-12-3653-2020.

Oppo, D. W., G. Gebbie, K. F. Huang, W. B. Curry, T. M. Marchitto, and K. R. Pietro. 2018. Data Constraints on Glacial Atlantic Water Mass Geometry and Properties. Paleoceanography and Paleoclimatology, 33(9):1013–1034, https://doi.org/10.1029/2018PA003408.

Orejas, C., C. Wienberg, J. Titschack, L. Tamborrino, A. Freiwald, and D. Hebbeln. 2021. Madrepora oculata forms large frameworks in hypoxic waters off Angola (SE Atlantic). Scientific Reports, 11(1):15170, https://doi.org/10.1038/s41598-021-94579-6.

Pahnke, K., S. L. Goldstein, and S. R. Hemming. 2008. Abrupt changes in Antarctic Intermediate Water circulation over the past 25,000 years. Nature Geoscience, 1(12):870–874, https://doi.org/10.1038/ngeo360.

Parrenin, F., V. Masson-Delmotte, P. Köhler, D. Raynaud, D. Paillard, J. Schwander, C. Barbante, A. Landais, A. Wegner, and J. Jouzel. 2013. Synchronous Change of Atmospheric CO2 and Antarctic Temperature During the Last Deglacial Warming. Science, 339(6123):1060–1063, https://doi.org/10.1126/science.1226368.

Pastor, M. V., P. Vélez-Belchí, and A. Hernández-Guerra. 2015. Water Masses in the Canary Current Large Marine Ecosystem; Pp. 73–79. In Oceanographic and biological features in the Canary Current Large Marine Ecosystem. L. Valdés, and I. Déniz-Golzáles, eds, Vol. 115. IOC-UNESCO, Paris.

Pena, L. D., S. L. Goldstein, S. R. Hemming, K. M. Jones, E. Calvo, C. Pelejero, and I. Cacho. 2013. Rapid changes in meridional advection of Southern Ocean intermediate waters to the tropical

Pacific during the last 30kyr. Earth and Planetary Science Letters, 368:20–32, https://doi.org/10.1016/j.epsl.2013.02.028.

Pflaumann, U., M. Sarnthein, M. Chapman, L. d'Abreu, B. Funnell, M. Huels, T. Kiefer, M. Maslin, H. Schulz, J. Swallow, S. van Kreveld, M. Vautravers, E. Vogelsang, and M. Weinelt. 2003. Glacial North Atlantic: Sea-surface conditions reconstructed by GLAMAP 2000. Paleoceanography, 18(3) https://doi.org/10.1029/2002pa000774.

Pires, D. O. 2007. The azooxanthellate coral fauna of Brazil. Conservations and Adaptative Management of Seamount and Deep-Sea Coral Ecosystems, (1976):265–272,.

Poggemann, D. W., D. Nürnberg, E. C. Hathorne, M. Frank, W. Rath, S. Reißig, and A. Bahr. 2018. Deglacial Heat Uptake by the Southern Ocean and Rapid Northward Redistribution Via Antarctic Intermediate Water. Paleoceanography and Paleoclimatology, 33(11):1292–1305, https://doi.org/10.1029/2017PA003284.

Poggemann, D.-W., E. C. Hathorne, D. Nürnberg, M. Frank, I. Bruhn, S. Reißig, and A. Bahr. 2017. Rapid deglacial injection of nutrients into the tropical Atlantic via Antarctic Intermediate Water. Earth and Planetary Science Letters, 463:118–126, https://doi.org/10.1016/j.epsl.2017.01.030.

Portilho-Ramos, R. da C., J. Titschack, C. Wienberg, M. G. Siccha Rojas, Y. Yokoyama, and D. Hebbeln. 2022. Major environmental drivers determining life and death of cold-water corals through time. PLOS Biology, 20(5) https://doi.org/10.1371/journal.pbio.3001628.

Pratt, N., T. Chen, T. Li, D. J. Wilson, T. van de Flierdt, S. H. Little, M. L. Taylor, L. F. Robinson, A. D. Rogers, and N. Santodomingo. 2019. Temporal distribution and diversity of cold-water corals in the southwest Indian Ocean over the past 25,000 years. Deep-Sea Research Part I: Oceanographic Research Papers, 149(May):103049, https://doi.org/10.1016/j.dsr.2019.05.009.

Raddatz, J., J. Titschack, N. Frank, A. Freiwald, A. Conforti, A. Osborne, S. Skornitzke, W. Stiller, A. Rüggeberg, S. Voigt, A. L. S. Albuquerque, A. Vertino, A. Schröder-Ritzrau, and A. Bahr. 2020. Solenosmilia variabilis-bearing cold-water coral mounds off Brazil. Coral Reefs, 39(1):69–83, https://doi.org/10.1007/s00338-019-01882-w.

Raddatz, J., V. Liebetrau, J. Trotter, A. Rüggeberg, S. Flögel, W.-C. Dullo, A. Eisenhauer, S. Voigt, and M. McCulloch. 2016. Environmental constraints on Holocene cold‐water coral reef growth off Norway: Insights from a multiproxy approach. Paleoceanography, 31(10):1350–1367, https://doi.org/10.1002/2016PA002974.

Raddatz, J., V. Liebetrau, A. Rüggeberg, E. Hathorne, A. Krabbenhöft, A. Eisenhauer, F. Böhm, H. Vollstaedt, J. Fietzke, M. López Correa, A. Freiwald, and W.-C. Dullo. 2013. Stable Sr-isotope, Sr/Ca, Mg/Ca, Li/Ca and Mg/Li ratios in the scleractinian cold-water coral Lophelia pertusa. Chemical Geology, 352:143–152, https://doi.org/10.1016/j.chemgeo.2013.06.013.

Rae, J. W. B., A. Burke, L. F. Robinson, J. F. Adkins, T. Chen, C. Cole, R. Greenop, T. Li, E. F. M. Littley, D. C. Nita, J. A. Stewart, and B. J. Taylor. 2018. CO2 storage and release in the deep Southern Ocean on millennial to centennial timescales. Nature, 562(7728):569–573, https://doi.org/10.1038/s41586-018-0614-0.

Rae, J. W. B., G. L. Foster, D. N. Schmidt, and T. Elliott. 2011. Boron isotopes and B/Ca in benthic foraminifera: Proxies for the deep ocean carbonate system. Earth and Planetary Science Letters, 302(3–4):403–413, https://doi.org/10.1016/j.epsl.2010.12.034.

Rafter, P. A., W. R. Gray, S. K. V. Hines, A. Burke, K. M. Costa, J. Gottschalk, M. P. Hain, J. W. B. Rae, J. R. Southon, M. H. Walczak, J. Yu, J. F. Adkins, and T. DeVries. 2022. Global

reorganization of deep-sea circulation and carbon storage after the last ice age. Science Advances, 8(46):1–10, https://doi.org/10.1126/sciadv.abq5434.

Rahmstorf, S., J. E. Box, G. Feulner, M. E. Mann, A. Robinson, S. Rutherford, and E. J. Schaffernicht. 2015. Exceptional twentieth-century slowdown in Atlantic Ocean overturning circulation. Nature Climate Change, 5(March):1–6, https://doi.org/10.1038/nclimate2554.

Rahmstorf, S. 2002. Ocean circulation and climate during the past 120,000 years. Nature, 419(September):207–214. https://doi.org/10.1038/nature01090.

Ramiro-Sánchez, B., J. M. González-Irusta, L.-A. Henry, J. Cleland, I. Yeo, J. R. Xavier, M. Carreiro-Silva, Í. Sampaio, J. Spearman, L. Victorero, C. G. Messing, G. Kazanidis, J. M. Roberts, and B. Murton. 2019. Characterization and Mapping of a Deep-Sea Sponge Ground on the Tropic Seamount (Northeast Tropical Atlantic): Implications for Spatial Management in the High Seas. Frontiers in Marine Science, 6(May):1–19, https://doi.org/10.3389/fmars.2019.00278.

Reimer, P. J., W. E. N. Austin, E. Bard, A. Bayliss, P. G. Blackwell, C. Bronk Ramsey, M. Butzin, H. Cheng, R. L. Edwards, M. Friedrich, P. M. Grootes, T. P. Guilderson, I. Hajdas, T. J. Heaton, A. G. Hogg, K. A. Hughen, B. Kromer, S. W. Manning, R. Muscheler, J. G. Palmer, C. Pearson, J. van der Plicht, R. W. Reimer, D. A. Richards, E. M. Scott, J. R. Southon, C. S. M. Turney, L. Wacker, F. Adolphi, U. Büntgen, M. Capano, S. M. Fahrni, A. Fogtmann-Schulz, R. Friedrich, P. Köhler, S. Kudsk, F. Miyake, J. Olsen, F. Reinig, M. Sakamoto, A. Sookdeo, and S. Talamo. 2020. The IntCal20 Northern Hemisphere Radiocarbon Age Calibration Curve (0–55 cal kBP). Radiocarbon, 62(4):725–757, https://doi.org/10.1017/RDC.2020.41.

Reimer, P. J., E. Bard, A. Bayliss, J. W. Beck, P. G. Blackwell, C. B. Ramsey, C. E. Buck, H. Cheng, R. L. Edwards, M. Friedrich, P. M. Grootes, T. P. Guilderson, H. Haflidason, I. Hajdas, C. Hatté, T. J. Heaton, D. L. Hoffmann, A. G. Hogg, K. A. Hughen, K. F. Kaiser, B. Kromer, S. W. Manning, M. Niu, R. W. Reimer, D. A. Richards, E. M. Scott, J. R. Southon, R. A. Staff, C. S. M. Turney, and J. van der Plicht. 2013. IntCal13 and Marine13 Radiocarbon Age Calibration Curves 0–50,000 Years cal BP. Radiocarbon, 55(4):1869–1887, https://doi.org/10.2458/azu_js_rc.55.16947.

Rhein, M., J. Fischer, W. M. Smethie, D. Smythe-Wright, R. F. Weiss, C. Mertens, D.-H. Min, U. Fleischmann, and A. Putzka. 2002. Labrador Sea Water: Pathways, CFC Inventory, and Formation Rates. Journal of Physical Oceanography, 32(2):648–665, https://doi.org/10.1175/1520-0485(2002)032<0648:LSWPCI>2.0.CO;2.

Roberts, J., J. Gottschalk, L. C. Skinner, V. L. Peck, S. Kender, H. Elderfield, C. Waelbroeck, N. Vázquez Riveiros, and D. A. Hodell. 2016. Evolution of South Atlantic density and chemical stratification across the last deglaciation. Proceedings of the National Academy of Sciences, 113(3):514–519, https://doi.org/10.1073/pnas.1511252113.

Roberts, J. M., A. Wheeler, A. Freiwald, and S. Cairns. 2009. Cold-Water Corals. Cambridge University Press, 1–350 pp. https://doi.org/10.1017/CBO9780511581588.

Roberts, J. M., A. J. Wheeler, and A. Freiwald. 2006. Reefs of the Deep: The Biology and Geology of Cold-Water Coral Ecosystems. Science, 312(5773):543–547, https://doi.org/10.1126/science.1119861.

Roberts, S., and M. Hirshfield. 2004. Deep Sea Corals: Out of Sight, But No Longer Out of Mind. Frontiers in Ecology and the Environment, https://doi.org/https://doi.org/10.1890/1540-9295(2004)002[0123:DCOOSB]2.0.CO;2.

Robinson, L. F., N. S. Belshaw, and G. M. Henderson. 2004a. U and Th concentrations and isotope ratios in modern carbonates and waters from the Bahamas. Geochimica et Cosmochimica Acta, 68(8):1777–1789, https://doi.org/10.1016/j.gca.2003.10.005.

Robinson, L. F., G. M. Henderson, L. Hall, and I. Matthews. 2004b. Climatic control of riverine and seawater uranium-isotope ratios. Science, 305(5685):851–854, https://doi.org/10.1126/science.1099673.

Robinson, L. F., J. F. Adkins, L. D. Keigwin, J. Southon, D. P. Fernandez, S.-L. Wang, and D. S. Scheirer. 2005. Radiocarbon Variability in the Western North Atlantic During the Last Deglaciation. Science, 310(5753):1469–1473, https://doi.org/10.1126/science.1114832.

Robinson, L. F., J. F. Adkins, D. P. Fernandez, D. S. Burnett, S. L. Wang, A. C. Gagnon, and N. Krakauer. 2006. Primary U distribution in scleractinian corals and its implications for U series dating. Geochemistry, Geophysics, Geosystems, 7(5) https://doi.org/10.1029/2005GC001138.

Robinson, L. F., J. F. Adkins, N. Frank, A. C. Gagnon, N. G. Prouty, E. Brendan Roark, and T. van de Flierdt. 2014. The geochemistry of deep-sea coral skeletons: A review of vital effects and applications for palaeoceanography. Deep-Sea Research Part II: Topical Studies in Oceanography, 99:184–198, https://doi.org/10.1016/j.dsr2.2013.06.005.

Robinson, L. F. 2014. RRS James Cook Cruise JC094, October 13 - Novemeber 30 2013, Tenerife - Trinidad. TROPICS, Tracing Oceanic Processes Using Corals and Sediments. Reconstructing Abrupt Changes in Chemistry and Circulation of the Equatorial Atlantic Ocean: Implications For . pp.

Rogerson, M., E. J. Rohling, P. P. E. Weaver, and J. W. Murray. 2005. Glacial to interglacial changes in the settling depth of the Mediterranean Outflow plume. Paleoceanography, 20(3):1–12, https://doi.org/10.1029/2004PA001106.

Romahn, S., A. Mackensen, J. Groeneveld, and J. Pätzold. 2014. Deglacial intermediate water reorganization: new evidence from the Indian Ocean. Climate of the Past, 10(1):293–303, https://doi.org/10.5194/cp-10-293-2014.

Romero, O. E., J.-H. Kim, and B. Donner. 2008. Submillennial-to-millennial variability of diatom production off Mauritania, NW Africa, during the last glacial cycle. Paleoceanography, 23(3):n/a-n/a, https://doi.org/10.1029/2008PA001601.

Rowland, G. H., L. F. Robinson, K. R. Hendry, H. C. Ng, D. McGee, and J. F. McManus. 2021. The Spatial Distribution of Aeolian Dust and Terrigenous Fluxes in the Tropical Atlantic Ocean Since the Last Glacial Maximum. Paleoceanography and Paleoclimatology, 36(2):1–17, https://doi.org/10.1029/2020PA004148.

Rühlemann, C., S. Mulitza, G. Lohmann, A. Paul, M. Prange, and G. Wefer. 2004. Intermediate depth warming in the tropical Atlantic related to weakened thermohaline circulation: Combining paleoclimate data and modeling results for the last deglaciation. Paleoceanography, 19(1):1–10, https://doi.org/10.1029/2003PA000948.

Santos, G. C., R. Kerr, J. L. L. Azevedo, C. R. B. Mendes, and L. C. da Cunha. 2016. Influence of Antarctic Intermediate Water on the deoxygenation of the Atlantic Ocean. Dynamics of Atmospheres and Oceans, 76:72–82, https://doi.org/10.1016/j.dynatmoce.2016.09.002.

Santos, T. P., M. H. Shimizu, R. A. Nascimento, I. M. Venancio, M. C. Campos, R. C. Portilho-Ramos, J. M. Ballalai, D. O. Lessa, S. Crivellari, R. H. Nagai, C. M. Chiessi, H. Kuhnert, A. Bahr, and A. L. S. Albuquerque. 2022. A data-model perspective on the Brazilian margin surface

warming from the Last Glacial Maximum to the Holocene. Quaternary Science Reviews, 286 https://doi.org/10.1016/j.quascirev.2022.107557.

Santos, T. P., D. O. Lessa, I. M. Venancio, C. M. Chiessi, S. Mulitza, H. Kuhnert, A. Govin, T. Machado, K. B. Costa, F. Toledo, B. B. Dias, and A. L. S. Albuquerque. 2017. Prolonged warming of the Brazil Current precedes deglaciations. Earth and Planetary Science Letters, 463:1–12, https://doi.org/10.1016/j.epsl.2017.01.014.

Schejter, L., C. S. Bremec, and S. D. Cairns. 2016. Scleractinian corals recorded in the argentinean antarctic expeditions between 2012 and 2014, with comments on Flabellum (flabellum) areum cairns, 1982. Polar Research, 35:1–7, https://doi.org/10.3402/polar.v35.29762.

Schneider von Deimling, T., A. Ganopolski, H. Held, and S. Rahmstorf. 2006. How cold was the Last Glacial Maximum? Geophysical Research Letters, 33(14):L14709, https://doi.org/10.1029/2006GL026484.

Scholz, D., A. Mangini, and T. Felis. 2004. U-series dating of diagenetically altered fossil reef corals. Earth and Planetary Science Letters, 218(1–2):163–178, https://doi.org/10.1016/S0012-821X(03)00647-2.

Schröder-Ritzrau, A., A. Freiwald, and A. Mangini. 2005. U/Th-dating of deep-water corals from the eastern North Atlantic and the western Mediterranean Sea; Pp. 157–172. In Cold-Water Corals and Ecosystems. A. Freiwald, and J. M. Roberts, eds, Springer-Verlag, Berlin/Heidelberg https://doi.org/10.1007/3-540-27673-4_8.

Schröder-Ritzrau, A., A. Mangini, and M. Lomitschka. 2003. Deep-sea corals evidence periodic reduced ventilation in the North Atlantic during the LGM/Holocene transition. Earth and Planetary Science Letters, 216(3):399–410, https://doi.org/10.1016/S0012-821X(03)00511-9.

Shakun, J. D., P. U. Clark, F. He, S. A. Marcott, A. C. Mix, Z. Liu, B. Otto-Bliesner, A. Schmittner, and E. Bard. 2012. Global warming preceded by increasing carbon dioxide concentrations during the last deglaciation. Nature, 484(7392):49–54, https://doi.org/10.1038/nature10915.

Shen, G. T., and E. A. Boyle. 1988. Determination of lead, cadmium and other trace metals in annually-banded corals. Chemical Geology, 67:47–62,.

Sherwood, O. A., R. E. Thresher, S. J. Fallon, D. M. Davies, and T. W. Trull. 2009. Multi-century time-series of 15N and 14C in bamboo corals from deep Tasmanian seamounts: Evidence for stable oceanographic conditions. Marine Ecology Progress Series, 397:209–218, https://doi.org/10.3354/meps08166.

Shevenell, A. E., A. E. Ingalls, E. W. Domack, and C. Kelly. 2011. Holocene Southern Ocean surface temperature variability west of the Antarctic Peninsula. Nature, 470(7333):250–254, https://doi.org/10.1038/nature09751.

Sigman, D. M., and M. P. Hain. 2012. The Biological Productivity of the Ocean | Learn Science at Scitable. Nature Education Knowledge, 3(6):1–16,.

Sigman, D. M., M. P. Hain, and G. H. Haug. 2010. The polar ocean and glacial cycles in atmospheric CO2 concentration. Nature, 466(7302):47–55, https://doi.org/10.1038/nature09149.

Sinclair, D. J., and M. J. Risk. 2006. A numerical model of trace-element coprecipitation in a physicochemical calcification system: Application to coral biomineralization and trace-element “vital effects.” Geochimica et Cosmochimica Acta, 70(15):3855–3868, https://doi.org/10.1016/j.gca.2006.05.019.

Skinner, L. C., F. Primeau, E. Freeman, M. de la Fuente, P. A. Goodwin, J. Gottschalk, E. Huang, I. N. McCave, T. L. Noble, and A. E. Scrivner. 2017. Radiocarbon constraints on the glacial ocean circulation and its impact on atmospheric CO2. Nature Communications, 8(1):16010, https://doi.org/10.1038/ncomms16010.

Skinner, L. C., C. Waelbroeck, A. E. Scrivner, and S. J. Fallon. 2014. Radiocarbon evidence for alternating northern and southern sources of ventilation of the deep Atlantic carbon pool during the last deglaciation. Proceedings of the National Academy of Sciences, 111(15):5480–5484, https://doi.org/10.1073/pnas.1400668111.

Skinner, L. C., S. Fallon, C. Waelbroeck, E. Michel, and S. Barker. 2010. Ventilation of the Deep Southern Ocean and Deglacial CO 2 Rise. Science, 328(5982):1147–1151, https://doi.org/10.1126/science.1183627.

Skinner, L. C., and N. J. Shackleton. 2004. Rapid transient changes in northeast Atlantic deep water ventilation age across Termination I. Paleoceanography, 19(2):n/a-n/a, https://doi.org/10.1029/2003PA000983.

Skinner, L. C., N. J. Shackleton, and H. Elderfield. 2003. Millennial-scale variability of deep-water temperature and δ18Odw indicating deep-water source variations in the Northeast Atlantic, 0-34 cal. ka BP. Geochemistry, Geophysics, Geosystems, 4(12) https://doi.org/10.1029/2003GC000585.

Skinner, L. C., and E. Bard. 2022. Radiocarbon as a Dating Tool and Tracer in Paleoceanography. Reviews of Geophysics, 60(1):1–64, https://doi.org/10.1029/2020RG000720.

Sortor, R. N., and D. C. Lund. 2011. No evidence for a deglacial intermediate water Δ14C anomaly in the SW Atlantic. Earth and Planetary Science Letters, 310(1–2):65–72, https://doi.org/10.1016/j.epsl.2011.07.017.

Southon, J., A. L. Noronha, H. Cheng, R. L. Edwards, and Y. Wang. 2012. A high-resolution record of atmospheric 14C based on Hulu Cave speleothem H82. Quaternary Science Reviews, 33:32–41, https://doi.org/10.1016/j.quascirev.2011.11.022.

Souza, A. G. Q. de, R. Kerr, and J. L. L. de Azevedo. 2018. On the influence of Subtropical Mode Water on the South Atlantic Ocean. Journal of Marine Systems, 185(October 2017):13–24, https://doi.org/10.1016/j.jmarsys.2018.04.006.

Spooner, P. T., L. F. Robinson, F. Hemsing, P. Morris, and J. A. Stewart. 2018. Extended calibration of cold-water coral Ba/Ca using multiple genera and co-located measurements of dissolved barium concentration. Chemical Geology, 499(September 2017):100–110, https://doi.org/10.1016/j.chemgeo.2018.09.012.

Spooner, P. T., T. Chen, L. F. Robinson, and C. D. Coath. 2016. Rapid uranium-series age screening of carbonates by laser ablation mass spectrometry. Quaternary Geochronology, 31:28–39, https://doi.org/10.1016/j.quageo.2015.10.004.

Spratt, R. M., and L. E. Lisiecki. 2016. A Late Pleistocene sea level stack. Climate of the Past, 12(4):1079–1092, https://doi.org/10.5194/cp-12-1079-2016.

Stewart, J. A., Robinson, L. F., Rae, J. W. B., Burke, A., Chen, T., Li, T., de Carvalho Ferreira, M. L., Fornari, D. Deep-sea corals reveal Antarctic climate pacing of low latitude deglacial warming. In review at Science Advances.

Stewart, J. A., T. Li, P. T. Spooner, A. Burke, T. Chen, J. Roberts, J. W. B. Rae, V. Peck, S. Kender, Q. Liu, and L. F. Robinson. 2021. Productivity and Dissolved Oxygen Controls on the Southern

Ocean Deep‐Sea Benthos During the Antarctic Cold Reversal. Paleoceanography and Paleoclimatology, 36(10) https://doi.org/10.1029/2021PA004288.

Stewart, J. A., L. F. Robinson, R. D. Day, I. Strawson, A. Burke, J. W. B. Rae, P. T. Spooner, A. Samperiz, P. J. Etnoyer, B. Williams, A. Paytan, M. J. Leng, V. Häussermann, L. N. Wickes, R. Bratt, and H. Pryer. 2020. Refining trace metal temperature proxies in cold-water scleractinian and stylasterid corals. Earth and Planetary Science Letters, 545:116412, https://doi.org/10.1016/j.epsl.2020.116412.

Stott, L., B. Davy, J. Shao, R. Coffin, I. Pecher, H. Neil, P. Rose, and J. Bialas. 2019. CO 2 Release From Pockmarks on the Chatham Rise‐Bounty Trough at the Glacial Termination. Paleoceanography and Paleoclimatology, 34(11):1726–1743, https://doi.org/10.1029/2019PA003674.

Stott, L., J. Southon, A. Timmermann, and A. Koutavas. 2009. Radiocarbon age anomaly at intermediate water depth in the Pacific Ocean during the last deglaciation. Paleoceanography, 24(2):1–10, https://doi.org/10.1029/2008PA001690.

Stuiver, M., and H. A. Polach. 1977. Discussion Reporting of 14C Data. Radiocarbon, 19(3):355–363, https://doi.org/10.1017/S0033822200003672.

Sumida, P. Y., A. F. Bernardino, and F. C. De Leo. 2020. Brazilian Deep-Sea Biodiversity. 1–273 pp. https://doi.org/10.1007/978-3-030-53222-2.

Sumida, P. Y. G., M. Y. Yoshinaga, L. A. S.-P. Madureira, and M. Hovland. 2004. Seabed pockmarks associated with deepwater corals off SE Brazilian continental slope, Santos Basin. Marine Geology, 207(1–4):159–167, https://doi.org/10.1016/j.margeo.2004.03.006.

Talley, L. 2013. Closure of the Global Overturning Circulation Through the Indian, Pacific, and Southern Oceans: Schematics and Transports. Oceanography, 26(1):80–97, https://doi.org/10.5670/oceanog.2013.07.

Talley, L. D., G. L. Pickard, W. J. Emery, and J. H. Swift. 2011a. Atlantic Ocean. Descriptive Physical Oceanography, (cm):1–43, https://doi.org/10.1016/B978-0-7506-4552-2.10021-6.

Talley, L. D., G. L. Pickard, W. J. Emery, and J. H. Swift. 2011b. Southern Ocean. Descriptive Physical Oceanography, 437–471, https://doi.org/10.1016/B978-0-7506-4552-2.10013-7.

Telesiński, M. M., M. M. Ezat, F. Muschitiello, H. A. Bauch, and R. F. Spielhagen. 2021. Ventilation History of the Nordic Seas Deduced From Pelagic‐Benthic Radiocarbon Age Offsets. Geochemistry, Geophysics, Geosystems, 22(4):1–10, https://doi.org/10.1029/2020GC009132.

Thiagarajan, N., A. V Subhas, J. R. Southon, J. M. Eiler, and J. F. Adkins. 2014. Abrupt pre-Bølling–Allerød warming and circulation changes in the deep ocean. Nature, 511(7507):75–78, https://doi.org/10.1038/nature13472.

Thiagarajan, N., D. Gerlach, M. L. Roberts, A. Burke, A. McNichol, W. J. Jenkins, A. V. Subhas, R. E. Thresher, and J. F. Adkins. 2013. Movement of deep-sea coral populations on climatic timescales. Paleoceanography, 28(2):227–236, https://doi.org/10.1002/palo.20023.

Thornalley, D. J. R., H. Elderfield, and I. N. McCave. 2011a. Reconstructing North Atlantic deglacial surface hydrography and its link to the Atlantic overturning circulation. Global and Planetary Change, 79(3–4):163–175, https://doi.org/10.1016/j.gloplacha.2010.06.003.

Thornalley, D. J. R. R., S. Barker, W. S. Broecker, H. Elderfield, and I. N. McCave. 2011b. The Deglacial Evolution of North Atlantic Deep Convection. Science, 331(6014):202–205, https://doi.org/10.1126/science.1196812.

Titschack, J., D. Baum, R. De Pol-Holz, M. López Correa, N. Forster, S. Flögel, D. Hebbeln, and A. Freiwald. 2015. Aggradation and carbonate accumulation of Holocene Norwegian cold-water coral reefs. Sedimentology, 62(7):1873–1898, https://doi.org/10.1111/sed.12206.

Toucanne, S., G. Soulet, N. Vázquez Riveiros, S. M. Boswell, B. Dennielou, C. Waelbroeck, G. Bayon, M. Mojtahid, M. Bosq, M. Sabine, S. Zaragosi, J. Bourillet, and H. Mercier. 2021. The North Atlantic Glacial Eastern Boundary Current as a Key Driver for Ice-Sheet—AMOC Interactions and Climate Instability. Paleoceanography and Paleoclimatology, 36(3):1–23, https://doi.org/10.1029/2020PA004068.

Trevizani, T. H., R. H. Nagai, R. C. L. Figueira, P. Y. G. Sumida, and M. M. De Mahiques. 2022. Chemical characterization of deep-sea corals from the continental slope of Santos Basin (southeastern Brazilian upper margin). Ocean and Coastal Research, 70(suppl 2):1–15, https://doi.org/10.1590/2675-2824070.21108tht.

Umling, N. E., D. W. Oppo, P. Chen, J. Yu, Z. Liu, M. Yan, G. Gebbie, D. C. Lund, K. R. Pietro, Z. D. Jin, K. -F. Huang, K. B. Costa, and F. A. L. Toledo. 2019. Atlantic Circulation and Ice Sheet Influences on Upper South Atlantic Temperatures During the Last Deglaciation. Paleoceanography and Paleoclimatology, 34(6):990–1005, https://doi.org/10.1029/2019PA003558.

Valley, S. G., J. Lynch-Stieglitz, and T. M. Marchitto. 2019. Intermediate water circulation changes in the Florida Straits from a 35 ka record of Mg/Li-derived temperature and Cd/Ca-derived seawater cadmium. Earth and Planetary Science Letters, 523:115692, https://doi.org/10.1016/j.epsl.2019.06.032.

Valley, S., J. Lynch-Stieglitz, and T. M. Marchitto. 2017. Timing of Deglacial AMOC Variability From a High-Resolution Seawater Cadmium Reconstruction. Paleoceanography, 32(11):1195–1203, https://doi.org/10.1002/2017PA003099.

van de Flierdt, T., L. F. Robinson, and J. F. Adkins. 2010. Deep-sea coral aragonite as a recorder for the neodymium isotopic composition of seawater. Geochimica et Cosmochimica Acta, 74(21):6014–6032, https://doi.org/10.1016/j.gca.2010.08.001.

van der Land, C., M. Eisele, F. Mienis, H. de Haas, D. Hebbeln, J. J. G. Reijmer, and T. C. E. van Weering. 2014. Carbonate mound development in contrasting settings on the Irish margin. Deep Sea Research Part II: Topical Studies in Oceanography, 99:297–306, https://doi.org/10.1016/j.dsr2.2013.10.004.

van der Land, C., F. Mienis, H. de Haas, N. Frank, R. Swennen, and T. C. E. van Weering. 2010. Diagenetic processes in carbonate mound sediments at the south-west Rockall Trough margin. Sedimentology, 57(3):912–931, https://doi.org/10.1111/j.1365-3091.2009.01125.x.

Vernet, M., I. H. Ellingsen, L. Seuthe, D. Slagstad, M. R. Cape, and P. A. Matrai. 2019. Influence of Phytoplankton Advection on the Productivity Along the Atlantic Water Inflow to the Arctic Ocean. Frontiers in Marine Science, 6(September):1–18, https://doi.org/10.3389/fmars.2019.00583.

Victorero, L., K. Robert, L. F. Robinson, M. L. Taylor, and V. A. I. Huvenne. 2018. Species replacement dominates megabenthos beta diversity in a remote seamount setting. Scientific Reports, 8(1):1–11, https://doi.org/10.1038/s41598-018-22296-8.

Victorero, L., D. Blamart, E. Pons-Branchu, M. N. Mavrogordato, and V. A. I. Huvenne. 2016. Reconstruction of the formation history of the Darwin Mounds, N Rockall Trough: How the dynamics of a sandy contourite affected cold-water coral growth. Marine Geology, 378:186–195, https://doi.org/10.1016/j.margeo.2015.12.001.

Wacker, L., M. Christl, and H. A. Synal. 2010. Bats: A new tool for AMS data reduction. Nuclear Instruments and Methods in Physics Research, Section B: Beam Interactions with Materials and Atoms, 268(7–8):976–979, https://doi.org/10.1016/j.nimb.2009.10.078.

Wagner, T. 2000. Control of organic carbon accumulation in the late Quaternary equatorial Atlantic (Ocean Drilling Program sites 664 and 663): Productivity versus terrigenous supply. Paleoceanography, 15(2):181–199, https://doi.org/10.1029/1999PA000406.

Weaver, A. J., C. M. Bitz, A. F. Fanning, and M. M. Holland. 1999. THERMOHALINE CIRCULATION: High-Latitude Phenomena and the Difference Between the Pacific and Atlantic. Annu. Rev. Earth Planet. Sci., 27:231–285, https://doi.org/0084-6597/99/0515-0231$08.00.

Wefing, A. M., J. Arps, P. Blaser, C. Wienberg, D. Hebbeln, and N. Frank. 2017. High precision U-series dating of scleractinian cold-water corals using an automated chromatographic U and Th extraction. Chemical Geology, 475(June):140–148, https://doi.org/10.1016/j.chemgeo.2017.10.036.

Weldeab, S., T. Friedrich, A. Timmermann, and R. R. Schneider. 2016. Strong middepth warming and weak radiocarbon imprints in the equatorial Atlantic during Heinrich 1 and Younger Dryas. Paleoceanography, 31(8):1070–1082, https://doi.org/10.1002/2016PA002957.

Wienberg, C., J. Titschack, N. Frank, R. De Pol-Holz, J. Fietzke, M. Eisele, A. Kremer, and D. Hebbeln. 2020. Deglacial upslope shift of NE Atlantic intermediate waters controlled slope erosion and cold-water coral mound formation (Porcupine Seabight, Irish margin). Quaternary Science Reviews, 237:106310, https://doi.org/10.1016/j.quascirev.2020.106310.

Wienberg, C., J. Titschack, A. Freiwald, N. Frank, T. Lundälv, M. Taviani, L. Beuck, A. Schröder-Ritzrau, T. Krengel, and D. Hebbeln. 2018. The giant Mauritanian cold-water coral mound province: Oxygen control on coral mound formation. Quaternary Science Reviews, 185:135–152, https://doi.org/10.1016/j.quascirev.2018.02.012.

Wienberg, C., and J. Titschack. 2015. Framework-Forming Scleractinian Cold-Water Corals Through Space and Time: A Late Quaternary North Atlantic Perspective; Pp. 1–34. In Marine Animal Forests. S. Rossi,, L. Bramanti,, A. Gori, and C. Orejas, eds, Springer International Publishing, Cham https://doi.org/10.1007/978-3-319-17001-5_16-1.

Wienberg, C., N. Frank, K. N. Mertens, J.-B. Stuut, M. Marchant, J. Fietzke, F. Mienis, and D. Hebbeln. 2010. Glacial cold-water coral growth in the Gulf of Cádiz: Implications of increased palaeo-productivity. Earth and Planetary Science Letters, 298(3–4):405–416, https://doi.org/10.1016/j.epsl.2010.08.017.

Wienberg, C., D. Hebbeln, H. G. Fink, F. Mienis, B. Dorschel, A. Vertino, M. L. Correa, and A. Freiwald. 2009. Scleractinian cold-water corals in the Gulf of Cádiz—First clues about their spatial and temporal distribution. Deep Sea Research Part I: Oceanographic Research Papers, 56(10):1873–1893, https://doi.org/10.1016/j.dsr.2009.05.016.

Xiao, X., M. Zhao, K. L. Knudsen, L. Sha, J. Eiríksson, E. Gudmundsdóttir, H. Jiang, and Z. Guo. 2017. Deglacial and Holocene sea–ice variability north of Iceland and response to ocean

circulation changes. Earth and Planetary Science Letters, 472:14–24, https://doi.org/10.1016/j.epsl.2017.05.006.

Xie, R. C., F. Marcantonio, and M. W. Schmidt. 2012. Deglacial variability of Antarctic Intermediate Water penetration into the North Atlantic from authigenic neodymium isotope ratios. Paleoceanography, 27(3):1–12, https://doi.org/10.1029/2012PA002337.

Yu, J., D. W. Oppo, Z. Jin, M. Lacerra, X. Ji, N. E. Umling, D. C. Lund, N. McCave, L. Menviel, J. Shao, and C. Xu. 2022. Millennial and centennial CO2 release from the Southern Ocean during the last deglaciation. Nature Geoscience, 15(4):293–299, https://doi.org/10.1038/s41561-022-00910-9.

Yu, J., H. Elderfield, and A. M. Piotrowski. 2008. Seawater carbonate ion-δ13C systematics and application to glacial-interglacial North Atlantic ocean circulation. Earth and Planetary Science Letters, 271(1–4):209–220, https://doi.org/10.1016/j.epsl.2008.04.010.

Zarriess, M., and A. Mackensen. 2010. The tropical rainbelt and productivity changes off northwest Africa: A 31,000-year high-resolution record. Marine Micropaleontology, 76(3–4):76–91, https://doi.org/10.1016/j.marmicro.2010.06.001.

APPENDIX I
DATA TABLES AND SUPPLEMENTARY FIGURES FOR CHAPTER 2 (PAPER CHAPTER)

Table S1: U-series ages of cold-water corals from east Equatorial Atlantic (east Eq. Atl.) and Reykjanes Ridge defined by laser ablation method. Depths of east Equatorial Atlantic corals was retrieved by ROV. Depths of Reykjanes Ridge corals corresponds to the mean depth of the dredge on and off bottom. Samples not included on age distribution discussion are shown in grey.

Sample ID	Taxa	Location	Latitude	Longitude	Depth water	Age	2s
			DecDeg (N)	DecDeg (E)	m	ka BP	ka
JC094-f0001car0002L	*Caryophyllia sp.*	east Eq. Atl.	9.22	-21.32	1080	22.17	0.77
JC094-f0001car0190L	*Caryophyllia sp.*	east Eq. Atl.	9.22	-21.32	1080	44.43	1.68
JC094-f0001carcs004o	*Caryophyllia sp.*	east Eq. Atl.	9.22	-21.32	1080	43.45	1.47
JC094-f0001carcs004y	*Caryophyllia sp.*	east Eq. Atl.	9.22	-21.32	1080	40.37	1.30
JC094-f0001carcs006	*Caryophyllia sp.*	east Eq. Atl.	9.22	-21.32	1080	46.51	1.56
JC094-f0001carcs007	*Caryophyllia sp.*	east Eq. Atl.	9.22	-21.32	1080	41.25	1.30
JC094-f0001carcs008	*Caryophyllia sp.*	east Eq. Atl.	9.22	-21.32	1080	34.90	1.18
JC094-f0001carcs010	*Caryophyllia sp.*	east Eq. Atl.	9.22	-21.32	1080	32.80	1.16
JC094-f0001carcs011	*Caryophyllia sp.*	east Eq. Atl.	9.22	-21.32	1080	2.57	0.32
JC094-f0001carcs014	*Caryophyllia sp.*	east Eq. Atl.	9.22	-21.32	1080	39.16	1.59
JC094-f0001carcs015	*Caryophyllia sp.*	east Eq. Atl.	9.22	-21.32	1080	1.12	0.24
JC094-f0001carcs016	*Caryophyllia sp.*	east Eq. Atl.	9.22	-21.32	1080	16.65	0.83
JC094-f0001carcs017	*Caryophyllia sp.*	east Eq. Atl.	9.22	-21.32	1080	4.83	0.40
JC094-f0001carcs018	*Caryophyllia sp.*	east Eq. Atl.	9.22	-21.32	1080	2.90	0.34
JC094-f0001carcs019	*Caryophyllia sp.*	east Eq. Atl.	9.22	-21.32	1080	1.54	0.43
JC094-f0001carcs020	*Caryophyllia sp.*	east Eq. Atl.	9.22	-21.32	1080	46.10	1.78
JC094-f0001carcs021	*Caryophyllia sp.*	east Eq. Atl.	9.22	-21.32	1080	4.03	0.52
JC094-f0001carcs022	*Caryophyllia sp.*	east Eq. Atl.	9.22	-21.32	1080	14.80	0.68
JC094-f0001carcs023	*Caryophyllia sp.*	east Eq. Atl.	9.22	-21.32	1080	2.31	0.34
JC094-f0001carcs024	*Caryophyllia sp.*	east Eq. Atl.	9.22	-21.32	1080	16.62	0.84
JC094-f0001carcs025	*Caryophyllia sp.*	east Eq. Atl.	9.22	-21.32	1080	14.61	0.75
JC094-f0001carcs026	*Caryophyllia sp.*	east Eq. Atl.	9.22	-21.32	1080	39.68	1.55
JC094-f0001carcs027	*Caryophyllia sp.*	east Eq. Atl.	9.22	-21.32	1080	13.08	0.77
JC094-f0001carcs028	*Caryophyllia sp.*	east Eq. Atl.	9.22	-21.32	1080	1.65	0.44

Sample ID	Taxa	Location	Latitude	Longitude	Depth water	Age	2s
JC094-f0001carcs029	*Caryophyllia sp.*	east Eq. Atl.	9.22	-21.32	1080	15.84	0.79
JC094-f0001carcs030	*Caryophyllia sp.*	east Eq. Atl.	9.22	-21.32	1080	35.02	1.97
JC094-f0001carcs031	*Caryophyllia sp.*	east Eq. Atl.	9.22	-21.32	1080	31.35	1.52
JC094-f0001carcs032	*Caryophyllia sp.*	east Eq. Atl.	9.22	-21.32	1080	11.93	0.69
JC094-f0001carcs033	*Caryophyllia sp.*	east Eq. Atl.	9.22	-21.32	1080	31.14	1.23
JC094-f0001carcs034	*Caryophyllia sp.*	east Eq. Atl.	9.22	-21.32	1080	33.47	1.60
JC094-f0001carcs035	*Caryophyllia sp.*	east Eq. Atl.	9.22	-21.32	1080	28.35	1.34
JC094-f0001carcs036	*Caryophyllia sp.*	east Eq. Atl.	9.22	-21.32	1080	13.54	0.82
JC094-f0001carcs037	*Caryophyllia sp.*	east Eq. Atl.	9.22	-21.32	1080	20.05	0.99
JC094-f0001carcs038	*Caryophyllia sp.*	east Eq. Atl.	9.22	-21.32	1080	9.43	0.53
JC094-f0001carcs040	*Caryophyllia sp.*	east Eq. Atl.	9.22	-21.32	1080	3.66	0.36
JC094-f0001carcs041	*Caryophyllia sp.*	east Eq. Atl.	9.22	-21.32	1080	32.37	1.61
JC094-f0001carcs042	*Caryophyllia sp.*	east Eq. Atl.	9.22	-21.32	1080	30.54	1.31
JC094-f0001carcs043	*Caryophyllia sp.*	east Eq. Atl.	9.22	-21.32	1080	15.06	0.87
JC094-f0001carcs044	*Caryophyllia sp.*	east Eq. Atl.	9.22	-21.32	1080	16.48	0.96
JC094-f0001carcs045	*Caryophyllia sp.*	east Eq. Atl.	9.22	-21.32	1080	5.01	0.45
JC094-f0001carcs046	*Caryophyllia sp.*	east Eq. Atl.	9.22	-21.32	1080	4.02	0.38
JC094-f0001carcs047	*Caryophyllia sp.*	east Eq. Atl.	9.22	-21.32	1080	34.53	1.45
JC094-f0001carcs048	*Caryophyllia sp.*	east Eq. Atl.	9.22	-21.32	1080	27.72	1.13
JC094-f0001carcs049	*Caryophyllia sp.*	east Eq. Atl.	9.22	-21.32	1080	14.23	1.02
JC094-f0001carcs050	*Caryophyllia sp.*	east Eq. Atl.	9.22	-21.32	1080	13.50	0.70
JC094-f0001carcs051	*Caryophyllia sp.*	east Eq. Atl.	9.22	-21.32	1080	18.80	0.86
JC094-f0001carcs052	*Caryophyllia sp.*	east Eq. Atl.	9.22	-21.32	1080	31.63	1.33
JC094-f0001carcs053	*Caryophyllia sp.*	east Eq. Atl.	9.22	-21.32	1080	40.57	1.67
JC094-f0001carcs054	*Caryophyllia sp.*	east Eq. Atl.	9.22	-21.32	1080	34.43	1.30
JC094-f0001carcs055	*Caryophyllia sp.*	east Eq. Atl.	9.22	-21.32	1080	35.33	1.34
JC094-f0001carcs056	*Caryophyllia sp.*	east Eq. Atl.	9.22	-21.32	1080	14.66	0.71
JC094-f0001carcs057	*Caryophyllia sp.*	east Eq. Atl.	9.22	-21.32	1080	28.27	1.18
JC094-f0001carcs059	*Caryophyllia sp.*	east Eq. Atl.	9.22	-21.32	1080	3.40	0.48

Sample ID	Taxa	Location	Latitude	Longitude	Depth water	Age	2s
JC094-f0001carcs060	*Caryophyllia sp.*	east Eq. Atl.	9.22	-21.32	1080	3.98	0.34
JC094-f0001carcs061	*Caryophyllia sp.*	east Eq. Atl.	9.22	-21.32	1080	16.44	0.61
JC094-f0001carcs062	*Caryophyllia sp.*	east Eq. Atl.	9.22	-21.32	1080	34.06	1.28
JC094-f0001carcs063	*Caryophyllia sp.*	east Eq. Atl.	9.22	-21.32	1080	60.22	2.45
JC094-f0001carcs064	*Caryophyllia sp.*	east Eq. Atl.	9.22	-21.32	1080	3.84	0.38
JC094-f0001carcs065	*Caryophyllia sp.*	east Eq. Atl.	9.22	-21.32	1080	16.91	0.71
JC094-f0001carcs067	*Caryophyllia sp.*	east Eq. Atl.	9.22	-21.32	1080	14.27	0.61
JC094-f0001carcs068	*Caryophyllia sp.*	east Eq. Atl.	9.22	-21.32	1080	35.46	1.43
JC094-f0001carcs069	*Caryophyllia sp.*	east Eq. Atl.	9.22	-21.32	1080	16.16	0.61
JC094-f0001carcs192	*Caryophyllia sp.*	east Eq. Atl.	9.22	-21.32	1080	32.77	1.31
JC094-f0001carcsm191	*Caryophyllia sp.*	east Eq. Atl.	9.22	-21.32	1080	37.24	1.42
JC094-f0001carns0001L	*Caryophyllia sp.*	east Eq. Atl.	9.22	-21.32	1080	0.37	0.17
JC094-f0001descm001	*Desmophyllum dianthus*	east Eq. Atl.	9.22	-21.32	1080	133.97	7.02
JC094-f0001pol002L	*Polymyces sp.*	east Eq. Atl.	9.22	-21.32	1080	30.63	1.26
JC094-f0002jav001L	*Javania sp.*	east Eq. Atl.	9.22	-21.32	1057	0.58	0.23
JC094-f0002javpm001	*Javania sp.*	east Eq. Atl.	9.22	-21.32	1057	0.36	0.13
JC094-f0003des001L	*Desmophyllum dianthus*	east Eq. Atl.	9.22	-21.32	994	16.02	0.81
JC094-f0005carnm001	*Caryophyllia sp.*	east Eq. Atl.	9.22	-21.32	994	15.79	0.82
JC094-f0005desnm001	*Desmophyllum dianthus*	east Eq. Atl.	9.22	-21.32	994	35.84	1.37
JC094-f0006carcm001	*Caryophyllia sp.*	east Eq. Atl.	9.22	-21.32	990	42.39	1.86
JC094-f0006carcs003	*Caryophyllia sp.*	east Eq. Atl.	9.22	-21.32	990	15.00	0.67
JC094-f0006carnm001	*Caryophyllia sp.*	east Eq. Atl.	9.22	-21.32	990	26.44	1.20
JC094-f0009carnm002	*Caryophyllia sp.*	east Eq. Atl.	9.22	-21.32	990	24.18	0.84
JC094-f0010carns001	*Caryophyllia sp.*	east Eq. Atl.	9.22	-21.32	990	0.58	0.24
JC094-f0011carcm001	*Caryophyllia sp.*	east Eq. Atl.	9.22	-21.32	990	25.12	0.91
JC094-f0011carnm001	*Caryophyllia sp.*	east Eq. Atl.	9.22	-21.32	990	42.36	1.49
JC094-f0012carcs001	*Caryophyllia sp.*	east Eq. Atl.	9.22	-21.32	990	54.73	2.07
JC094-f0012carcs002	*Caryophyllia sp.*	east Eq. Atl.	9.22	-21.32	990	58.27	2.50
JC094-f0012carns001	*Caryophyllia sp.*	east Eq. Atl.	9.22	-21.31	671	1.19	0.42

Sample ID	Taxa	Location	Latitude	Longitude	Depth water	Age	2s
JC094-f0012carns002	*Caryophyllia sp.*	east Eq. Atl.	9.22	-21.31	671	50.49	2.42
JC094-f0012carns003	*Caryophyllia sp.*	east Eq. Atl.	9.22	-21.31	671	1.50	0.35
JC094-f0012carns004	*Caryophyllia sp.*	east Eq. Atl.	9.22	-21.31	671	1.24	0.29
JC094-f0012carns005	*Caryophyllia sp.*	east Eq. Atl.	9.22	-21.31	671	55.98	2.62
JC094-f0012carns006	*Caryophyllia sp.*	east Eq. Atl.	9.22	-21.31	671	54.25	2.61
JC094-f0012carns007	*Caryophyllia sp.*	east Eq. Atl.	9.22	-21.31	671	58.11	3.90
JC094-f0012carQcs001	*Caryophyllia sp.*	east Eq. Atl.	9.22	-21.31	671	60.97	2.66
JC094-f0012carQcs002	*Caryophyllia sp.*	east Eq. Atl.	9.22	-21.31	671	60.82	2.83
JC094-f0012carQcs003	*Caryophyllia sp.*	east Eq. Atl.	9.22	-21.31	671	28.98	1.13
JC094-f0012carQcs004	*Caryophyllia sp.*	east Eq. Atl.	9.22	-21.31	671	59.83	2.72
JC094-f0012carQns001	*Caryophyllia sp.*	east Eq. Atl.	9.22	-21.31	671	62.69	2.87
JC094-f0012carQns002	*Caryophyllia sp.*	east Eq. Atl.	9.22	-21.31	671	63.61	2.37
JC094-f0012carQns003	*Caryophyllia sp.*	east Eq. Atl.	9.22	-21.31	671	31.80	2.13
JC094-f0012descm001	*Desmophyllum dianthus*	east Eq. Atl.	9.22	-21.31	671	86.94	5.22
JC094-f0012descm002	*Desmophyllum dianthus*	east Eq. Atl.	9.22	-21.31	671	30.37	1.11
JC094-f0012descm003	*Desmophyllum dianthus*	east Eq. Atl.	9.22	-21.31	671	71.71	3.05
JC094-f0012descm004	*Desmophyllum dianthus*	east Eq. Atl.	9.22	-21.31	671	61.97	2.83
JC094-f0013carnm001	*Caryophyllia sp.*	east Eq. Atl.	9.22	-21.32	639	24.57	0.92
JC094-f0013desps001	*Desmophyllum dianthus*	east Eq. Atl.	9.22	-21.32	639	0.58	0.19
JC094-f0015dasnf007	*Dasmosmillia sp.*	east Eq. Atl.	9.24	-21.32	265	0.53	0.32
JC094-f0015dasnm001	*Dasmosmillia sp.*	east Eq. Atl.	9.24	-21.32	265	0.56	0.42
JC094-f0019carns001	*Caryophyllia sp.*	east Eq. Atl.	9.2	-21.29	1829	33.93	1.26
JC094-f0019carns003	*Caryophyllia sp.*	east Eq. Atl.	9.2	-21.29	1829	53.68	2.38
JC094-f0019carns004	*Caryophyllia sp.*	east Eq. Atl.	9.2	-21.29	1829	16.20	0.77
JC094-f0019carns005	*Caryophyllia sp.*	east Eq. Atl.	9.2	-21.29	1829	34.21	1.58
JC094-f0019carns006	*Caryophyllia sp.*	east Eq. Atl.	9.2	-21.29	1829	16.20	0.69
JC094-f0019carns007	*Caryophyllia sp.*	east Eq. Atl.	9.2	-21.29	1829	54.13	1.79
JC094-f0019carns008	*Caryophyllia sp.*	east Eq. Atl.	9.2	-21.29	1829	41.09	1.61
JC094-f0019carns009	*Caryophyllia sp.*	east Eq. Atl.	9.2	-21.29	1829	36.08	1.38

Sample ID	Taxa	Location	Latitude	Longitude	Depth water	Age	2s
JC094-f0019carns010	*Caryophyllia sp.*	east Eq. Atl.	9.2	-21.29	1829	33.27	1.43
JC094-f0019carns011	*Caryophyllia sp.*	east Eq. Atl.	9.2	-21.29	1829	36.41	1.50
JC094-f0019carns013	*Caryophyllia sp.*	east Eq. Atl.	9.2	-21.29	1829	14.62	0.76
JC094-f0019carns014	*Caryophyllia sp.*	east Eq. Atl.	9.2	-21.29	1829	79.94	3.09
JC094-f0019carns015-2	*Caryophyllia sp.*	east Eq. Atl.	9.2	-21.29	1829	16.81	0.80
JC094-f0019enacm004d	*Enallopsammia sp.*	east Eq. Atl.	9.2	-21.29	1829	12.02	0.51
JC094-f0019enacm004e	*Enallopsammia sp.*	east Eq. Atl.	9.2	-21.29	1829	49.51	1.87
JC094-f0019enacs005a	*Enallopsammia sp.*	east Eq. Atl.	9.2	-21.29	1829	15.33	0.79
JC094-f0019enacs005b	*Enallopsammia sp.*	east Eq. Atl.	9.2	-21.29	1829	12.19	0.52
JC094-f0019enacs005c	*Enallopsammia sp.*	east Eq. Atl.	9.2	-21.29	1829	15.88	0.59
JC094-f0019enacs005e	*Enallopsammia sp.*	east Eq. Atl.	9.2	-21.29	1829	11.49	0.47
JC094-f0019othnm001	*unidentified sp.*	east Eq. Atl.	9.2	-21.29	1829	16.32	0.66
JC094-f0021carcm001	*Caryophyllia sp.*	east Eq. Atl.	9.2	-21.29	1545	12.56	0.69
JC094-f0021despm001	*Desmophyllum dianthus*	east Eq. Atl.	9.2	-21.29	1545	0.47	0.24
JC094-f0021madQnm001c	*Madrepora sp.*	east Eq. Atl.	9.2	-21.29	1545	14.72	0.70
JC094-f0021madQnm001d	*Madrepora sp.*	east Eq. Atl.	9.2	-21.29	1545	14.98	0.63
JC094-f0021madQnm001e	*Madrepora sp.*	east Eq. Atl.	9.2	-21.29	1545	16.51	0.77
JC094-f0023carcs001	*Caryophyllia sp.*	east Eq. Atl.	9.2	-21.3	1524	12.17	0.52
JC094-f0026enacm001a	*Enallopsammia sp.*	east Eq. Atl.	9.2	-21.3	1506	1.31	0.28
JC094-f0026enacm001b	*Enallopsammia sp.*	east Eq. Atl.	9.2	-21.3	1506	3.32	0.35
JC094-f0027carns001	*Caryophyllia sp.*	east Eq. Atl.	9.21	-21.3	1431	12.76	0.74
JC094-f0027carns002	*Caryophyllia sp.*	east Eq. Atl.	9.21	-21.3	1431	15.03	0.70
JC094-f0027carns003	*Caryophyllia sp.*	east Eq. Atl.	9.21	-21.3	1431	12.02	0.56
JC094-f0027carns004	*Caryophyllia sp.*	east Eq. Atl.	9.21	-21.3	1431	10.74	0.58
JC094-f0027carns005	*Caryophyllia sp.*	east Eq. Atl.	9.21	-21.3	1431	13.13	0.62
JC094-f0027carns006	*Caryophyllia sp.*	east Eq. Atl.	9.21	-21.3	1431	12.29	0.74
JC094-f0027carns007	*Caryophyllia sp.*	east Eq. Atl.	9.21	-21.3	1431	12.60	0.64
JC094-f0027carns008	*Caryophyllia sp.*	east Eq. Atl.	9.21	-21.3	1431	12.24	0.84
JC094-f0027carns009	*Caryophyllia sp.*	east Eq. Atl.	9.21	-21.3	1431	14.79	0.82

Sample ID	Taxa	Location	Latitude	Longitude	Depth water	Age	2s
JC094-f0027carns012	*Caryophyllia sp.*	east Eq. Atl.	9.21	-21.3	1431	13.52	0.64
JC094-f0027carns014	*Caryophyllia sp.*	east Eq. Atl.	9.21	-21.3	1431	13.56	0.77
JC094-f0027carns015	*Caryophyllia sp.*	east Eq. Atl.	9.21	-21.3	1431	139.48	7.16
JC094-f0027carns016	*Caryophyllia sp.*	east Eq. Atl.	9.21	-21.3	1431	15.96	0.80
JC094-f0027carns017	*Caryophyllia sp.*	east Eq. Atl.	9.21	-21.3	1431	15.32	1.19
JC094-f0027carns018	*Caryophyllia sp.*	east Eq. Atl.	9.21	-21.3	1431	12.24	0.63
JC094-f0027descs004	*Desmophyllum dianthus*	east Eq. Atl.	9.21	-21.3	1431	15.36	0.69
JC094-f0029carcs004	*Caryophyllia sp.*	east Eq. Atl.	9.21	-21.3	1413	16.32	0.80
JC094-f0029carcs005	*Caryophyllia sp.*	east Eq. Atl.	9.21	-21.3	1413	16.46	0.71
JC094-f0029carcsm001	*Caryophyllia sp.*	east Eq. Atl.	9.21	-21.3	1413	18.68	0.83
JC094-f0029carns001	*Caryophyllia sp.*	east Eq. Atl.	9.21	-21.3	1413	1.45	0.33
JC094-f0029carns002	*Caryophyllia sp.*	east Eq. Atl.	9.21	-21.3	1413	0.53	0.31
JC094-f0029enacl002a	*Enallopsammia sp.*	east Eq. Atl.	9.21	-21.3	1413	1.97	0.21
JC094-f0029enacl002b	*Enallopsammia sp.*	east Eq. Atl.	9.21	-21.3	1413	2.87	0.28
JC094-f0029enacl002c	*Enallopsammia sp.*	east Eq. Atl.	9.21	-21.3	1413	1.75	0.16
JC094-f0029enapsm001a	*Enallopsammia sp.*	east Eq. Atl.	9.21	-21.3	1413	1.27	0.26
JC094-f0029enapsm001b	*Enallopsammia sp.*	east Eq. Atl.	9.21	-21.3	1413	0.68	0.35
JC094-f0029enapsm001c	*Enallopsammia sp.*	east Eq. Atl.	9.21	-21.3	1413	0.40	0.28
JC094-f0030carcs001	*Caryophyllia sp.*	east Eq. Atl.	9.21	-21.3	1380	14.84	0.65
JC094-f0030carcs002	*Caryophyllia sp.*	east Eq. Atl.	9.21	-21.3	1380	17.02	0.90
JC094-f0030carcs003	*Caryophyllia sp.*	east Eq. Atl.	9.21	-21.3	1380	12.03	0.79
JC094-f0030carcs004	*Caryophyllia sp.*	east Eq. Atl.	9.21	-21.3	1380	16.46	0.77
JC094-f0030carcs005	*Caryophyllia sp.*	east Eq. Atl.	9.21	-21.3	1380	13.49	0.55
JC094-f0030carcs006	*Caryophyllia sp.*	east Eq. Atl.	9.21	-21.3	1380	12.63	0.54
JC094-f0030carcs007	*Caryophyllia sp.*	east Eq. Atl.	9.21	-21.3	1380	11.06	0.53
JC094-f0030carcs008	*Caryophyllia sp.*	east Eq. Atl.	9.21	-21.3	1380	2.52	0.34
JC094-f0030carcs009	*Caryophyllia sp.*	east Eq. Atl.	9.21	-21.3	1380	15.53	0.77
JC094-f0030carcs010	*Caryophyllia sp.*	east Eq. Atl.	9.21	-21.3	1380	11.83	0.63
JC094-f0030carcs011	*Caryophyllia sp.*	east Eq. Atl.	9.21	-21.3	1380	14.90	0.69

Sample ID	Taxa	Location	Latitude	Longitude	Depth water	Age	2s
JC094-f0030carcs012	*Caryophyllia sp.*	east Eq. Atl.	9.21	-21.3	1380	15.61	0.80
JC094-f0030carps001	*Caryophyllia sp.*	east Eq. Atl.	9.21	-21.3	1380	14.78	0.59
JC094-f0030carps002	*Caryophyllia sp.*	east Eq. Atl.	9.21	-21.3	1380	12.11	0.48
JC094-f0030jav001L	*Javania sp.*	east Eq. Atl.	9.21	-21.3	1380	17.20	0.72
JC094-f0031carcm001	*Caryophyllia sp.*	east Eq. Atl.	9.21	-21.3	1380	127.76	6.48
JC094-f0031desnm001	*Desmophyllum dianthus*	east Eq. Atl.	9.21	-21.3	1380	133.80	7.07
JC094-f0040carcs001	*Caryophyllia sp.*	east Eq. Atl.	9.2	-21.28	2160	49.75	1.84
JC094-f0040des001L	*Desmophyllum dianthus*	east Eq. Atl.	9.2	-21.28	2160	47.36	1.90
JC094-f0040des002L	*Desmophyllum dianthus*	east Eq. Atl.	9.2	-21.28	2160	94.79	3.69
JC094-f0040des003L	*Desmophyllum dianthus*	east Eq. Atl.	9.2	-21.28	2160	95.67	4.30
JC094-f0040des004L	*Desmophyllum dianthus*	east Eq. Atl.	9.2	-21.28	2160	49.88	2.18
JC094-f0040des005L	*Desmophyllum dianthus*	east Eq. Atl.	9.2	-21.28	2160	147.41	8.76
JC094-f0040descs001	*Desmophyllum dianthus*	east Eq. Atl.	9.2	-21.28	2160	48.72	2.05
JC094-f0040descs003	*Desmophyllum dianthus*	east Eq. Atl.	9.2	-21.28	2160	86.16	4.06
JC094-f0042des001L	*Desmophyllum dianthus*	east Eq. Atl.	9.2	-21.28	2100	147.65	9.11
JC094-f0042des002L	*Desmophyllum dianthus*	east Eq. Atl.	9.2	-21.28	2100	145.42	8.93
JC094-f0042enacsm002	*Enallopsammia sp.*	east Eq. Atl.	9.2	-21.28	2100	146.05	8.55
JC094-f0044carcs015	*Caryophyllia sp.*	east Eq. Atl.	9.21	-21.3	1345	16.42	0.66
JC094-f0044carcsm001	*Caryophyllia sp.*	east Eq. Atl.	9.21	-21.3	1345	18.71	0.89
JC094-f0044carcsm002	*Caryophyllia sp.*	east Eq. Atl.	9.21	-21.3	1345	38.13	1.54
JC094-f0044carcsm004	*Caryophyllia sp.*	east Eq. Atl.	9.21	-21.3	1345	14.90	0.82
JC094-f0044carcsm005	*Caryophyllia sp.*	east Eq. Atl.	9.21	-21.3	1345	1.24	0.26
JC094-f0044carcsm006	*Caryophyllia sp.*	east Eq. Atl.	9.21	-21.3	1345	13.55	0.61
JC094-f0044carcsm007	*Caryophyllia sp.*	east Eq. Atl.	9.21	-21.3	1345	17.76	0.73
JC094-f0044carcsm008	*Caryophyllia sp.*	east Eq. Atl.	9.21	-21.3	1345	14.80	0.76
JC094-f0044carcsm009	*Caryophyllia sp.*	east Eq. Atl.	9.21	-21.3	1345	14.74	0.74
JC094-f0044carps002	*Caryophyllia sp.*	east Eq. Atl.	9.21	-21.3	1345	2.41	0.26
JC094-f0044carps003	*Caryophyllia sp.*	east Eq. Atl.	9.21	-21.3	1345	1.10	0.24
JC094-f0044descs001	*Desmophyllum dianthus*	east Eq. Atl.	9.21	-21.3	1345	19.67	0.77

Sample ID	Taxa	Location	Latitude	Longitude	Depth water	Age	2s
JC094-f0046carns001	*Caryophyllia sp.*	east Eq. Atl.	9.21	-21.3	1326	1.11	0.22
JC094-f0047carcs024	*Caryophyllia sp.*	east Eq. Atl.	9.21	-21.3	1366	14.30	0.59
JC094-f0047carcs025	*Caryophyllia sp.*	east Eq. Atl.	9.21	-21.3	1366	138.43	8.37
JC094-f0047carcs027	*Caryophyllia sp.*	east Eq. Atl.	9.21	-21.3	1366	141.90	7.24
JC094-f0047carcs028	*Caryophyllia sp.*	east Eq. Atl.	9.21	-21.3	1366	123.48	5.81
JC094-f0047carcsm002	*Caryophyllia sp.*	east Eq. Atl.	9.21	-21.3	1366	15.65	0.86
JC094-f0047carcsm003	*Caryophyllia sp.*	east Eq. Atl.	9.21	-21.3	1366	40.21	1.84
JC094-f0047carcsm004	*Caryophyllia sp.*	east Eq. Atl.	9.21	-21.3	1366	44.18	1.82
JC094-f0047carcsm006	*Caryophyllia sp.*	east Eq. Atl.	9.21	-21.3	1366	131.75	6.30
JC094-f0047carcsm019	*Caryophyllia sp.*	east Eq. Atl.	9.21	-21.3	1366	16.85	0.76
JC094-f0047carcsm036	*Caryophyllia sp.*	east Eq. Atl.	9.21	-21.3	1366	145.39	8.89
JC094-f0047carcsm037	*Caryophyllia sp.*	east Eq. Atl.	9.21	-21.3	1366	77.89	3.17
JC094-f0047descm001	*Desmophyllum dianthus*	east Eq. Atl.	9.21	-21.3	1366	134.86	6.72
JC094-f0047enacsm001a	*Enallopsammia sp.*	east Eq. Atl.	9.21	-21.3	1366	1.45	0.38
JC094-f0047enacsm001b	*Enallopsammia sp.*	east Eq. Atl.	9.21	-21.3	1366	140.59	7.64
JC094-f0048carcs001	*Caryophyllia sp.*	east Eq. Atl.	9.21	-21.3	1365	47.81	1.63
JC094-f0048carcs004	*Caryophyllia sp.*	east Eq. Atl.	9.21	-21.3	1365	34.87	1.44
JC094-f0048carcs005	*Caryophyllia sp.*	east Eq. Atl.	9.21	-21.3	1365	16.85	0.70
JC094-f0048carcs009	*Caryophyllia sp.*	east Eq. Atl.	9.21	-21.3	1365	142.66	8.98
JC094-f0049carns001	*Caryophyllia sp.*	east Eq. Atl.	9.21	-21.3	1375	0.69	0.23
JC094-f0052carcs010	*Caryophyllia sp.*	east Eq. Atl.	9.22	-21.31	973	2.34	0.27
JC094-f0052carcs011	*Caryophyllia sp.*	east Eq. Atl.	9.22	-21.31	973	0.39	0.22
JC094-f0052carcs012	*Caryophyllia sp.*	east Eq. Atl.	9.22	-21.31	973	0.47	0.18
JC094-f0052carcs013	*Caryophyllia sp.*	east Eq. Atl.	9.22	-21.31	973	1.60	0.24
JC094-f0052carcs014	*Caryophyllia sp.*	east Eq. Atl.	9.22	-21.31	973	0.89	0.25
JC094-f0052carcs015	*Caryophyllia sp.*	east Eq. Atl.	9.22	-21.31	973	1.73	0.28
JC094-f0052carcs017	*Caryophyllia sp.*	east Eq. Atl.	9.22	-21.31	973	1.10	0.23
JC094-f0052carcs018	*Caryophyllia sp.*	east Eq. Atl.	9.22	-21.31	973	2.53	0.20
JC094-f0052carcs019	*Caryophyllia sp.*	east Eq. Atl.	9.22	-21.31	973	9.65	0.46

Sample ID	Taxa	Location	Latitude	Longitude	Depth water	Age	2s
JC094-f0052carcs020	*Caryophyllia sp.*	east Eq. Atl.	9.22	-21.31	973	2.51	0.24
JC094-f0052carcs021	*Caryophyllia sp.*	east Eq. Atl.	9.22	-21.31	973	71.00	2.93
JC094-f0052carcs022	*Caryophyllia sp.*	east Eq. Atl.	9.22	-21.31	973	30.96	1.18
JC094-f0052carcsm039L	*Caryophyllia sp.*	east Eq. Atl.	9.22	-21.31	973	34.31	1.33
JC094-f0052carcsm040L	*Caryophyllia sp.*	east Eq. Atl.	9.22	-21.31	973	24.42	0.95
JC094-f0052carcsm043	*Caryophyllia sp.*	east Eq. Atl.	9.22	-21.31	973	1.61	0.24
JC094-f0052carns003	*Caryophyllia sp.*	east Eq. Atl.	9.22	-21.31	973	0.79	0.23
JC094-f0053carcm028	*Caryophyllia sp.*	east Eq. Atl.	9.22	-21.31	800	8.64	0.52
JC094-f0053carcs034	*Caryophyllia sp.*	east Eq. Atl.	9.22	-21.31	800	34.50	1.67
JC094-f0053carcsm001	*Caryophyllia sp.*	east Eq. Atl.	9.22	-21.31	800	24.09	0.97
JC094-f0053carcsm003	*Caryophyllia sp.*	east Eq. Atl.	9.22	-21.31	800	28.32	1.15
JC094-f0053carcsm006	*Caryophyllia sp.*	east Eq. Atl.	9.22	-21.31	800	42.94	1.61
JC094-f0053carcsm007	*Caryophyllia sp.*	east Eq. Atl.	9.22	-21.31	800	24.26	0.92
JC094-f0053carcsm008	*Caryophyllia sp.*	east Eq. Atl.	9.22	-21.31	800	44.52	1.57
JC094-f0053carcsm009	*Caryophyllia sp.*	east Eq. Atl.	9.22	-21.31	800	71.28	4.34
JC094-f0053carcsm010	*Caryophyllia sp.*	east Eq. Atl.	9.22	-21.31	800	48.83	1.58
JC094-f0053carcsm011	*Caryophyllia sp.*	east Eq. Atl.	9.22	-21.31	800	25.95	0.99
JC094-f0053carcsm020	*Caryophyllia sp.*	east Eq. Atl.	9.22	-21.31	800	30.07	1.24
JC094-f0053carcsm021	*Caryophyllia sp.*	east Eq. Atl.	9.22	-21.31	800	71.46	3.35
JC094-f0053carcsm022	*Caryophyllia sp.*	east Eq. Atl.	9.22	-21.31	800	27.28	1.33
JC094-f0053carcsm023	*Caryophyllia sp.*	east Eq. Atl.	9.22	-21.31	800	36.43	1.41
JC094-f0053carcsm024	*Caryophyllia sp.*	east Eq. Atl.	9.22	-21.31	800	69.28	2.84
JC094-f0053carcsm025	*Caryophyllia sp.*	east Eq. Atl.	9.22	-21.31	800	13.43	0.82
JC094-f0053carcsm026	*Caryophyllia sp.*	east Eq. Atl.	9.22	-21.31	800	36.50	1.46
JC094-f0053carcsm027	*Caryophyllia sp.*	east Eq. Atl.	9.22	-21.31	800	27.40	1.15
JC094-f0053carcsm029	*Caryophyllia sp.*	east Eq. Atl.	9.22	-21.31	800	29.51	1.34
JC094-f0053carcsm030	*Caryophyllia sp.*	east Eq. Atl.	9.22	-21.31	800	31.85	1.42
JC094-f0053carcsm031	*Caryophyllia sp.*	east Eq. Atl.	9.22	-21.31	800	27.11	1.15
JC094-f0053carcsm032	*Caryophyllia sp.*	east Eq. Atl.	9.22	-21.31	800	34.31	1.28

Sample ID	Taxa	Location	Latitude	Longitude	Depth water	Age	2s
JC094-f0054carcm021	*Caryophyllia sp.*	east Eq. Atl.	9.22	-21.31	800	31.36	1.32
JC094-f0054carcm022	*Caryophyllia sp.*	east Eq. Atl.	9.22	-21.31	800	24.21	1.11
JC094-f0054carcm024	*Caryophyllia sp.*	east Eq. Atl.	9.22	-21.31	800	9.02	0.51
JC094-f0054carcm025	*Caryophyllia sp.*	east Eq. Atl.	9.22	-21.31	800	25.08	0.94
JC094-f0054carcm026	*Caryophyllia sp.*	east Eq. Atl.	9.22	-21.31	800	43.28	1.65
JC094-f0054carcm027	*Caryophyllia sp.*	east Eq. Atl.	9.22	-21.31	800	19.98	0.80
JC094-f0054carcm029	*Caryophyllia sp.*	east Eq. Atl.	9.22	-21.31	800	23.02	0.98
JC094-f0054carcm030	*Caryophyllia sp.*	east Eq. Atl.	9.22	-21.31	800	71.89	3.00
JC094-f0054carcm031	*Caryophyllia sp.*	east Eq. Atl.	9.22	-21.31	800	37.79	1.57
JC094-f0054carcm033	*Caryophyllia sp.*	east Eq. Atl.	9.22	-21.31	800	36.00	1.47
JC094-f0054carcs001	*Caryophyllia sp.*	east Eq. Atl.	9.22	-21.31	800	30.89	1.12
JC094-f0054carcs002	*Caryophyllia sp.*	east Eq. Atl.	9.22	-21.31	800	24.96	0.91
JC094-f0054carcs003	*Caryophyllia sp.*	east Eq. Atl.	9.22	-21.31	800	23.31	0.90
JC094-f0054carns012	*Caryophyllia sp.*	east Eq. Atl.	9.22	-21.31	800	25.20	1.20
JC094-f0054carns013	*Caryophyllia sp.*	east Eq. Atl.	9.22	-21.31	800	25.21	1.15
JC094-f0054carns016	*Caryophyllia sp.*	east Eq. Atl.	9.22	-21.31	800	33.57	1.33
JC094-f0054carns017	*Caryophyllia sp.*	east Eq. Atl.	9.22	-21.31	800	43.25	1.48
JC094-f0054carns018	*Caryophyllia sp.*	east Eq. Atl.	9.22	-21.31	800	24.99	0.93
JC094-f0054carns019	*Caryophyllia sp.*	east Eq. Atl.	9.22	-21.31	800	26.41	1.24
JC094-f0054carns020	*Caryophyllia sp.*	east Eq. Atl.	9.22	-21.31	798	2.00	0.42
JC094-f0054carpm002	*Caryophyllia sp.*	east Eq. Atl.	9.22	-21.31	798	0.66	0.35
JC094-f0054carQcs050	*Caryophyllia sp.*	east Eq. Atl.	9.22	-21.31	798	33.94	1.34
JC094-f0054carQcs051	*Caryophyllia sp.*	east Eq. Atl.	9.22	-21.31	798	23.34	0.96
JC094-f0054carQcs052	*Caryophyllia sp.*	east Eq. Atl.	9.22	-21.31	798	34.92	1.30
JC094-f0054carQcs053	*Caryophyllia sp.*	east Eq. Atl.	9.22	-21.31	798	21.15	1.06
JC094-f0054carQcsm036L	*Caryophyllia sp.*	east Eq. Atl.	9.22	-21.31	798	15.79	0.78
JC094-f0054carQcsm038L	*Caryophyllia sp.*	east Eq. Atl.	9.22	-21.31	798	36.35	1.51
JC094-f0054carQcsm039L	*Caryophyllia sp.*	east Eq. Atl.	9.22	-21.31	798	19.68	0.94
JC094-f0054carQcsm042L	*Caryophyllia sp.*	east Eq. Atl.	9.22	-21.31	798	30.05	1.20

Sample ID	Taxa	Location	Latitude	Longitude	Depth water	Age	2s
JC094-f0054carQcsm044L	*Caryophyllia sp.*	east Eq. Atl.	9.22	-21.31	798	19.05	0.80
JC094-f0054carQcsm048L	*Caryophyllia sp.*	east Eq. Atl.	9.22	-21.31	798	128.34	7.50
JC094-f0054descm001	*Desmophyllum dianthus*	east Eq. Atl.	9.22	-21.31	798	68.22	2.99
JC094-f0054othcml001	*unidentified sp.*	east Eq. Atl.	9.22	-21.31	798	31.72	1.15
JC094-f0057carcm007	*Caryophyllia sp.*	east Eq. Atl.	9.22	-21.31	746	27.74	1.25
JC094-f0057carcsm001L	*Caryophyllia sp.*	east Eq. Atl.	9.22	-21.31	746	17.20	0.82
JC094-f0057carcsm002	*Caryophyllia sp.*	east Eq. Atl.	9.22	-21.31	746	45.00	1.71
JC094-f0057carcsm003	*Caryophyllia sp.*	east Eq. Atl.	9.22	-21.31	746	15.36	0.63
JC094-f0057carcsm007L	*Caryophyllia sp.*	east Eq. Atl.	9.22	-21.31	747	25.73	1.03
JC094-f0059carcs003	*Caryophyllia sp.*	east Eq. Atl.	9.21	-21.3	1354	15.50	0.79
JC094-f0059carcs004	*Caryophyllia sp.*	east Eq. Atl.	9.21	-21.3	1354	1.49	0.21
JC094-f0059polcm001	*Polymyces sp.*	east Eq. Atl.	9.21	-21.3	1354	12.83	0.69
JC094-f0060carnm001	*Caryophyllia sp.*	east Eq. Atl.	5.6	-26.97	1985	15.22	0.79
JC094-f0060carnm003	*Caryophyllia sp.*	east Eq. Atl.	5.6	-26.97	1985	15.44	0.79
JC094-f0060carnm004	*Caryophyllia sp.*	east Eq. Atl.	5.6	-26.97	1985	15.64	0.58
JC094-f0060carnm006	*Caryophyllia sp.*	east Eq. Atl.	5.6	-26.97	1985	15.39	0.81
JC094-f0060carnm008	*Caryophyllia sp.*	east Eq. Atl.	5.6	-26.97	1985	2.32	0.30
JC094-f0060carnm009	*Caryophyllia sp.*	east Eq. Atl.	5.6	-26.97	1985	2.05	0.27
JC094-f0060carnm010	*Caryophyllia sp.*	east Eq. Atl.	5.6	-26.97	1985	14.44	0.99
JC094-f0060carnm011	*Caryophyllia sp.*	east Eq. Atl.	5.6	-26.97	1985	14.66	0.98
JC094-f0060carnm015	*Caryophyllia sp.*	east Eq. Atl.	5.6	-26.97	1985	14.08	0.93
JC094-f0060carnm017	*Caryophyllia sp.*	east Eq. Atl.	5.6	-26.97	1985	14.54	0.66
JC094-f0060carnm018	*Caryophyllia sp.*	east Eq. Atl.	5.6	-26.97	1985	15.16	0.63
JC094-f0060carnm019	*Caryophyllia sp.*	east Eq. Atl.	5.6	-26.97	1985	14.69	0.59
JC094-f0060carnm022	*Caryophyllia sp.*	east Eq. Atl.	5.6	-26.97	1985	15.65	0.67
JC094-f0060carnm024	*Caryophyllia sp.*	east Eq. Atl.	5.6	-26.97	1985	13.83	0.71
JC094-f0060carnm025	*Caryophyllia sp.*	east Eq. Atl.	5.6	-26.97	1985	14.94	0.61
JC094-f0060carnm034	*Caryophyllia sp.*	east Eq. Atl.	5.6	-26.97	1985	14.35	0.59
JC094-f0060carnm039	*Caryophyllia sp.*	east Eq. Atl.	5.6	-26.97	1985	14.95	0.77

Sample ID	Taxa	Location	Latitude	Longitude	Depth water	Age	2s
JC094-f0060carnm044	*Caryophyllia sp.*	east Eq. Atl.	5.6	-26.97	1985	15.19	0.66
JC094-f0060carnm050	*Caryophyllia sp.*	east Eq. Atl.	5.6	-26.97	1985	14.35	0.58
JC094-f0060carnm051	*Caryophyllia sp.*	east Eq. Atl.	5.6	-26.97	1985	14.57	0.64
JC094-f0060carnm059	*Caryophyllia sp.*	east Eq. Atl.	5.6	-26.97	1985	15.67	0.55
JC094-f0060carns001	*Caryophyllia sp.*	east Eq. Atl.	5.6	-26.97	1985	2.18	0.42
JC094-f0060carns002	*Caryophyllia sp.*	east Eq. Atl.	5.6	-26.97	1985	15.80	0.94
JC094-f0061carnm006	*Caryophyllia sp.*	east Eq. Atl.	5.6	-26.97	1966	14.23	0.80
JC094-f0061carnm007	*Caryophyllia sp.*	east Eq. Atl.	5.6	-26.97	1966	14.97	0.69
JC094-f0061carnm011	*Caryophyllia sp.*	east Eq. Atl.	5.6	-26.97	1966	15.01	0.82
JC094-f0061carnm013	*Caryophyllia sp.*	east Eq. Atl.	5.6	-26.97	1966	14.03	0.63
JC094-f0061carnm014	*Caryophyllia sp.*	east Eq. Atl.	5.6	-26.97	1966	13.98	0.61
JC094-f0061carnm019	*Caryophyllia sp.*	east Eq. Atl.	5.6	-26.97	1966	15.26	0.83
JC094-f0061carnm022	*Caryophyllia sp.*	east Eq. Atl.	5.6	-26.97	1966	14.73	0.66
JC094-f0061carnm026	*Caryophyllia sp.*	east Eq. Atl.	5.6	-26.97	1966	14.25	0.52
JC094-f0061carnm027	*Caryophyllia sp.*	east Eq. Atl.	5.6	-26.97	1966	15.37	0.52
JC094-f0061carnm028	*Caryophyllia sp.*	east Eq. Atl.	5.6	-26.97	1966	14.21	0.59
JC094-f0061carnm029	*Caryophyllia sp.*	east Eq. Atl.	5.6	-26.97	1966	14.97	0.56
JC094-f0061carnm030	*Caryophyllia sp.*	east Eq. Atl.	5.6	-26.97	1966	15.39	0.82
JC094-f0061carnm032	*Caryophyllia sp.*	east Eq. Atl.	5.6	-26.97	1966	14.14	0.71
JC094-f0061carnm034	*Caryophyllia sp.*	east Eq. Atl.	5.6	-26.97	1966	14.29	0.55
JC094-f0061carnm035	*Caryophyllia sp.*	east Eq. Atl.	5.6	-26.97	1966	13.79	0.59
JC094-f0061carnm036	*Caryophyllia sp.*	east Eq. Atl.	5.6	-26.97	1966	15.38	0.50
JC094-f0061carnm039	*Caryophyllia sp.*	east Eq. Atl.	5.6	-26.97	1966	15.45	0.67
JC094-f0061carnm041	*Caryophyllia sp.*	east Eq. Atl.	5.6	-26.97	1966	2.44	0.27
JC094-f0061carnm043	*Caryophyllia sp.*	east Eq. Atl.	5.6	-26.97	1966	14.56	0.62
JC094-f0061carnm044	*Caryophyllia sp.*	east Eq. Atl.	5.6	-26.97	1966	15.35	0.70
JC094-f0061carnm045	*Caryophyllia sp.*	east Eq. Atl.	5.6	-26.97	1966	2.74	0.44
JC094-f0061carnm046	*Caryophyllia sp.*	east Eq. Atl.	5.6	-26.97	1966	1.46	0.32
JC094-f0061carnm047	*Caryophyllia sp.*	east Eq. Atl.	5.6	-26.97	1966	14.57	0.60

Sample ID	Taxa	Location	Latitude	Longitude	Depth water	Age	2s
JC094-f0061carnm048	*Caryophyllia sp.*	east Eq. Atl.	5.6	-26.97	1966	15.04	0.59
JC094-f0061carnm049	*Caryophyllia sp.*	east Eq. Atl.	5.6	-26.97	1966	1.02	0.22
JC094-f0061carnm050	*Caryophyllia sp.*	east Eq. Atl.	5.6	-26.97	1966	0.85	0.30
JC094-f0062carpm001	*Caryophyllia sp.*	east Eq. Atl.	5.6	-26.96	1853	1.25	0.46
JC094-f0065carcs003	*Caryophyllia sp.*	east Eq. Atl.	5.61	-26.96	1574	29.92	1.24
JC094-f0065carcs004	*Caryophyllia sp.*	east Eq. Atl.	5.61	-26.96	1574	24.01	0.96
JC094-f0065carcs005	*Caryophyllia sp.*	east Eq. Atl.	5.61	-26.96	1574	143.87	8.50
JC094-f0065carcsm001L	*Caryophyllia sp.*	east Eq. Atl.	5.61	-26.96	1574	139.12	7.28
JC094-f0065descm001	*Desmophyllum dianthus*	east Eq. Atl.	5.61	-26.96	1574	59.80	2.39
JC094-f0069enacsm001	*Enallopsammia sp.*	east Eq. Atl.	5.61	-26.96	1445	2.36	0.23
JC094-f0073carcs003	*Caryophyllia sp.*	east Eq. Atl.	5.63	-26.97	1264	12.42	0.60
JC094-f0073carcs004	*Caryophyllia sp.*	east Eq. Atl.	5.63	-26.97	1264	15.84	0.77
JC094-f0073carcs005	*Caryophyllia sp.*	east Eq. Atl.	5.63	-26.97	1264	16.13	0.97
JC094-f0074descm001	*Desmophyllum dianthus*	east Eq. Atl.	5.63	-26.96	997	15.48	0.58
JC094-f0075carcs001	*Caryophyllia sp.*	east Eq. Atl.	5.63	-26.95	915	2.91	0.35
JC094-f0075carcs002	*Caryophyllia sp.*	east Eq. Atl.	5.63	-26.95	915	1.18	0.32
JC094-f0076carcm030	*Caryophyllia sp.*	east Eq. Atl.	5.63	-26.95	845	16.68	0.77
JC094-f0076carcs003	*Caryophyllia sp.*	east Eq. Atl.	5.63	-26.95	845	18.55	0.67
JC094-f0076carcs004	*Caryophyllia sp.*	east Eq. Atl.	5.63	-26.95	845	23.46	0.83
JC094-f0076carcs007	*Caryophyllia sp.*	east Eq. Atl.	5.63	-26.95	845	0.41	0.31
JC094-f0076carcs008	*Caryophyllia sp.*	east Eq. Atl.	5.63	-26.95	845	22.13	1.01
JC094-f0076carcs009	*Caryophyllia sp.*	east Eq. Atl.	5.63	-26.95	845	25.74	0.88
JC094-f0076carcs021	*Caryophyllia sp.*	east Eq. Atl.	5.63	-26.95	845	37.89	1.52
JC094-f0076descm001L	*Desmophyllum dianthus*	east Eq. Atl.	5.63	-26.95	845	18.01	0.82
JC094-f0077carcs002	*Caryophyllia sp.*	east Eq. Atl.	5.63	-26.95	773	0.52	0.27
JC094-f0077javcm001	*Javania sp.*	east Eq. Atl.	5.63	-26.95	773	1.63	0.35
JC094-f0077javcm002	*Javania sp.*	east Eq. Atl.	5.63	-26.95	773	0.97	0.26
JC094-f0079carcs001	*Caryophyllia sp.*	east Eq. Atl.	5.63	-26.95	749	0.66	0.27
JC094-f0079carcs003	*Caryophyllia sp.*	east Eq. Atl.	5.63	-26.95	749	1.49	0.27

Sample ID	Taxa	Location	Latitude	Longitude	Depth water	Age	2s
JC094-f0079carcs004	*Caryophyllia sp.*	east Eq. Atl.	5.63	-26.95	749	0.52	0.35
JC094-f0079carcs005	*Caryophyllia sp.*	east Eq. Atl.	5.63	-26.95	749	2.66	0.31
JC094-f0079carcs006	*Caryophyllia sp.*	east Eq. Atl.	5.63	-26.95	749	3.38	0.45
JC094-f0079carcs008	*Caryophyllia sp.*	east Eq. Atl.	5.63	-26.95	761	0.97	0.24
JC094-f0085carpm001	*Caryophyllia sp.*	east Eq. Atl.	5.59	-26.99	2599	0.43	0.20
JC094-f0087carpm001	*Caryophyllia sp.*	east Eq. Atl.	5.6	-27	2475	0.23	0.17
JC094-f0091carcm001	*Caryophyllia sp.*	east Eq. Atl.	5.6	-26.97	2170	0.45	0.24
JC094-f0091carcm002	*Caryophyllia sp.*	east Eq. Atl.	5.6	-26.97	2170	0.81	0.24
JC094-f0091carcm003	*Caryophyllia sp.*	east Eq. Atl.	5.6	-26.97	2170	1.82	0.24
JC094-f0092descm001	*Desmophyllum dianthus*	east Eq. Atl.	5.62	-26.96	1164	135.13	8.03
JC094-f0092descm002	*Desmophyllum dianthus*	east Eq. Atl.	5.62	-26.96	1164	125.87	5.90
JC094-f0093carcs001	*Caryophyllia sp.*	east Eq. Atl.	5.62	-26.96	1164	16.08	0.70
JC094-f0093carcs002	*Caryophyllia sp.*	east Eq. Atl.	5.62	-26.96	1164	19.74	0.81
JC094-f0093carcs004	*Caryophyllia sp.*	east Eq. Atl.	5.62	-26.96	1164	12.31	0.52
JC094-f0093carcs005	*Caryophyllia sp.*	east Eq. Atl.	5.62	-26.96	1164	7.62	0.40
JC094-f0093carcs006	*Caryophyllia sp.*	east Eq. Atl.	5.62	-26.96	1164	10.08	0.48
JC094-f0093carcs007	*Caryophyllia sp.*	east Eq. Atl.	5.62	-26.96	1164	61.78	2.40
JC094-f0093carcs008	*Caryophyllia sp.*	east Eq. Atl.	5.62	-26.96	1164	7.33	0.44
JC094-f0093carcs009	*Caryophyllia sp.*	east Eq. Atl.	5.62	-26.96	1164	9.89	0.43
JC094-f0093carcs010	*Caryophyllia sp.*	east Eq. Atl.	5.62	-26.96	1164	6.28	0.37
JC094-f0093carcs011	*Caryophyllia sp.*	east Eq. Atl.	5.62	-26.96	1164	13.22	0.57
JC094-f0093carcs041	*Caryophyllia sp.*	east Eq. Atl.	5.62	-26.96	1164	12.78	0.62
JC094-f0093carns001	*Caryophyllia sp.*	east Eq. Atl.	5.62	-26.96	1164	125.49	6.01
JC094-f0093carns002	*Caryophyllia sp.*	east Eq. Atl.	5.62	-26.96	1164	8.36	0.40
JC094-f0093carns004	*Caryophyllia sp.*	east Eq. Atl.	5.62	-26.96	1164	1.32	0.21
JC094-f0093carps002	*Caryophyllia sp.*	east Eq. Atl.	5.62	-26.96	1164	9.48	0.56
JC094-f0093descm001L	*Desmophyllum dianthus*	east Eq. Atl.	5.62	-26.96	1164	141.65	7.71
JC094-f0093descm002L	*Desmophyllum dianthus*	east Eq. Atl.	5.62	-26.96	1164	17.05	0.78
JC094-f0093descm003L	*Desmophyllum dianthus*	east Eq. Atl.	5.62	-26.96	1164	135.17	7.21

Sample ID	Taxa	Location	Latitude	Longitude	Depth water	Age	2s
JC094-f0093descm004L	*Desmophyllum dianthus*	east Eq. Atl.	5.62	-26.96	1164	67.25	3.09
JC094-f0093desnm001L	*Desmophyllum dianthus*	east Eq. Atl.	5.62	-26.96	1164	131.33	6.88
JC094-f0093desnm002	*Desmophyllum dianthus*	east Eq. Atl.	5.62	-26.96	1164	145.64	6.71
JC094-f0093desnm002L	*Desmophyllum dianthus*	east Eq. Atl.	5.62	-26.96	1164	142.24	7.78
JC094-f0094descm003	*Desmophyllum dianthus*	east Eq. Atl.	5.62	-26.96	1162	134.51	6.37
JC094-f0095carcs002	*Caryophyllia sp.*	east Eq. Atl.	5.62	-26.96	1162	38.45	1.28
JC094-f0095carcs003	*Caryophyllia sp.*	east Eq. Atl.	5.62	-26.96	1162	39.28	1.59
JC094-f0095carcs004	*Caryophyllia sp.*	east Eq. Atl.	5.62	-26.96	1162	64.82	2.39
JC094-f0095carns001	*Caryophyllia sp.*	east Eq. Atl.	5.62	-26.96	1162	11.47	0.73
JC094-f0095carns002	*Caryophyllia sp.*	east Eq. Atl.	5.62	-26.96	1162	2.00	0.26
JC094-f0095carns003	*Caryophyllia sp.*	east Eq. Atl.	5.62	-26.96	1162	20.53	0.78
JC094-f0095carns004	*Caryophyllia sp.*	east Eq. Atl.	5.62	-26.96	1162	1.04	0.26
JC094-f0095carns005	*Caryophyllia sp.*	east Eq. Atl.	5.62	-26.96	1162	5.12	0.40
JC094-f0095carps001	*Caryophyllia sp.*	east Eq. Atl.	5.62	-26.96	1162	145.88	9.42
JC094-f0096carns001	*Caryophyllia sp.*	east Eq. Atl.	5.62	-26.96	1035	16.12	0.88
JC094-f0096carns002	*Caryophyllia sp.*	east Eq. Atl.	5.62	-26.96	1035	3.28	0.42
JC094-f0096carns028	*Caryophyllia sp.*	east Eq. Atl.	5.62	-26.96	1035	36.24	1.52
JC094-f0096carns029	*Caryophyllia sp.*	east Eq. Atl.	5.62	-26.96	1035	4.56	0.32
JC094-f0096carns030	*Caryophyllia sp.*	east Eq. Atl.	5.62	-26.96	1035	5.80	0.43
JC094-f0097carcm001	*Caryophyllia sp.*	east Eq. Atl.	5.59	-26.98	2309	1.26	0.27
CE0806-Dr02A-1-c-s-001	*Solitary Scleractinian*	Reykjanes Ridge	55.7	-35	2022	0.87	0.31
CE0806-Dr02A-2-col-n-s-001	*Colonial Scleractinian*	Reykjanes Ridge	55.7	-35	2022	0.41	0.34
CE0806-Dr02A-4-n-s-001	*Solitary Scleractinian*	Reykjanes Ridge	55.7	-35	2022	0.82	0.20
CE0806-Dr02A-8-col-c-s-001	*Colonial Scleractinian*	Reykjanes Ridge	55.7	-35	2022	0.87	0.24
CE0806-DR04-10	*Solitary Scleractinian*	Reykjanes Ridge	56.3	-34.5	1290	0.29	0.07
CE0806-Dr04-1-c-m-001	*Solitary Scleractinian*	Reykjanes Ridge	56.3	-34.5	1290	0.33	0.14
CE0806-DR04-2	*Solitary Scleractinian*	Reykjanes Ridge	56.3	-34.5	1290	10.59	0.43
CE0806-DR04-3	*Solitary Scleractinian*	Reykjanes Ridge	56.3	-34.5	1290	1.57	0.18
CE0806-Dr04-4-col-c-s-001	*Colonial Scleractinian*	Reykjanes Ridge	56.3	-34.5	1290	12.84	1.02

Sample ID	Taxa	Location	Latitude	Longitude	Depth water	Age	2s
CE0806-Dr04-6-c-m-001	*Solitary Scleractinian*	Reykjanes Ridge	56.3	-34.5	1290	2.27	0.32
CE0806-DR04-7	*Solitary Scleractinian*	Reykjanes Ridge	56.3	-34.5	1290	2.20	0.17
CE0806-Dr09-12-n-l-001	*Solitary Scleractinian*	Reykjanes Ridge	56.8	-34.2	1464	54.99	2.69
CE0806-Dr09-5-col-c-s-001	*Colonial Scleractinian*	Reykjanes Ridge	56.8	-34.2	1464	8.13	0.59
CE0806-Dr09-7-col-c-m-001	*Colonial Scleractinian*	Reykjanes Ridge	56.8	-34.2	1464	10.32	0.62
CE0806-DR14-1	*Solitary Scleractinian*	Reykjanes Ridge	57.7	-33.2	1795	6.73	0.25
CE0806-Dr15-10-col-p-m-001	*Colonial Scleractinian*	Reykjanes Ridge	57.7	-33.2	1361	0.73	0.24
CE0806-DR15-6	*Solitary Scleractinian*	Reykjanes Ridge	57.7	-33.2	1361	9.36	0.41
CE0806-DR15-8	*Solitary Scleractinian*	Reykjanes Ridge	57.7	-33.2	1361	9.35	0.37
CE0806-Dr15-9-col-c-l-001	*Colonial Scleractinian*	Reykjanes Ridge	57.7	-33.2	1361	3.78	0.42
CE0806-DR16-11	*Solitary Scleractinian*	Reykjanes Ridge	57.9	-32.9	1680	10.33	0.51
CE0806-DR16-12	*Solitary Scleractinian*	Reykjanes Ridge	57.9	-32.9	1680	0.36	0.17
CE0806-DR16-14-COL.	*Colonial Scleractinian*	Reykjanes Ridge	57.9	-32.9	1680	0.41	0.10
CE0806-DR16-14-SOL.	*Solitary Scleractinian*	Reykjanes Ridge	57.9	-32.9	1680	0.38	0.14
CE0806-DR16-15	*Solitary Scleractinian*	Reykjanes Ridge	57.9	-32.9	1680	0.92	0.22
CE0806-DR16-16	*Solitary Scleractinian*	Reykjanes Ridge	57.9	-32.9	1680	96.42	3.56
CE0806-Dr16-19-col-n-l-001	*Colonial Scleractinian*	Reykjanes Ridge	57.9	-32.9	1680	3.17	0.35
CE0806-Dr16-20-col-c-m-001	*Colonial Scleractinian*	Reykjanes Ridge	57.9	-32.9	1680	0.45	0.32
CE0806-DR16-22	*Solitary Scleractinian*	Reykjanes Ridge	57.9	-32.9	1680	0.51	0.14
CE0806-DR16-24	*Solitary Scleractinian*	Reykjanes Ridge	57.9	-32.9	1680	0.50	0.08
CE0806-DR16-26	*Solitary Scleractinian*	Reykjanes Ridge	57.9	-32.9	1680	0.23	0.10
CE0806-Dr16-3-c-m-001	*Solitary Scleractinian*	Reykjanes Ridge	57.9	-32.9	1680	0.63	0.50
CE0806-DR16-4	*Solitary Scleractinian*	Reykjanes Ridge	57.9	-32.9	1680	47.13	1.72
CE0806-DR16-6	*Solitary Scleractinian*	Reykjanes Ridge	57.9	-32.9	1680	42.20	1.38
CE0806-DR16-7	*Solitary Scleractinian*	Reykjanes Ridge	57.9	-32.9	1680	0.37	0.18
CE0806-DR16-8-COL.	*Colonial Scleractinian*	Reykjanes Ridge	57.9	-32.9	1680	0.76	0.14
CE0806-DR16-8-SOL.	*Solitary Scleractinian*	Reykjanes Ridge	57.9	-32.9	1680	0.90	0.15
CE0806-Dr17-2-col-c-m-001	*Colonial Scleractinian*	Reykjanes Ridge	58.2	-32.6	1284	13.92	0.73
CE0806-Dr17-3-col-n-m-001	*Colonial Scleractinian*	Reykjanes Ridge	58.2	-32.6	1284	0.55	0.23

Sample ID	Taxa	Location	Latitude	Longitude	Depth water	Age	2s
CE0806-Dr18-10-col-p-m-001	*Colonial Scleractinian*	Reykjanes Ridge	58.5	-32.3	1385	0.86	0.16
CE0806-Dr18-10-col-p-m-002	*Colonial Scleractinian*	Reykjanes Ridge	58.5	-32.3	1385	0.44	0.14
CE0806-DR18-2	*Solitary Scleractinian*	Reykjanes Ridge	58.5	-32.3	1385	73.32	2.62
CE0806-Dr18-4-col-p-l-001	*Colonial Scleractinian*	Reykjanes Ridge	58.5	-32.3	1385	0.25	0.23
CE0806-Dr18-5-col-c-s-001	*Colonial Scleractinian*	Reykjanes Ridge	58.5	-32.3	1385	8.32	0.57
CE0806-DR18-6	*Solitary Scleractinian*	Reykjanes Ridge	58.5	-32.3	1385	79.78	3.47
CE0806-Dr18-9-col-c-s-001	*Colonial Scleractinian*	Reykjanes Ridge	58.5	-32.3	1385	11.67	0.52
CE0806-Dr18A-1-col-p-m-001	*Colonial Scleractinian*	Reykjanes Ridge	58.5	-32.3	1369	0.44	0.08
CE0806-Dr18A-1-col-p-s-001	*Colonial Scleractinian*	Reykjanes Ridge	58.5	-32.3	1369	0.61	0.10
CE0806-DR18A-2	*Solitary Scleractinian*	Reykjanes Ridge	58.5	-32.3	1369	6.45	0.33
CE0806-Dr18A-2-col-c-l-001	*Colonial Scleractinian*	Reykjanes Ridge	58.5	-32.3	1369	6.68	0.39
CE0806-Dr18A-2-col-c-l-002	*Colonial Scleractinian*	Reykjanes Ridge	58.5	-32.3	1369	0.61	0.08
CE0806-Dr18A-4	*Solitary Scleractinian*	Reykjanes Ridge	58.5	-32.3	1369	1.09	0.14
CE0806-DR19-1	*Solitary Scleractinian*	Reykjanes Ridge	58.8	-32	1646	0.45	0.09
CE0806-DR19-1	*Solitary Scleractinian*	Reykjanes Ridge	58.8	-32	1646	0.45	0.17
CE0806-DR19-2	*Solitary Scleractinian*	Reykjanes Ridge	58.8	-32	1646	0.31	0.07
CE0806-DR19-3	*Solitary Scleractinian*	Reykjanes Ridge	58.8	-32	1646	8.89	0.49
CE0806-DR19-4	*Solitary Scleractinian*	Reykjanes Ridge	58.8	-32	1646	0.55	0.11
CE0806-DR19-4	*Solitary Scleractinian*	Reykjanes Ridge	58.8	-32	1646	0.44	0.09
CE0806-DR19A-1	*Solitary Scleractinian*	Reykjanes Ridge	58.8	-32	1545	54.06	1.76
CE0806-DR19A-10	*Solitary Scleractinian*	Reykjanes Ridge	58.8	-32	1545	95.48	3.76
CE0806-DR19A-1COL.	*Colonial Scleractinian*	Reykjanes Ridge	58.8	-32	1545	0.77	0.14
CE0806-Dr19A-1-n-l-001	*Solitary Scleractinian*	Reykjanes Ridge	58.8	-32	1545	0.23	0.09
CE0806-DR19A-4	*Solitary Scleractinian*	Reykjanes Ridge	58.8	-32	1545	74.22	2.70
CE0806-DR19A-5	*Solitary Scleractinian*	Reykjanes Ridge	58.8	-32	1545	75.51	2.66
CE0806-Dr19A-6-col-p-m-001	*Colonial Scleractinian*	Reykjanes Ridge	58.8	-32	1545	0.39	0.10
CE0806-DR19A-7	*Solitary Scleractinian*	Reykjanes Ridge	58.8	-32	1545	4.52	0.25
CE0806-DR19A-7	*Solitary Scleractinian*	Reykjanes Ridge	58.8	-32	1545	0.61	0.20
CE0806-DR19A-9	*Solitary Scleractinian*	Reykjanes Ridge	58.8	-32	1545	0.34	0.12

Sample ID	Taxa	Location	Latitude	Longitude	Depth water	Age	2s
CE0806-Dr19A-9-col-n-m-001	*Colonial Scleractinian*	Reykjanes Ridge	58.8	-32	1545	0.82	0.13
CE0806-Dr19B-04-col-p-m-001	*Solitary Scleractinian*	Reykjanes Ridge	58.8	-32	1429	0.34	0.12
CE0806-DR19B-11	*Solitary Scleractinian*	Reykjanes Ridge	58.8	-32	1429	9.50	0.50
CE0806-DR19B-2	*Solitary Scleractinian*	Reykjanes Ridge	58.8	-32	1429	51.33	1.64
CE0806-DR19B-6	*Solitary Scleractinian*	Reykjanes Ridge	58.8	-32	1429	0.47	0.23
CE0806-DR19B-8	*Solitary Scleractinian*	Reykjanes Ridge	58.8	-32	1429	7.98	0.44
CE0806-DR20-1	*Solitary Scleractinian*	Reykjanes Ridge	59.35	-31.48	1528	0.73	0.17
CE0806-Dr20-1-col-n-m-001	*Colonial Scleractinian*	Reykjanes Ridge	59.35	-31.48	1528	0.44	0.09
CE0806-DR20-2	*Solitary Scleractinian*	Reykjanes Ridge	59.35	-31.48	1528	0.72	0.10
CE0806-DR21A-2	*Solitary Scleractinian*	Reykjanes Ridge	59.35	-31.48	1427	12.38	0.54
CE0806-DR21A-3	*Solitary Scleractinian*	Reykjanes Ridge	59.35	-31.48	1427	8.77	0.47
CE0806-Dr22A-1	*Solitary Scleractinian*	Reykjanes Ridge	60.1	-30.65	1607	7.40	0.37
CE0806-Dr22A-2	*Solitary Scleractinian*	Reykjanes Ridge	60.1	-30.65	1607	0.38	0.08
CE0806-Dr22A-3	*Solitary Scleractinian*	Reykjanes Ridge	60.1	-30.65	1607	0.39	0.17
CE0806-Dr22A-4	*Solitary Scleractinian*	Reykjanes Ridge	60.1	-30.65	1607	1.76	0.19
CE0806-DR24-1	*Solitary Scleractinian*	Reykjanes Ridge	60.1	-30.65	1038	4.21	0.34
CE0806-DR24-1	*Solitary Scleractinian*	Reykjanes Ridge	60.1	-30.65	1038	0.97	0.12
CE0806-DR25-3	*Solitary Scleractinian*	Reykjanes Ridge	60.68	-29.2	1416	0.32	0.09
CE0806-DR25-5	*Solitary Scleractinian*	Reykjanes Ridge	60.68	-29.2	1416	0.44	0.14
CE0806-Dr26-1	*Solitary Scleractinian*	Reykjanes Ridge	60.68	-29.2	1210	49.39	2.24
CE0806-Dr26-2	*Solitary Scleractinian*	Reykjanes Ridge	60.7	-29.4	1210	76.34	3.00
CE0806-DR26-8	*Solitary Scleractinian*	Reykjanes Ridge	60.7	-29.4	1210	48.21	1.64
CE0806-DR26A-3	*Solitary Scleractinian*	Reykjanes Ridge	60.7	-29.4	1142	5.52	0.33
CE0806-DR26A-4	*Solitary Scleractinian*	Reykjanes Ridge	60.7	-29.4	1142	0.22	0.10
CE0806-DR26A-5	*Solitary Scleractinian*	Reykjanes Ridge	60.7	-29.4	1142	5.33	0.38
CE0806-DR26A-6	*Solitary Scleractinian*	Reykjanes Ridge	60.7	-29.4	1142	40.43	1.34
CE0806-Dr26A-7	*Solitary Scleractinian*	Reykjanes Ridge	60.7	-29.4	1142	3.78	0.29
CE0806-Dr26A-8	*Solitary Scleractinian*	Reykjanes Ridge	60.7	-29.4	1142	4.91	0.34
CE0806-DR27-6	*Solitary Scleractinian*	Reykjanes Ridge	61.18	-28.87	1314	2.51	0.31

Sample ID	Taxa	Location	Latitude	Longitude	Depth water	Age	2s
CE0806-DR27-8	*Solitary Scleractinian*	Reykjanes Ridge	61.18	-28.87	1314	5.10	0.32
CE0806-DR28-1	*Solitary Scleractinian*	Reykjanes Ridge	61.18	-28.87	1211	0.42	0.19
CE0806-Dr29-1-n-s-001	*Solitary Scleractinian*	Reykjanes Ridge	61.4	-27.9	994	2.23	0.40
CE0806-Dr29A-1-n-m-001	*Solitary Scleractinian*	Reykjanes Ridge	61.4	-27.9	997	0.35	0.26
CE0806-DR29A-3	*Solitary Scleractinian*	Reykjanes Ridge	61.4	-27.9	997	44.86	1.62
CE0806-DR31-3	*Solitary Scleractinian*	Reykjanes Ridge	61.9	-27	768	0.45	0.09
CE0806-Dr31A-7	*Solitary Scleractinian*	Reykjanes Ridge	61.9	-27	768	0.13	0.09
CE0806-Dr31A-8	*Solitary Scleractinian*	Reykjanes Ridge	61.9	-27	768	0.21	0.10
CE0806-Dr32-1-col-p-s-001	*Colonial Scleractinian*	Reykjanes Ridge	62.1	-26.6	843	0.16	0.09
CE0806-Dr32-2	*Solitary Scleractinian*	Reykjanes Ridge	62.1	-26.6	843	0.11	0.10
CE0806-Dr32-3	*Solitary Scleractinian*	Reykjanes Ridge	62.1	-26.6	843	0.40	0.09
CE0806-Dr9-14-col-n-s-001	*Colonial Scleractinian*	Reykjanes Ridge	56.8	-34.2	1464	2.17	0.74
CE0806-DR9-8	*Solitary Scleractinian*	Reykjanes Ridge	56.8	-34.2	1464	11.26	0.47
JC094-f0015dasnf006	*Dasmosmillia sp.*	east Eq. Atl.	9.24	21.32	265	0.28	0.38
JC094-f0015dasns005	*Dasmosmillia sp.*	east Eq. Atl.	9.24	21.32	265	0.35	0.40
JC094-f0015dasps001	*Dasmosmillia sp.*	east Eq. Atl.	9.24	21.32	265	0.41	0.59
JC094-f0044carps001	*Caryophyllia sp.*	east Eq. Atl.	9.21	21.3	1345	0.11	0.16
JC094-f0046carpm003	*Caryophyllia sp.*	east Eq. Atl.	9.21	21.3	1326	0.13	0.17
JC094-f0046carpm004	*Caryophyllia sp.*	east Eq. Atl.	9.21	21.3	1326	0.11	0.30
JC094-f0052carcs016	*Caryophyllia sp.*	east Eq. Atl.	9.22	21.31	973	0.12	0.23
JC094-f0052carps001	*Caryophyllia sp.*	east Eq. Atl.	9.22	21.31	973	0.13	0.29
JC094-f0059carns001	*Caryophyllia sp.*	east Eq. Atl.	9.21	21.3	1354	0.03	0.22
JC094-f0062carpm002	*Caryophyllia sp.*	east Eq. Atl.	5.6	26.96	1853	0.17	0.42
JC094-f0076carcs006	*Caryophyllia sp.*	east Eq. Atl.	5.63	26.95	845	0.10	0.35
JC094-f0079carcs007	*Caryophyllia sp.*	east Eq. Atl.	5.63	26.95	749	0.47	0.44
JC094-f0095carps002	*Caryophyllia sp.*	east Eq. Atl.	5.62	26.96	1162	0.06	0.20
CE0806-Dr02A-9-n-l-001	*Solitary Scleractinian*	Reykjanes Ridge	55.7	-35	2022	0.17	0.21
CE0806-Dr04A-1-n-m-001	*Solitary Scleractinian*	Reykjanes Ridge	56.3	-34.5	1290	0.21	0.24
CE0806-Dr09-3-p-s-001	*Solitary Scleractinian*	Reykjanes Ridge	56.8	-34.2	1464	0.01	0.14

Sample ID	Taxa	Location	Latitude	Longitude	Depth water	Age	2s
CE0806-DR16-16	*Solitary Scleractinian*	Reykjanes Ridge	57.9	-32.9	1680	166.81	8.28
CE0806-Dr16-20-col-n-5-001	*Colonial Scleractinian*	Reykjanes Ridge	57.9	-32.9	1680	0.19	0.33
CE0806-Dr17-4-col-p-s-001	*Colonial Scleractinian*	Reykjanes Ridge	58.2	-32.6	1284	0.12	0.22
CE0806-Dr18-10-col-p-m-001	*Colonial Scleractinian*	Reykjanes Ridge	58.5	-32.3	1385	30.41	75.95
CE0806-Dr18-10-col-p-m-002	*Colonial Scleractinian*	Reykjanes Ridge	58.5	-32.3	1385	41.58	107.23
CE0806-Dr18-9-col-c-s-001	*Colonial Scleractinian*	Reykjanes Ridge	58.5	-32.3	1385	12.08	46.39
CE0806-Dr18A-1-col-p-m-001	*Colonial Scleractinian*	Reykjanes Ridge	58.5	-32.3	1369	37.14	145.31
CE0806-Dr18A-2-col-c-l-001	*Colonial Scleractinian*	Reykjanes Ridge	58.5	-32.3	1369	25.87	199.41
CE0806-Dr18A-2-col-c-l-002	*Colonial Scleractinian*	Reykjanes Ridge	58.5	-32.3	1369	41.37	107.12
CE0806-DR19-1	*Solitary Scleractinian*	Reykjanes Ridge	58.8	-32	1646	0.45	0.09
CE0806-DR19-4	*Solitary Scleractinian*	Reykjanes Ridge	58.8	-32	1646	0.55	0.11
CE0806-DR19A-2	*Solitary Scleractinian*	Reykjanes Ridge	58.8	-32	1545	0.15	0.19
CE0806-DR19A-7	*Solitary Scleractinian*	Reykjanes Ridge	58.8	-32	1545	0.61	0.20
CE0806-Dr19A-9-col-n-m-001	*Colonial Scleractinian*	Reykjanes Ridge	58.8	-32	1545	4.61	18.65
CE0806-Dr20-1-col-n-m-001	*Colonial Scleractinian*	Reykjanes Ridge	59.35	-31.48	1528	17.12	64.95
CE0806-Dr22A-5	*Solitary Scleractinian*	Reykjanes Ridge	60.1	-30.65	1607	9.88	4.60
CE0806-DR24-1	*Solitary Scleractinian*	Reykjanes Ridge	60.1	-30.65	1038	4.21	0.34
CE0806-Dr24-3	*Solitary Scleractinian*	Reykjanes Ridge	60.1	-30.65	1038	80.07	44.20
CE0806-Dr24-4	*Solitary Scleractinian*	Reykjanes Ridge	60.1	-30.65	1038	18.46	3.57
CE0806-Dr25-02-col-p-s-001	*Colonial Scleractinian*	Reykjanes Ridge	60.68	-29.2	1416	40.27	14.91
CE0806-Dr25-10-col-p-s-001	*Colonial Scleractinian*	Reykjanes Ridge	60.68	-29.2	1416	17.85	6.10
CE0806-DR25-4	*Solitary Scleractinian*	Reykjanes Ridge	60.68	-29.2	1416	188.75	12.67
CE0806-Dr26-4	*Solitary Scleractinian*	Reykjanes Ridge	60.7	-29.4	1210	22.57	4.29
CE0806-Dr26-6	*Solitary Scleractinian*	Reykjanes Ridge	60.7	-29.4	1210	26.06	3.89
CE0806-DR-27-4	*Solitary Scleractinian*	Reykjanes Ridge	61.18	-28.87	1314	1.70	0.20
CE0806-Dr30A-1	*Solitary Scleractinian*	Reykjanes Ridge	61.9	-27	944	19.02	2.38
CE0806-Dr32A3-c-l-001	*Solitary Scleractinian*	Reykjanes Ridge	62.1	-26.6	843	0.69	0.72
CE0806-Dr9-10-col-c-s-001	*Colonial Scleractinian*	Reykjanes Ridge	56.8	-34.2	1464	11.20	9.19

Table S2: Uranium series dated cold-water corals from Tropic Seamount, Reykjanes Ridge, and seamounts of the east Equatorial Atlantic. Ages are reported in years before present (BP; where present is the year of 1950 CE) both uncorrected and corrected for initial 232Th. Greyed out samples did not pass our quality control. Selection code column indicates samples not included on age distribution discussion: [238U] <2 ppm (Low U), [232Th] >6 ppb (High Th), [δ234Ui] >157‰ (High δU) and lowest quality sub-sample (duplicate).

Location	Full Sample ID	Depth	Age uncorr	2s	Age corr	2s	$\delta^{234}U$ m	2s	$\delta^{234}Ui$	2s	^{238}U	2s	^{232}Th	2s	$^{230}Th/^{238}U$	2s	Selection code
		m	ka BP		ka BP		‰		‰		ppm		ppb		activity ratio		
Tropic Seamount	JC142-009-011-cl-001	1027	20.42	0.11	20.349	0.127	140.9	1.0	149.3	1.1	3.908	0.008	0.583	0.003	0.196	0.001	
Tropic Seamount	JC142-009-011-cm-001	1027	24.28	0.15	23.892	0.416	135.9	1.1	145.5	1.2	4.035	0.009	3.374	0.016	0.228	0.001	
Tropic Seamount	JC142-009-011-cm-001	1027	24.19	0.16	23.786	0.429	136.0	1.0	145.7	1.0	3.991	0.010	3.453	0.015	0.227	0.001	duplicate
Tropic Seamount	JC142-009-011-n-col-001	1027	22.20	0.14	22.005	0.239	136.4	1.0	145.1	1.1	4.245	0.009	1.801	0.008	0.210	0.001	
Tropic Seamount	JC142-047-002-c-col-001	994	142.10	1.72	142.04	1.72	105.7	1.0	158.0	1.5	4.191	0.010	0.572	0.003	0.819	0.005	
Tropic Seamount	JC142-047-003-c-col-001	994	148.67	1.46	148.445	1.48	111.0	1.0	169.0	1.5	3.926	0.007	1.959	0.008	0.842	0.004	High δU
Tropic Seamount	JC142-047-003-pl-001	994	148.47	1.47	148.417	1.469	104.7	1.0	159.3	1.5	4.580	0.009	0.556	0.002	0.836	0.004	
Tropic Seamount	JC142-047-006-c-col-001	995	32.07	0.24	30.529	1.571	133.3	1.0	146.0	1.1	5.066	0.013	16.812	0.075	0.290	0.002	High Th
Tropic Seamount	JC142-047-006-c-col-001	995	31.34	0.18	30.363	1.006	134.1	1.0	146.1	1.1	5.315	0.012	11.227	0.048	0.285	0.001	High Th
Tropic Seamount	JC142-047-006-c-col-001	995	31.11	0.26	30.039	1.106	132.6	1.1	144.4	1.3	5.627	0.014	13.010	0.056	0.283	0.002	High Th
Tropic Seamount	JC142-047-006-cl-001	995	32.61	0.22	31.889	0.75	131.7	1.0	144.1	1.2	5.189	0.012	8.023	0.035	0.294	0.002	High Th
Tropic Seamount	JC142-047-006-cl-001	995	32.84	0.25	31.746	1.125	133.5	1.1	146.0	1.2	4.693	0.010	11.066	0.048	0.297	0.002	High Th
Tropic Seamount	JC142-047-006-cl-001A	995	29.95	0.19	29.604	0.391	134.7	1.0	146.4	1.1	4.509	0.010	3.342	0.014	0.274	0.001	

Location	Full Sample ID	Depth	Age uncorr	2s	Age corr	2s	$\delta^{234}U$ m	2s	$\delta^{234}Ui$	2s	^{238}U	2s	^{232}Th	2s	$^{230}Th/^{238}U$	2s	Selection code
Tropic Seamount	JC142-047-006-cl-002	995	29.17	0.22	29.132	0.22	135.4	1.0	147.0	1.1	4.453	0.010	0.317	0.001	0.268	0.002	
Tropic Seamount	JC142-047-006-cm-001	995	30.47	0.18	30.208	0.321	136.4	1.0	148.6	1.1	4.687	0.010	2.690	0.012	0.279	0.001	
Tropic Seamount	JC142-047-006-cm-002	995	30.23	0.20	30.085	0.244	133.8	1.0	145.7	1.0	4.096	0.010	1.258	0.006	0.276	0.002	
Tropic Seamount	JC142-047-006-cm-003	995	29.93	0.18	29.744	0.262	134.8	1.0	146.7	1.1	4.393	0.010	1.794	0.008	0.274	0.001	
Tropic Seamount	JC142-047-006-nl-001	995	29.28	0.23	29.234	0.23	135.1	1.0	146.8	1.1	4.670	0.011	0.505	0.002	0.269	0.002	
Tropic Seamount	JC142-047-006-nl-002	995	29.85	0.21	29.548	0.368	133.6	1.0	145.3	1.1	3.597	0.009	2.359	0.010	0.273	0.002	
Tropic Seamount	JC142-058-039-cm-001	970	13.78	0.08	13.734	0.087	144.4	1.0	150.1	1.0	3.712	0.009	0.332	0.002	0.137	0.001	
Tropic Seamount	JC142-100-003B-n-col-001	1406	83.10	0.60	82.939	0.623	119.9	1.0	151.6	1.3	4.234	0.009	1.477	0.006	0.604	0.003	
Tropic Seamount	JC142-100-003C-cl-001	1406	18.38	0.13	18.243	0.192	142.1	1.0	149.7	1.0	3.233	0.008	0.989	0.004	0.178	0.001	duplicate
Tropic Seamount	JC142-100-003C-cl-001	1406	18.37	0.11	18.227	0.176	142.8	1.1	150.4	1.1	3.235	0.008	0.987	0.005	0.178	0.001	
Tropic Seamount	JC142-100-003C-cm-001	1406	15.35	0.10	14.855	0.506	144.3	1.1	150.5	1.2	3.638	0.008	3.904	0.017	0.151	0.001	
Tropic Seamount	JC142-100-003C-cm-001	1406	16.24	0.13	15.384	0.871	143.8	1.0	150.2	1.1	3.724	0.009	6.927	0.031	0.159	0.001	High Th
Tropic Seamount	JC142-113-007-cl-001	1797	32.35	0.27	31.91	0.519	134.9	1.0	147.7	1.1	3.391	0.007	3.232	0.014	0.293	0.002	
Tropic Seamount	JC142-113-007-cl-002	1797	32.43	0.29	32.05	0.478	129.6	1.0	141.9	1.1	3.824	0.010	3.138	0.014	0.292	0.002	
Tropic Seamount	JC142-113-007-cl-002	1797	32.27	0.19	31.692	0.61	131.4	1.0	144.0	1.0	3.666	0.008	4.559	0.020	0.292	0.001	duplicate
Tropic Seamount	JC142-113-007-cs-001	1797	33.10	0.27	32.624	0.546	130.0	1.0	142.5	1.2	3.296	0.007	3.380	0.014	0.298	0.002	
Tropic Seamount	JC142-113-007-cs-002	1797	32.67	0.18	32.221	0.485	138.5	1.0	151.8	1.1	3.080	0.006	3.014	0.012	0.297	0.001	
Tropic Seamount	JC142-113-015-c-col-001	1464	22.25	0.15	20.578	1.676	138.5	1.0	146.9	1.2	1.644	0.004	5.875	0.026	0.211	0.001	Low U

Location	Full Sample ID	Depth	Age uncorr	2s	Age corr	2s	$\delta^{234}U$ m	2s	$\delta^{234}Ui$	2s	^{238}U	2s	^{232}Th	2s	$^{230}Th/^{238}U$	2s	Selection code
Tropic Seamount	JC142-113-015-c-col-001	1464	17.01	0.13	16.593	0.443	147.0	1.5	154.1	1.6	0.293	0.001	0.269	0.001	0.167	0.001	Low U
Tropic Seamount	JC142-113-015-cl-001	1464	19.49	0.11	19.415	0.132	137.6	1.0	145.5	1.0	3.738	0.009	0.571	0.003	0.187	0.001	
Tropic Seamount	JC142-113-015-cl-002	1464	19.21	0.11	19.114	0.141	141.5	0.9	149.4	1.0	3.266	0.008	0.663	0.003	0.185	0.001	
Tropic Seamount	JC142-113-015-cl-003	1464	19.21	0.12	19.098	0.166	138.9	1.0	146.6	1.1	3.411	0.008	0.851	0.004	0.185	0.001	
Tropic Seamount	JC142-113-015-cl-003	1464	19.17	0.14	19.056	0.18	138.5	1.0	146.3	1.0	3.409	0.008	0.861	0.004	0.185	0.001	duplicate
Tropic Seamount	JC142-113-015-cl-004	1464	19.67	0.11	19.491	0.209	140.8	1.0	148.8	1.0	3.225	0.007	1.243	0.006	0.189	0.001	
Tropic Seamount	JC142-113-015-cl-005	1464	19.73	0.11	19.531	0.23	137.9	1.0	145.8	1.0	3.763	0.009	1.661	0.007	0.189	0.001	
Tropic Seamount	JC142-113-015-cl-006	1464	19.51	0.11	19.41	0.146	142.5	1.1	150.6	1.1	3.310	0.008	0.687	0.003	0.188	0.001	
Tropic Seamount	JC142-113-015-cl-006	1464	19.41	0.11	19.261	0.179	136.9	1.0	144.7	1.0	3.547	0.008	1.095	0.005	0.186	0.001	duplicate
Tropic Seamount	JC142-113-015-cl-007	1464	19.54	0.13	19.428	0.172	137.4	1.0	145.2	1.0	3.623	0.008	0.898	0.004	0.188	0.001	
Tropic Seamount	JC142-58-041-n-col-001	970	0.213	0.003	0.127	0.085	145.6	1.0	145.7	1.0	4.473	0.010	0.825	0.004	0.003	0	
Tropic Seamount	JC142-58-041-n-col-001	970	0.488	0.004	0.265	0.224	145.9	1.1	146.0	1.1	3.930	0.007	1.896	0.008	0.006	0	duplicate
Tropic Seamount	JC142-58-041-n-col-001	970	1.81	0.02	0.741	1.072	145.0	1.2	145.8	1.2	0.533	0.001	1.223	0.005	0.019	0	Low U
Tropic Seamount	JC142-58-041-n-col-001	970	-0.01	0.09	non determined		140.9	3.5	140.5	3.5	0.041	0.000	0.014	0.001	-0.009	0.004	Low U
Tropic Seamount	JC142-58-041-n-col-001	970	1.58	0.03	0.47	1.11	146.9	1.1	147.1	1.2	0.320	0.001	0.766	0.003	0.017	0	Low U
Tropic Seamount	JC142-58-042-cs-001	970	13.12	0.07	12.76	0.36	142.9	1.0	148.3	1.0	3.522	0.008	2.727	0.012	0.130	0.001	
Tropic Seamount	JC142-58-042-cs-001	970	13.76	0.09	12.90	0.86	142.8	1.0	148.2	1.1	3.773	0.009	6.941	0.032	0.136	0.001	High Th

Location	Full Sample ID	Depth	Age uncorr	2s	Age corr	2s	$\delta^{234}U$ m	2s	$\delta^{234}Ui$	2s	^{238}U	2s	^{232}Th	2s	$^{230}Th/^{238}U$	2s	Selection code
Tropic Seamount	JC142-58-042-cs-001	970	13.68	0.10	13.31	0.38	143.3	1.1	148.8	1.2	3.375	0.007	2.713	0.011	0.136	0.001	duplicate
Tropic Seamount	JC142-61-011-cm-001	1223	13.11	0.08	12.99	0.15	144.6	1.0	150.1	1.0	3.905	0.009	1.055	0.005	0.130	0.001	
Tropic Seamount	JC142-61-011-cm-002	1223	13.81	0.09	13.38	0.44	147.4	1.0	153.2	1.1	3.562	0.008	3.305	0.016	0.137	0.001	
Tropic Seamount	JC142-61-011-cm-002	1223	13.85	0.08	13.28	0.58	146.3	1.0	152.1	1.0	3.639	0.009	4.498	0.020	0.138	0.001	duplicate
Tropic Seamount	JC142-61-011-cm-003	1223	13.28	0.10	13.06	0.24	145.0	1.1	150.5	1.1	3.494	0.007	1.679	0.007	0.132	0.001	
Tropic Seamount	JC142-61-011-cm-004	1223	17.49	0.13	13.64	3.92	147.6	1.0	153.4	2.0	0.626	0.001	5.147	0.022	0.171	0.001	Low U
Tropic Seamount	JC142-61-011-n-col-001	1223	19.93	0.14	19.71	0.26	139.9	1.0	148.0	1.0	3.344	0.007	1.605	0.007	0.191	0.001	
Tropic Seamount	JC142-61-011-n-col-002	1223	19.82	0.11	19.62	0.23	139.0	0.9	147.1	1.0	3.267	0.008	1.444	0.007	0.190	0.001	
Tropic Seamount	JC142-61-012-n-col-001	1193	0.315	0.004	0.21	0.10	146.2	1.0	146.4	1.0	4.079	0.010	0.909	0.004	0.004	0	
Tropic Seamount	JC142-ROV320-cm-001	1780	56.72	0.35	56.55	0.39	121.0	1.1	141.9	1.2	4.496	0.009	1.702	0.007	0.458	0.002	
Tropic Seamount	JC142-113-ROV320-c-col-001	1464	48.07	0.30	47.44	0.70	173.5	1.0	198.4	1.2	0.998	0.002	1.433	0.006	0.422	0.002	Low U
Reykjanes Ridge	CE0806-Dr04-3	1290	0.199	0.002	0.07	0.06	147.8	1.1	147.8	1.1	4.169	0.012	0.516	0.002	0.002	0	
Reykjanes Ridge	CE0806-Dr15-1	1361	69.67	0.41	69.33	0.41	120.0	0.6	146.1	0.9	3.408	0.011	0.686	0.002	0.534	0.002	
Reykjanes Ridge	CE0806-Dr15-3	1361	69.61	0.40	69.16	0.40	129.9	0.6	158.1	1.0	3.058	0.010	0.851	0.003	0.538	0.0019	High δU
Reykjanes Ridge	CE0806-Dr15-6a	1361	9.28	0.05	9.10	0.12	146.3	1.1	150.2	1.1	4.164	0.015	1.039	0.002	0.094	0.0005	
Reykjanes Ridge	CE0806-Dr15-8	1361	9.16	0.05	9.00	0.10	146.4	1.1	150.2	1.1	4.660	0.016	0.857	0.002	0.092	0.0004	
Reykjanes Ridge	CE0806-Dr16-1	1680	73.83	0.43	73.59	0.44	115.2	0.5	141.8	0.9	4.636	0.015	0.593	0.002	0.554	0.002	

Location	Full Sample ID	Depth	Age uncorr	2s	Age corr	2s	$\delta^{234}U$ m	2s	$\delta^{234}Ui$	2s	^{238}U	2s	^{232}Th	2s	$^{230}Th/^{238}U$	2s	Selection code
Reykjanes Ridge	CE0806-Dr16-5	1680	36.71	0.19	36.41	0.20	127.4	0.7	141.3	0.9	4.021	0.015	0.696	0.002	0.324	0.0013	
Reykjanes Ridge	CE0806-Dr16-5b	1680	36.35	0.18	35.76	0.20	128.9	0.6	142.8	0.9	3.358	0.011	1.262	0.004	0.322	0.0012	
Reykjanes Ridge	CE0806-Dr16-5b	1680	36.44	0.19	35.83	0.21	126.7	0.6	140.4	0.9	3.158	0.011	1.232	0.004	0.322	0.0012	
Reykjanes Ridge	CE0806-Dr18-1	1385	109.96	0.79	109.67	0.80	107.4	0.5	146.5	1.0	5.031	0.017	0.808	0.003	0.713	0.0027	
Reykjanes Ridge	CE0806-Dr18A-2	1369	5.95	0.03	5.84	0.06	146.8	1.0	149.3	1.1	2.969	0.010	0.332	0.006	0.061	0.0003	
Reykjanes Ridge	CE0806-Dr18A-4	1369	1.09	0.01	0.95	0.07	147.4	1.0	147.8	1.0	4.443	0.011	0.629	0.003	0.011	0.0001	
Reykjanes Ridge	CE0806-Dr19A-3	1545	72.65	0.42	71.84	0.44	123.5	0.6	151.5	1.1	3.170	0.010	1.683	0.006	0.552	0.002	
Reykjanes Ridge	CE0806-Dr19B-11a	1429	51.29	0.30	51.18	0.31	130.1	1.1	150.4	1.2	3.633	0.016	0.299	0.002	0.427	0.0019	
Reykjanes Ridge	CE0806-Dr19B-5	1429	9.33	0.04	8.96	0.07	143.9	0.7	147.7	0.8	3.731	0.012	0.810	0.003	0.094	0.0004	
Reykjanes Ridge	CE0806-Dr19B-8	1429	8.00	0.04	7.88	0.07	145.5	1.1	148.8	1.1	3.822	0.010	0.438	0.002	0.081	0.0004	
Reykjanes Ridge	CE0806-Dr20-01	1528	0.38	0.02	0.22	0.09	146.6	1.0	146.7	1.0	4.005	0.011	0.802	0.002	0.004	0.0002	
Reykjanes Ridge	CE0806-Dr21A-2a	1427	10.92	0.06	10.78	0.09	145.5	1.1	150.0	1.1	3.852	0.012	0.592	0.002	0.109	0.0005	
Reykjanes Ridge	CE0806-Dr21A-3a	1427	8.73	0.04	8.62	0.07	144.4	1.1	148.0	1.1	3.725	0.015	0.380	0.002	0.088	0.0004	
Reykjanes Ridge	CE0806-Dr25-10	1416	14.51	0.10	14.41	0.10	147.9	2.6	154.1	2.7	2.063	0.016	0.126	0.002	0.143	0.0008	
Reykjanes Ridge	CE0806-Dr25-3	1416	0.184	0.002	0.04	0.08	147.2	1.1	147.2	1.1	3.224	0.015	0.553	0.001	0.002	0	
Reykjanes Ridge	CE0806-Dr25-5	1416	0.189	0.002	0.01	0.11	146.9	1.0	146.9	1.0	2.767	0.016	0.652	0.003	0.002	0	
Reykjanes Ridge	CE0806-Dr25-7	1416	14.58	0.08	14.51	0.08	142.6	1.0	148.6	1.0	4.699	0.010	0.061	0.002	0.143	0.0007	
Reykjanes Ridge	CE0806-Dr25-7	1416	14.51	0.07	14.37	0.07	144.1	0.7	150.2	0.7	4.458	0.015	0.224	0.002	0.143	0.0005	

Location	Full Sample ID	Depth	Age uncorr	2s	Age corr	2s	$\delta^{234}U$ m	2s	$\delta^{234}Ui$	2s	^{238}U	2s	^{232}Th	2s	$^{230}Th/^{238}U$	2s	Selection code
Reykjanes Ridge	CE0806-Dr26A-1	1142	4.53	0.02	4.42	0.03	144.4	0.7	146.3	0.8	4.730	0.016	0.502	0.002	0.047	0.0002	
Reykjanes Ridge	CE0806-Dr27-3	1314	4.39	0.02	4.24	0.05	150.1	0.7	152.0	0.8	3.221	0.010	0.570	0.002	0.045	0.0002	
Reykjanes Ridge	CE0806-Dr27-4	1314	0.552	0.003	0.43	0.03	146.8	0.7	147.0	0.8	3.441	0.011	0.478	0.002	0.006	0	
Reykjanes Ridge	CE0806-Dr27-6	1314	2.24	0.01	2.16	0.02	148.3	1.1	149.2	1.1	2.736	0.011	0.080	0.002	0.023	0.0001	
Reykjanes Ridge	CE0806-Dr27-8	1314	4.30	0.02	4.20	0.04	146.5	1.0	148.3	1.0	3.190	0.011	0.208	0.002	0.044	0.0002	
Reykjanes Ridge	CE0806-Dr29-2	994	1.15	0.01	1.06	0.02	147.1	0.8	147.5	0.8	4.082	0.015	0.255	0.001	0.012	0.0001	
Reykjanes Ridge	CE0806-Dr29-3	994	14.59	0.10	14.49	0.11	143.7	0.7	149.7	0.8	4.350	0.016	0.099	0.063	0.143	0.0008	
Reykjanes Ridge	CE0806-Dr29A-2	997	43.29	0.22	42.06	0.29	126.9	0.6	143.3	1.2	4.686	0.015	3.864	0.013	0.371	0.0013	
Reykjanes Ridge	CE0806-Dr31A-1	768	9.87	0.05	9.39	0.08	144.3	0.7	148.3	0.9	3.267	0.011	0.965	0.003	0.099	0.0004	
Reykjanes Ridge	CE0806-Dr31A-2	768	0.034	0.001	0.000	0.008	148.5	0.7	148.5	0.7	3.775	0.012	0.125	0.001	0.000	0	
east Equatorial Atlantic	JC094-f0001carcs016	1080	15.44	0.08	15.16	0.23	143.8	1.4	150.1	1.4	4.330	0.010	2.011	0.009	0.151	0.001	
east Equatorial Atlantic	JC094-f0001carcs017	1080	7.37	0.05	6.03	1.28	145.9	1.0	148.4	1.1	3.918	0.008	10.754	0.045	0.075	0.001	High Th
east Equatorial Atlantic	JC094-f0001carcs018	1080	3.36	0.02	2.81	0.48	147.7	1.1	148.9	1.1	3.712	0.008	3.862	0.017	0.035	0.001	
east Equatorial Atlantic	JC094-f0001carcs027	1080	12.79	0.07	12.43	0.30	142.3	1.4	147.4	1.4	4.883	0.010	3.156	0.013	0.127	0.001	
east Equatorial Atlantic	JC094-f0001carcs028	1080	2.52	0.01	2.15	0.30	146.9	1.0	147.9	1.0	4.118	0.009	2.666	0.012	0.026	0.001	

Location	Full Sample ID	Depth	Age uncorr	2s	Age corr	2s	$\delta^{234}U$ m	2s	$\delta^{234}Ui$	2s	^{238}U	2s	^{232}Th	2s	$^{230}Th/^{238}U$	2s	Selection code
east Equatorial Atlantic	JC094-f0001carcs045	1080	3.91	0.02	3.59	0.26	146.9	1.0	148.4	1.1	5.090	0.011	2.873	0.012	0.040	0.001	
east Equatorial Atlantic	JC094-f0001carcs050	1080	13.00	0.10	12.65	0.30	143.2	1.0	148.4	1.1	4.925	0.010	3.007	0.013	0.129	0.001	
east Equatorial Atlantic	JC094-f0001carcs060	1080	4.01	0.03	3.80	0.16	146.5	1.0	148.1	1.1	4.879	0.010	1.639	0.007	0.041	0.001	
east Equatorial Atlantic	JC094-f0001carcs064	1080	3.70	0.02	3.48	0.16	146.1	1.3	147.5	1.3	4.834	0.012	1.693	0.007	0.038	0.001	
east Equatorial Atlantic	JC094-f0001carns0001L	1080	1.85	0.01	1.07	0.79	147.2	1.0	147.6	1.1	4.093	0.009	6.914	0.029	0.019	0.001	High Th
east Equatorial Atlantic	JC094-f0053carcsm022	800	25.56	0.17	25.31	0.26	132.8	1.1	142.6	1.2	4.105	0.009	1.680	0.007	0.237	0.001	
east Equatorial Atlantic	JC094-f0057carcm007	746	25.89	0.17	25.61	0.28	133.4	1.0	143.5	1.1	3.771	0.009	1.738	0.007	0.240	0.001	
east Equatorial Atlantic	JC094-f0065carcs004	1574	24.11	0.25	23.70	0.42	130.8	1.2	139.9	1.4	4.752	0.018	3.440	0.028	0.225	0.001	
east Equatorial Atlantic	JC094-f0074descm001	997	17.91	0.14	15.89	1.97	141.0	1.2	147.5	2.1	4.350	0.013	18.141	0.116	0.173	0.001	High Th
east Equatorial Atlantic	JC094-f0075carcs001	915	2.75	0.02	2.14	0.55	146.5	1.1	147.4	1.1	4.946	0.011	5.902	0.025	0.029	0.001	
east Equatorial Atlantic	JC094-f0079carcs003	749	2.28	0.02	1.29	0.93	146.5	1.4	147.0	1.4	4.737	0.011	9.427	0.044	0.024	0.001	High Th
east Equatorial Atlantic	JC094-f0093carcs004	1164	1.20	0.01	0.94	0.20	148.4	1.1	148.8	1.1	3.995	0.008	1.692	0.007	0.013	0.001	

Location	Full Sample ID	Depth	Age uncorr	2s	Age corr	2s	$\delta^{234}U$ m	2s	$\delta^{234}Ui$	2s	^{238}U	2s	^{232}Th	2s	$^{230}Th/^{238}U$	2s	Selection code
east Equatorial Atlantic	JC094-f0093carcs005	1164	13.45	0.07	13.23	0.16	141.7	1.3	147.2	1.4	4.493	0.010	1.448	0.006	0.133	0.001	
east Equatorial Atlantic	JC094-f0093carcs006	1164	9.61	0.08	9.42	0.15	144.7	1.1	148.7	1.1	4.991	0.010	1.388	0.007	0.097	0.001	
east Equatorial Atlantic	JC094-f0093carcs041	1164	12.22	0.08	12.02	0.15	142.6	1.1	147.6	1.2	3.726	0.008	1.035	0.005	0.121	0.001	
east Equatorial Atlantic	JC094-f0095carns001	1162	12.25	0.08	11.98	0.23	144.4	1.0	149.4	1.0	3.969	0.008	1.810	0.008	0.122	0.001	
east Equatorial Atlantic	JC094-f0096carns001	1035	16.36	0.09	15.85	0.46	143.4	1.2	150.0	1.3	5.740	0.016	5.599	0.022	0.160	0.001	

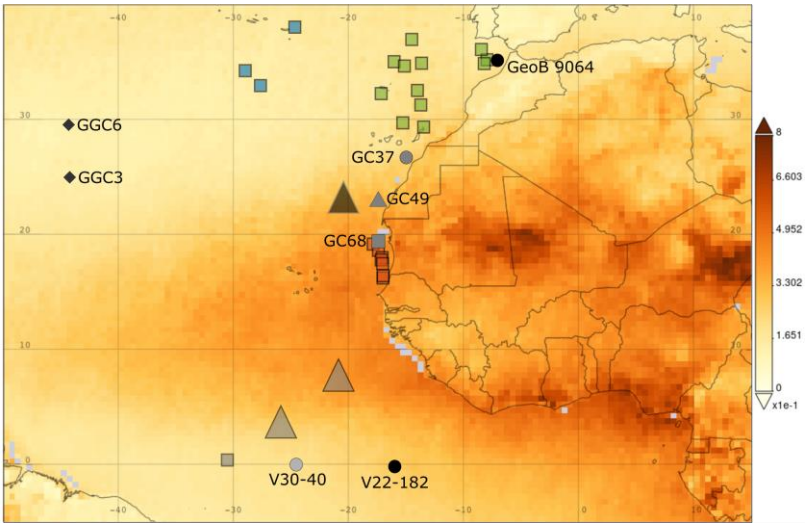

Figure S1: Map of sediment core and cold-water coral sites (published coral data indicated by squares, new coral data by triangles, and diamonds for sediment cores see Figure 1 for details) discussed in the text and Figure 5 and satellite aerosol optical depth 555 nm for 2013 to 2017 (from MISR satellite, daily and 0.5° resolution at https://giovanni.gsfc.nasa.gov). Darker colours indicate larger amounts of aerosols interpreted as dust emission. Sediment cores for dust flux: OC437-7 GC68, GC49, GC37 (McGee et al., 2013), KN207-2 GGC3, GGC6 (Middleton et al., 2018); productivity index: GeoB 9064 (Wienberg et al., 2010); opal flux: V22-182, V30-40 (Bradtmiller et al., 2007).

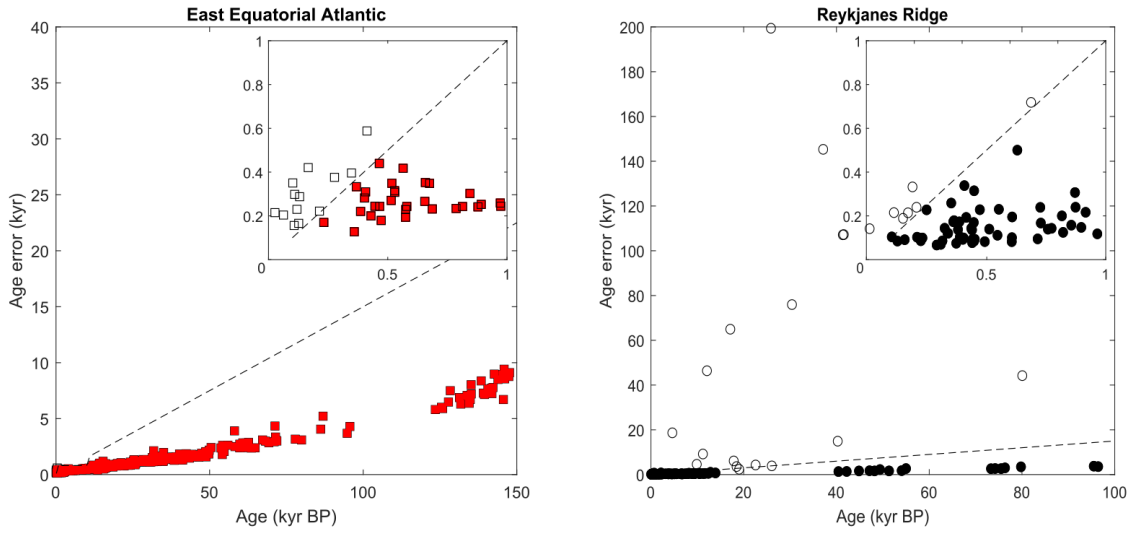

Figure S2: New U-series laser ablation ages of cold-water corals from east Equatorial Atlantic (left) and Reykjanes Ridge (right), please note both charts are in different scales. Dashed line correspond to the projected uncertainty from the method, it was interpolated using uncertainties of 0.8 kyr, 1.5 kyr and 15 kyr at 10 kyr BP, 20 kyr BP and 125 kyr BP (Spooner et al., 2016). Insert charts show ages younger than 1 kyr BP but in this case, dashed line corresponds to 100% error on the age, thus all samples above the dashed line show uncertainty higher than the age itself. Filled symbols have an analytical error lower that the projected uncertainty so they are included at the compilation. Hollow symbols are not included.

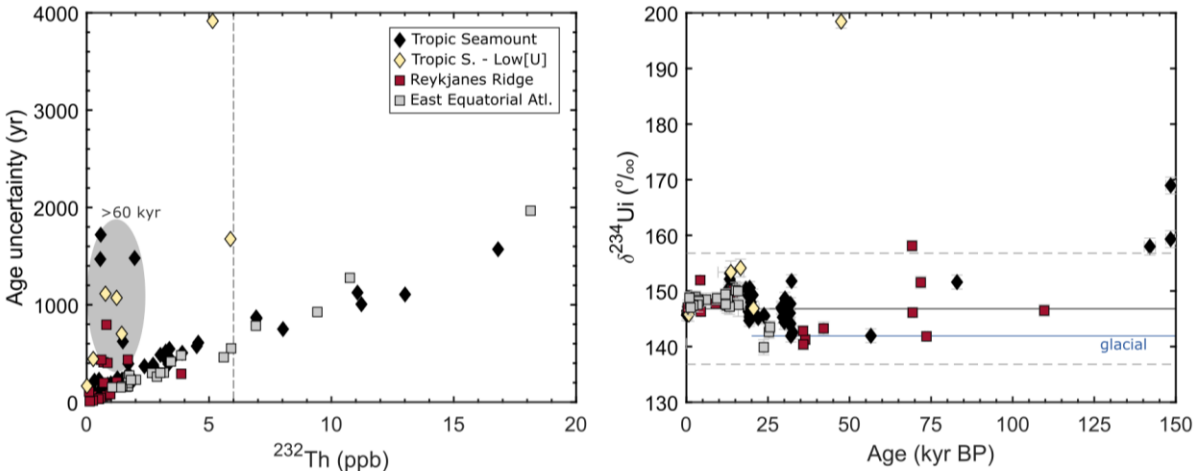

Figure S3: U-series isotope dilution data from Tropic Seamount (diamonds), Reykjanes Ridge (red squares) and east Equatorial Atlantic (grey squares). Tropic Seamount samples with ^{238}U concentration lower than 3 ppm are indicated by yellow diamonds. Left: age uncertainty against ^{232}Th concentration. As expected a positive trend is observed, excluding samples with low ^{238}U concentration (yellow diamonds) and samples older than 60 kyr BP (grey ellipse). Dashed line indicates the cut-off value of ^{232}Th (6 ppb, see text for details). Right: initial $\delta^{234}U$ against corrected age. Age uncertainties are ±2s. Black line indicates modern seawater $\delta^{234}U_i$ (146.8‰; Andersen et al., 2010), dashed grey lines indicate ±10‰ range about this modern value, and blue line indicates $\delta^{234}U_i$ prior 17 kyr BP (Chen et al., 2016a).

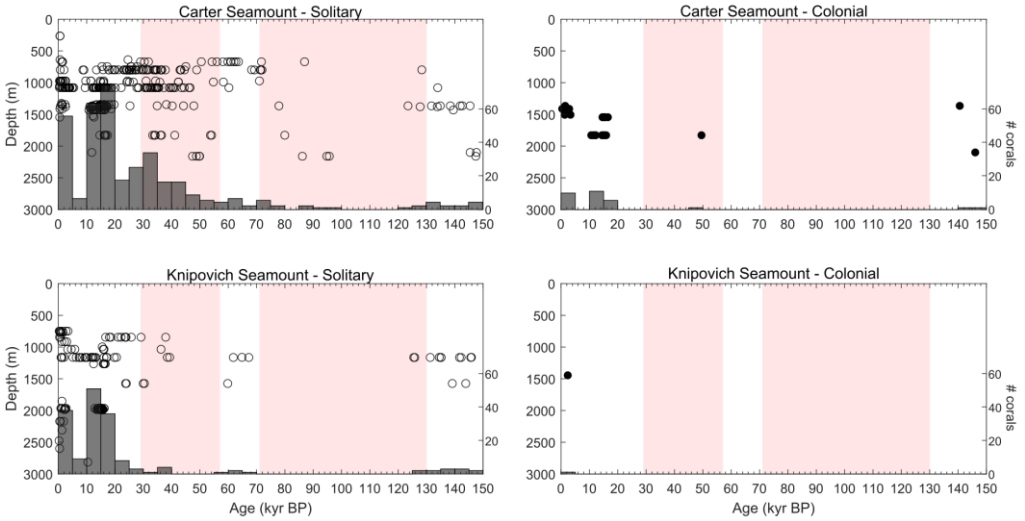

Figure S4: Temporal distribution of new and published (Chen et al., 2015c, 2016a, 2020) cold-water corals from east Equatorial Atlantic. U-series ages plotted against sample depth (symbols, left y axis). Histograms show number of corals dated, with bins of 5 kyr (right y axis). Top: Carter Seamount (9°N, 21°W). Bottom: Knipovich Seamount (5°N, 26°W). Left: solitary cold-water corals. Right: colonial cold-water corals. Red shadings indicate MIS 3 and MIS 5.

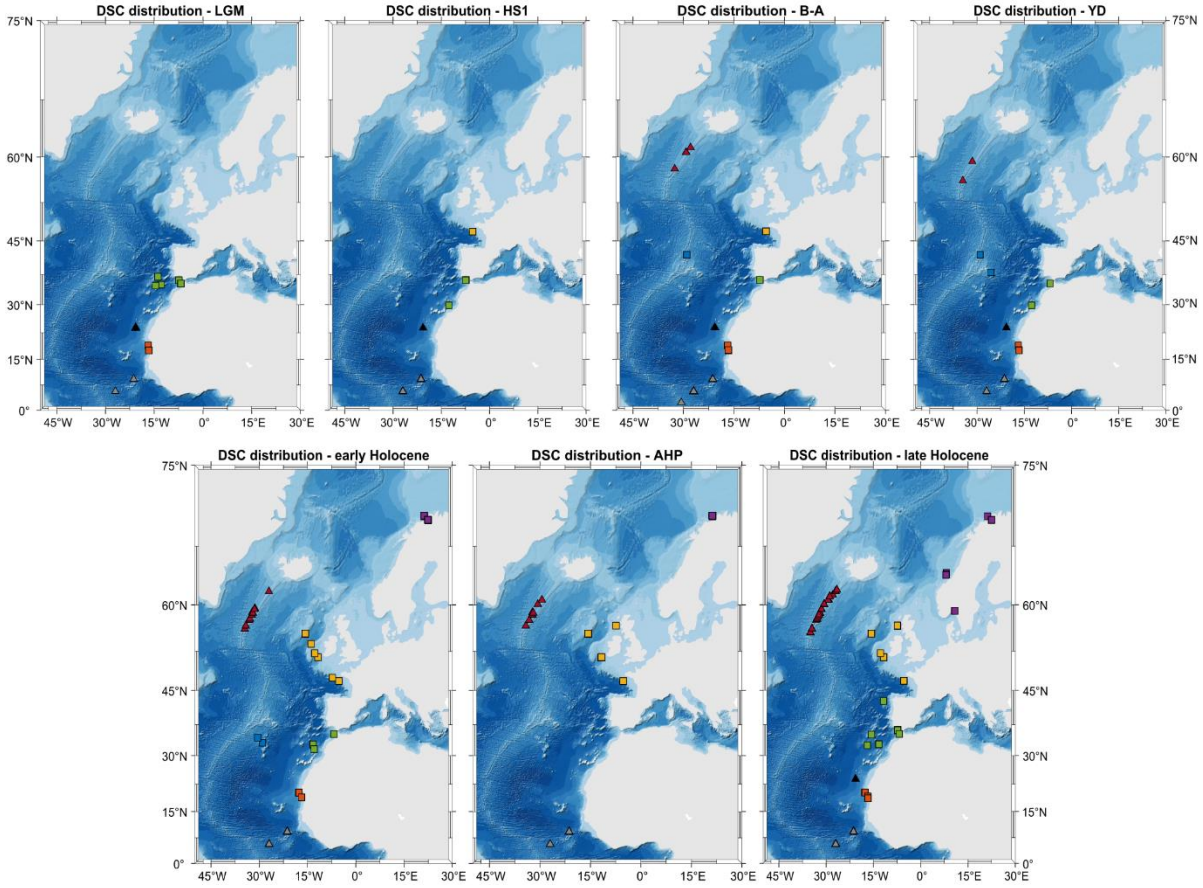

Figure S5: Cold-water coral distribution at Northeast Atlantic at 8 times in the past linked to climatic events (from top left to bottom right): Last Glacial Maximum (22 to 18 kyr BP), Heinrich Stadial 1 (18 to 14.7 kyr BP), Bølling–Allerød (14.7 to 13 kyr BP), Younger Dryas (13 to 11.7 kyr BP), early-Holocene (11.7 to 8.4 kyr BP), African Humid Period (8.2 to 5.5 kyr BP), late-Holocene (2 kyr BP to present).

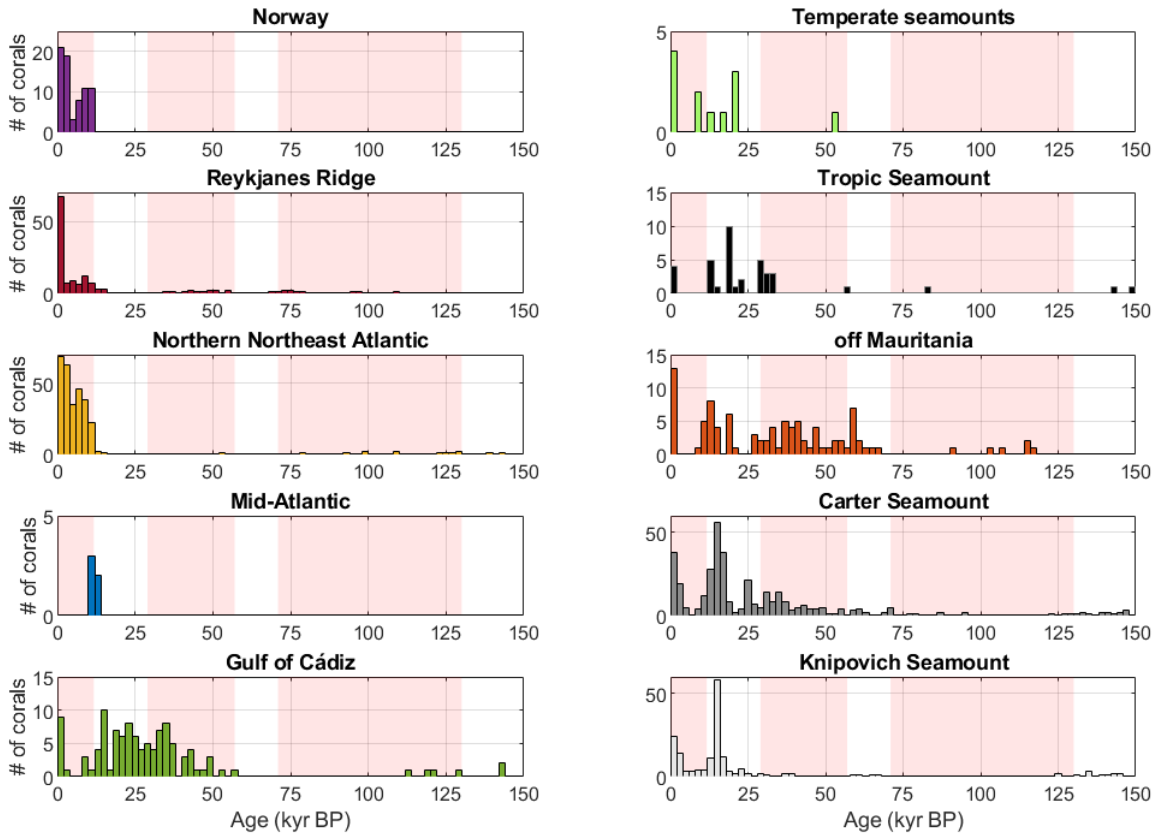

Figure S6: Age distribution of cold-water corals for each region discussed in the text (Table 2) including new sites published in this study: Reykjanes Ridge, Tropic Seamount, Carter Seamount and Knipovich Seamount. Histograms show number of corals dated, with bins of 2 kyr.

APPENDIX II

DATA TABLES FOR CHAPTER 3

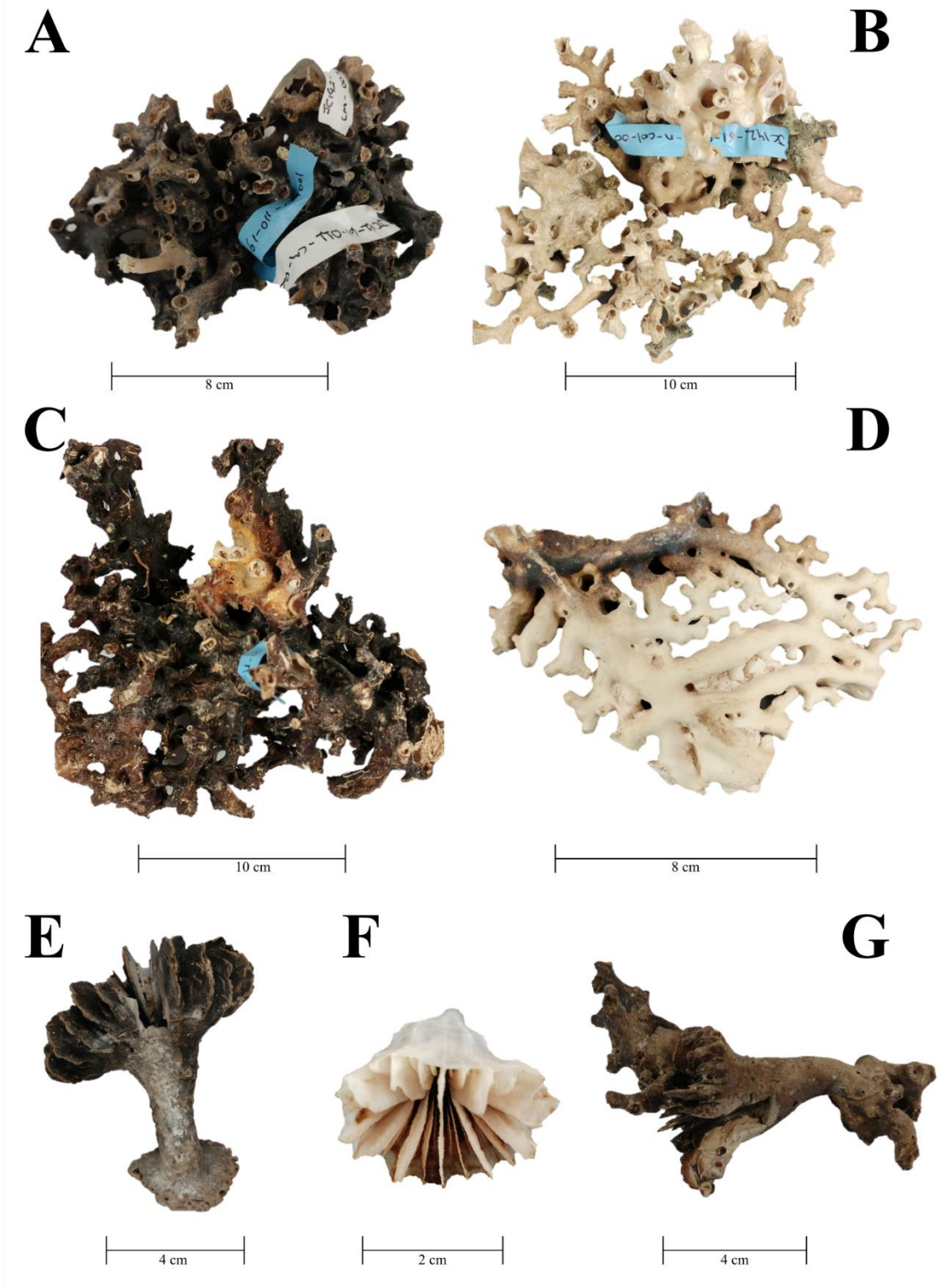

Plate 1: Cold-water corals from Tropic Seamount. (A), (B) and (C) *Solenosmilia variabilis* colony view (JC142-61-011-cm-003, JC142-61-012-n-col-001; JC142-61-011-n-col-001); (D) *Madrepora oculata* colony view (JC142-047-003-pl); € *Desmophyllum dianthus* lateral view (JC142-100-003C-cl-001); (F) Javania caelleti calicular view (JC142-020-010-pm-001); (G) *Desmophyllum dianthus* lateral view (JC142-009-011-cl-001) growing on a colonial coral (likely *Solenosmilia variabilis*).

Table 1: Uranium series dated cold-water corals from Tropic Seamount. Ages are reported in years before present (BP; where present is the year of 1950 CE) both uncorrected and corrected for initial 232Th. Greyed out samples did not pass our quality control. Selection code column indicates samples with [238U] <2 ppm (Low U), or [232Th] >6 ppb (High Th), or [δ234Ui] >157‰ (High δU) and sub-sample (duplicate).

Full Sample ID	Species	Lat	Lon	Depth	Age uncorr	2s	Age corr	2s	$\delta^{234}U$ m	2s	$\delta^{234}Ui$	2s	^{238}U	2s	^{232}Th	2s	$^{230}Th/^{238}U$	2s	Selection code
		DecDeg (N)	DecDeg €	m	yrs BP		yrs BP		‰		‰		ppm		ppb		activity ratio		
JC142-58-041-n-col-001	*Solenosmilia variabilis*	23.89	-20.67	970	213	3	127	85	145.6	1.0	145.7	1.0	4.5	0.010	0.8	0.004	0.003	0.000	
JC142-61-012-n-col-001	*Solenosmilia variabilis*	23.95	-20.69	1193	315	4	212	102	146.2	1.0	146.4	1.0	4.1	0.010	0.9	0.004	0.004	0.000	
JC142-58-041-n-col-001	*Solenosmilia variabilis*	23.89	-20.67	970	488	4	265	224	145.9	1.1	146.0	1.1	3.9	0.007	1.9	0.008	0.006	0.000	duplicate
JC142-58-041-n-col-001	*Solenosmilia variabilis*	23.89	-20.67	970	1577	25	468	1114	146.9	1.1	147.1	1.2	0.3	0.001	0.8	0.003	0.017	0.000	Low U
JC142-58-041-n-col-001	*Solenosmilia variabilis*	23.89	-20.67	970	1806	22	741	1072	145.0	1.2	145.8	1.2	0.5	0.001	1.2	0.005	0.019	0.000	Low U
JC142-58-042-cs-001	*Solenosmilia sp.*	23.89	-20.67	970	13116	69	12758	364	142.9	1.0	148.3	1.0	3.5	0.008	2.7	0.012	0.130	0.001	
JC142-58-042-cs-001	*Solenosmilia sp.*	23.89	-20.67	970	13756	93	12904	860	142.8	1.0	148.2	1.1	3.8	0.009	6.9	0.032	0.136	0.001	High Th
JC142-61-011-cm-001	*Desmophyllum dianthus*	23.95	-20.68	1223	13114	84	12990	150	144.6	1.0	150.1	1.0	3.9	0.009	1.1	0.005	0.130	0.001	
JC142-61-011-cm-003	*Solenosmilia variabilis*	23.95	-20.68	1223	13276	102	13055	243	145.0	1.1	150.5	1.1	3.5	0.007	1.7	0.007	0.132	0.001	

Full Sample ID	Species	Lat	Lon	Depth	Age uncorr	2s	Age corr	2s	$\delta^{234}U$ m	2s	$\delta^{234}Ui$	2s	^{238}U	2s	^{232}Th	2s	$^{230}Th/^{238}U$	2s	Selection code
JC142-61-011-cm-002	*Desmophyllum dianthus*	23.95	-20.68	1223	13854	81	13284	575	146.3	1.0	152.1	1.0	3.6	0.009	4.5	0.020	0.138	0.001	duplicate
JC142-58-042-cs-001	*Solenosmilia sp.*	23.89	-20.67	970	13677	102	13305	384	143.3	1.1	148.8	1.2	3.4	0.007	2.7	0.011	0.136	0.001	duplicate
JC142-61-011-cm-002	*Desmophyllum dianthus*	23.95	-20.68	1223	13806	94	13379	437	147.4	1.0	153.2	1.1	3.6	0.008	3.3	0.016	0.137	0.001	
JC142-61-011-cm-004	*Solenosmilia variabilis*	23.95	-20.68	1223	17492	128	13636	3916	147.6	1.0	153.4	2.0	0.6	0.001	5.1	0.022	0.171	0.001	Low U
JC142-058-039-cm-001	*Desmophyllum dianthus*	23.89	-20.67	970	13775	77	13734	87	144.4	1.0	150.1	1.0	3.7	0.009	0.3	0.002	0.137	0.001	
JC142-100-003C-cm-001	*Caryophyllia sp.*	23.86	-20.68	1406	15350	103	14855	506	144.3	1.1	150.5	1.2	3.6	0.008	3.9	0.017	0.151	0.001	
JC142-100-003C-cm-001	*Caryophyllia sp.*	23.86	-20.68	1406	16244	129	15384	871	143.8	1.0	150.2	1.1	3.7	0.009	6.9	0.031	0.159	0.001	High Th
JC142-113-015-c-col-001	*Desmophyllum dianthus*	23.80	-20.72	1464	17014	133	16593	443	147.0	1.5	154.1	1.6	0.3	0.001	0.3	0.001	0.167	0.001	Low U
JC142-100-003C-cl-001	*Desmophyllum dianthus*	23.86	-20.68	1406	18367	108	18227	176	142.8	1.1	150.4	1.1	3.2	0.008	1.0	0.005	0.178	0.001	
JC142-100-003C-cl-001	*Desmophyllum dianthus*	23.86	-20.68	1406	18383	130	18243	192	142.1	1.0	149.7	1.0	3.2	0.008	1.0	0.004	0.178	0.001	duplicate
JC142-113-	*Desmophyllum dianthus*	23.80	-20.72	1464	19173	138	19056	180	138.5	1.0	146.3	1.0	3.4	0.008	0.9	0.004	0.185	0.001	duplicate

Full Sample ID	Species	Lat	Lon	Depth	Age uncorr	2s	Age corr	2s	$\delta^{234}U$ m	2s	$\delta^{234}Ui$	2s	^{238}U	2s	^{232}Th	2s	$^{230}Th/^{238}U$	2s	Selection code
015-cl-003																			
JC142-113-015-cl-003	*Desmophyllum dianthus*	23.80	-20.72	1464	19212	119	19098	166	138.9	1.0	146.6	1.1	3.4	0.008	0.9	0.004	0.185	0.001	
JC142-113-015-cl-002	*Desmophyllum dianthus*	23.80	-20.72	1464	19208	106	19114	141	141.5	0.9	149.4	1.0	3.3	0.008	0.7	0.003	0.185	0.001	
JC142-113-015-cl-006	*Caryophyllia sp.*	23.80	-20.72	1464	19405	107	19261	179	136.9	1.0	144.7	1.0	3.5	0.008	1.1	0.005	0.186	0.001	duplicate
JC142-113-015-cl-006	*Caryophyllia sp.*	23.80	-20.72	1464	19505	110	19410	146	142.5	1.1	150.6	1.1	3.3	0.008	0.7	0.003	0.188	0.001	
JC142-113-015-cl-001	*Desmophyllum dianthus*	23.80	-20.72	1464	19485	113	19415	132	137.6	1.0	145.5	1.0	3.7	0.009	0.6	0.003	0.187	0.001	
JC142-113-015-cl-007	*Desmophyllum dianthus*	23.80	-20.72	1464	19542	129	19428	172	137.4	1.0	145.2	1.0	3.6	0.008	0.9	0.004	0.188	0.001	
JC142-113-015-cl-004	*Desmophyllum dianthus*	23.80	-20.72	1464	19668	108	19491	209	140.8	1.0	148.8	1.0	3.2	0.007	1.2	0.006	0.189	0.001	
JC142-113-015-cl-005	*Desmophyllum dianthus*	23.80	-20.72	1464	19734	110	19531	230	137.9	1.0	145.8	1.0	3.8	0.009	1.7	0.007	0.189	0.001	
JC142-61-011-	*Solenosmilia variabilis*	23.95	-20.68	1223	19819	107	19615	231	139.0	0.9	147.1	1.0	3.3	0.008	1.4	0.007	0.190	0.001	

Full Sample ID	Species	Lat	Lon	Depth	Age uncorr	2s	Age corr	2s	$\delta^{234}U$ m	2s	$\delta^{234}Ui$	2s	^{238}U	2s	^{232}Th	2s	$^{230}Th/^{238}U$	2s	Selection code
n-col-002																			
JC142-61-011-n-col-001	*Solenosmilia variabilis*	23.95	-20.68	1223	19931	137	19709	260	139.9	1.0	148.0	1.0	3.3	0.007	1.6	0.007	0.191	0.001	
JC142-009-011-cl-001	*Desmophyllum dianthus*	23.85	-20.74	1027	20417	108	20349	127	140.9	1.0	149.3	1.1	3.9	0.008	0.6	0.003	0.196	0.001	
JC142-113-015-c-col-001	*Desmophyllum dianthus*	23.80	-20.72	1464	22245	149	20578	1676	138.5	1.0	146.9	1.2	1.6	0.004	5.9	0.026	0.211	0.001	Low U
JC142-009-011-n-col-001	*Solenosmilia sp.*	23.85	-20.74	1027	22201	136	22005	239	136.4	1.0	145.1	1.1	4.2	0.009	1.8	0.008	0.210	0.001	
JC142-009-011-cm-001	*Caryophyllia sp.*	23.85	-20.74	1027	24185	155	23786	429	136.0	1.0	145.7	1.0	4.0	0.010	3.5	0.015	0.227	0.001	duplicate
JC142-009-011-cm-001	*Caryophyllia sp.*	23.85	-20.74	1027	24278	151	23892	416	135.9	1.1	145.5	1.2	4.0	0.009	3.4	0.016	0.228	0.001	
JC142-047-006-cl-002	*Desmophyllum dianthus*	23.89	-20.72	995	29166	218	29132	220	135.4	1.0	147.0	1.1	4.5	0.010	0.3	0.001	0.268	0.002	
JC142-047-006-nl-001	*Desmophyllum dianthus*	23.89	-20.72	995	29283	225	29234	230	135.1	1.0	146.8	1.1	4.7	0.011	0.5	0.002	0.269	0.002	
JC142-047-	*Desmophyllum dianthus*	23.89	-20.72	995	29852	211	29548	368	133.6	1.0	145.3	1.1	3.6	0.009	2.4	0.010	0.273	0.002	

Full Sample ID	Species	Lat	Lon	Depth	Age uncorr	2s	Age corr	2s	$\delta^{234}U$ m	2s	$\delta^{234}Ui$	2s	^{238}U	2s	^{232}Th	2s	$^{230}Th/^{238}U$	2s	Selection code
006-nl-002																			
JC142-047-006-cl-001A	*Desmophyllum dianthus*	23.89	-20.72	995	29946	187	29604	391	134.7	1.0	146.4	1.1	4.5	0.010	3.3	0.014	0.274	0.001	
JC142-047-006-cm-003	*Desmophyllum dianthus*	23.89	-20.72	995	29933	183	29744	262	134.8	1.0	146.7	1.1	4.4	0.010	1.8	0.008	0.274	0.001	
JC142-047-006-c-col-001	*Desmophyllum dianthus*	23.89	-20.72	995	31114	257	30039	1106	132.6	1.1	144.4	1.3	5.6	0.014	13.0	0.056	0.283	0.002	High Th
JC142-047-006-cm-002	*Desmophyllum dianthus*	23.89	-20.72	995	30228	198	30085	244	133.8	1.0	145.7	1.0	4.1	0.010	1.3	0.006	0.276	0.002	
JC142-047-006-cm-001	*Caryophyllia sp.*	23.89	-20.72	995	30473	183	30208	321	136.4	1.0	148.6	1.1	4.7	0.010	2.7	0.012	0.279	0.001	
JC142-047-006-c-col-001	*Desmophyllum dianthus*	23.89	-20.72	995	31344	184	30363	1006	134.1	1.0	146.1	1.1	5.3	0.012	11.2	0.048	0.285	0.001	High Th
JC142-047-006-c-col-001	*Desmophyllum dianthus*	23.89	-20.72	995	32073	236	30529	1571	133.3	1.0	146.0	1.1	5.1	0.013	16.8	0.075	0.290	0.002	High Th
JC142-113-007-cl-002	*Desmophyllum dianthus*	23.78	-20.72	1797	32270	192	31692	610	131.4	1.0	144.0	1.0	3.7	0.008	4.6	0.020	0.292	0.001	duplicate
JC142-047-	*Desmophyllum dianthus*	23.89	-20.72	995	32841	251	31746	1125	133.5	1.1	146.0	1.2	4.7	0.010	11.1	0.048	0.297	0.002	High Th

Full Sample ID	Species	Lat	Lon	Depth	Age uncorr	2s	Age corr	2s	$\delta^{234}U$ m	2s	$\delta^{234}Ui$	2s	^{238}U	2s	^{232}Th	2s	$^{230}Th/^{238}U$	2s	Selection code
006-cl-001																			
JC142-047-006-cl-001	*Desmophyllum dianthus*	23.89	-20.72	995	32606	222	31889	750	131.7	1.0	144.1	1.2	5.2	0.012	8.0	0.035	0.294	0.002	High Th
JC142-113-007-cl-001	*Desmophyllum dianthus*	23.78	-20.72	1797	32350	274	31910	519	134.9	1.0	147.7	1.1	3.4	0.007	3.2	0.014	0.293	0.002	
JC142-113-007-cl-002	*Desmophyllum dianthus*	23.78	-20.72	1797	32431	288	32050	478	129.6	1.0	141.9	1.1	3.8	0.010	3.1	0.014	0.292	0.002	
JC142-113-007-cs-002	*Desmophyllum dianthus*	23.78	-20.72	1797	32671	182	32221	485	138.5	1.0	151.8	1.1	3.1	0.006	3.0	0.012	0.297	0.001	
JC142-113-007-cs-001	*Desmophyllum dianthus*	23.78	-20.72	1797	33101	269	32624	546	130.0	1.0	142.5	1.2	3.3	0.007	3.4	0.014	0.298	0.002	
JC142-113-ROV320-c-col-001	*Solenosmilia variabilis*	23.47	-21.28	1464	48071	299	47436	702	173.5	1.0	198.4	1.2	1.0	0.002	1.4	0.006	0.422	0.002	Low U
JC142-ROV320-cm-001	*Desmophyllum dianthus*	23.78	-20.72	1780	56722	353	56546	394	121.0	1.1	141.9	1.2	4.5	0.009	1.7	0.007	0.458	0.002	
JC142-100-003B-n-col-001	*Solenosmilia variabilis*	23.86	-20.68	1406	83100	601	82939	623	119.9	1.0	151.6	1.3	4.2	0.009	1.5	0.006	0.604	0.003	
JC142-047-	*Madrepora oculata*	23.89	-20.72	994	142101	1720	142040	1720	105.7	1.0	158.0	1.5	4.2	0.010	0.6	0.003	0.819	0.005	

Full Sample ID	Species	Lat	Lon	Depth	Age uncorr	2s	Age corr	2s	$\delta^{234}U$ m	2s	$\delta^{234}Ui$	2s	^{238}U	2s	^{232}Th	2s	$^{230}Th/^{238}U$	2s	Selection code
002-c-col-001																			
JC142-047-003-pl-001	*Madrepora oculata*	23.89	-20.72	994	148473	1465	148417	1469	104.7	1.0	159.3	1.5	4.6	0.009	0.6	0.002	0.836	0.004	
JC142-047-003-c-col-001	*Madrepora oculata*	23.89	-20.72	994	148674	1461	148445	1480	111.0	1.0	169.0	1.5	3.9	0.007	2.0	0.008	0.842	0.004	High δU
JC142-58-041-n-col-001	*Solenosmilia variabilis*	23.89	-20.67	970	-6	90	non determined		140.9	3.5	140.5	3.5	0.04	0.000	0.01	0.001	-0.009	0.004	Low U

Table 2: Radiocarbon parameters of deep-sea corals from Tropic Seamount. All Desmophyllum sp. are solitary corals. Fm correspond to blank corrected fraction modern.

Full Sample ID	**Taxa**	**Late**	**Lon**	**Depth**	**U-series age**	**2 s**	**^{14}C age**	**2s**	**Fm**	**1s**	**$\Delta^{14}C$**	**2s**	**$\Delta\Delta^{14}C$**	**2s**	**B-atm**	**2s**
		DecDeg (N)	**DecDЄ(E)**	**m**	**yr BP**	**yr**	**yr**	**yr**			**‰**		**‰**	**‰**	**yr**	**yr**
JC142-113-010-pm-001	*Javania caelleti*	23.80	-20.72	1783	Live		759	50	0.9098	0.0028	-90	7	-66	8	559	66
JC142-61-012-n-col-001	*Solenosmilia variabilis*	23.95	-20.69	1193	212	102	833	50	0.9015	0.0028	-67	16	-74	27	615	220
JC142-58-042-cs-001	*Solenosmilia sp.*	23.89	-20.67	970	12758	364	11351	31	0.2434	0.0010	148	62	-71	82	478	561
JC142-61-011-cm-001	*Desmophyllum sp.*	23.95	-20.68	1223	12990	150	11803	64	0.2301	0.0009	116	27	-99	36	677	262
JC142-61-011-cm-003	*Solenosmilia sp.*	23.95	-20.68	1223	13055	243	11779	64	0.2308	0.0009	129	42	-82	54	561	377
JC142-61-011-cm-002	*Desmophyllum sp.*	23.95	-20.68	1223	13378	437	11669	58	0.2340	0.0009	189	76	-14	87	94	590
JC142-058-039-cm-001	*Desmophyllum sp.*	23.89	-20.67	970	13734	87	12362	33	0.2146	0.0009	140	16	-60	29	406	199
JC142-100-003C-cm-001	*Caryophyllia sp.*	23.86	-20.68	1406	14855	506	13121	68	0.1953	0.0008	188	91	-85	56	545	390
JC142-100-003C-cl-001	*Desmophyllum sp.*	23.86	-20.68	1406	18227	176	16083	103	0.1350	0.0009	236	39	-167	75	1009	435
JC142-113-015-cl-003	*Desmophyllum sp.*	23.80	-20.72	1464	19098	166	17041	86	0.1199	0.0006	217	34	-187	34	1144	226
JC142-113-015-cl-002	*Desmophyllum sp.*	23.80	-20.72	1464	19114	141	17110	85	0.1188	0.0006	211	31	-194	31	1197	202
JC142-113-015-cl-006	*Caryophyllia sp.*	23.80	-20.72	1464	19410	146	16948	86	0.1213	0.0007	280	32	-138	43	825	254
JC142-113-015-cl-001	*Desmophyllum sp.*	23.80	-20.72	1464	19415	132	17211	85	0.1174	0.0006	240	29	-178	41	1077	256
JC142-113-015-cl-007	*Desmophyllum dianthus*	23.80	-20.72	1464	19428	172	17042	88	0.1199	0.0007	267	36	-149	49	893	299
JC142-113-015-cl-004	*Desmophyllum sp.*	23.80	-20.72	1464	19491	209	16989	86	0.1206	0.0006	286	45	-128	56	761	338
JC142-113-015-cl-005	*Desmophyllum sp.*	23.80	-20.72	1464	19531	230	17374	90	0.1150	0.0006	232	44	-182	53	1105	337
JC142-61-011-n-col-002	*Solenosmilia sp.*	23.95	-20.68	1223	19615	231	17147	88	0.1183	0.0007	280	47	-136	44	813	274

Full Sample ID	Taxa	Late	Lon	Depth	U-series age	2 s	^{14}C age	2s	Fm	1s	Δ^{14}C	2s	$\Delta\Delta^{14}$C	2s	B-atm	2s
JC142-61-011-n-col-001	*Solenosmilia sp.*	23.95	-20.68	1223	19709	260	17203	88	0.1175	0.0006	284	52	-137	43	812	280
JC142-113-015-c-col-001	*Desmophyllum dianthus*	23.80	-20.72	1464	20008	711	17308	88	0.1159	0.0006	317	137	-116	114	683	719
JC142-009-011-cl-001	*Desmophyllum sp.*	23.85	-20.74	1027	20349	127	17643	117	0.1112	0.0008	315	34	-131	40	768	235
JC142-009-011-n-col-001	*Solenosmilia sp.*	23.85	-20.74	1027	22005	239	19016	100	0.0937	0.0006	354	52	-160	57	902	330
JC142-009-011-cm-001	*Caryophyllia sp.*	23.85	-20.74	1027	23891	416	20357	112	0.0793	0.0006	442	93	-75	113	422	624
JC142-047-006-cl-002	*Desmophyllum sp.*	23.89	-20.72	995	29132	220	25219	172	0.0433	0.0005	482	62	-36	100	197	550
JC142-047-006-nl-001	*Desmophyllum sp.*	23.89	-20.72	995	29234	230	25744	176	0.0406	0.0005	406	60	-105	77	589	448
JC142-047-006-nl-002	*Desmophyllum sp.*	23.89	-20.72	995	29548	368	25914	180	0.0397	0.0004	430	87	-111	68	599	391
JC142-047-006-cl-001A	*Desmophyllum dianthus*	23.89	-20.72	995	29604	391	25618	176	0.0412	0.0005	492	97	-51	84	269	454
JC142-047-006-cm-003	*Desmophyllum sp.*	23.89	-20.72	995	29744	262	25256	168	0.0431	0.0005	587	73	31	85	-160	433
JC142-047-006-cm-002	*Desmophyllum sp.*	23.89	-20.72	995	30085	244	25791	176	0.0403	0.0004	547	68	27	100	-144	535
JC142-047-006-cm-001	*Caryophyllia sp.*	23.89	-20.72	995	30208	321	25568	176	0.0415	0.0005	615	89	100	111	-513	542
JC142-047-006-c-col-001	*Desmophyllum dianthus*	23.89	-20.72	995	30362	1006	25941	180	0.0396	0.0004	581	237	57	275	-236	1399
JC142-047-006-cl-001	*Desmophyllum sp.*	23.89	-20.72	995	31889	750	27506	210	0.0326	0.0004	544	176	88	188	-443	993
JC142-113-007-cl-001	*Desmophyllum sp.*	23.78	-20.72	1797	31910	519	26668	262	0.0362	0.0006	733	155	282	161	-1427	742
JC142-113-007-cl-002	*Desmophyllum sp.*	23.78	-20.72	1797	32050	478	27366	178	0.0318	0.0004	617	123	165	119	-850	625
JC142-113-007-cl-002	*Desmophyllum sp.*	23.78	-20.72	1797	32050	478	27706	216	0.0318	0.0004	532	119	82	123	-454	673
JC142-113-007-cs-002	*Desmophyllum dianthus*	23.78	-20.72	1797	32222	485	28444	200	0.0290	0.0004	444	115	-20	86	127	510
JC142-113-007-cs-001	*Desmophyllum dianthus*	23.78	-20.72	1797	32624	546	29342	218	0.0252	0.0004	352	118	-158	87	895	503

Full Sample ID	Taxa	Late	Lon	Depth	U-series age	2 s	^{14}C age	2s	Fm	1s	$\Delta^{14}C$	2s	$\Delta\Delta^{14}C$	2s	B-atm	2s
JC142-113-007-cs-001	*Desmophyllum dianthus*	23.78	-20.72	1797	32624	546	29572	264	0.0252	0.0004	306	119	-197	89	1141	510

Table 3: Trace elements of deep-sea corals from Tropic Seamount.

Full Sample ID	Taxa	Lat	Lon	Depth	U-series age	2 s	[Ca]	Li/Ca	Mg/Ca	Al/Ca	Mn/Ca	Fe/Ca	Li/Mg	Temperature (from Li/Mg)
		DecDeg (N)	D¢eg (E)	m	yr BP	yr	mM	µmol/mol	mmol/mol	µmol/mol	µmol/mol	µmol/mol	mmol/mol	°C
JC142-020-010-ps-001	*Javania caelleti*	23.88	-20.71	995	Live		3.73	12.17	2.98	1.23	0.35	0.70	4.09	5.64
JC142-113-010-pm-001	*Javania caelleti*	23.80	-20.72	1783	Live		3.81	11.67	2.45	1.73	0.29	0.58	4.77	2.57
JC142-61-012-n-col-001	*Solenosmilia variabilis*	23.95	-20.69	1193	212	102	3.41	8.63	2.05	1.34	0.47	1.97	4.20	5.09
JC142_094_032-1	*Solenosmilia sp.*	23.90	-20.70	1328	12304	609	3.82	12.21	2.67	26.24	1.26	16.95	4.58	3.38
JC142-58-042-cs-001	*Solenosmilia sp.*	23.89	-20.67	970	12758	364	4.02	12.09	2.89	57.94	6.14	7.46	4.18	5.21
JC142-61-011-cm-001	*Desmophyllum sp.*	23.95	-20.68	1223	12990	150	4.01	12.67	2.94	16.69	1.76	7.45	4.31	4.60
JC142-61-011-cm-003	*Solenosmilia variabilis*	23.95	-20.68	1223	13055	243	3.73	12.13	2.83	42.74	2.39	2.35	4.29	4.67
JC142-61-011-cm-002	*Desmophyllum dianthus*	23.95	-20.68	1223	13378	437	3.80	12.94	2.83	12.24	1.48	1.25	4.57	3.42
JC142-058-039-cm-001	*Desmophyllum sp.*	23.89	-20.67	970	13734	87	3.73	10.52	2.47	10.37	1.05	4.28	4.25	4.87
JC142-100-003C-cm-001	*Caryophyllia sp.*	23.86	-20.68	1406	14855	506	3.92	10.99	2.61	20.57	3.61	17.15	4.21	5.04
JC142-100-003C-cl-001	*Desmophyllum sp.*	23.86	-20.68	1406	18227	176	3.66	15.27	2.37	5.19	0.73	3.46	6.42	-3.40
JC142-113-015-cl-003	*Desmophyllum sp.*	23.80	-20.72	1464	19098	166	3.55	11.62	1.87	3.16	1.09	7.48	6.21	-2.71
JC142-113-015-cl-002	*Desmophyllum sp.*	23.80	-20.72	1464	19114	141	3.46	13.44	2.10	2.00	0.18	1.39	6.41	-3.36
JC142-113-015-cl-006	*Caryophyllia sp.*	23.80	-20.72	1464	19410	146	3.97	17.10	2.60	5.42	0.50	6.71	6.58	-3.88
JC142-113-015-cl-001	*Desmophyllum sp.*	23.80	-20.72	1464	19415	132	4.04	13.26	2.03	2.05	0.41	1.63	6.52	-3.69

Full Sample ID	Taxa	Lat	Lon	Depth	U-series age	2 s	[Ca]	Li/Ca	Mg/Ca	Al/Ca	Mn/Ca	Fe/Ca	Li/Mg	Temperature (from Li/Mg)
JC142-113-015-cl-007	*Desmophyllum dianthus*	23.80	-20.72	1464	19428	172	4.01	11.30	1.79	0.99	0.10	1.32	6.32	-3.06
JC142-113-015-cl-004	*Desmophyllum sp.*	23.80	-20.72	1464	19491	209	3.91	14.71	2.43	9.70	1.23	3.84	6.04	-2.18
JC142-113-015-cl-005	*Desmophyllum sp.*	23.80	-20.72	1464	19531	230	3.49	13.22	2.12	1.11	0.18	1.28	6.25	-2.83
JC142-61-011-n-col-002	*Solenosmilia sp.*	23.95	-20.68	1223	19615	231	3.62	14.43	2.48	7.28	1.12	8.36	5.82	-1.43
JC142-61-011-n-col-001	*Solenosmilia sp.*	23.95	-20.68	1223	19709	260	4.00	12.69	2.26	6.79	0.79	10.91	5.62	-0.72
JC142-113-015-c-col-001	*Desmophyllum dianthus*	23.80	-20.72	1464	20008	711	3.64	16.02	2.69	80.35	6.47	1.42	6.01	-2.05
JC142-009-011-cl-001	*Desmophyllum sp.*	23.85	-20.74	1027	20349	127	3.81	14.18	2.52	7.52	1.06	3.21	5.63	-0.77
JC142-009-011-n-col-001	*Solenosmilia sp.*	23.85	-20.74	1027	22005	239	3.90	14.89	2.82	13.05	0.93	7.61	5.28	0.54
JC142-009-011-cm-001	*Caryophyllia sp.*	23.85	-20.74	1027	23891	416	4.01	12.63	2.47	20.78	2.78	2.76	5.11	1.19
JC142-047-006-cl-002	*Desmophyllum sp.*	23.89	-20.72	995	29132	220	3.83	11.35	2.23	3.22	0.34	1.69	5.09	1.26
JC142-047-006-nl-001	*Desmophyllum sp.*	23.89	-20.72	995	29234	230	3.65	11.65	2.38	3.78	0.09	1.02	4.89	2.05
JC142-047-006-nl-002	*Desmophyllum sp.*	23.89	-20.72	995	29548	368	3.93	10.39	1.98	5.59	0.41	2.67	5.25	0.65
JC142-047-006-cl-001A	*Desmophyllum dianthus*	23.89	-20.72	995	29604	391	3.80	9.64	1.76	0.46	LOD	LOD	5.47	-0.17
JC142-047-006-cm-003	*Desmophyllum sp.*	23.89	-20.72	995	29744	262	4.06	10.11	1.99	1.19	0.06	0.70	5.10	1.23
JC142-047-006-cm-002	*Desmophyllum sp.*	23.89	-20.72	995	30085	244	3.81	10.83	1.96	9.14	1.49	3.65	5.58	-0.58
JC142-047-006-cm-001	*Caryophyllia sp.*	23.89	-20.72	995	30208	321	3.98	12.70	2.51	11.55	2.79	7.96	5.06	1.37
JC142-047-006-c-col-001	*Desmophyllum dianthus*	23.89	-20.72	995	30362	1006	3.91	10.05	1.71	15.82	3.51	NO DATA	5.89	-1.67
JC142-047-006-cl-001	*Desmophyllum sp.*	23.89	-20.72	995	31889	750	3.87	12.70	2.22	13.79	3.22	2.90	5.71	-1.05

Full Sample ID	Taxa	Lat	Lon	Depth	U-series age	2 s	[Ca]	Li/Ca	Mg/Ca	Al/Ca	Mn/Ca	Fe/Ca	Li/Mg	Temperature (from Li/Mg)
JC142-113-007-cl-001	*Desmophyllum sp.*	23.78	-20.72	1797	31910	519	3.74	11.21	2.02	8.58	2.24	3.50	5.55	-0.49
JC142-113-007-cl-002	*Desmophyllum sp.*	23.78	-20.72	1797	32050	478	3.79	11.87	2.14	18.53	1.09	4.63	5.54	-0.44
JC142-113-007-cs-002	*Desmophyllum dianthus*	23.78	-20.72	1797	32222	485	4.00	8.56	1.65	1.41	0.57	1.10	5.24	0.68
JC142-113-007-cs-001	*Desmophyllum dianthus*	23.78	-20.72	1797	32624	546	4.16	13.19	2.38	87.05	8.54	NO DATA	5.52	-0.37
JC142_094_001A	*Desmophyllum sp.*	23.90	-20.70	1952	34182	272	3.72	8.64	1.59	4.34	0.97	3.91	5.43	-0.04

Table 4: Trace elements duplicates.

Full Sample ID	Taxa	Latitude	Longitude	Depth	U-series age	2 s	[Ca]	Li/Ca	Mg/Ca	Al/Ca	Mn/Ca	Fe/Ca	Li/Mg
		DecDeg (N)	DecDeg €	m	yr BP	yr	mM	µmol/mol	mmol/mol	µmol/mol	µmol/mol	µmol/mol	mmol/mol
JC142-020-010-ps-001	*Javania caelleti*	23.88	-20.71	995	Live		3.45	11.53	2.83	1.24	0.12	0.27	4.07
JC142-020-010-ps-001	*Javania caelleti*	23.88	-20.71	995	Live		4.02	12.81	3.12	1.23	0.58	1.13	4.10
JC142-113-010-pm-001	*Javania caelleti*	23.80	-20.72	1783	Live		3.65	11.75	2.46	2.72	0.25	0.77	4.78
JC142-113-010-pm-001	*Javania caelleti*	23.80	-20.72	1783	Live		3.97	11.60	2.44	0.73	0.34	0.39	4.76
JC142-61-012-n-col-001	*Solenosmilia sp.*	23.95	-20.69	1223	212	102	2.90	8.76	2.09	2.11	0.09	1.80	4.19
JC142-61-012-n-col-001	*Solenosmilia sp.*	23.95	-20.69	1223	212	102	3.91	8.51	2.02	0.57	0.85	2.14	4.22
JC142_094_032-1	*Solenosmilia sp.*	23.90	-20.70	1328	12304	609	3.83	11.82	2.57	42.28	1.92	26.95	4.59
JC142_094_032-1	*Solenosmilia sp.*	23.90	-20.70	1328	12304	609	3.81	12.61	2.76	10.19	0.60	6.96	4.56
JC142-58-042-cs-001	*Solenosmilia?*	23.89	-20.67	970	12757	364	4.11	10.64	2.83	22.38	1.22	7.46	3.76
JC142-58-042-cs-001	*Solenosmilia?*	23.89	-20.67	970	12757	364	3.93	13.53	2.95	93.49	11.06	NO DATA	4.59
JC142-61-011-cm-001	*Desmophyllum sp.*	23.95	-20.68	1223	12990	150	4.07	12.95	2.98	11.52	1.72	7.45	4.35
JC142-61-011-cm-001	*Desmophyllum sp.*	23.95	-20.68	1223	12990	150	3.95	12.39	2.91	21.85	1.79	NO DATA	4.26
JC142-61-011-cm-003	*Solenosmilia sp.*	23.95	-20.68	1223	13055	243	3.71	11.82	2.75	3.22	0.12	2.35	4.30
JC142-61-011-cm-003	*Solenosmilia sp.*	23.95	-20.68	1223	13055	243	3.75	12.45	2.91	82.27	4.66	NO DATA	4.28
JC142-61-011-cm-002	*Desmophyllum sp.*	23.95	-20.68	1223	13379	437	3.56	14.20	2.93	2.83	0.13	1.25	4.84
JC142-61-011-cm-002	*Desmophyllum sp.*	23.95	-20.68	1223	13379	437	4.03	11.68	2.72	21.66	2.82	NO DATA	4.29
JC142-058-039-cm-001	*Desmophyllum sp.*	23.89	-20.67	970	13734	87	3.55	12.74	2.95	12.58	1.61	4.49	4.32
JC142-058-039-cm-001	*Desmophyllum sp.*	23.89	-20.67	970	13734	87	3.92	8.30	1.99	8.16	0.48	4.06	4.18

Full Sample ID	Taxa	Latitude	Longitude	Depth	U-series age	2 s	[Ca]	Li/Ca	Mg/Ca	Al/Ca	Mn/Ca	Fe/Ca	Li/Mg
JC142-100-003C-cm-001	*Caryophyllia sp.*	23.86	-20.68	1406	14853	506	4.41	11.08	2.58	31.48	6.25	28.34	4.30
JC142-100-003C-cm-001	*Caryophyllia sp.*	23.86	-20.68	1406	14855	506	3.44	10.89	2.64	9.66	0.96	5.96	4.12
JC142-100-003C-cl-001	*Desmophyllum sp.*	23.86	-20.68	1406	18227	176	3.38	16.28	2.47	5.98	1.02	3.46	6.58
JC142-100-003C-cl-001	*Desmophyllum sp.*	23.86	-20.68	1406	18227	176	3.93	14.26	2.27	4.40	0.45	NO DATA	6.27
JC142-113-015-cl-003	*Desmophyllum sp.*	23.80	-20.72	1464	19097	166	3.09	11.57	1.86	4.12	1.55	7.48	6.20
JC142-113-015-cl-003	*Desmophyllum sp.*	23.80	-20.72	1464	19097	166	4.01	11.68	1.88	2.19	0.63	NO DATA	6.21
JC142-113-015-cl-002	*Desmophyllum sp.*	23.80	-20.72	1464	19114	141	3.47	13.19	2.08	3.10	0.12	1.39	6.33
JC142-113-015-cl-002	*Desmophyllum sp.*	23.80	-20.72	1464	19114	141	3.46	13.70	2.11	0.90	0.24	NO DATA	6.49
JC142-113-015-cl-006	*Caryophyllia sp.*	23.80	-20.72	1464	19410	146	4.17	17.24	2.62	2.94	0.60	6.71	6.58
JC142-113-015-cl-006	*Caryophyllia sp.*	23.80	-20.72	1464	19410	146	3.78	16.96	2.58	7.90	0.40	NO DATA	6.59
JC142-113-015-cl-001	*Desmophyllum sp.*	23.80	-20.72	1464	19415	132	4.02	15.52	2.37	LOD	LOD	1.63	6.56
JC142-113-015-cl-001	*Desmophyllum sp.*	23.80	-20.72	1464	19415	132	4.06	11.01	1.70	3.79	0.77	NO DATA	6.48
JC142-113-015-cl-007	*Desmophyllum dianthus*	23.80	-20.72	1464	19428	172	4.13	12.33	1.97	LOD	LOD	1.21	6.27
JC142-113-015-cl-007	*Desmophyllum dianthus*	23.80	-20.72	1464	19428	172	3.90	10.27	1.62	1.62	0.12	1.43	6.36
JC142-113-015-cl-004	*Desmophyllum sp.*	23.80	-20.72	1464	19491	209	4.03	13.83	2.32	3.69	0.56	3.84	5.96
JC142-113-015-cl-004	*Desmophyllum sp.*	23.80	-20.72	1464	19491	209	3.79	15.60	2.55	15.72	1.89	NO DATA	6.12
JC142-113-015-cl-005	*Desmophyllum sp.*	23.80	-20.72	1464	19530	230	2.99	14.62	2.35	LOD	LOD	1.12	6.23
JC142-113-015-cl-005	*Desmophyllum sp.*	23.80	-20.72	1464	19530	230	4.00	11.82	1.89	1.21	0.14	1.45	6.26
JC142-61-011-n-col-002	*Solenosmilia sp.*	23.95	-20.68	1223	19614	231	3.37	15.04	2.63	9.81	0.60	8.36	5.71

Full Sample ID	Taxa	Latitude	Longitude	Depth	U-series age	2 s	[Ca]	Li/Ca	Mg/Ca	Al/Ca	Mn/Ca	Fe/Ca	Li/Mg
JC142-61-011-n-col-002	*Solenosmilia sp.*	23.95	-20.68	1223	19614	231	3.87	13.82	2.33	4.74	1.64	NO DATA	5.93
JC142-61-011-n-col-001	*Solenosmilia sp.*	23.95	-20.68	1223	19709	260	4.14	12.94	2.38	7.06	LOD	10.91	5.43
JC142-61-011-n-col-001	*Solenosmilia sp.*	23.95	-20.68	1223	19709	260	3.86	12.44	2.14	6.52	0.63	LOD	5.80
JC142-113-015-c-col-001	*Desmophyllum dianthus*	23.80	-20.72	1464	20010	711	3.44	15.10	2.37	20.42	0.82	1.42	6.38
JC142-113-015-c-col-001	*Desmophyllum dianthus*	23.80	-20.72	1464	20010	711	3.83	16.93	3.01	140.28	12.12	NO DATA	5.63
JC142-009-011-cl-001	*Desmophyllum sp.*	23.85	-20.74	1027	20349	127	3.59	13.48	2.41	4.84	0.43	3.21	5.59
JC142-009-011-cl-001	*Desmophyllum sp.*	23.85	-20.74	1027	20349	127	4.03	14.88	2.62	10.20	1.69	NO DATA	5.67
JC142-009-011-n-col-001	*Solenosmilia sp.*	23.85	-20.74	1027	22005	239	3.93	14.23	2.69	8.02	0.73	6.87	5.28
JC142-009-011-n-col-001	*Solenosmilia sp.*	23.85	-20.74	1027	22005	239	3.87	15.55	2.95	18.09	1.14	8.34	5.27
JC142-009-011-cm-001	*Caryophyllia sp.*	23.85	-20.74	1027	23891	416	4.11	12.43	2.48	3.29	0.46	2.76	5.02
JC142-009-011-cm-001	*Caryophyllia sp.*	23.85	-20.74	1027	23891	416	3.90	12.83	2.47	38.26	5.09	NO DATA	5.19
JC142-047-006-cl-002	*Desmophyllum sp.*	23.89	-20.72	995	29132	220	3.60	11.32	2.19	4.51	0.18	2.24	5.16
JC142-047-006-cl-002	*Desmophyllum sp.*	23.89	-20.72	995	29132	220	4.06	11.38	2.27	1.92	0.50	1.13	5.02
JC142-047-006-nl-001	*Desmophyllum sp.*	23.89	-20.72	995	29233	230	3.47	11.63	2.35	2.66	0.09	0.94	4.94
JC142-047-006-nl-001	*Desmophyllum sp.*	23.89	-20.72	995	29233	230	3.83	11.68	2.41	4.89	LOD	1.10	4.84
JC142-047-006-nl-002	*Desmophyllum sp.*	23.89	-20.72	995	29548	368	3.97	10.76	2.08	8.16	0.53	3.69	5.18
JC142-047-006-nl-002	*Desmophyllum sp.*	23.89	-20.72	995	29548	368	3.89	10.02	1.89	3.03	0.28	1.66	5.32
JC142-047-006-cl-001A	*Desmophyllum sp.*	23.89	-20.72	995	29604	391	3.61	9.77	1.80	0.54	LOD	NO DATA	5.44
JC142-047-006-cl-001A	*Desmophyllum sp.*	23.89	-20.72	995	29604	391	3.98	9.51	1.73	0.38	LOD	LOD	5.49

Full Sample ID	Taxa	Latitude	Longitude	Depth	U-series age	2 s	[Ca]	Li/Ca	Mg/Ca	Al/Ca	Mn/Ca	Fe/Ca	Li/Mg
JC142-047-006-cm-003	*Desmophyllum sp.*	23.89	-20.72	995	29744	262	4.20	11.10	2.25	1.78	0.06	0.92	4.94
JC142-047-006-cm-003	*Desmophyllum sp.*	23.89	-20.72	995	29744	262	3.91	9.12	1.74	0.59	LOD	0.49	5.26
JC142-047-006-cm-002	*Desmophyllum sp.*	23.89	-20.72	995	30085	244	3.76	9.41	1.62	2.18	LOD	3.65	5.82
JC142-047-006-cm-002	*Desmophyllum sp.*	23.89	-20.72	995	30085	244	3.87	12.25	2.30	16.10	2.85	NO DATA	5.34
JC142-047-006-cm-001	*Caryophyllia sp.*	23.89	-20.72	995	30208	321	3.80	11.86	2.35	8.39	2.54	7.96	5.05
JC142-047-006-cm-001	*Caryophyllia sp.*	23.89	-20.72	995	30208	321	4.16	13.55	2.67	14.72	3.04	NO DATA	5.08
JC142-047-006-c-col-001	*Desmophyllum dianthus*	23.89	-20.72	995	30362	1006	4.09	10.53	1.83	7.16	6.34	NO DATA	5.75
JC142-047-006-c-col-001	*Desmophyllum dianthus*	23.89	-20.72	995	30362	1006	3.73	9.58	1.59	24.47	0.68	NO DATA	6.04
JC142-047-006-cl-001	*Desmophyllum sp.*	23.89	-20.72	995	31889	750	3.52	13.12	2.25	3.90	0.54	2.90	5.82
JC142-047-006-cl-001	*Desmophyllum sp.*	23.89	-20.72	995	31889	750	4.21	12.28	2.19	23.68	5.89	NO DATA	5.60
JC142-113-007-cl-001	*Desmophyllum sp.*	23.78	-20.72	1797	31910	519	3.49	11.25	2.02	6.66	0.26	3.50	5.58
JC142-113-007-cl-001	*Desmophyllum sp.*	23.78	-20.72	1797	31910	519	3.99	11.17	2.02	10.50	4.22	NO DATA	5.53
JC142-113-007-cl-002	*Desmophyllum sp.*	23.78	-20.72	1797	32049	478	3.52	11.56	2.09	7.82	0.38	4.63	5.53
JC142-113-007-cl-002	*Desmophyllum sp.*	23.78	-20.72	1797	32049	478	4.05	12.19	2.20	29.24	1.79	NO DATA	5.55
JC142-113-007-cs-002	*Desmophyllum dianthus*	23.78	-20.72	1797	32221	485	4.27	9.58	1.95	LOD	LOD	1.10	4.92
JC142-113-007-cs-002	*Desmophyllum dianthus*	23.78	-20.72	1797	32221	485	3.74	7.53	1.36	2.37	1.04	NO DATA	5.56
JC142-113-007-cs-001	*Desmophyllum dianthus*	23.78	-20.72	1797	32624	546	4.21	10.79	2.03	11.62	2.09	NO DATA	5.32
JC142-113-007-cs-001	*Desmophyllum dianthus*	23.78	-20.72	1797	32624	546	4.11	15.58	2.72	162.48	14.99	NO DATA	5.73
JC142_094_001A	*Desmophyllum sp.*	23.90	-20.70	1952	34182	272	3.74	8.23	1.49	4.25	1.50	5.56	5.53

Full Sample ID	Taxa	Latitude	Longitude	Depth	U-series age	2 s	[Ca]	Li/Ca	Mg/Ca	Al/Ca	Mn/Ca	Fe/Ca	Li/Mg
JC142_094_001A	*Desmophyllum sp.*	23.90	-20.70	1952	34182	272	3.69	9.06	1.70	4.43	0.44	2.25	5.33

Table 5: Measurement of trace elements of the standards 8301f, 8301c, JCP.

STD		Li/Ca µmol/mol	B/Ca µmol/mol	Mg/Ca mmol/mol	Al/Ca µmol/mol	Mn/Ca µmol/mol	Ni/Ca µmol/mol	Cu/Ca umol/mol	Zn/Ca µmol/mol	Sr/Ca mmol/mol	Cd/Ca µmol/mol	Sn/Ca nmol/mol	Ba/Ca µmol/mol	Nd/Ca µmol/mol	U/Ca nmol/mol	Na/Ca mmol/mol	Fe/Ca µmol/mol	Co/Ca µmol/mol
8301f																		
	AVERAGE	8.79	138.58	2.63	89.87	48.19	9.03	5.95	10.68	1.35	0.57	66.92	4.06	5.13	68.89	3.01	18.33	0.52
	%RSD	0.3%	0.8%	0.6%	1.7%	0.5%	5.3%	3.1%	9.3%	0.5%	1.0%	148.5%	2.8%	0.4%	0.9%	0.7%	4.2%	1.9%
	Lit value	9.01	138.91	2.62	90.91	49.40	7.93	5.68	10.78	1.34	0.58	78.34	3.90	5.06	68.69	3.06	25.42	0.79
	%off lit value	-2.5%	-0.2%	0.7%	-1.2%	-2.5%	12.1%	4.5%	-1.0%	0.6%	-1.8%	-17.1%	3.9%	1.5%	0.3%	-1.6%	-38.7%	-51.3%
8301c																		
	AVERAGE	5.34	523.15	4.14	47.02	2.48	9.20	19.63	39.74	8.24	0.20	88.07	6.13	0.15	831.10	20.14	10.47	1.02
	%RSD	1.7%	1.5%	0.8%	5.3%	1.9%	4.9%	2.8%	12.4%	0.8%	1.8%	129.8%	1.0%	5.9%	1.8%	1.9%	16.5%	2.9%
	Lit value	5.40	528.12	4.11	48.13	2.59	8.10	19.61	38.83	8.10	0.20	81.60	5.92	0.16	828.90	20.04	15.44	1.11
	%off lit value	-1.1%	-0.9%	0.7%	-2.3%	-4.7%	11.9%	0.1%	2.3%	1.7%	0.3%	7.3%	3.4%	-0.6%	0.3%	0.5%	-47.4%	-9.1%
JCP																		
	AVERAGE	6.16	457.09	4.23	112.87	1.18	7.41	0.97	3.90	8.90	0.03	57.21	7.49	0.02	1197.09	20.08	12.94	0.44
	%RSD	1.5%	1.7%	0.9%	73.3%	4.2%	16.7%	21.4%	165.6%	0.9%	8.0%	40.5%	2.0%	11.5%	1.9%	1.3%	10.5%	16.2%
	Lit value	6.19	459.60	4.20						8.84			7.47		1192.00			
	%off lit value	-0.5%	-0.5%	0.8%						0.7%			0.3%		0.4%			

APPENDIX III

DATA TABLES FOR CHAPTER 4

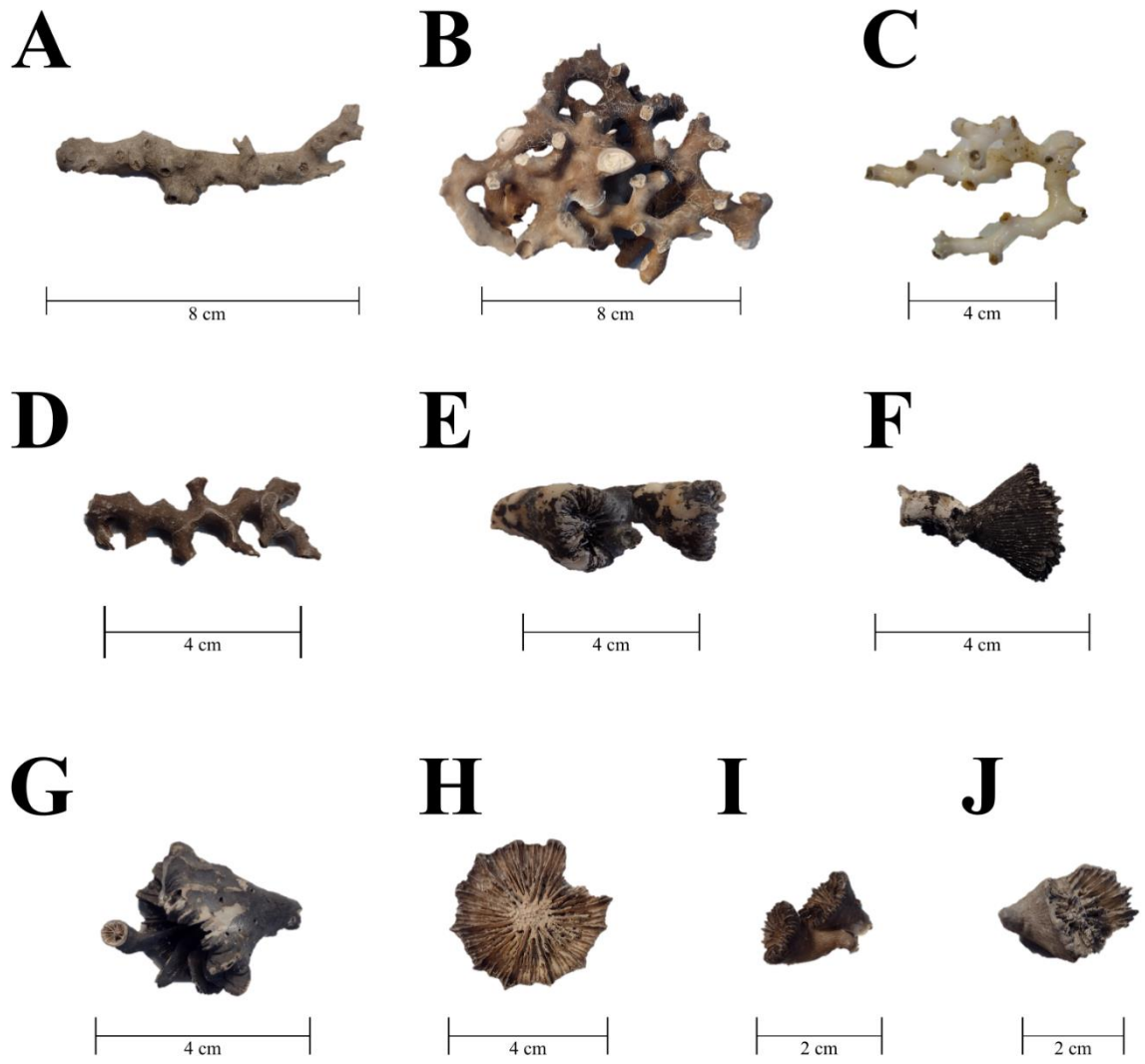

Plate 2: Cold-water corals from Rio Grande Rise and Brazilian shelf. (A) *Enallopsammia* sp. colony view (DY094-St23-Ena2); (B) and (C) *Solenosmilia variabilis* colony view (MNRJ-5739, MNRJ-5742-2); (D) *Madrepora oculata* colony view (MNRJ-9000); (E) *Caryophyllia berteriana* lateral view (MNRJ-8861); (F) *Paracyathus* sp. lateral view (MNRJ-8789); (G) *Desmophyllum dianthus* lateral view (MNRJ-8848); (H) *Stephanocyathus diadema* calicular view (MNRJ-5038-2); (I) *Trochocyathus rawsonii* lateral view (MNRJ-9028); (J) *Caryophyllia scobinosa* lateral view (MNRJ-9031).

Table 1: U-series laser ablation ages of deep-sea corals from Rio Grande Rise. Selection code column indicates the samples selected for U-series isotope dilution dating.

Full Sample ID	Taxa	Latitude	Longitude	Depth	Age uncorr	2s	$^{230}Th/^{238}U$	2s	Selection code
		DecDeg (N)	DecDeg (E)	m	yrs BP				
DY094-St23-ena2	*Enallopsammia sp.*	-30.82	-35.97	786	304	99	0.0039	0.0005	Selec. I.D.
MNRJ 9000	*Madrepora oculata*	-30.75	-34.74	900	412	175	0.0051	0.0009	Selec. I.D.
MNRJ-8875-ENA2	*Enallopsammia rostrata*	-30.66	-36.10	1150	582	255	0.0068	0.0013	
DY094-St23-ena1	*Enallopsammia sp.*	-30.82	-35.97	786	1553	121	0.0169	0.0006	
MNRJ-9052	*Enallopsammia rostrata*	-31.16	-32.21	830	2207	201	0.0237	0.0010	
MNRJ 9044	*Caryophyllia berteriana*	-30.34	-36.07		2474	268	0.0264	0.0014	
MNRJ 9052	*Enallopsammia rostrata*	-31.16	-32.21	830	2503	266	0.0267	0.0014	
MNRJ-9031	*Caryophyllia scobinosa*	-31.15	-34.80	1987	2652	251	0.0282	0.0013	Selec. I.D.
MNRJ 9028	*Trochocyathus rawsonii*	-29.84	-36.55	912	2858	341	0.0303	0.0017	Selec. I.D.
MNRJ 9021	*Trochocyathus rawsonii*	-31.37	-34.42	2314	3711	184	0.0390	0.0009	
MNRJ 9022	*Caryophylliidae sp.*	-31.14	-35.61		3783	499	0.0397	0.0025	Selec. I.D.
MNRJ 8900	*Enallopsammia rostrata*	-31.16	-32.21	830	4431	274	0.0463	0.0014	
MNRJ 8873	*Caryophyllia berteriana*	-32.11	-32.84	2350	4750	329	0.0495	0.0016	Selec. I.D.
MNRJ-9034	*Enallopsammia rostrata*	-30.62	-36.81	1575	5008	325	0.0520	0.0016	
MNRJ 8977	*Caryophylliidae*	-32.10	-32.66	1798	5038	365	0.0523	0.0018	
MNRJ 9017	*Caryophyllia berteriana*	-32.71	-32.71	1250	5215	356	0.0541	0.0017	
MNRJ 9034	*Enallopsammia rostrata*	-30.62	-36.81	1575	5552	338	0.0575	0.0017	
MNRJ-8875-ENA1	*Enallopsammia rostrata*	-30.66	-36.10	1150	7399	479	0.0757	0.0023	
DY094-St23-car	*Caryophylliidae*	-30.82	-35.97	786	8237	530	0.0838	0.0025	Selec. I.D.
MNRJ 9058	*Enallopsammia rostrata*	-30.49	-36.30	990	8993	509	0.0911	0.0024	
MNRJ-8994	*Enallopsammia rostrata*	-30.73	-35.97	1060	9166	484	0.0928	0.0023	
MNRJ 8847	*Caryophyllia berteriana*	-33.46	-31.31	1878	9305	568	0.0942	0.0027	Selec. I.D.
MNRJ 9070	*Caryophylliidae*	-34.19	-30.97	2600	11300	512	0.1131	0.0023	Selec. I.D.

Full Sample ID	Taxa	Latitude	Longitude	Depth	Age uncorr	2s	$^{230}Th/^{238}U$	2s	Selection code
MNRJ 8993	*Caryophylliidae*	-32.10	-32.82	1148	12106	531	0.1207	0.0024	Selec. I.D.
MNRJ-8865	*Caryophyllia berteriana*	-32.13	-32.78	1631	13863	583	0.1370	0.0026	
MNRJ 8861	*Caryophyllia berteriana*	-33.81	-30.70	1680	14032	666	0.1385	0.0030	Selec. I.D.
MNRJ 8797	*Caryophylliidae*	-34.12	-30.95	2172	14321	585	0.1411	0.0026	Selec. I.D.
DY094_032_G002-2	*Caryophylliidae*	-30.74	-35.95	1504	14775	657	0.1453	0.0029	Selec. I.D.
MNRJ 8789	*Paracyathus sp.*	-30.19	-36.41		14964	646	0.1470	0.0028	Selec. I.D.
MNRJ 8916	*Desmophyllum dianthus*	-32.71	-32.80	1050	20006	765	0.1918	0.0032	Selec. I.D.
MNRJ 8791	*Caryophyllia berteriana*	-31.05	-35.82	1330	24204	821	0.2274	0.0032	Selec. I.D.
MNRJ 9025	*Caryophyllia sp.*	-32.71	-32.71	1250	25052	867	0.2344	0.0034	Selec. I.D.
MNRJ 8906-DES	*Desmophyllum dianthus*	-33.62	-31.13	2500	25508	981	0.2382	0.0039	
MNRJ 9040	*Caryophyllia berteriana*	-30.58	-36.14	1500	29426	980	0.2698	0.0036	Selec. I.D.
MNRJ-8848	*Desmophyllum dianthus*	-30.10	-36.83	1542	30157	1152	0.2756	0.0043	
MNRJ 9004	*Caryophyllia berteriana*	-33.63	-30.90	1550	32875	1272	0.2967	0.0047	Selec. I.D.
DY094_032_G002-1	*Caryophylliidae*	-30.74	-35.95	1504	33158	988	0.2988	0.0035	Selec. I.D.
MNRJ-8875-DES	*Desmophyllum dianthus*	-30.66	-36.10	1150	34733	1381	0.3108	0.0050	
MNRJ 8860	*Crispatotrochus squiresi*	-31.13	-35.41	1087	35800	1572	0.3187	0.0056	
MNRJ 8882	*Caryophylliidae*	-30.62	-36.81	1575	37494	1227	0.3312	0.0042	Selec. I.D.
MNRJ-8875-CAR	*Caryophyllia berteriana*	-30.66	-36.10	1150	37884	1321	0.3341	0.0045	Selec. I.D.
MNRJ 8976	*Caryophyllia berteriana*	-32.13	-32.78	1631	38900	1334	0.3415	0.0045	Selec. I.D.
MNRJ 9015	*Caryophyllia berteriana*	-30.75	-35.06	1600	39528	1721	0.3460	0.0060	Selec. I.D.
MNRJ 8773	*Caryophyllia berteriana*	-30.95	-35.04	1740	43144	2003	0.3715	0.0067	
MNRJ 9063-2	*Caryophyllia berteriana*	-32.10	-32.66	1798	60531	2674	0.4825	0.0075	
MNRJ-8886	*Caryophyllia berteriana*	-30.34	-36.07		60976	2434	0.4852	0.0067	
MNRJ 9063-1	*Caryophyllia berteriana*	-32.10	-32.66	1798	75276	2572	0.5631	0.0061	
MNRJ 8955	*Caryophyllia berteriana*	-30.10	-36.83	1542	89481	3761	0.6305	0.0078	
MNRJ 8906-SOL	*Solenosmilia variabilis*	-33.62	-31.13	2500	95517	4080	0.6564	0.0080	
MNRJ 9097	*Caryophylliidae*	-30.46	-36.56	1387	113283	4617	0.7243	0.0075	

Full Sample ID	Taxa	Latitude	Longitude	Depth	Age uncorr	2s	$^{230}Th/^{238}U$	2s	Selection code
MNRJ 9012	*Caryophylliidae*	-30.89	-34.79	1900	148530	7603	0.8279	0.0088	
MNRJ 9064	*Solenosmilia variabilis*	-31.16	-35.39	1220	199632	18029	0.9250	0.0125	
MNRJ 8843	*Bathelia candida*	-31.17	-34.80	870	262827	36892	0.9900	0.0123	

Table 2: U-series laser ablation ages of deep-sea corals from the Brazilian margin. Selection code column indicates the samples selected for U-series isotope dilution dating.

Full Sample ID	Taxa	Latitude	Longitude	Depth	Age uncorr	2s	$^{230}Th/^{238}U$	2s	Selection code
		DecDeg (N)	DecDeg (E)	m	yrs BP				
MNRJ-6443	*Enallopsammia rostrata*	-26.92	-47.00	766	257	190	0.0034	0.0010	
MNRJ-6663-1	*Solenosmilia variabilis*	-22.43	-39.96	1077	263	213	0.0035	0.0011	
MNRJ-6431	*Solenosmilia variabilis*	-34.55	-51.82	629	320	179	0.0041	0.0009	
MNRJ-6410	*Solenosmilia variabilis*	-26.48	-45.69	861	385	266	0.0048	0.0014	
MNRJ-6712	*Enallopsammia rostrata*	-2.26	-38.27	240	502	155	0.0060	0.0008	
MNRJ-6688-2	*Solenosmilia variabilis*	-22.36	-40.18	867	769	213	0.0088	0.0011	
MNRJ-6692	*Solenosmilia variabilis*	-22.43	-39.96	1077	898	219	0.0101	0.0011	Selec. I.D.
MNRJ-5683	*Solenosmilia variabilis*	-22.40	-39.91	1150	1039	186	0.0116	0.0010	Selec. I.D.
MNRJ-6415	*Enallopsammia rostrata*	-28.35	-46.82	768	1112	161	0.0124	0.0008	
MNRJ-6688-1	*Solenosmilia variabilis*	-22.36	-40.18	867	1212	214	0.0134	0.0011	
MNRJ-6663-2	*Solenosmilia variabilis*	-22.43	-39.96	1077	1212	224	0.0134	0.0012	
MNRJ-6698	*Solenosmilia variabilis*	-22.43	-39.96	1073	1786	217	0.0193	0.0011	Selec. I.D.
MNRJ-6297	*Enallopsammia rostrata*	-24.27	-43.40	600	2970	242	0.0315	0.0012	
MNRJ-5038-2	*Stephanocyathus diadema*	-25.93	-43.93	2212	3495	364	0.0368	0.0018	Selec. I.D.
MNRJ-5038-1	*Stephanocyathus diadema*	-25.93	-43.93	2212	5381	387	0.0558	0.0019	Selec. I.D.
MNRJ-6414	*Solenosmilia variabilis*	-34.38	-46.82	768	6243	398	0.0643	0.0019	
MNRJ-6392	*Solenosmilia variabilis*	-28.35	-46.82	768	6515	586	0.0670	0.0029	
MNRJ-5742	*Solenosmilia variabilis*	-22.22	-39.87	1059	6662	514	0.0684	0.0025	Selec. I.D.
MNRJ-5739	*Solenosmilia variabilis*	-22.40	-39.91	1150	6904	341	0.0708	0.0016	Selec. I.D.
MNRJ-6393-des	*Desmophyllum dianthus*	-28.35	-46.82	768	7083	463	0.0726	0.0022	Selec. I.D.
MNRJ-6393-sol	*Solenosmilia variabilis*	-28.35	-46.82	768	7384	431	0.0755	0.0021	
MNRJ-6005	*Solenosmilia variabilis*	-21.38	-40.18	625	13401	653	0.1327	0.0029	Selec. I.D.
MNRJ-6405	*Solenosmilia variabilis*	-24.27	-43.40	600	17848	855	0.1729	0.0037	Selec. I.D.
MNRJ-5737	*Solenosmilia variabilis*	-22.41	-39.93	1105	45944	2043	0.3907	0.0067	Selec. I.D.

Table 3: U-series isotope dilution ages of deep-sea corals from Rio Grande Rise. Selection code column indicates the samples not included in the discussion and includes the rationale (see text for details).

Full Sample ID	**Taxa**	**Lat**	**Lon**	**Depth**	**Age uncorr**	**2s**	**Age corr**	**2s**	**δ^{234}Um**	**2s**	**δ^{234}Ui**	**2s**	**^{238}U**	**2s**	**^{232}Th**	**2s**	**^{230}Th/^{238}U corrected**	**2s**
		DecDeg (N)	**DecDeg (E)**	**m**	**yrs**		**yrs BP**		**‰**		**‰**		**ppm**		**ppb**		**activity ratio**	
DY094_032_G002-1	*Caryophylliidae*	-30.74	-35.95	1504	38890	218	38739	232	124.5	1.1	138.9	1.2	4.6	0.009	0.8	0.0033	0.3389	0.001
DY094_032_G002-2	*Caryophylliidae*	-30.74	-35.95	1504	15699	80	15419	222	139.5	1.1	145.8	1.1	4.0	0.008	1.8	0.0075	0.1530	0.0007
DY094-St23-car	*Caryophylliidae*	-30.82	-35.97	786	8627	43	8264	294	145.3	1.1	148.7	1.2	3.8	0.008	2.4	0.0099	0.0871	0.0004
DY094-St23-ena2	*Enallopsammia sp.*	-30.82	-35.97	786	150	1.8	68	10	146.0	1.4	146.1	1.4	4.7	0.013	0.1	0.0005	0.0016	0.00002
MNRJ 8773-1	*Caryophyllia berteriana*	-30.95	-35.04	1740	48001	283	47723	347	124.9	1.2	143.0	1.4	3.0	0.006	1.3	0.0057	0.4030	0.0018
MNRJ 8789	*Paracyathus sp.*	-30.19	-36.41		16322	82	15945	316	140.9	1.2	147.4	1.3	3.4	0.007	2.3	0.0092	0.1588	0.0007
MNRJ 8791	*Caryophyllia berteriana*	-31.05	-35.82	1330	30539	165	30293	239	129.8	1.2	141.4	1.3	3.9	0.008	1.5	0.0061	0.2770	0.0013
MNRJ 8797	*Caryophylliidae*	-34.12	-30.95	2172	16267	83	16010	203	139.9	1.1	146.4	1.1	4.3	0.009	1.7	0.0072	0.1582	0.0007
MNRJ 8847	*Caryophyllia berteriana*	-33.46	-31.31	1878	10094	52	9730	298	142.9	1.0	146.9	1.1	3.5	0.007	2.2	0.0094	0.1011	0.0005
MNRJ 8861-1	*Caryophyllia berteriana*	-33.81	-30.70	1680	13076	68	12874	147	141.9	1.2	147.2	1.3	4.3	0.009	1.2	0.0051	0.1292	0.0006
MNRJ 8861-2	*Caryophyllia berteriana*	-33.81	-30.70	1680	12705	66	12392	250	142.2	1.2	147.3	1.2	4.4	0.009	2.3	0.0096	0.1257	0.0006
MNRJ 8873	*Caryophyllia berteriana*	-32.11	-32.84	2350	5558	29	5361	128	144.6	1.2	146.9	1.2	4.0	0.009	1.1	0.0045	0.0569	0.0003
MNRJ 8882	*Caryophylliidae*	-30.62	-36.81	1575	39742	223	39299	432	125.1	1.0	139.9	1.1	5.3	0.011	4.2	0.0176	0.3453	0.0016

Full Sample ID	Taxa	Lat	Lon	Depth	Age uncorr	2s	Age corr	2s	δ^{234}Um	2s	δ^{234}Ui	2s	^{238}U	2s	^{232}Th	2s	^{230}Th/^{238}U corrected	2s
MNRJ 8906-DES	*Desmophyllum dianthus*	-33.62	-31.13	2500	24311	128	23736	519	142.0	1.1	151.9	1.2	3.3	0.007	3.6	0.0149	0.2289	0.0011
MNRJ 8916	*Desmophyllum dianthus*	-32.71	-32.80	1050	21597	114	21199	346	133.3	1.2	141.6	1.2	4.7	0.011	3.3	0.0139	0.2041	0.00095
MNRJ 8976	*Caryophyllia berteriana*	-32.13	-32.78	1631	39319	219	39140	244	125.3	1.1	140.0	1.2	4.3	0.009	1.0	0.0041	0.3423	0.00155
MNRJ 8977	*Caryophylliidae*	-32.10	-32.66	1798	6283	33	6119	97	145.1	1.1	147.7	1.1	3.8	0.008	0.8	0.0032	0.0641	0.00032
MNRJ 8993-1	*Caryophylliidae*	-32.10	-32.82	1148	15298	79	15145	113	138.8	1.1	144.9	1.1	3.1	0.006	0.6	0.0023	0.1493	0.00070
MNRJ 8993-2	*Caryophylliidae*	-32.10	-32.82	1148	15471	80	15224	192	139.3	1.1	145.4	1.1	5.8	0.012	2.2	0.0092	0.1509	0.00072
MNRJ 9000	*Madrepora oculata*	-30.75	-34.74	900	574	3.9	484	19	145.3	1.1	145.5	1.1	4.8	0.010	0.2	0.0010	0.0060	0.00004
MNRJ 9004	*Caryophyllia berteriana*	-33.63	-30.90	1550	33165	189	32854	305	127.6	1.2	140.1	1.3	4.7	0.010	2.4	0.0101	0.2969	0.00141
MNRJ 9015	*Caryophyllia berteriana*	-30.75	-35.06	1600	47691	278	47438	330	123.3	1.1	141.1	1.2	3.8	0.008	1.5	0.0062	0.4003	0.00182
MNRJ 9022	*Caryophyllia sp.*	-31.14	-35.61		3593	19	3406	116	146.4	1.2	147.9	1.2	3.4	0.007	0.8	0.0035	0.0371	0.00019
MNRJ 9025	*Caryophyllia sp.*	-32.71	-32.71	1250	29059	154	28610	409	129.4	1.1	140.3	1.2	4.7	0.010	3.8	0.0158	0.2651	0.00121
MNRJ 9028	*Trochocyathus rawsonii*	-29.84	-36.55	912	2943	15	2789	83	145.7	1.0	146.9	1.0	4.7	0.010	0.8	0.0035	0.0305	0.00015
MNRJ 9040	*Caryophyllia berteriana*	-30.58	-36.14	1500	32286	179	32006	275	128.0	1.2	140.1	1.3	4.9	0.011	2.2	0.0092	0.2902	0.00136
MNRJ 9044	*Caryophyllia berteriana*	-30.34	-36.07		2575	14	2450	55	145.3	1.1	146.4	1.1	3.5	0.007	0.4	0.0017	0.0267	0.00014
MNRJ 9070	*Caryophylliidae*	-34.19	-30.97	2600	13932	70	13553	315	142.4	1.1	148.0	1.1	4.8	0.010	3.2	0.0132	0.1372	0.00063
MNRJ-8849	*Desmophyllum dianthus*	-30.10	-36.83	1542	32001	172	31672	311	129.9	1.2	142.1	1.3	3.7	0.007	2.1	0.0085	0.2885	0.00131
MNRJ-8865	*Caryophyllia berteriana*	-32.13	-32.78	1631	1814	9.3	1629	114	146.0	1.1	146.7	1.1	9.3	0.017	2.3	0.0092	0.0189	0.00009
MNRJ-8865	*Caryophyllia berteriana*	-32.13	-32.78	1631	18923	967	18221	1150	137.2	1.1	144.5	1.3	1.2	0.007	1.7	0.0640	0.1815	0.00847

Full Sample ID	Taxa	Lat	Lon	Depth	Age uncorr	2s	Age corr	2s	δ^{234}Um	2s	δ^{234}Ui	2s	^{238}U	2s	^{232}Th	2s	^{230}Th/^{238}U corrected	2s
MNRJ-8875-CAR	*Caryophyllia berteriana*	-30.66	-36.10	1150	38401	206	37784	587	125.9	1.2	140.1	1.3	5.7	0.011	6.7	0.0271	0.3358	0.00147
MNRJ-9031	*Caryophyllia scobinosa*	-31.15	-34.80	1987	3332	17	3197	65	145.4	1.1	146.8	1.1	5.2	0.011	0.7	0.0031	0.0344	0.00017

Table 4: U-series isotope dilution ages of deep-sea corals from the Brazilian margin.

Full Sample ID	**Taxa**	**Lat**	**Lon**	**Depth**	**Age uncorr**	**2s**	**Age corr**	**2s**	**$\delta^{234}U$ m**	**2s**	**$\delta^{234}Ui$**	**2s**	**^{238}U**	**2s**	**^{232}Th**	**2s**	**$^{230}Th/^{238}U$**	**2s**
		DecDeg (N)	**DecDeg (E)**	**m**	**yrs**		**yrs BP**		**‰**		**‰**		**ppm**		**ppb**		**activity ratio**	
MNRJ-5742-2	*Solenosmilia variabilis*	-22.22	-39.87	1059	113	1.4	90	23	146.4	1.1	146.4	1.1	3.6	0.007	0.2	0.0008	0.0012	0.00001
MNRJ-5683	*Solenosmilia variabilis*	-22.40	-39.91	1150	827	5.6	699	128	145.4	1.1	145.7	1.1	5.1	0.010	1.4	0.0059	0.0086	0.00006
MNRJ-6692	*Solenosmilia variabilis*	-22.43	-39.96	1077	780	4.8	729	51	146.1	1.1	146.4	1.1	4.1	0.008	0.5	0.0020	0.0082	0.00005
MNRJ-6698	*Solenosmilia variabilis*	-22.43	-39.96	1073	1291	8	1190	102	145.9	1.1	146.3	1.1	4.2	0.008	0.9	0.0038	0.0135	0.00008
MNRJ-5038-2	*Stephanocyathus diadema*	-25.93	-43.93	2212	3821	20	3202	621	145.8	1.1	147.1	1.2	4.2	0.008	5.7	0.0235	0.0394	0.00020
MNRJ-5038-1	*Stephanocyathus diadema*	-25.93	-43.93	2212	5865	31	4852	1019	145.2	1.1	147.2	1.2	4.4	0.009	9.6	0.0404	0.0599	0.00030
MNRJ-6393-des	*Desmophyllum dianthus*	-28.35	-46.82	768	6507	34	6343	167	146.6	1.0	149.2	1.1	3.2	0.006	1.1	0.0049	0.0664	0.00033
MNRJ-5739	*Solenosmilia variabilis*	-22.40	-39.91	1150	6911	34	6849	71	144.5	1.1	147.3	1.1	4.6	0.009	0.6	0.0026	0.0703	0.00033
MNRJ-5742-1	*Solenosmilia variabilis*	-22.22	-39.87	1059	7123	36	7098	44	144.0	1.1	146.9	1.1	3.9	0.008	0.2	0.0011	0.0723	0.00035
MNRJ-6005	*Solenosmilia variabilis*	-21.38	-40.18	625	14112	72	14018	118	141.0	1.1	146.7	1.1	3.5	0.007	0.7	0.0030	0.1387	0.00065
MNRJ-6405	*Solenosmilia variabilis*	-24.27	-43.40	600	17919	94	17831	128	138.8	1.1	146.0	1.1	3.8	0.008	0.7	0.0030	0.1729	0.00082
MNRJ-5737	*Solenosmilia variabilis*	-22.41	-39.93	1105	51038	302	50941	317	125.3	1.0	144.7	1.1	3.1	0.006	0.7	0.0028	0.4234	0.00195

Table 5: Radiocarbon parameters of deep-sea corals from Rio Grande Rise.

Full Sample ID	**Taxa**	**Latitude**	**Longitude**	**Depth**	**U-series age**	**2 s**	**^{14}C age**	**2s**	**Fraction modern (Fm)**	**1s**	**$\Delta^{14}C$**	**2s**	**$\Delta\Delta^{14}C$**	**2s**	**B-atmosphere**	**2s**
		°N	**°E**	**m**	**yr BP**	**yr**	**yr**	**yr**			**‰**		**‰**	**‰**	**yr**	**yr**
DY094-St23-ena2	Enallopsammia sp.	-30.82	-35.97	786	68	10	855	48	0.8991	0.0027	-86	7	-86	9	722	81
MNRJ 9000	Madrepora oculata	-30.75	-34.74	900	484	19	1320	48	0.8485	0.0026	-93	7	-86	13	725	108
MNRJ 9028	Trochocyathus rawsonii	-29.84	-36.55	912	2789	83	3173	50	0.6737	0.0021	-48	14	-49	15	405	126
MNRJ-9031	Caryophyllia scobinosa	-31.15	-34.80	1987	3197	65	3811	50	0.6223	0.0019	-76	11	-90	11	748	93
DY094-St23-car	Caryophylliidae	-30.82	-35.97	786	8264	294	7781	54	0.8991	0.0027	41	47	-33	54	250	420
MNRJ 8861-2	Caryophyllia berteriana	-33.81	-30.70	1680	12392	250	10734	66	0.2628	0.0011	186	45	-42	40	282	245
MNRJ 8861-1	Caryophyllia berteriana	-33.81	-30.70	1680	12874	147	11232	68	0.2470	0.0011	183	29	-30	25	206	172
DY094_032_G002-2	Caryophylliidae	-30.74	-35.95	1504	15419	222	13594	60	0.1841	0.0007	199	41	-101	32	649	215
MNRJ 8797	Caryophylliidae	-34.12	-30.95	2172	16010	203	14150	62	0.1718	0.0007	202	38	-123	30	787	200
MNRJ 8916	Desmophyllum dianthus	-32.71	-32.80	1050	21199	346	18441	74	0.1007	0.0005	320	69	-144	50	838	319

Table 6: Radiocarbon parameters of deep-sea corals from the Brazilian margin.

Full Sample ID	Taxa	Latitude	Longitude	Depth	U-series age	2 s	^{14}C age	2s	Fraction modern (Fm)	1s	$\Delta^{14}C$	2s	$\Delta\Delta^{14}C$	2s	B-atm	2s
		°N	°E	m	yr BP	yr	yr	yr			‰		‰	‰	yr	yr
MNRJ-5742-2	Solenosmilia variabilis	-22.22	-39.87	1059	18	23	851	48	0.8995	0.0027	-91	7	-86	7	726	61
MNRJ-6698	Solenosmilia variabilis	-22.43	-39.96	1073	1118	102	2060	50	0.7738	0.0024	-106	15	-94	16	806	139
MNRJ-5038-2	Stephanocyathus diadema	-25.93	-43.93	2212	3130	621	3562	50	0.6419	0.0020	-54	85	-65	74	539	616
MNRJ-6393-des	Desmophyllum dianthus	-28.35	-46.82	768	6271	167	6327	52	0.4549	0.0015	-20	26	-99	34	771	262
MNRJ-5739	Solenosmilia variabilis	-22.40	-39.91	1150	6777	71	6831	52	0.4273	0.0014	-22	13	-105	12	822	99
MNRJ-5742-1	Solenosmilia variabilis	-22.22	-39.87	1059	7026	44	7174	52	0.4094	0.0013	-34	10	-127	12	989	90
MNRJ-6005	Solenosmilia variabilis	-21.38	-40.18	625	13946	118	12556	76	0.2095	0.0010	142	24	-68	34	463	239
MNRJ-6405	Solenosmilia variabilis	-24.27	-43.40	600	17759	128	15440	64	0.1463	0.0006	265	27	-148	37	889	224

Table 7: Mean values of trace elements measurements of deep-sea corals from Rio Grande Rise.

Full Sample ID	Taxa	Lat	Lon	Depth	U-series age	2 s	[Ca]	Li/Ca	Mg/Ca	Al/Ca	Mn/Ca	Fe/Ca	Li/Mg	Selection code
		DecDeg (N)	DecDeg (E)	m	yr BP	yr	mM	µmol/mol	mmol/mol	µmol/mol	µmol/mol	µmol/mol	mmol/mol	
DY094-St23-ena2	*Enallopsammia sp.*	-30.82	-35.97	786	68	10	4.12	9.50	2.32	1.91	0.50	0.54	4.10	
MNRJ 9000	*Madrepora oculata*	-30.75	-34.74	900	484	19	3.97	10.53	2.41	2.70	1.14	1.51	4.38	
MNRJ-8865	*Caryophyllia berteriana*	-32.13	-32.78	1631	1629	114	3.97	6.72	1.31	0.89	0.19	0.25	5.12	High 238U
MNRJ 9044	*Caryophyllia berteriana*	-30.34	-36.07		2450	55	4.07	9.41	2.16	2.41	1.17	1.86	4.36	No depth info
MNRJ 9028	*Trochocyathus rawsonii*	-29.84	-36.55	912	2789	83	3.81	10.93	2.50	3.05	1.98	1.92	4.37	
MNRJ-9031	*Caryophyllia scobinosa*	-31.15	-34.80	1987	3197	65	4.02	7.87	1.54	12.47	1.67	5.10	5.13	
MNRJ 9022	*Caryophylliidae sp.*	-31.14	-35.61		3406	116	4.07	10.80	2.33	2.75	2.24	1.39	4.63	No depth info
MNRJ 8873	*Caryophyllia berteriana*	-32.11	-32.84	2350	5361	128	3.83	9.60	2.18	2.34	2.97	6.64	4.41	
MNRJ 8977	*Caryophylliidae*	-32.10	-32.66	1798	6119	97	3.92	8.79	1.93	5.02	0.93	2.43	4.56	
DY094-St23-car	*Caryophylliidae*	-30.82	-35.97	786	8264	294	3.92	11.42	2.72	4.33	1.53	6.56	4.20	
MNRJ 8847	*Caryophyllia berteriana*	-33.46	-31.31	1878	9730	298	3.91	10.25	2.36	4.07	4.34	4.66	4.34	
MNRJ 8861-2	*Caryophyllia berteriana*	-33.81	-30.70	1680	12392	250	3.85	7.45	1.55	3.07	1.90	1.26	4.81	
MNRJ 8861-1	*Caryophyllia berteriana*	-33.81	-30.70	1680	12874	147	3.94	8.06	1.67	1.47	0.44	0.64	4.82	
MNRJ 9070	*Caryophylliidae*	-34.19	-30.97	2600	13553	315	4.17	9.77	1.91	25.54	5.53	13.86	5.11	
MNRJ 8993-1	*Caryophylliidae*	-32.10	-32.82	1148	15145	113	3.75	11.06	2.39	0.69	0.61	2.92	4.63	
DY094_032_G002-2	*Caryophylliidae*	-30.74	-35.95	1504	15419	222	4.02	9.45	2.05	1.17	0.88	0.93	4.61	

Full Sample ID	Taxa	Lat	Lon	Depth	U-series age	2 s	[Ca]	Li/Ca	Mg/Ca	Al/Ca	Mn/Ca	Fe/Ca	Li/Mg	Selection code
MNRJ 8789	*Paracyathus sp.*	-30.19	-36.41		15945	316	4.01	13.00	2.65	3.83	13.58	5.69	4.90	No depth info
MNRJ 8797	*Caryophylliidae*	-34.12	-30.95	2172	16010	203	4.00	11.16	2.09	3.77	3.78	4.39	5.35	
MNRJ-8865	*Caryophyllia berteriana*	-32.13	-32.78	1631	18221	1150	4.11	9.58	1.64	4.51	3.48	8.73	5.83	Low 238U
MNRJ 8916	*Desmophyllum dianthus*	-32.71	-32.80	1050	21199	346	3.99	13.83	2.41	5.03	0.71	2.58	5.73	
MNRJ 8906-DES	*Desmophyllum dianthus*	-33.62	-31.13	2500	23736	519	3.81	16.30	2.65	36.49	10.82	26.25	6.15	High δ234 Ui
MNRJ 9025	*Caryophyllia sp.*	-32.71	-32.71	1250	28610	409	4.00	10.97	1.88	1.98	0.96	1.71	5.83	
MNRJ 8791	*Caryophyllia berteriana*	-31.05	-35.82	1330	30293	239	3.78	11.86	1.98	5.38	2.09	8.98	5.99	
MNRJ-8848	*Desmophyllum dianthus*	-30.10	-36.83	1542	31672	311	4.00	11.02	1.96	11.91	2.33	13.90	5.61	
MNRJ 9040	*Caryophyllia berteriana*	-30.58	-36.14	1500	32006	275	4.04	12.15	1.96	10.75	2.07	10.10	6.21	
MNRJ 9004	*Caryophyllia berteriana*	-33.63	-30.90	1550	32854	305	5.86	8.65	1.47	7.22	1.77	4.27	5.88	
MNRJ-8875-CAR	*Caryophyllia berteriana*	-30.66	-36.10	1150	37784	587	3.99	10.69	2.20	7.32	5.98	9.82	4.86	
DY094_032_G002-1	*Caryophylliidae*	-30.74	-35.95	1504	38739	232	3.87	8.54	1.82	3.88	3.60	4.63	4.69	
MNRJ 8976	*Caryophyllia berteriana*	-32.13	-32.78	1631	39140	244	3.82	11.95	2.45	1.02	0.31	0.77	4.88	
MNRJ 8882	*Caryophylliidae*	-30.62	-36.81	1575	39299	432	3.83	9.52	1.80	2.42	0.33	1.18	5.28	
MNRJ 9015	*Caryophyllia berteriana*	-30.75	-35.06	1600	47438	330	3.82	9.40	1.94	4.19	1.72	4.39	4.86	
MNRJ 8773-1	*Caryophyllia berteriana*	-30.95	-35.04	1740	47723	347	2.80	11.92	2.46	11.71	2.04	6.59	4.85	
MNRJ 8773-2	*Caryophyllia berteriana*	-30.95	-35.04	1740	247530	4260	3.56	8.43	1.84	1.19	0.35	0.30	4.58	Too old

Table 8: Mean values of trace elements measurements of deep-sea corals from the Brazilian margin.

Full Sample ID	**Taxa**	**Lat**	**Lon**	**Depth**	**U-series age**	**2 s**	**[Ca]**	**Li/Ca**	**Mg/Ca**	**Al/Ca**	**Mn/Ca**	**Fe/Ca**	**Li/Mg**
		DecDeg (N)	**DecDeg (E)**	**m**	**yr BP**	**yr**	**mM**	**µmol/mol**	**mmol/mol**	**µmol/mol**	**µmol/mol**	**µmol/mol**	**mmol/mol**
MNRJ-5742-2	*Solenosmilia variabilis*	-22.22	-39.87	1059	18	23	3.88	12.04	2.70	3.02	<LOD	0.73	4.46
MNRJ-5683	*Solenosmilia variabilis*	-22.40	-39.91	1150	627	128	3.77	11.87	2.59	8.98	<LOD	3.86	4.59
MNRJ-6692	*Solenosmilia variabilis*	-22.43	-39.96	1077	657	51	3.92	11.04	2.47	7.62	2.34	2.11	4.48
MNRJ-6698	*Solenosmilia variabilis*	-22.43	-39.96	1073	1118	102	3.86	10.86	2.47	6.68	2.61	5.90	4.40
MNRJ-5038-2	*Stephanocyathus diadema*	-25.93	-43.93	2212	3130	621	4.09	11.06	2.21	19.57	3.49	14.04	5.00
MNRJ-5038-1	*Stephanocyathus diadema*	-25.93	-43.93	2212	4780	1019	3.88	9.79	1.92	76.29	9.08	56.42	5.10
MNRJ-6393-des	*Desmophyllum dianthus*	-28.35	-46.82	768	6271	167	3.70	12.78	2.93	5.16	24.28	35.79	4.36
MNRJ-5739	*Solenosmilia variabilis*	-22.40	-39.91	1150	6777	71	3.99	10.12	2.38	1.67	<LOD	1.71	4.26
MNRJ-5742-1	*Solenosmilia variabilis*	-22.22	-39.87	1059	7026	44	3.93	9.48	2.41	2.25	<LOD	1.15	3.93
MNRJ-6005	*Solenosmilia variabilis*	-21.38	-40.18	625	13946	118	4.02	11.42	3.03	5.27	<LOD	13.39	3.77
MNRJ-6405	*Solenosmilia variabilis*	-24.27	-43.40	600	17759	128	3.60	13.17	2.73	3.96	8.74	8.20	4.83
MNRJ-5737	*Solenosmilia variabilis*	-22.41	-39.93	1105	50869	317	4.09	13.08	2.99	7.44	9.46	22.68	4.38

Table 9: Replicates of trace elements measurements of deep-sea corals from Rio Grande Rise.

Full Sample ID	Taxa	Lat	Lon	Depth	U-series age	2 s	[Ca]	Li/Ca	Mg/Ca	Al/Ca	Mn/Ca	Fe/Ca	Li/Mg	Selection code
		DecDeg (N)	DecDeg (E)	m	yr BP	yr	mM	µmol/mol	mmol/mol	µmol/mol	µmol/mol	µmol/mol	mmol/mol	
DY094-St23-ena2	*Enallopsammia sp.*	-30.82	-35.97	786	68	10	4.15	9.34	2.32	1.74	0.23	0.51	4.03	
DY094-St23-ena2	*Enallopsammia sp.*	-30.82	-35.97	786	68	10	4.09	9.66	2.32	2.08	0.78	0.58	4.17	
MNRJ 9000	*Madrepora oculata*	-30.75	-34.74	900	484	19	3.97	10.34	2.35	3.32	1.22	1.80	4.40	
MNRJ 9000	*Madrepora oculata*	-30.75	-34.74	900	484	19	3.96	10.73	2.46	2.08	1.06	1.21	4.35	
MNRJ-8865	*Caryophyllia berteriana*	-32.13	-32.78	1631	1629	114	4.10	6.80	1.29	1.10	0.16	0.14	5.26	High 238U
MNRJ-8865	*Caryophyllia berteriana*	-32.13	-32.78	1631	1629	114	3.83	6.64	1.34	0.69	0.22	0.36	4.97	High 238U
MNRJ 9044	*Caryophyllia berteriana*	-30.34	-36.07		2450	55	3.98	8.10	1.86	1.79	0.79	1.55	4.34	No depth info
MNRJ 9044	*Caryophyllia berteriana*	-30.34	-36.07		2450	55	4.15	10.73	2.45	3.03	1.55	2.16	4.38	No depth info
MNRJ 9028	*Trochocyathus rawsonii*	-29.84	-36.55	912	2789	83	3.89	10.19	2.33	2.07	1.23	1.03	4.37	
MNRJ 9028	*Trochocyathus rawsonii*	-29.84	-36.55	912	2789	83	3.72	11.66	2.66	4.03	2.74	2.82	4.38	
MNRJ-9031	*Caryophyllia scobinosa*	-31.15	-34.80	1987	3197	65	4.07	8.88	1.81	20.45	3.02	9.87	4.89	
MNRJ-9031	*Caryophyllia scobinosa*	-31.15	-34.80	1987	3197	65	3.97	6.87	1.26	4.49	0.32	0.33	5.46	
MNRJ 9022	*Caryophylliidae sp.*	-31.14	-35.61		3406	116	4.12	10.93	2.35	3.45	2.58	1.84	4.64	No depth info
MNRJ 9022	*Caryophylliidae sp.*	-31.14	-35.61		3406	116	4.02	10.67	2.31	2.05	1.90	0.95	4.61	No depth info
MNRJ 8873	*Caryophyllia berteriana*	-32.11	-32.84	2350	5361	128	3.79	8.68	2.05	1.67	3.38	11.32	4.23	

Full Sample ID	Taxa	Lat	Lon	Depth	U-series age	2 s	[Ca]	Li/Ca	Mg/Ca	Al/Ca	Mn/Ca	Fe/Ca	Li/Mg	Selection code
MNRJ 8873	*Caryophyllia berteriana*	-32.11	-32.84	2350	5361	128	3.87	10.53	2.30	3.00	2.56	1.97	4.58	
MNRJ 8977	*Caryophylliidae*	-32.10	-32.66	1798	6119	97	3.91	8.58	1.97	2.46	1.38	2.05	4.36	
MNRJ 8977	*Caryophylliidae*	-32.10	-32.66	1798	6119	97	3.92	9.00	1.88	7.58	0.48	2.80	4.77	
DY094-St23-car	*Caryophylliidae*	-30.82	-35.97	786	8264	294	3.78	11.50	2.76	3.76	1.31	5.32	4.17	
DY094-St23-car	*Caryophylliidae*	-30.82	-35.97	786	8264	294	4.07	11.34	2.68	4.89	1.75	7.80	4.24	
MNRJ 8847	*Caryophyllia berteriana*	-33.46	-31.31	1878	9730	298	3.99	10.49	2.41	3.88	3.39	3.49	4.36	
MNRJ 8847	*Caryophyllia berteriana*	-33.46	-31.31	1878	9730	298	3.82	10.00	2.31	4.25	5.30	5.83	4.33	
MNRJ 8861-2	*Caryophyllia berteriana*	-33.81	-30.70	1680	12392	250	4.12	7.82	1.67	1.88	3.21	1.77	4.69	
MNRJ 8861-2	*Caryophyllia berteriana*	-33.81	-30.70	1680	12392	250	3.58	7.08	1.43	4.26	0.60	0.75	4.95	
MNRJ 8861-1	*Caryophyllia berteriana*	-33.81	-30.70	1680	12874	147	3.71	7.94	1.59	2.17	0.61	0.98	4.99	
MNRJ 8861-1	*Caryophyllia berteriana*	-33.81	-30.70	1680	12874	147	4.17	8.18	1.76	0.76	0.28	0.29	4.66	
MNRJ 9070	*Caryophylliidae*	-34.19	-30.97	2600	13553	315	4.25	9.38	1.80	14.21	5.27	13.30	5.23	
MNRJ 9070	*Caryophylliidae*	-34.19	-30.97	2600	13553	315	4.08	10.15	2.03	36.87	5.78	14.42	5.00	
MNRJ 8993-1	*Caryophylliidae*	-32.10	-32.82	1148	15145	113	3.71	11.16	2.40	0.63	<LOD	2.48	4.66	
MNRJ 8993-1	*Caryophylliidae*	-32.10	-32.82	1148	15145	113	3.80	10.96	2.38	0.75	0.61	3.36	4.61	
DY094_032_G002-2	*Caryophylliidae*	-30.74	-35.95	1504	15419	222	3.94	9.36	1.99	1.38	1.47	1.12	4.70	
DY094_032_G002-2	*Caryophylliidae*	-30.74	-35.95	1504	15419	222	4.09	9.54	2.11	0.95	0.29	0.75	4.52	
MNRJ 8789	*Paracyathus sp.*	-30.19	-36.41		15945	316	3.99	12.60	2.57	3.28	7.73	1.94	4.90	
MNRJ 8789	*Paracyathus sp.*	-30.19	-36.41		15945	316	4.04	13.41	2.73	4.38	19.44	9.44	4.90	
MNRJ 8797	*Caryophylliidae*	-34.12	-30.95	2172	16010	203	3.91	11.31	2.12	5.04	2.82	3.36	5.33	
MNRJ 8797	*Caryophylliidae*	-34.12	-30.95	2172	16010	203	4.10	11.02	2.05	2.50	4.75	5.42	5.38	
MNRJ-8865	*Caryophyllia berteriana*	-32.13	-32.78	1631	18221	1150	4.15	9.92	1.74	2.13	1.70	2.49	5.69	Low 238U
MNRJ-8865	*Caryophyllia berteriana*	-32.13	-32.78	1631	18221	1150	4.07	9.25	1.54	6.89	5.25	14.98	5.99	Low 238U

Full Sample ID	Taxa	Lat	Lon	Depth	U-series age	2 s	[Ca]	Li/Ca	Mg/Ca	Al/Ca	Mn/Ca	Fe/Ca	Li/Mg	Selection code
MNRJ 8916	*Desmophyllum dianthus*	-32.71	-32.80	1050	21199	346	4.15	12.42	2.23	3.95	0.71	2.64	5.58	
MNRJ 8916	*Desmophyllum dianthus*	-32.71	-32.80	1050	21199	346	3.84	15.24	2.60	6.12	0.72	2.52	5.86	
MNRJ 8906-DES	*Desmophyllum dianthus*	-33.62	-31.13	2500	23736	519	3.83	15.78	2.67	32.76	4.54	18.54	5.92	High δ234Ui
MNRJ 8906-DES	*Desmophyllum dianthus*	-33.62	-31.13	2500	23736	519	3.79	16.82	2.64	40.21	17.09	33.96	6.38	High δ234Ui
MNRJ 9025	*Caryophyllia sp.*	-32.71	-32.71	1250	28610	409	3.86	11.16	1.97	1.65	0.76	1.84	5.68	
MNRJ 9025	*Caryophyllia sp.*	-32.71	-32.71	1250	28610	409	4.14	10.79	1.80	2.32	1.15	1.59	6.00	
MNRJ 8791	*Caryophyllia berteriana*	-31.05	-35.82	1330	30293	239	3.76	11.72	1.97	5.83	2.63	10.60	5.96	
MNRJ 8791	*Caryophyllia berteriana*	-31.05	-35.82	1330	30293	239	3.79	12.00	1.99	4.93	1.55	7.37	6.03	
MNRJ-8848	*Desmophyllum dianthus*	-30.10	-36.83	1542	31672	311	3.88	10.97	1.97	10.45	3.20	10.02	5.58	
MNRJ-8848	*Desmophyllum dianthus*	-30.10	-36.83	1542	31672	311	4.12	11.07	1.96	13.38	1.46	17.77	5.65	
MNRJ 9040	*Caryophyllia berteriana*	-30.58	-36.14	1500	32006	275	4.01	11.89	1.86	10.99	0.90	9.61	6.38	
MNRJ 9040	*Caryophyllia berteriana*	-30.58	-36.14	1500	32006	275	4.06	12.41	2.05	10.52	3.23	10.58	6.06	
MNRJ 9004	*Caryophyllia berteriana*	-33.63	-30.90	1550	32854	305	5.11	8.59	1.47	6.86	1.11	3.39	5.85	
MNRJ 9004	*Caryophyllia berteriana*	-33.63	-30.90	1550	32854	305	6.61	8.71	1.47	7.57	2.43	5.16	5.92	
MNRJ-8875-CAR	*Caryophyllia berteriana*	-30.66	-36.10	1150	37784	587	4.13	9.99	2.07	9.63	9.41	14.19	4.83	
MNRJ-8875-CAR	*Caryophyllia berteriana*	-30.66	-36.10	1150	37784	587	3.86	11.40	2.33	5.00	2.55	5.46	4.88	
DY094_032_G002-1	*Caryophylliidae*	-30.74	-35.95	1504	38739	232	4.01	8.20	1.75	6.74	6.52	7.89	4.69	
DY094_032_G002-1	*Caryophylliidae*	-30.74	-35.95	1504	38739	232	3.72	8.88	1.89	1.02	0.68	1.37	4.69	
MNRJ 8976	*Caryophyllia berteriana*	-32.13	-32.78	1631	39140	244	3.97	13.22	2.63	1.16	0.38	0.58	5.02	
MNRJ 8976	*Caryophyllia berteriana*	-32.13	-32.78	1631	39140	244	3.67	10.68	2.27	0.88	0.24	0.96	4.71	

Full Sample ID	Taxa	Lat	Lon	Depth	U-series age	2 s	[Ca]	Li/Ca	Mg/Ca	Al/Ca	Mn/Ca	Fe/Ca	Li/Mg	Selection code
MNRJ 8882	*Caryophylliidae*	-30.62	-36.81	1575	39299	432	3.77	9.46	1.78	1.36	0.27	0.97	5.30	
MNRJ 8882	*Caryophylliidae*	-30.62	-36.81	1575	39299	432	3.90	9.57	1.82	3.47	0.38	1.39	5.26	
MNRJ 9015	*Caryophyllia berteriana*	-30.75	-35.06	1600	47438	330	3.76	9.31	1.92	5.12	0.58	3.45	4.84	
MNRJ 9015	*Caryophyllia berteriana*	-30.75	-35.06	1600	47438	330	3.88	9.49	1.95	3.26	2.86	5.32	4.87	
MNRJ 8773-1	*Caryophyllia berteriana*	-30.95	-35.04	1740	47723	347	2.42	12.07	2.51	2.02	1.80	1.48	4.81	
MNRJ 8773-1	*Caryophyllia berteriana*	-30.95	-35.04	1740	47723	347	3.18	11.77	2.41	21.41	2.29	11.70	4.89	
MNRJ 8773-2	*Caryophyllia berteriana*	-30.95	-35.04	1740	247530	4260	3.99	8.39	1.83	0.70	0.20	0.18	4.58	Too old
MNRJ 8773-2	*Caryophyllia berteriana*	-30.95	-35.04	1740	247530	4260	3.14	8.47	1.85	1.68	0.50	0.41	4.59	Too old

Table 10: Replicates of trace elements measurements of deep-sea corals from the Brazilian margin.

Full Sample ID	Taxa	Lat	Lon	Depth	U-series age	2 s	[Ca]	Li/Ca	Mg/Ca	Al/Ca	Mn/Ca	Fe/Ca	Li/Mg	Selection code
		DecDeg (N)	DecDeg (E)	m	yr BP	yr	mM	µmol/mol	mmol/mol	µmol/mol	µmol/mol	µmol/mol	mmol/mol	
MNRJ-5742-2	*Solenosmilia variabilis*	-22.22	-39.87	1059	18	23	3.88	12.13	2.70	4.34	<LOD	1.18	4.49	
MNRJ-5742-2	*Solenosmilia variabilis*	-22.22	-39.87	1059	18	23	3.89	11.95	2.70	1.69	<LOD	0.28	4.43	
MNRJ-5683	*Solenosmilia variabilis*	-22.40	-39.91	1150	627	128	3.57	12.44	2.62	9.14	<LOD	4.18	4.75	
MNRJ-5683	*Solenosmilia variabilis*	-22.40	-39.91	1150	627	128	3.98	11.31	2.56	8.82	<LOD	3.54	4.42	
MNRJ-6692	*Solenosmilia variabilis*	-22.43	-39.96	1077	657	51	3.92	11.04	2.47	7.62	2.34	2.11	4.48	
MNRJ-6692	*Solenosmilia variabilis*	-22.43	-39.96	1077	657	51	4.13	14.41	2.58	148.63	4.08	12.47	5.59	Rejected
MNRJ-6698	*Solenosmilia variabilis*	-22.43	-39.96	1073	1118	102	3.86	10.81	2.44	4.98	<LOD	4.52	4.43	
MNRJ-6698	*Solenosmilia variabilis*	-22.43	-39.96	1073	1118	102	3.87	10.92	2.49	8.37	2.61	7.27	4.38	
MNRJ-5038-2	*Stephanocyathus diadema*	-25.93	-43.93	2212	3130	621	4.09	10.95	2.17	28.61	3.49	19.75	5.06	
MNRJ-5038-2	*Stephanocyathus diadema*	-25.93	-43.93	2212	3130	621	4.09	11.17	2.26	10.54	<LOD	8.33	4.94	
MNRJ-5038-1	*Stephanocyathus diadema*	-25.93	-43.93	2212	4780	1019	3.83	9.97	2.00	58.36	8.29	45.83	5.00	
MNRJ-5038-1	*Stephanocyathus diadema*	-25.93	-43.93	2212	4780	1019	3.93	9.62	1.84	94.23	9.87	67.02	5.22	
MNRJ-6393-des	*Desmophyllum dianthus*	-28.35	-46.82	768	6271	167	3.75	12.84	2.96	5.81	23.33	55.25	4.34	
MNRJ-6393-des	*Desmophyllum dianthus*	-28.35	-46.82	768	6271	167	3.65	12.73	2.91	4.51	25.23	16.33	4.38	
MNRJ-5739	*Solenosmilia variabilis*	-22.40	-39.91	1150	6777	71	3.86	10.18	2.40	2.12	<LOD	2.62	4.24	
MNRJ-5739	*Solenosmilia variabilis*	-22.40	-39.91	1150	6777	71	4.12	10.05	2.35	1.22	<LOD	0.80	4.27	
MNRJ-5742-1	*Solenosmilia variabilis*	-22.22	-39.87	1059	7026	44	3.94	9.27	2.35	1.90	<LOD	0.85	3.94	

Full Sample ID	Taxa	Lat	Lon	Depth	U-series age	2 s	[Ca]	Li/Ca	Mg/Ca	Al/Ca	Mn/Ca	Fe/Ca	Li/Mg	Selection code
MNRJ-5742-1	*Solenosmilia variabilis*	-22.22	-39.87	1059	7026	44	3.92	9.70	2.48	2.61	<LOD	1.44	3.92	
MNRJ-6005	*Solenosmilia variabilis*	-21.38	-40.18	625	13946	118	4.02	11.69	3.09	4.40	<LOD	11.87	3.78	
MNRJ-6005	*Solenosmilia variabilis*	-21.38	-40.18	625	13946	118	4.03	11.15	2.97	6.15	<LOD	14.91	3.75	
MNRJ-6405	*Solenosmilia variabilis*	-24.27	-43.40	600	17759	128	3.42	13.33	2.75	2.21	<LOD	4.21	4.85	
MNRJ-6405	*Solenosmilia variabilis*	-24.27	-43.40	600	17759	128	3.78	13.01	2.71	5.72	8.74	12.20	4.80	
MNRJ-5737	*Solenosmilia variabilis*	-22.41	-39.93	1105	50869	317	4.12	12.63	2.97	6.33	5.34	15.71	4.26	
MNRJ-5737	*Solenosmilia variabilis*	-22.41	-39.93	1105	50869	317	4.07	13.54	3.01	8.54	13.57	29.65	4.49	